Editorial: THE DEVELOPING TECHNOLOGY OF TRANSMUTATION

Index pg 3 First article pg 5
Title pg 235 Front cover pg 233

This third issue of the *Journal of New Energy* will become an historic publication. Thanks to the efforts of Distinguished Professor of Chemistry at Texas A&M, John O'Malley Bockris (and his associate Dr. G. H. Lin) and co-host George Miley, editor of *Fusion Technology*, the second conference on **Low-Energy Nuclear Reactions**, September 13-14, 1996, College Station, Texas, is an historic event. This issue publishes most of the papers presented at that historic conference.

These proceedings, and the recentlt past conference, mark the beginnings of a new understanding of some of the many and varied low-energy nuclear reactions. The phrase **low-energy nuclear reactions** is a euphemism for **transmutation**. The word **transmutation** may be offensive to many members of scientific academia who have thoroughly accepted the currently-taught model of the atomic nucleus. The belief that there are no possible low-energy methods to create nuclear reactions is strongly taught and strongly accepted by many scientists.

To our valued academic friends, we strongly encourage you to read carefully the detailed paper by Kenneth & Steve Shoulders. For over a decade, Kenneth Shoulders has been developing a variety of devices (inventions) based on the generation and control of high-density charge clusters (EVs). In his conference presentation, Shoulders offered specific experimental information on the role of the fracto-emission of EVs that may account for some, most, or all of the nuclear reactions in a variety of cold fusion devices. This insight into the role of nuclear Evs as an explanation for some of the experimental observations has prompted this editor to highlight (bold type) a few of the observations made in some of the papers herein.

On rare occasions, a variety of concepts presented in a conference results in a scientific or technological breakthrough. **Such an event was the result of this conference.** Because of the importance of this new understanding, a paper has been prepared and is included in this issue. This paper by Fox, Bass, and Jin has been peer-reviewed and approved for publication. In one sense, the paper summarizes and extends concepts presented in the conference. In this editor's judgement, this paper represents the culmination of over seven years of a struggle to understand the real nature of low-energy nuclear reactions found in the study of cold nuclear fusion. In addition, a patent application has been filed with claims of a method and apparatus to produce thermal energy, ameliorate radioactive wastes, and transmute many of the elements in the periodic table. **A new science and a new technology have begun!**

Hal Fox, Editor

Attendees of the Second International Low Energy Nuclear Reactions Conference

First row: Roberto Monti, ? , Charles Becker, Yeong Kim, Albert Cau, John O'M. Bockris, Don Rott, Barry Merriman, ? , Stanley Spzak, Tadayoshi Ohmori.

Second row: Michael Robert, Guang H. Lin, Toby Grotz, Hal Fox, Jerry W. Decker, Ernst Bauer, Emre Brooks, Andrew Michrowski, Dan York, Richard Murray, Russ George, Lee Don Biewski, Tom Claytor, Edmund Storms, Mitchel Swartz, Edward Lewis, George Miley, David Nagel, Ken Shoulders, Yan Kucherovm, Georgiy Rabzi.

JOURNAL OF NEW ENERGY

Proceedings of the Second International Low Energy
Nuclear Reactions Conference
College Station, Texas, September 13-14, 1996

Additional Conference Papers by

Z. Minevski: New Elements Formed in the Electrolysis of Light Water on Palladium
R. George: Isotopic Ratio Anomalies Induced in Palladium by the Application of Intense Ultrasound
R. Notoya: Evidence of Nuclear Reactions Found by Measurement of Radioactivity in Electrolytic Cells
R.J. Kovac: Unusual Reactions of Mass 5 with Helium and Catalytic Metals, with Proposed Mathematical Interpretation
E. Lewis: Novel Hypothesis Concerning the Production of Elements, Superconductivity and Anomalous Radiation

were unavailable at press time and may be printed at a later date.

NUCLEAR TRANSMUTATIONS IN THIN-FILM NICKEL COATINGS UNDERGOING ELECTROLYSIS

George H. Miley [1] and James A. Patterson [2]

ABSTRACT

Experiments using 1-mm plastic and glass microspheres coated with single and multilayers of thin films of various metals such as palladium and nickel, used in a packed-bed electrolytic cell (Patterson Power Cell ™ configuration), have apparently produced a variety of nuclear reaction products. The analysis of a run with 650-Å film of Ni is presented here. Following a two-week electrolytic run, the Ni film was found to contain Fe, Ag, Cu, Mg, and Cr, in concentrations exceeding 2 atom % each, plus a number of additional trace elements. These elements were at the most, only present in the initial film and the electrolyte plus other accessible cell components in much smaller amounts. That fact, combined with other data, such as deviations from natural isotope abundances, seemingly eliminates the alternate explanation of impurities concentrating in the film.

A 1-molar lithium sulfate solution in light water was employed for the electrolyte. A small excess heat of approximately 0.5 ± 0.4 watts was recorded throughout the run. Reaction products were analyzed using a combination of secondary ion mass spectrometry (SIMS), Auger electron spectrometry (AES), energy dispersive x-ray (EDX) analysis, and neutron activation analysis (NAA).

Results showing a broad array of products such as found here have also been obtained with thin film coatings of other materials, e.g., Pd and multi-layers of Pd and Ni. The yields of the major elements contributing depend on the film material, however. Some of that work is still being analyzed and will be presented at ICCF-6 [15].

The array of products found in these experiments is consistent with recent studies of solid Pd and Au electrodes by Mizuno et al. [19] and Ohmori and Enyo [22] , respectively. A distinct advantage of thin electrode construction used here, however, is that the reaction zone becomes well defined, enabling quantitative measurements of the amounts of various products.

To explain the observation of products with atomic numbers both well above and below Ni, a reaction model is being developed that involves proton-induced excited complexes, followed in some cases by a fission of the unstable compound nucleus

INTRODUCTION

Various nuclear transmutation products generated during electrolytic cell operation, typically employing Pd and heavy or light water with various electrolytes such as Na_2CO_3 and LiOH, have previously been reported, e.g., see the proceedings of the first conference in this series (Bockris and Lin [1]). Most of these reports have dealtwith impurity level quantities of specific elements, such as Sr, Rb or tritium, although some workers, such as Mizuno

[1] Fusion Studies Laboratory, U. of Illinois, 103 S. Goodwin Avenue,Urbana, IL 61801-2984
Ph. 217-333-3772 Fax 217-333-2906 E-mail: g-miley@uiuc. edu

[2] Clean Energy Technologies, Inc., 1 Lincoln Center, 5400 LBJ Freeway, Suite 950, Dallas, TX 75240
Ph. 972-982-8340 Fax 972-982-8349

et al.[19], Ohmori and Enyo [22] , and Karabut et al.[7] report on a wide variety of isotopes occurring at impurity levels. Several investigators, e.g., Miles and Bush [10], have concentrated on ^4He, which they view as a logical reaction product for nuclear reactions in solids.

While the occurrence of this number of independent observations strongly implies that chemically assisted nuclear reactions in solids are possible, the quantification and the credibility of the results have suffered from low, impurity-level yields and non-reproducibility. In sharp contrast, the thin (<2000Å) films used in present work result in transmutation of a significant percentage of the metal in the thin-film cathode due to the "small" number of host atoms. (While, as stressed later, impurity contributions can not be completely ruled out, the term "transmutation products" is used here due to the overwhelming evidence in favor of this identification.)

Over a dozen experiments with various types of thin-film coatings have been carried out in different cells (Miley and Patterson [17]). Thin-film coatings on 1-mm-diameter plastic/glass microspheres, ranging from 500-Å-thick single layers of Pd or Ni to multiple Ni/Pd layers, were used in a flowing packed-bed-type electrolytic cell with a 1-molar Li_2SO_4 light water electrolyte. Nuclear reaction products were obtained in all cases, with several runs resulting in over 40 atomic % of the original coating materials being transmuted to reaction products such as Fe, Si, Mg, Cu, Cr, Zn, and Ag. The present paper deals with the specific case of a single nickel thin film, since it has been analyzed most thoroughly to date and appears to be representative of the behavior observed in the other runs.

The "normal" Patterson Power Cell employs electrolytically coated layers of Ni and Pd on microspheres, and this composition has been extensively studied for power production (Patterson [24]). The Ni-coated thin film microspheres described here were developed explicitly for reaction product studies, although power production with "conventional" thick Ni electrodes in light water cells has been widely studied (e.g., see I. Myers et al. and references therein [20]).

The use of thin-film coatings originates from the "swimming electron layer" (SEL) theory proposed earlier (Hora, Miley, et al. [5]; Miley et al.[12]; Miley et al.[14]), which suggests that nuclear reactions are assisted by the use of multilayer thin films with alternating metals that have large differences in Fermi energy levels. The resulting increase in electron density at the film interface is shown to "squeeze" excess electrons between ions, greatly reducing the Coulombic barrier, thus enhancing nuclear reactions. This theory was first studied using thin-film Pd/Ti coatings sputtered onto a large stainless steel substrate electrode (Miley et al. [14]). Those experiments were terminated due to flaking of the films off of the electrode soon after loading and heating occurred. However, the results were very encouraging, since high excess heat (estimated to be kW/cm^3 at the interface regions) was observed for minutes prior to the disintegration of the thin films. Subsequently, J. Patterson [24] developed a unique electrode configuration using electrochemical deposition of relatively thick (mm) coatings of Ni/Pd layers on millimeter diameter cross-linked polymer microspheres. These microspheres were then employed in a flowing packed-bed-type electrolytic cell (Patterson Power Cell). The coatings, while thicker than the earlier thin-film studies, were found to be quite stable in this configuration, so experiments with thin films (300- to 2000-Å thick) on such microspheres were undertaken in the present work.

The thin films were laid down using a special sputtering process (Miley, Name, et al.[18]), where the microspheres are suspended in a fluidized state during the spraying process. The metallurgy of the films themselves has been studied before and after electrolysis, using both Auger electron probe techniques and electron microscopic surface analysis.

Reaction product measurements have utilized a combination of secondary ion mass spectrometry (SIMS), Energy Dispersive X-ray (EDX) analysis, Auger Electron Spectroscopy (AES), and neutron activation analysis (NAA). SIMS is used to obtain a broad view of both high and low concentration isotopes present and their isotopic ratios, while NAA provides a quantitative measure of the masses of key elements. EDX provides confirmatory data for

elements having high concentrations, while AES is used for depth-profiling of high concentration elements. NAA can obtain total quantities of elements in a sample typically containing 10 microspheres, while the other techniques are restricted to probing a local area on single microspheres. Due to variations among microspheres due to location in the packed bed and other effects, this difference in samples becomes very important in present work. The analysis techniques and the nuclear reaction products observed are described further in following sections

ELECTROLYTIC CELL DESCRIPTION AND OPERATION

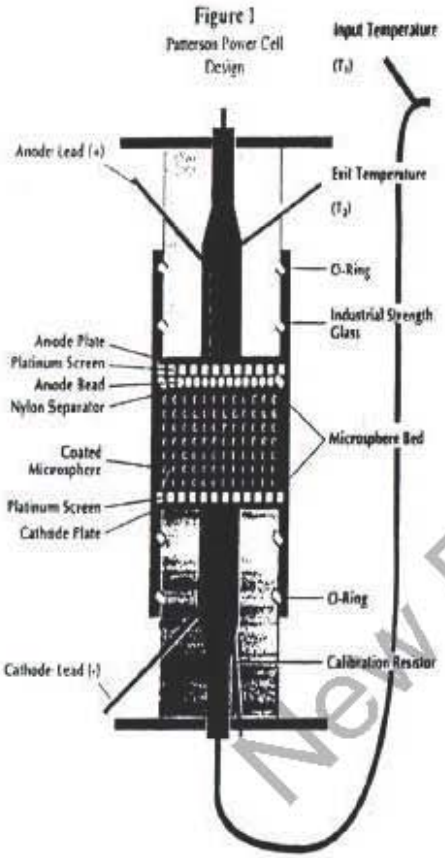

Fig. 1a. Schematic Diagram of a Patterson Cell

The general configuration of the Patterson-type electrolytic cell employed is shown in Fig. 1a. About 1000 microspheres (~0.5 cm^3 volume) were used in the packed-bed cell. Titanium electrodes were employed in the present Ni run and in most other runs, except for a few cases where Pt electrodes were used for comparison purposes.

A flow diagram is shown in Fig. 1b. A preheater allowed control of the temperature of the electrolyte entering the cell from 20-70° C, with flow rates of ~11 ml/min. Voltages across the bed were held at ~2-3 V, with several mA of current, giving an electrical input power of approximately 0.06 W. The pump and preheater consume an additional 5 W, but this input does not enter into the energy balance across the cell, hence the 5 W is not involved in the computation of excess heat production. Inlet-outlet thermocouples provide a measure of the temperature increase of the flowing electrolyte typical values ranged from 0.1 to 4° C, corresponding to about 0.1 to 4 W output, depending on the films used. Positive outputs were observed in all cases, but due to the calorimeter technique, the values are only considered to be accurate to ±0.4 W. More precise calorimetry is in use in several laboratories studying excess power from the Patterson cell, but here the cell design was focused on ease of reaction product measurement. In view of the positive results reported here, further work with improved calorimetry and periodic sampling of microspheres during runs is warranted to obtain a quantitative relation between the power (or energy production/run) and the various reaction products.

Such studies are now in progress. Still, the present reaction product data provides a first insight into this important new field of chemically-assisted nuclear reactions using thin-film electrolysis.

Loading of hydrogen into the thin film is typically done at low (25° C) temperatures and requires several hours, as observed by an initial increase in the voltage across the bed, i.e., the change in film resistance, followed by an eventual equilibrium voltage level of +2 to 3 V. The loading time, defined as the time to reach this equilibrium

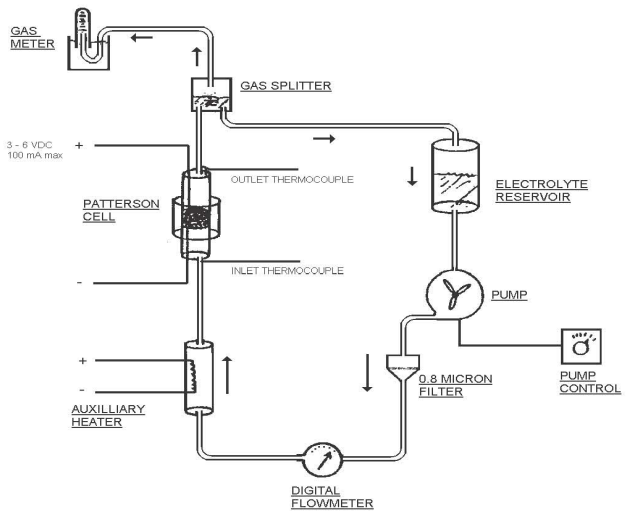

Fig. 1 b. Schematic of flow system.

state, was about an hour for the present Ni run. Thus this loading time was negligible compared to the two-week run time. A quantitative measurement of the loading was not attempted, although there is strong evidence presented by others that loadings in excess of 0.85 atoms of hydrogen or deuterium (H/D) per atom Pd are required in conventional solid Pd electrodes to produce heat (Crouch-Baker et al. [3]). After an equilibrium was achieved, the cell inlet temperature was raised slowly (over several hours) to the desired operating temperature of 60-70° C.

Further details about construction and operation of this type of cell is given in Patterson [24], Cravens [2], and Nix et al. [21].

NICKEL-FILM RUN

The run lasted for 310 hours and employed an entering electrolyte temperature of approximately 60° C. Termination of the run was made prior to any noticeable deterioration of thermal performance. A temperature rise across the cell of less than 0.5° C was obtained throughout the run, representing an output of 0.5 ± 0.4 watts. Calibration corrections due to heat losses and flow-pattern variations prevented a more accurate measurement, but the output always indicated a positive excess heat.

The cell employed for the run used all plastic fittings with the exception of the pressure and flow meters and the pump. (To further decrease possible impurity sources, a loop with all plastic components except for the electrodes was developed for subsequent runs. As noted later, this modification did not cause a noticeable change in film products.) Titanium electrodes were used. A filter fitted with 0.8-μm pore size filter paper was inserted in the loop to collect any fine particles entering the electrolyte, either from film surfaces or from other parts of the system.

Characteristics of the 650-Å Ni film microspheres used in this run (#8) are summarized in Table 1. A 650Å-thick Ni film was laid down by sputtering the Ni on to a 1-mm plastic core. The thickness of the layer was determined by weighing a calibration sample coated under the same conditions as the microspheres in the sputtering unit. Some coating variations, estimated to be ±30%, can occur among the 1000 microspheres used in the cell, however. Measurements with an Auger electron probe on select microspheres confirmed the film thickness to be reasonably uniform (±20%).

Table 1. Data for nickel coated microspheres

Layer	Diameter (cm)	Volume (cc)	Mass of layer (g)	# of atoms
PS	0.106	6.22×10^{-4}	6.09×10^{-4}	
Ni(605A)	0.106	2.29×10^{-7}	2.04×10^{-6}	2.09×10^{16}

Total Mass of a microsphere 6.11×10^{-4} g.
Total Mass of metal on a microsphere 2.04×10^{-6}
Total Atoms of metal 2.09×10^{16}

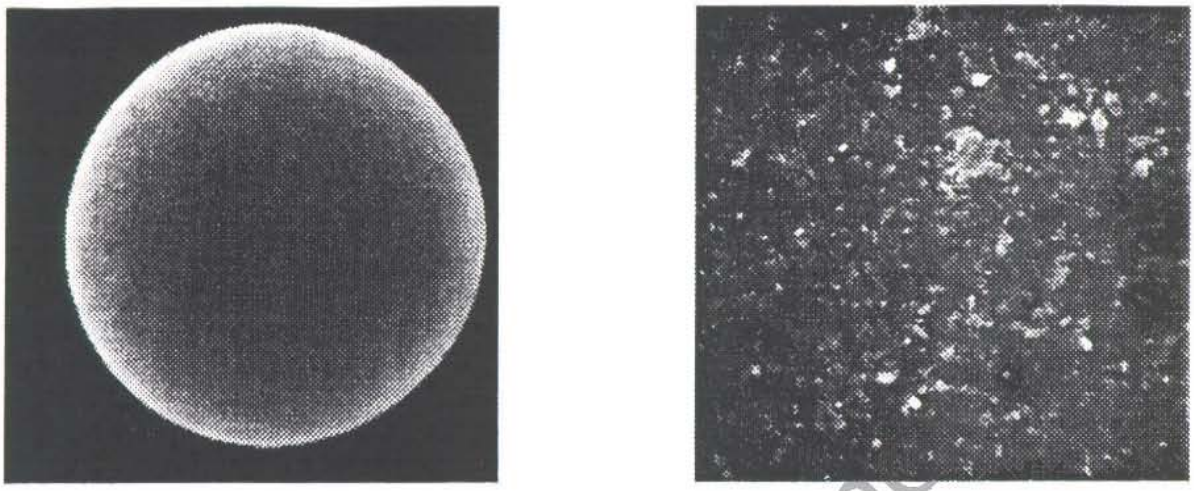

Fig. 2a. SEM photographs of the microsphere before a run (80X magnification on left & 1000X magnification on right).

The mass of the metallic film on these microspheres was less than 1% of the total microsphere mass (see Table 1), giving a most unique electrode configuration for the electrolytic cell. Photographs of the outer surface of the microspheres, using a scanning electron microscope (SEM), confirmed that a very smooth surface was achieved with the sputtering process (Fig. 2a), while a high magnification photo shows a small-scale, rough structure uniformly distributed over the surface. Some erosion of small particles from the surface occurs during operation, however, as detected by placing a filter with 0.8-μm filter paper in the flow loop. Concurrently, various fragile looking bead-like and fiber-like structures are typically visible on the film surface after electrolysis, e.g., see Fig. 2b.

REACTION PRODUCT ANALYSIS METHODS

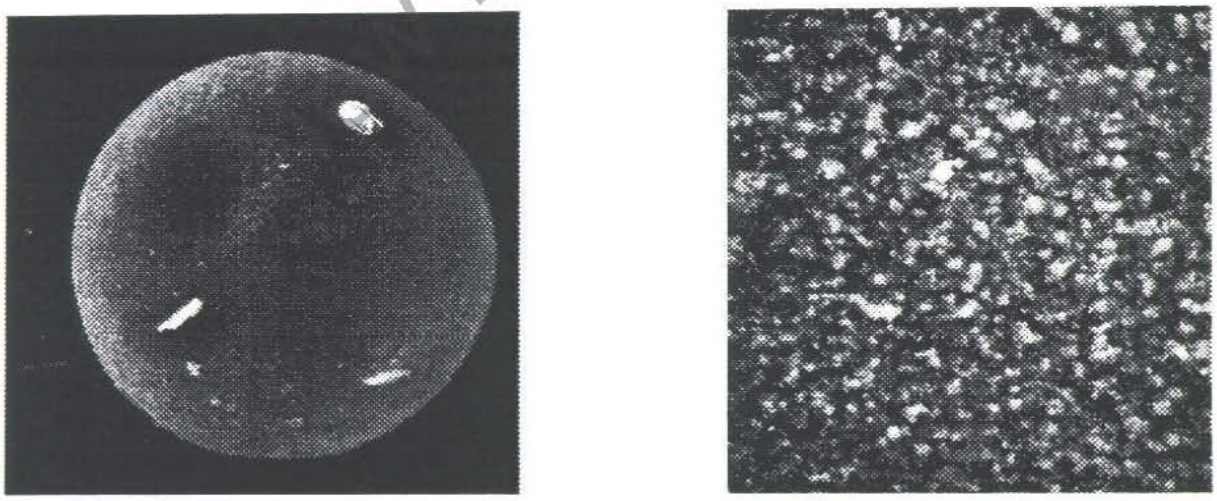

Fig. 2 b. SEM photographs of the microsphere after a run (80X on left & 1000X on right).

SIMS, EDX, AES and NAA methods were employed to analyze the microspheres before and after the run. Sampling was done by disassembling the cell after a run and removing microspheres from the top (cathode end) layer of the packed bed. (The 1000 microspheres in the bed result in roughly 3-5 layers total). These microspheres were selected for reasons of accessibility and the fact that the higher electric field in that region is expected to make this layer most reactive.

This limited selection procedure raises key issues about the reactivity in other layers. Thus, an uncertainty arises when it is desired to extrapolate the results to predict total cell characteristics (element yields or cell power). To study these effects in more detail, a new sampling technique employing a small plastic tube that is plunged into the bed to extract a "core sample" of microspheres has now been developed.

The SIMS analysis employed a Cameca IMS 5F unit operating with 8-keV oxygen primary beam in the positive ion mode (Wilson et al.[27]). Scans of key isotopes were made using single microspheres in a low-resolution (2,000 mass resolution) mode at several depths of interest (typically near the surface and interfaces) (see Fig. 3a). High-resolution (40,000 mass resolution) scans were then done to resolve any interferences involving important isotopes (e.g., see Cu-63 and Ag-107 in Fig. 3b). Although the SIMS gives the relative amounts of isotopes for a given element accurately, the variation of isotopes with depth and the lack of reference samples for calibration of the SIMS sensitivity made it difficult to determine absolute concentrations of isotopes with this technique alone. Thus NAA was used to determine total concentrations of Al, Cu, Mg, Cr, Fe, Zn, V, and Ag (subsequently termed "NAA elements") in the microspheres. This data was, in turn, used as a calibration for the SIMS sensitivity to find concentrations of the other "non-NAA" elements, as described next.

SIMS scan of a fresh microsphere (See all figures at end of paper.)
Fig. 3a. Typical low resolution SIMS scan (before the run).
Fig. 3a. Typical low resolution SIMS scan after the run (average of microspheres in 3 layers in the cell).
Fig. 3b. High Resolution SIMS scan for Cu(63) after the run.
Fig. 3b. High Resolution SIMS scan for Ag(107) after the run.

Interpretation of the SIMS count data of Fig. 3 requires a knowledge of sensitivities (RSF values) for sputtering of each isotope out of the host matrix by the SIMS's primary beam (Wilson et al. [27])

For accurate analysis, the RSF should be determined by implanting a known quantity of the isotope of interest in a sample of the host matrix and measuring the RSF in the SIMS under the actual conditions employed. Since such a calibration is not available for thin film Ni, an alternate technique was employed. Theoretically (Wilson et al. [27]), the RSF is an exponential function of the ionization potential (IP) for non-gaseous isotopes in a fixed host matrix. This functional relation was employed, but a RSF-IP slope from Ni matrix studies by Wilson and Stevie [28][29], and Wilson [28] was assumed and fit through data for the nine NAA elements to obtain a RSF value for the remaining SIMS values. One refinement found necessary was to separate elements into two groups, one having concentrations >0.1% and one <0.1%, each group having a different RSF functional fit. (SIMS intensities tend to saturate at high concentrations.) With this technique, an uncertainty factor of 2 is estimated for the absolute values for non-NAA element percentages. (Note: due to changes in the RSF correlation employed, results presented here differ somewhat for those in an earlier draft of this paper, cf. G. Miley and J. Patterson [16]).

NAA was carried out at the University of Illinois (UI) TRIGA research reactor (Landsberger [9]). Samples consisted of 10 microspheres. Techniques for short-lived NAA (Parry [23]) were initially performed to determine the presence of Ag, Cu, Al, and V in the electrodes. (Subsequently, analysis of Fe, Cr and Zn was done in a similar fashion.) Epithermal NAA was used for Ag in conjunction with the $^{109}Ag(n, \gamma)^{110}Ag^{m}$ reaction using the 657.1-keV gamma ray. A 10-sec irradiation time at a flux of 2.1×10^{11} n/cm^2·sec, with a 20-sec decay time and a 75-sec counting time was used, along with a pneumatic transfer facility. Typical detection limits for Ag were of the order of 2 ppm, with a precision of ±10 to 15%. A typical gamma spectrum for the Ag analysis is shown in Fig 4a.

Fig. 4a. Typical NAA gamma spectrum for Ag.
Fig. 4b. NAA gamma spectrum for Cu.

Thermal NAA was also used for Cu, Al, and V in conjunction with $^{65}Cu(n,\gamma)^{66}Cu$, $^{27}Al(n,\gamma)^{28}Al$, and $^{51}V(n,\gamma)^{52}V$, using the 1039.1-keV, 1778.9-keV, and the 1434.2-keV decay gamma rays, respectively. A representative gamma spectrum for Cu-66 is shown in Fig. 4b. Typically, a 2-min irradiation time with a flux of $4x10^{11}$ n/cm^2-sec, followed by a 2-3-min decay time and a 5-min counting time was used with the same pneumatic transfer facility. Detection limits were several ppm for Cu and less than 1 ppm for V and Al, with a precision of several percent for these elements. Calibration used certified liquid standards from the National Institute of Standards and Technology. Ores containing known quantities of these elements were analyzed for quality control. All such NAA results agreed within the error limits of the reference materials.

As a supplement to SIMS analysis, NAA was also employed to study key isotope ratios for comparison to natural abundance. Cu and Ag are of particular interest in the present work. Then, for example, an NAA measurement of the Cu63/65 ratio was carried out. Cu-63 was determined using the $^{63}Cu(n,\gamma)^{64}Cu$ reaction with the resulting 511-keV gamma ray to determine Cu-63. Cu-65 was determined using the $^{65}Cu(n,\gamma)^{66}Cu$ reaction using the 1039-keV gamma ray (see Fig. 4b).

The EDX analysis used a Field Emission Electron Microscope (Hitachi S800) operating in the energy dispersion analysis mode with the electron energy set at 20 kV to detect elements with atomic concentrations above about 1%. LINK software was utilized to derive the elemental concentrations from the energy spectrum. Due to the unique geometry with the curved film-plastic interface, the measurement accuracy was limited to 10%.

AES was used in a sputtering mode to perform semi-quantitative depth profiling for the major element species above 1 atom %. Two instruments were employed, PHI models 660 and 595, providing a resolution of approximately 25 nm. Depth profiles were also run with the SIMS, but the higher sputtering rates for SIMS greatly limited the spatial resolution in the thin film.

RESULTS

ELEMENT AND ISOTOPE CONCENTRATIONS

Results from NAA and EDX analysis of high concentration elements (Mg, Al, Si, Ag, Cr, Fe, Zn, and Cu) in the Ni run are summarized and compared in Table 2. (Two NAA runs on the microspheres yielded values within 10% of those shown for NAA in the table). The variation in the concentrations observed is attributed to the fact that each analysis used a different sampling of microspheres taken from various locations in the packed bed at the end of the run. Some differences are expected from microsphere to microsphere due to variations in location and coating. Further, the NAA results provide total concentrations for a sample of 10 microspheres, while EDX examined only a small volume of an individual microsphere. Still, the important point is that these independent measurements confirm that following a run, over 40 atom % of the film consists of these product elements, the remainder being the host Ni plus trace elements.

Table 2. Comparison of NAA and EDX analyses for several microspheres

ANALYSIS COMPARISON (Atomic %) *

TYPE	NAA	EDX	EDX
Sample #	N3.3	N3.3	N3.3
Mg	NA	5.6	5.0
Al	0.51	2.3	2.2
Si	NA	7.3	6.1
S	NA	1.1	NL
Ag	6.61	17.0	30.7
Cr	5.94	6.9	6.5
Fe	14.53	17.2	10.3
Ni**	62.31	32.3	29.0
Cu	7.96	10.3	10.2
V	0.01	NL	NL
Co	0.10	NL	NL
Zn	2.04	NL	NL
Total	100.0	100.0	100.0

** microspheres taken from same location in the packed bed.*
*** Ni % (from NAA) adjusted for a total of 100%*
NA: Not included in analysis
NL: Percentage below detection limit

To evaluate the other major **non-NAA** elements present and to obtain isotopic concentrations, SIMS and NAA data have been combined in Table 3. **NAA elements** are listed in bold. (Light elements, still under study, and other isotopes not observed are omitted from Table 3.) This table shows the yield, i.e., the difference between the final and initial weight for each isotope (fourth column). NAA only measured the elemental (isotopic) concentrations; therefore the NAA values for a given element have been pro-rated between isotopes according to the SIMS isotopic analysis. Corresponding values for the number of atoms of each isotope before ("fresh MS") and after ("reacted MS") a run follow in the fifth and sixth columns. Non-NAA elements used the SIMS data directly for both the element yield and the isotope values, based on the RSF interpretation discussed earlier.

Table 3. Yield Data from the Combined SIMS/NAA Analysis [see remaining figures at end of paper.]

Despite the uncertainties associated with the RSF correlation for non-NAA elements, the values shown in Table 3 should still provide a first estimate of ***non-NAA*** isotopes in the film. Note that the isotopic yields for **NAA elements** should be quite accurate, since the RSF values are essentially constant for isotopes of a given element, while the total concentrations of these elements come directly from the NAA measurement, avoiding RSF issues.

The isotopic atomic percents in the metal film are then calculated from the increased number of atoms for each element (column 7) and tabulated in the column labeled "SIMS". Comparison of this result with natural abundance values ("Natural a/o" in column 3) gives the "difference in a/o" shown in the final column. This data in Table 3 is used later to obtain figures for element production rates (Fig. 7 and Fig. 8), element yields (Fig. 9a and Fig. 9b), and isotope shifts (Fig. 11) vs. mass or Z. The systematics of the data will become clearer when these figures are discussed.

ELEMENT DEPTH PROFILES

Data from AES profile measurements on a typical microsphere are presented in Fig. 5 for the higher concentration elements. While the isotopes' profile behaviors are hard to interpret quantitatively, several observations can be made. Most profiles peak in the nickel volume or near the film-plastic interface, suggesting an internal source rather than diffusion in from the surface. For example, the key elements Ag and Fe peak near the Ni-plastic interface, (at ~ 650 Å corresponding to about 12 min. sputtering time). Cu peaks further out in the film. However the amplitude of the peaks is too small to draw definitive conclusions about diffusion vs. an internal source.

The product concentrations decrease into the plastic substrate. However, the decrease is gradual, indicating strong interdiffusion has occurred under run conditions. This interdiffusion of products can explain some differences between NAA and EDX values noted earlier in Table 2, since NAA, in contrast to EDX, measures total amounts of elements throughout both the film and the core of the microsphere. This distinction also applies to NAA vs. SIMS measurements.

Approximate Depth (Å)	0	100	700	2000
	Relative Atomic %			
C	20.00	-	-	61.23
Ag	2.68	9.94	11.77	3.07
Fe	7.72	10.02	10.45	5.12
Ni	9.99	12.30	22.28	12.56
Cu	4.17	7.64	7.61	5.38
Zn	11.12	10.48	9.22	-
Mg	10.78	13.75	-	-
Cr	-	-	3.66	4.99

Fig. 5. Tabulated atomic % vs. depth from AES scan.

NUCLEAR RADIATION EMISSION

In view of the evidence that products are formed at a significant rate (order of 10^{15} reactions/s-cm^3, cf. Table 5, discussed later) in an operating cell, measurable radiation emission would normally be expected, assuming normal nuclear reactions. However, so far attempts to measure nuclear radiation emission-neutrons, gammas, or x-rays-during cell operation have not detected any measurable quantities above background. A ^{3}He detector was employed for neutron measurements, and a cooled NaI crystal detector was used for gammas and x-rays. In one run, a 5-mm-thick Be window was placed over a small hole drilled into the side of the cell to allow measurement of softer x-rays (estimated lower limit of 20 kV), but after a four-hour run, none were detected. It is planned to repeat these measurements in a shielded area to reduce the background; however, if radiation emissions are escaping the cell, they are very low in intensity.

Another measurement used a liquid-scintillation detector to search for tritium in a sample of electrolyte immediately following a run. This measurement was repeated, and a sample was also sent out for independent analysis, but in no case was tritium detected. An experiment to measure the presence of tritium in the off gas, along with other possible products such as ^{4}He, is under consideration, but due to the very low concentrations involved, such measurements become very demanding.

Two attempts to measure beta or x-ray emission from the microspheres after a run were made by placing them on the face of a liquid N_2 cooled NaI crystal detector covered with a thin Be foil, but without positive results. Next, a set of microspheres was placed on medical X-ray film for a 3-day exposure – again negative results. Subsequently, a sample of microspheres run several months earlier were placed in a liquid scintillator and counted for three hours, using a Packard Tri-Carb 1500 dual-channel liquid-scintillation detector. No significant reading above background was obtained.

Recently, several sets of microspheres (run about 4 months earlier) were exposed to high-speed ASA 3000 film for a 4-day period with positive results as shown in Fig. 6 (Klema, 1996 [8]). Unfortunately, these experiments are not yet reproducible. A second positive exposure has been obtained, but three additional attempts failed. The technique is under study, and if verified, will demonstrate emission of low-energy beta rays or soft x-rays (estimated to be of the order of 20 keV for the geometry of Fig. 6).

Fig. 6. Nickel Microsphere Exposure on Kodak ASA 3000 Polaroid Film.

In summary, there is very preliminary evidence for soft x-ray (<20 keV) or beta emission from microspheres after operation. There is not an easily measurable emission of other high-energy radiation from the microspheres after operation or from the cell during operation. These facts must be considered when possible reaction mechanisms are sought to explain the present results. Much more study is needed, however, to fully define possible radiation emission for these cells.

MASS BALANCES AND IMPURITY ISSUES

The use of thin films introduces a problem in reaction product studies due to the small volume occupied by the film vs. the large volume of the electrolyte – about 100 cm^3 electrolyte vs. 3 x 10^{-4} cm^3 film for 1000 microspheres in the bed (cf. Table 1), a volume ratio of $\approx 10^5$:1. The corresponding mass ratio is roughly the same; consequently a low ppm impurity in the electrolyte could, if concentrated in the film, give a very high ppm there.

Note that some of the key elements are present in trace (but measurable) quantities in the applied thin film; e.g., recall Table 3. However, the initial values are typically a small fraction of the final, and they are always subtracted from the analysis of the increase in concentration of an element used to report yields and production

rates. Thus the key issue is whether there is another source of these isotopes in the cell or loop. Potential sources of impurities include the Li_2SO_4 itself, the cell glass, the insulating anode salt beads, the Ti (or Pt_{in} some cases) electrodes, and other loop components. Those components which were easily accessible plus the electrolyte and filter paper were analyzed by NAA since higher precision is required than is possible using manufacturer's specifications for impurities.

Masses for representative key elements (Ag, Al, Cu and V) based on NAA analyses of the microspheres, the electrolyte, and the filter paper are summarized in Table 4a. The key potential source of impurities in the microsphere film is the electrolyte. However, as seen from the table, the ratio of total mass of the four key elements in the electrolyte to that in the thin film was < 10% for Ag, Cu, and V, but was comparable for Al. Thus, at least for the first three elements, impurities in the electrolyte could not possibly account for present observations

Table 4a. Key element mass balances from NAA on microspheres, electrolyte and filter paper before and after a run. (see next page)

Impurities on the filter paper itself are also negligible. The total impurity masses in the electrodes are larger, but most of it is not "accessible." For example, while the Ti electrode was 100 μg Cu, if it is assumed as much as 1% of the Ti in the anode was dissolved and deposited in the Ni film, the Cu would be only 1 μg, or 0.1% of the increased Cu found there. Examination of anode surfaces after the runs indicates no observable erosion. Further, if large erosion occurred, more Ti would be expected on the microsphere surfaces than was found. Thus, the 1% erosion assumed here is, if anything, a gross overestimate. For these reasons, the Ti anode cannot account for the observed elements in the Ni film, and the ppm of other elements in the electrode rule it out as their source also. Analyses of the plastic components and other fittings leads to a similar conclusion for them. In no case is the upper limit for the amount of accessible material in any system component (singularly or taken together) enough to account for the key element concentrations found in the microsphere films, Al being a notable exception.

Balances for the many other elements found in the film have not been carried out (other than for subtraction of initial amounts found in the film by NAA or SIMS prior to a run). Thus, there remains a concern that some may be associated with trace impurities. Still, a number of the products found are not nominally anticipated to be present in materials used in the experiment. Thus, the likelihood that the entire array could have this origin seems unlikely.

Several additional checks on possible component contamination were run. In one, special microspheres with a conducting surface created by sulfonation were run in the cell with a voltage-current applied to simulate a Ni run. Subsequent NAA analysis of the microspheres (see Table 4b) and the filter paper showed that no build up of the important elements occurred on them. In this case, if impurities were present from a loop component, larger changes in the element concentration on the sulfonated beads than seen in Table 4b would be expected. (Changes there lie within the accuracy limits for NAA and microsphere-to-microsphere variation.) In another run, the cell was filled with glass microspheres and run at elevated (~60° C) temperature but without an applied voltage. Again no impurity build up was found.

Additional strong evidence was obtained in more recent work where runs are done in a special "clean" cell where all plastic parts are used in the loop except for the electrodes. The electrolyte is further purified by pre-test runs. Results from operation with this new cell are still being analyzed, but preliminary results confirm that the elements reported here are still formed despite the further reduction of possible impurities.

There is additional extremely strong evidence that the reaction products are not from external source contamination. First, many of the products observed show shifts from isotopic ratios in natural elements (seeFig. 11, discussed later), uncharacteristic of normal impurities. Second, in the other runs (not presented here) many

Table 4a.

Key element mass balances from NAA on microspheres, electrolyte and filter paper before and after a run

Microspheres

Element	ppm (fresh)	ppm (used)	Mass diff (g) / 1000MS
Ag	125.4	2594.9	1.51E-03
Al	11.2	50.2	2.38E-05
Cu	27.0	1840.9	1.11E-03
V	0.1	2.6	1.52E-06
Cr	2.9	1126.4	6.87E-04
Ni	1821.0	4420.5	1.59E-03
Fe	217.2	2956.6	1.67E-03
Zn	15.4	488.8	2.89E-04
Co	0.6	20.5	1.22E-05

used det. limit for ppm of Fe & Zn

Filter Paper

Element	ppm (fresh)	Mass in sample
Ag	0.0	8.79E-09
Al	0.9	7.07E-07
Cu	2.0	1.62E-06
V	0.0	7.79E-09

Filter Paper

S.No:	89.0
M(sample):	0.81

Electrolyte

Element	ppm (fresh)	Mass in system
Ag	0.03	3.00E-06
Al	2.2	2.20E-04
Cu	0.8	8.00E-05
V	0.01	9.00E-07

Electrolyte

S.No:	83.0
M(sample):	0.82
Initial Vol.(ml)	100.0
Times Filed	1.0
M(in system)	100.0

Electrode Material (Ti; two electrodes)

Element	ppm (fresh)	Mass in sample
Ag	1.3	1.15E-06
Al	84	7.46E-05
Cu	120	1.07E-04
V	215	1.91E-04

Ti electrode

S.No:	85.0
M(sample):	0.044
M(of electrode):	0.444
# of electrodes:	2.0
M(in system):	0.89

* all masses are expressed in grams
* M : abbreviation for Mass
* S. No. : abbreviation for Serial Number
* MS : abbreviation for Microsphere

Table 4b.

NAA result for sulfonated polystyrene microspheres

Element	ppm (before run)	ppm(after run)
Ag	0.7	2.9
Al	123.0	133.2
Cu	64.2	35.1
V	0.8	0.2

different elements are found, varying according to the material used for the thin film. If the source were elsewhere in the loop, the same elements would be expected, irrespective of the specific film material. Third, as discussed later, the yields of key elements appear to be consistent with independent results from different, but related experiments by Mizuno et al.[19], and Ohmori and Enyo [22]. Such a coincidence seems unlikely if impurities were involved due to the differences in experimental set-ups.

A noteworthy point related to mass balances is that noticeable quantities of materials were collected on the filter paper during the run, but this material is attributed to particles breaking off of the film surface under operating conditions. A SEM photograph of the debris on the filter paper after the nickel run is shown in Fig. 7. A thin solid layer of cake-like material is visible, with larger flakes on top plus small droplets, both of which appear to come from the bead surface (cf Fig. 2). Additional evidence that this material came from the film is based on runs where conducting plastic or glass microspheres were employed and material paper on the filter did not collect, confirming that this material does not originate from the electrode, cell walls or other loop components. NAA shows a composition similar to the film. Thus if elements contained in these materials were included in the analysis as belonging to the film, even larger yields would be reported.

Fig. 7. SEM photograph of debris on filter paper.

In summary, the finding that the masses of the key isotopes are large compared to possible sources of such isotopes from loop components, the negative results from simulation runs without Ni films, the observation of isotope shifts from natural abundance, and the observation that the isotopes vary with film material, combine to provide very strong evidence that the products reported are due to nuclear reactions. The next issue is to consider what reactions can account for these observations.

REACTION PRODUCT SYSTEMATICS

PRODUCTION RATES

Based on the yield data presented earlier, time-averaged element production rates are computed in Table 5 and plotted in Fig. 8a and Fig. 8b in terms of weight fraction of the metal film/s-cm^3 of film and atoms/s-cm^3 of film, respectively. These figures assume that the production rate was constant

Table 5 Production rate data.

Z	Element	Atomic Wt.	Yield (per microsphere) (frxn./s/cc)	(atom/s/cc)
14	Si	28.09	1.08E-01	2.25E+15
16	S	32.06	3.37E-02	7.04E+14
21	Sc	44.96	1.12E-04	2.34E+12
22	Ti	47.88	9.88E-03	2.06E+14
23	V	50.94	4.46E-04	9.31E+12
24	Cr	52.00	2.27E-01	4.75E+15
26	Fe	55.85	2.70E-01	5.64E+15
25	Mn	54.94	1.50E-01	3.13E+15
27	Co	58.93	2.96E-03	6.18E+13
29	Cu	63.55	2.78E-01	5.81E+15
30	Zn	65.39	6.15E-02	1.28E+15
31	Ga	69.72	2.26E-04	4.73E+12
32	Ge	72.59	1.75E-02	3.65E+14
34	Se	78.96	1.88E-01	3.92E+15
33	As	74.92	7.37E-02	1.54E+15
38	Sr	87.62	2.74E-05	5.72E+11
37	Rb	85.47	1.07E-06	2.24E+10
39	Y	88.91	4.28E-05	8.93E+11
40	Zr	91.22	9.25E-05	1.93E+12
42	Mo	95.94	4.29E-04	8.96E+12
41	Nb	92.91	9.89E-05	2.06E+12
46	Pd	106.42	1.26E-02	2.62E+14
48	Cd	112.41	2.12E-01	4.43E+15
47	Ag	107.87	1.69E-01	3.53E+15
50	Sn	118.71	5.77E-03	1.21E+14
49	In	114.82	4.78E-05	9.97E+11
52	Te	127.60	1.40E-02	2.93E+14
51	Sb	121.75	4.72E-03	9.85E+13
56	Ba	137.33	4.88E-04	1.02E+13
62	Sm	150.36	8.52E-05	1.78E+12
63	Eu	151.96	3.91E-05	8.16E+11
64	Gd	157.25	3.15E-04	6.57E+12
66	Dy	162.50	2.01E-05	4.20E+11
67	Ho	164.93	2.34E-05	4.89E+11
70	Yb	173.04	3.44E-05	7.19E+11
82	Pb	207.20	5.50E-03	1.15E+14

over the 310 hour run. There is some preliminary indication that the rate is higher at the start, and the time dependence, along with the effect of microsphere location, is now under study.
As seen from Fig. 8a, the large yield elements Cr, Fe, Se, Cu, Cd, and Ag have weight fraction (μg of element per μg metal film at start of run) production rates exceeding 0.1/s-cm^3. This corresponds to a rate of roughly 10^{-4} μg/sec for the full 1000-microsphere cell, or a run total of roughly 1 mg/element. In terms of atoms produced, the high yield elements have rates of ~10^{16}/s-cm^3, suggesting a nuclear reaction rate of corresponding magnitude.

Then assuming these five elements dominate and are created at 10^{16}/s-cm^3 each, operation at 0.5 watts for the 1000-microsphere cell corresponds to an average energy release of roughly 6 x 10^{-2} MeV/atom reacting Such an energy release is easily obtained by various exothermic nuclear reactions (Miley [13]) but as discussed later, due to the formation of heavy elements like Cu, Ag, and Cd, some endothermic reactions "absorb" energy. Thus the 0.5 W excess must be viewed as a "net" energy release from these various reactions.

The corresponding total increase in element masses, or in element atoms, are presented in Fig. 9a and Fig 9b, respectively. Consistent with the production rate graphs, these figures show total yields per microsphere approaching 0.1-0.2 μg per high yield element, or 3-6 atomic % in the metallic film.

It is interesting to compare these results to those reported by Mizuno et al. [18], who ran a high-current-density Pd electrode in a cell at high pressure and temperature with a heavy water Li_2CO_3 electrolyte. They report a rich variety of reaction products at 1-mm depth, concentrated in groups with atomic numbers 6 , 20-30, 46-54, and 72-82. Earlier, Bockris and Minevski [0] had reported a similar array of elements beneath the surface of a Pd electrode, separated from surface impurities. While isotope shift studies were not undertaken, they argued that these elements were not impurities based on diffusion considerations. While a one-per-one comparison is not possible since the present study used Ni rather than Pd, this distinct grouping of products is consistent with the present results where major products group between Z = 12-14, 20-30, and 46-56. The resemblance is seen from Fig. 10, where Mizuno et al.'s (and also Bockris and Minevski's) results are superimposed on the present data. Since neither Mizuno et al. nor Bockris and Minevski reported absolute yield values or rates, for comparison, their results have arbitrarily been normalized to the present Cu production rate. With this normalization, a number of the production rates for other high yield products agree reasonably well with Mizuno et al's results, e.g., note from Fig. 10 that Si, Cr, Fe, and Cd lie close together. Agreement with the Zn and Ag yields from Bockris and Minevski's experiment is good, but their other high yield products (Mg, Si, Ca, Fe, Pt) have somewhat higher production rates than found in the present Ni microspheres. A larger variation in lower yield elements is observed among these three experiments where various elements are found in one experiment and not the others. Two noticeable differences are the high yield of gases (Xe and O) and the yields at high Z72-82 group, including Os, Au, Hg found by Mizuno et al., and Pt found by Bockris and Minevski. Differences in gas yields might be anticipated. Gases are expected to diffuse out of the thin films used in present work, hence would not be found in SIMS results. The reduction of other products in the 72-82 group in present experiments is probably associated with the use of the lower Z Ni host material (vs. Pd). In conclusion, the resemblance of certain key features of the present results and those of Mizuno et al., and also Bockris and Minevski, is striking. In niew of the major differences in cell construction, this resemblance adds credence to the already strong arguments by all three experimental groups that the observed elements are not impurities.

Fig. 10. Comparison of present production rate data with Mizuno et al. and Bockris and Minevski.

The large production rate of Fe found here also has a resemblance to the observation by Ohmori and Enyo [22] that notable amounts of Fe was formed in electrolytic cells with Au and Pd electrodes and various light water electrolytes. They report Fe yields of ~10^{16} atom/cm^2 (17μg and 38μg maximum from Au and Pd electrodes, respectively). The present Fe production rate of 5.4 x 10^{15} atoms/s-cm^3 (cf Fig. 8b or Fig. 10) corresponds to 5.9 x 10^{21} Fe atoms/cm^3-film. For the 650-Å film thickness, this is equivalent to about 3.8 x 10^{16} Fe atoms/cm^2, in reasonable agreement with Ohmori and Enyo's measurements. The yield of Fe in present work from Fig. 9a

is ~0.22μg/microsphere, or ~0.2 mg total for the 1000 microsphere cell -- about 10 times the Ohmori-Enyo yield. A major factor in the higher yield is probably the larger surface area (~32 cm^2) of the microspheres vs. the 5-cm^2 plates used by Ohmori-Enyo. Other factors, such as input power, electrolyte, etc. must also affect the results, but attempts to optimize cell conditions in these varied experiments seem to have resulted in amazingly similar Fe production rates.

ISOTOPE SHIFTS FROM NATURAL ABUNDANCE

Differences between the isotopic percentage concentrations observed with the SIMS vs. those for natural abundance for the reaction product elements, listed earlier in Table 3, are summarized in Fig. 11. The accuracy of these measurements is estimated to be of order of ±3% in the difference when high resolution is employed. High resolution was used to eliminate possible line overlap in all important cases, but with the large number of elements found, this was not possible for all of the lower yield isotopes. Thus, those results must be viewed as less certain. Of the higher concentration elements, Fe and Zn, show significant deviations. Cr and Ag are in the ±3-5% range, while Cu is in the ±1% range. Many low-concentration elements show quite large differences e.g., Ti-50, +77.7%; Ge-72, +21%; Se-82, +32%; Zr-96, +97%; etc. There are no obvious patterns, however.

Fig. 11. Isotope shifts (percent SIMS - percent natural abundance) vs. Mass Number, A.

To further study the deviation from natural abundance for the vital isotopes of Cu (Cu-63 and Cu-65) and Ag (Ag-107 and Ag-109) special NAA isotope measurements (described earlier) are underway. First results for the present Ni run, based on a sample of 10 microspheres, indicates a deviation from natural % abundance of +3.6 ± 1.6% for Cu-63 and -8.1 ± 3.6% for Cu-65. (Since the two results are from different lines, unlike SIMS, slightly different values can occur in the + and - values for pairs.) These results are to be compared to a deviation of +0.8% for Cu-63 and -0.8% for Cu-65 from the SIMS data. The reason for larger percent differences with NAA than SIMS is not clear. A possible explanation is that as stressed earlier, the SIMS results are localized on a spot on a single bead film whereas the NAA value represents the ratio of total amounts of each isotope contained in films on the 10 microsphere sample. These issues are now under study employing multiple measurements with a sample matrix of microspheres.

The trend in the Cu shifts found here is similar, but smaller, than reported by Mizuno et al. [19] who cite Cu-63, +25% and Cu-65, -25%. Shifts for Fe have been reported by Mizuno et al. and also by Ohmori and Enyo [22], and are compared to present results in Table 6. While differences are observed, two isotopes, 56 and 57, do show the same trend for all cases.

Table 6 Isotope shifts reported for Fe in various systems.

		Difference from a/o, in percentage			
		Present	Ohmori/Enyo		Mizuno et al
		Ni*	Au	Pd	Pd
	Nat a/o				
Fe-54	5.8	-0.1	+0.7	+2.0	(a)
56	91.7	-4.8	-14.2	-6.3	-21
57	2.2	+5.2	+12.3	+4.0	+20
58	0.3	-0.3	+1.2	+0.3	(a)

*Electrode Material
(a) Not Reported

While a more detailed comparison of the various shifts is not possible due to material differences, the observation of a large number of isotope shifts in Fig. 11 is consistent with the large number of deviations reported by Mizuno et al. [19] They used this observation to argue that the elements observed were due to nuclear reactions, rather

than impurities. The possibility exists for some isotope separation due to diffusion in the host metal, but that effect seems unlikely to account for the varied changes observed. In conclusion, Mizuno et al's isotope shift argument against impurity sources applies to the present results also, and, combined with the large product yields compared to possible impurity sources, strongly supports the nuclear reaction hypothesis.

REACTION MECHANISM CONSIDERATIONS

A nuclear explanation for the products observed here requires an entirely new theory for chemically assisted reactions in solids. Here it is possible only to point out some features that should be considered in such a theory.

As several workers have stressed (Miley et al. [11], Preparata [26], Hagelstein [4]), any theory for reactions in solids must explain: 1) how the reacting ions overcome the Coulombic barrier, and 2) what reactions take place after the ions interact. In the present case, the SEL theory cited earlier offers a possible explanation for overcoming the Coulombic barrier between ions in a thin-film electrode. While only a single film was used in the Ni run, a Fermi level difference can develop at the plastic/film interface or at any oxidized region on the outer surface. More work, is needed to obtain definitive evidence for the validity of this theory, however. And even if SEL theory is accepted, the key issue of what reactions occur after barrier penetration remains open.

In view of the large yields obtained, the reactants must involve some of the key species present, namely: Li, S, or O from the electrolyte; C and H from the plastic microsphere core; Ni from the thin films (cathode); and protons (p) from the light water. The isotope yield profiles do not indicate that elements from the electrolyte participated in the transmutations. Further, unpublished results (J. Patterson, 1996b [25]), indicate that operation with a Na-based electrolyte (vs. Li) results in similar heating rates. Carbon from the plastic can not be ruled out, but is viewed as an unlikely participant. For these reasons, the following assumes that the main reactions involve p-Ni interactions, with protons possibly coming from the plastic core as well as the electrolyte.

The concept that excess heat from electrolytic cells originates from reactions involving the electrode material, e.g. Pd electrode, is not new. Indeed, Ragheb and Miley [11], originally proposed that in a heavy water cell, Oppenheimer-Phillips-type neutron-stripping reactions between the D and Pd might explain early observations. Later, Miley (Appendix B in Hoffman [13]) summarized the status of such theories, and ironically introduced a table of possible p-Pd reactions (including examples of fission-type reactions). The present Ni results add a new dimension to these thoughts, however.

The present data provides information on a number of characteristics that any successful model must explain. Most importantly, the model must predict the large yields of the high-concentration elements, without introducing added products not observed. This fact alone rules out many possibilities, e.g., a simple p-Ni reaction followed by a succession of p reactions with products, plus fission of some elements (cf the multi-D Pd chain proposed by Mizuno et al. [19] to explain their Pd-heavy water results) fails this test.

In this respect, one aspect of present data noted earlier, is that gaseous products can diffuse out of the thin films. Thus, theoretical models with gaseous products, e.g., He, Xe, and Kr, should not be ruled out based on present data.

Other key features observed in Fig. 8 and Fig. 9 that must be accounted for by any theory include the "gaps" between high yield products and the high Ag and Cd yields. Ag (and Cd) production is particularly challenging, since Ag occurs in large quantities but is not favored energetically. Ag's position, well to the lower binding energy side of Ni, infers an endothermic reaction (negative Q-value), which in turn suggests energy transfer to the reactants must occur to drive the reaction. (This is analogous to driving negative Q-value reactions by colliding high-energy reactants using accelerated beams. As defined here, Q values are the energy released due to the mass difference between reactants and products, assuming that the reactants enter with zero kinetic or

excitation energy.) Consequently, the model must contain a mechanism for energy storage/transfer to reactions involved in high Z element production.

A postulated reaction model, RIFEX (Reaction in a Film-Excited CompleX), is under development to satisfy these key characteristics. A major feature of RIFEX is that protons (p) interacting with the host Ni and neighboring isotopes produces a relatively long lived atom-p complex with excitation energies of orders of several MeV. This allows production of elements such as Ag with −Q-value reactions. Other products are produced by negative Q-value reactions via fission of compound nuclei. This model will be presented in detail in a future publication.

CONCLUSIONS

The results presented here defy conventional views in many ways. First, chemically-assisted nuclear reactions are not widely accepted by the scientific community. The present results not only confront that disbelief, but add a new dimension to the issue by reporting copious light and heavy element reaction products that seem to imply multi-body reactions due to the formation of heavier elements such as Cu and Ag from Ni. Further, a reaction which does not emit intense high-energy gammas is required by the experimental results. All of these features are difficult to comprehend and at first glance seem to point to impurities. However, as stressed, an extensive effort to find an impurity source has not uncovered one. Also, there is other strong evidence (such as isotope shifts, the different products occurring when the coating material is changed, and the similarity in yield trends with results from other workers), which supports the conclusion that the elements observed are reaction products.

Fortunately, cell experiments of this type are relatively straightforward and inexpensive. Thus far, reaction products, such as reported here, have been detected by the authors in all dozen experiments of this type performed, using a variety of metallic films. In this sense, the phenomenon seems highly reproducible. The use of thin films as developed here offers a way to simplify the analysis since a large fraction of the film contains the new elements and their localization in the film allows a qualitative determination. Hopefully, open-minded scientists will attempt to replicate the experiments to convince themselves. If verified, the thin-film approach to chemically assisted nuclear reactions opens the way to a whole new field of science.

[For another explanation of overcoming the Coulomb barrier, see Shoulders & Shoulders, and Fox, Jin, & Bass papers in this issue. -Ed.]

REFERENCES

1a. J.O'M. Bockris and Z. Minevski, "Two Zones of Impurities Observed after Prolonged Electrolysis on Palladium," *Infinite Energy*, vol 1, no 5 & 6 (1996), pp 67-69.

1b. Bockris, J.O'M and G.H. Lin (organizers) (1996), Proceedings of the 1996 Low Energy Nuclear Reactions Conference, *J. New Energy*, vol 1, no 3.

2. Dennis Cravens (1995), "Flowing Electrolyte Calorimetry," Proc. 5th Intern. Conf. on Cold Fusion, Valbonne, France, IMRA Europe, pp 79-86.

3. S. Crouch-Baker, M.C.H. McKubre, F.L. Tanzella (1995), "Some Thermodynamic Properties of the H(D)-Pd System," Proc. 5th Intern. Conf. on Cold Fusion, Valbonne, France, IMRA Europe, pp 431-440.

4. Peter Hagelstein (1995), "Update on Neutron Transfer Reactions," Proc. 5th Intern. Conf. on Cold Fusion, Valbonne, France, IMRA Europe, pp 327-337.

5. H. Hora, J.C. Kelly, J.U. Patel, M.A. Prelas, G.H. Miley, and J.W. Tompkins (1993), "Screening in Cold Fusion Derived from D-D Reactions," *Physics Letters A*, vol 175, pp 138-143.

6. A.B. Karabut, Ya.R. Kucherov, and I.B. Savvatimova (1991), "The Investigation of Deuterium Nuclei Fusion at Glow Discharge Cathode," *Fusion Technol.*, vol 20, pg 924.

7. A.B Karabut, Ya.R. Kucherov, and I.B. Savvatimova (1992), "Nuclear Product Ratio for Glow Discharge in Deuterium," *Physics Letters A*, vol 170, pp 265.

8. E. Klema (1996), Tufts University, Medford, MA. Private communication.

9. Sheldon Landsberger (1996), Dept. of Nuc. Eng., U. of Illinois, private communication.
10. M.H. Miles, and B.F. Bush (1994), "Heat and Helium Measurements in Deuterated Palladium," *Trans. Fusion Technol.*, vol 26, no 4T, Part 2, pp 157-159.
11. George H. Miley, Magdi Ragheb, and Heinrich Hora (1989), "Comments about Nuclear Reaction Products from Cold Fusion," NSF/EPRI Workshop, Washington D.C., 16-18 October 1989.
12. G.H. Miley, J.U. Patel, J. Javedani, H. Hora, J.C. Kelly, and J. Tompkins (1993), "Multilayer Thin Film Electrodes for Cold Fusion," Proc. 3rd Int. Conf. Cold Fusion (Frontiers in Science Series no. 4), ed. H. Ikegami, Universal Academy Press, pp 659-663.
13. G.H. Miley, (1995); in Hoffman, Nate (1995), A Dialogue on Chemically Induced Nuclear Effects: A Guide for the Perplexed about Cold Fusion, La Grange Park, IL, The American Nuclear Society, Appendix C, pp 146-154.
14. G.H. Miley, H. Hora, E.G., Batyrbekov, R.L. Zich (1994), "Electrolytic Cell with Multilayer Thin-Film Electrodes," *Trans. Fusion Technol.*, vol 26, no 4T, Part 2, pp 313-320.
15. G.H. Miley, J.A. Patterson (1996), "Experimental Observation of Massive Transmutations Occurring in Multi-Layer Thin-Film Microspheres After Electrolysis," Abstracts, *Sixth International Conference on Cold Fusion*, Hokkaido, Japan.
16. G.H. Miley, and J.A. Patterson (1996), "Massive Nuclear Transmutations in Thin-Film Coatings on Microspheres Undergoing Electrolysis, Part 1--Nickel Films," Workshop, Clean Energy Technologies, Inc., Dallas TX, July 1996.
17. G.H. Miley, and J.A. Patterson (1996), "Design Considerations for Multilayer Thin-Film Patterson-Type Microspheres," Abstracts, *Sixth International Conference on Cold Fusion*, Hokkaido, Japan.
18. G.H. Miley, G. Name, M.J. Williams, J.A. Patterson, J. Nix, D. Cravens, H. Hora (1996), "Multilayer Thin-Film Microspheres after Electrolysis," Sixth International Conference on Cold Fusion, Hokkaido, Japan.
19. T. Mizuno, T. Ohmori, and M. Enyo (1996), "Changes of Isotope Distribution Deposited on Palladium Induced by Electrochemical Reaction," Preprint. [See also Mizuno et al. this issue. -Ed.]
20. Ira Myers, Gustave C. Frolick, and Richard S. Baldwin (1996), "Replication of the Apparent Excess Heat Effect in a Light Water–Potassium Carbonate--Nickel Electrolytic Cell," NASA Tech Memo 107167, NASA Lewis Research Center, Cleveland, Ohio.
21. John Nix (1996), "Revised Protocol for Patterson+ Cell Assembly and Operation," Confidential Memorandum, Clean Energy Technologies, Inc., 3 May 1996.
22. T. Ohmori, and M. Enyo (1996), "Iron Formation in Gold and Palladium Cathodes," *J. New Energy*, vol 1, no 1, pp 15-22.
23. Susan J. Parry (1991), "Activation Spectrometry in Chemical Analysis," in Chemical Analysis, ed. J.D. Winefordner, vol19, John Wiley and Sons, New York.
24. James A. Patterson (1996), "System for Electrolysis," U.S. Patent #5,494,559, 27 February 1996.
25. James A. Patterson (1996), Clean Energy Technologies, Inc., private communication.
26. G. Preparata (1991), "Cold Fusion: What Do the Laws of Nature Allow and Forbid?," The Science of Cold Fusion, Conf. Proc. 33, eds. T. Bressani, E. Del Giudice, and G. Preparata, Bologna, Societa Italiana di Fisica, pp 419-443.
27. R.G. Wilson, F.A. Stevie, C.W. Magee (1989), Secondary Ion Mass Spectrometry: A Practical Handbook for Depth Profiling and Bulk Impurity Analysis, New York, John Wiley & Sons. Wilson, R.G., 1996, Hughes Research Laboratories, private communication.
28. R.G. Wilson, F.A. Stevie (1996), "Secondary Ion Mass Spectrometry Depth Profiling and Relative Sensitivity Factors for Elements from Hydrogen to Uranium Implanted in Metal Matrices (Be, Al, Ti, Ni, Cu, W and Au)," private communication.
29. R.G. Wilson, F.A. Stevie (1991), "Secondary Ion Mass Spectrometry Depth Profiling and Relative Sensitivity Factors/Relative Ion Yields and Systematics for Elements from Hydrogen to Uranium Implanted in Metal Matrices (Be, Al, r, Ni, Cu, W and Au)," Proceedings of the Eighth International Conference on Secondary Ion Mass Spectrometry, John Wiley & Sons.

ACKNOWLEDGMENTS

This work was supported by a grant from CETI. The authors wish to acknowledge essential contributions to this effort by a number of individuals. G. Narne carried out experiments at the UI and assisted in both SIMS and NAA measurements. M. Williams (UI) was responsible for microsphere coating and for cell mechanics, and he coordinated microsphere analysis. J. Baker and staff at the Center for Microanalysis of Materials, UI, supervised the SIMS analysis and consulted on its interpretation. S. Landsberger (UI) carried out the NAA analysis and provided important insight into its interpretation. D. Cravens (CETI) was instrumental in the cell design, in

helping with numerous problems that arose during operation. J. Reding (CETI) helped coordinate the UI and CETI efforts and has provided most valuable encouragement and enthusiasm. R. Twardock (UI), carried out independent radiation measurements on the microspheres. E. Klema (Tufts U) carried out film exposures on the microspheres and provided valuable insights. H. Hora (UNSW) consulted on SEL and other theoretical aspects. Valuable comments on an earlier draft, by M. McKubre (SRI) and P. Hagelstein (MIT) are also gratefully acknowledged.

FIGURES

FIGURES

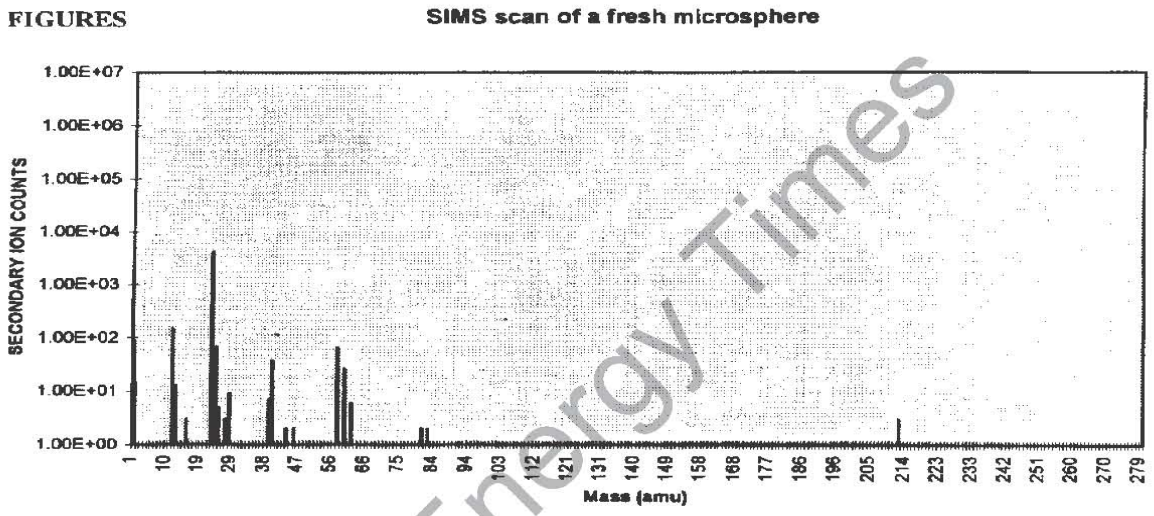

Fig. 3a. Typical low resolution SIMS scan (before the run).

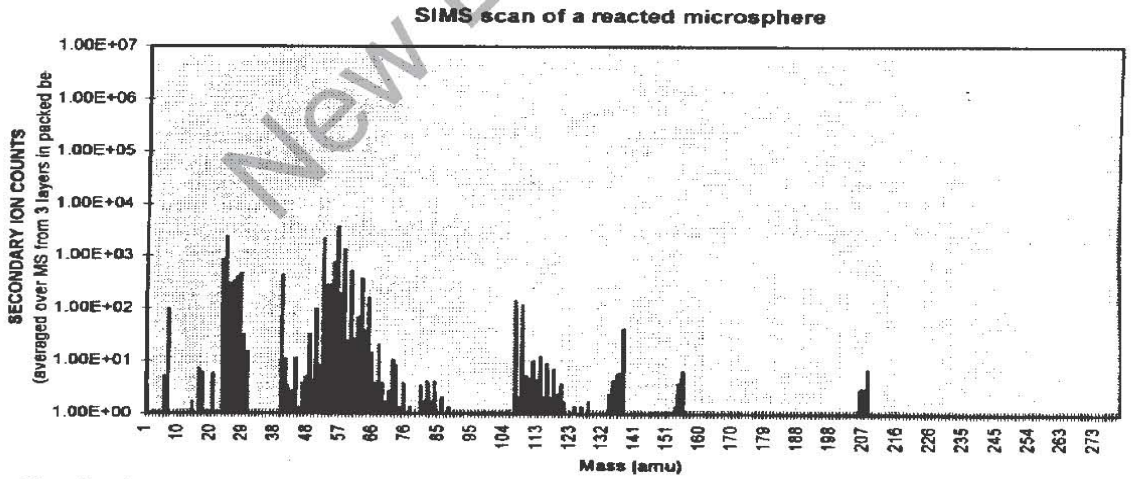

Fig. 3a. Typical low resolution SIMS scan after the run (average of microspheres in 3 layers in the cell).

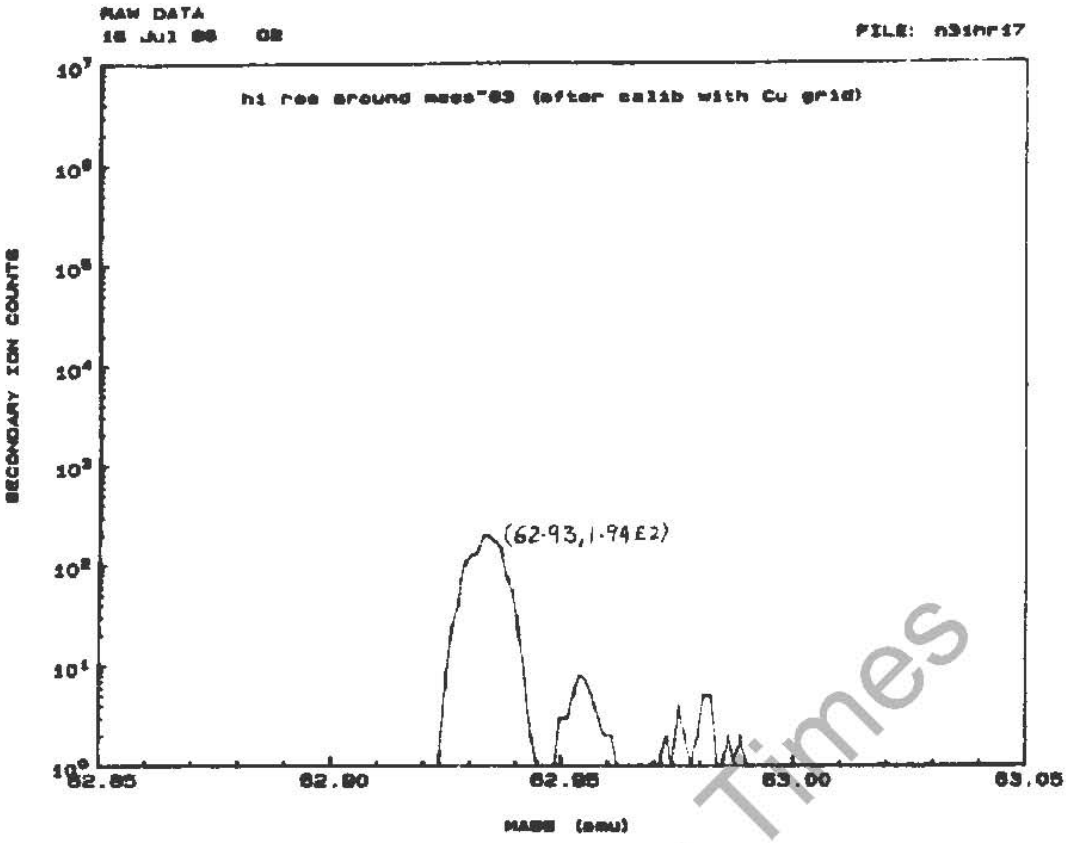

Fig. 3b. High resolution SIMS scan for Cu(63) after the run.

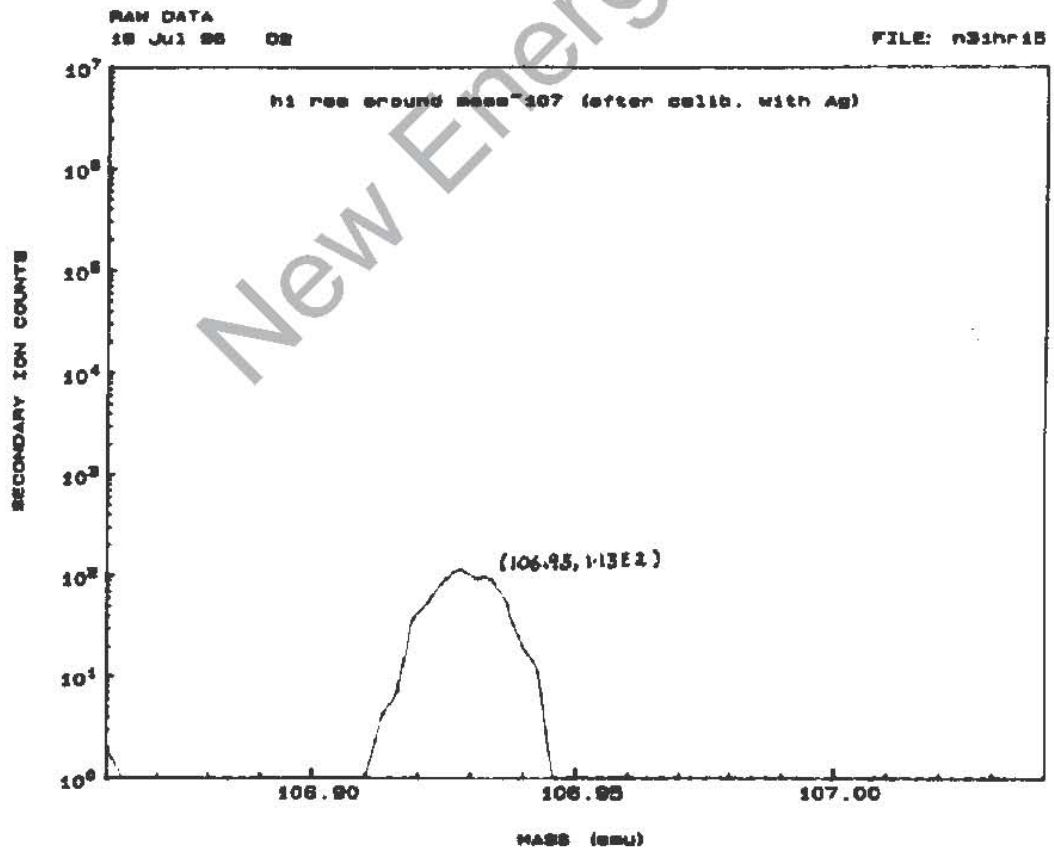

Fig. 3b. High resolution SIMS scan for Ag(107) after the run.

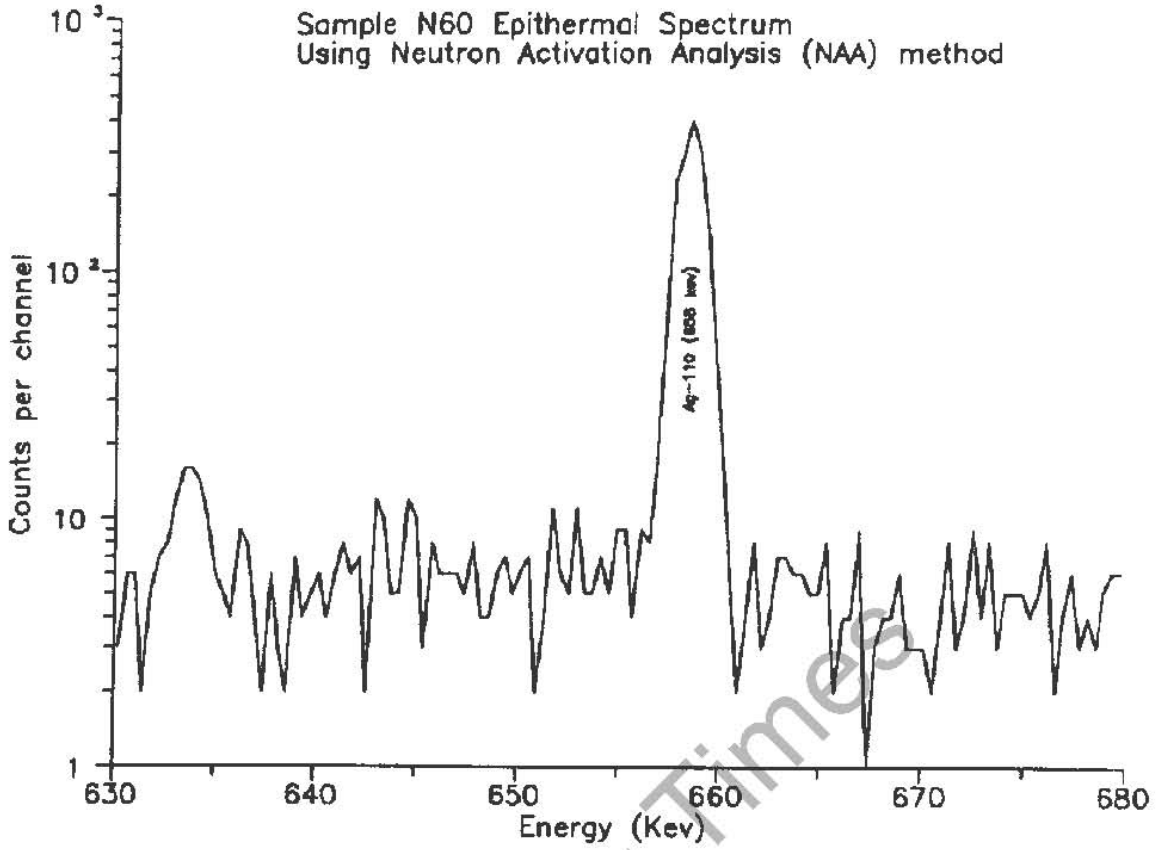

Fig. 4a. Typical NAA gamma spectrum for Ag.

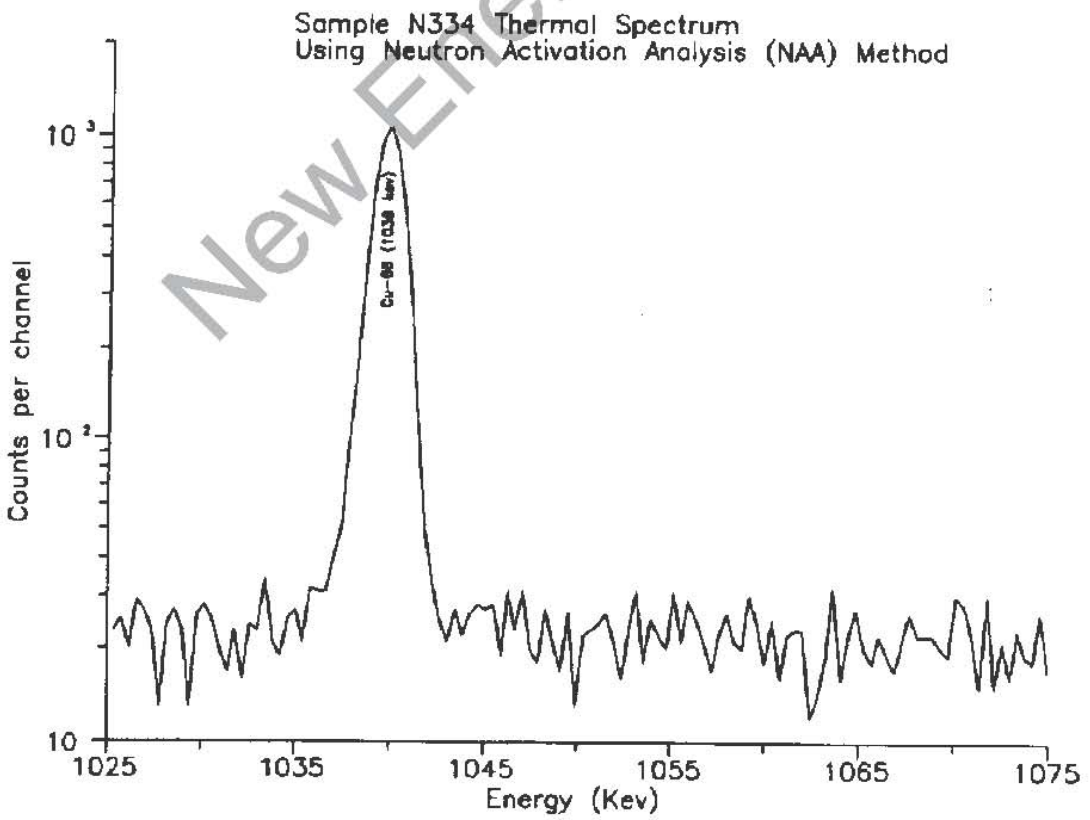

Fig. 4b. NAA gamma spectrum for Cu.

Table 3

Data sheet for change in isotope atom % in metal film after run; comparison to natural abundance (Data from SIMS; isotopes in "bold" use NAA element weight)

Mass No.	Element	Natural a/o	Change (Reacted-Fresh) (in micro-grams)	Fresh MS Atoms	Reacted MS Atoms	Difference % Metal (atomic)	SIMS a/o	Difference in a/o (SIMS-Natural)
28	Si	0.92	1.02E-01	8.14E+16	3.02E+17	1.29E+00	4.67E-01	-45.46
29	Si	0.05	9.80E-03	0.00E+00	2.04E+16	9.79E-01	3.55E-01	30.81
30	Si	0.03	5.07E-03	0.00E+00	1.02E+16	4.89E-01	1.78E-01	14.66
32	S	0.95	9.54E-03	0.00E+00	1.80E+16	8.63E-01	1.00E+00	5.00
45	Sc	1.00	4.45E-05	0.00E+00	5.96E+13	2.87E-03	1.00E+00	0.00
46	Ti	0.08	2.00E-04	0.00E+00	2.62E+14	1.26E-02	4.98E-02	-2.95
47	Ti	0.07	2.79E-04	0.00E+00	3.58E+14	1.72E-02	6.79E-02	-0.49
49	Ti	0.06	2.52E-04	0.00E+00	3.10E+14	1.49E-02	5.88E-02	0.37
50	Ti	0.05	3.60E-03	0.00E+00	4.34E+15	2.08E-01	8.24E-01	77.01
50	**V**	**0.00**	**5.52E-07**	**3.54E+10**	**7.01E+11**	**2.79E-05**	**2.45E-03**	**0.00**
51	**V**	**1.00**	**2.30E-04**	**1.44E+13**	**2.86E+14**	**1.14E-02**	**9.98E-01**	**-0.04**
52	**Cr**	**0.84**	**9.22E-02**	**5.63E+14**	**1.07E+17**	**5.07E+00**	**8.70E-01**	**3.21**
53	**Cr**	**0.10**	**1.19E-02**	**6.27E+13**	**1.36E+16**	**6.42E-01**	**1.10E-01**	**1.51**
54	**Cr**	**0.02**	**2.27E-03**	**1.53E+13**	**2.55E+15**	**1.20E-01**	**2.06E-02**	**-0.30**
54	**Fe**	**0.06**	**1.34E-02**	**2.82E+15**	**1.78E+16**	**3.96E-01**	**5.72E-02**	**-0.10**
55	Mn	1.00	7.30E-02	0.00E+00	8.00E+16	3.85E+00	1.00E+00	0.00
56	**Fe**	**0.92**	**2.11E-01**	**4.29E+16**	**2.70E+17**	**6.01E+00**	**8.69E-01**	**-4.82**
57	**Fe**	**0.02**	**1.24E-02**	**1.01E+15**	**1.41E+16**	**5.14E-01**	**7.42E-02**	**5.23**
59	**Co**	**1.00**	**1.63E-03**	**1.23E+14**	**1.99E+15**	**7.58E-02**	**1.00E+00**	**0.00**
63	**Cu**	**0.69**	**1.17E-01**	**3.57E+15**	**1.16E+17**	**4.99E+00**	**7.00E-01**	**0.80**
64	**Zn**	**0.49**	**1.63E-02**	**1.42E+15**	**1.67E+16**	**5.74E-01**	**3.64E-01**	**-12.47**
65	**Cu**	**0.31**	**5.19E-02**	**1.54E+15**	**4.97E+16**	**2.14E+00**	**3.00E-01**	**-0.80**
66	**Zn**	**0.28**	**9.24E-03**	**7.82E+14**	**9.22E+15**	**3.16E-01**	**2.01E-01**	**-7.72**
67	**Zn**	**0.04**	**2.28E-03**	**1.14E+14**	**2.18E+15**	**8.55E-02**	**5.43E-02**	**1.32**
68	**Zn**	**0.19**	**1.41E-02**	**5.08E+14**	**1.30E+16**	**5.42E-01**	**3.44E-01**	**15.84**
69	Ga	0.60	7.59E-05	0.00E+00	8.64E+13	3.19E-03	5.50E-01	-5.40
70	**Zn**	**0.01**	**1.42E-03**	**1.64E+13**	**1.24E+15**	**5.70E-02**	**3.62E-02**	**3.00**
71	Ga	0.40	6.39E-05	0.00E+00	5.43E+13	2.61E-03	4.50E-01	5.40
72	Ge	0.27	5.39E-03	0.00E+00	4.51E+15	2.17E-01	4.84E-01	21.04
73	Ge	0.08	4.23E-03	0.00E+00	3.49E+15	1.68E-01	3.75E-01	29.74
74	Ge	0.37	8.94E-04	0.00E+00	7.28E+14	3.50E-02	7.81E-02	-28.69
75	As	1.00	4.89E-02	0.00E+00	3.93E+16	1.89E+00	1.00E+00	0.00
76	Ge	0.08	7.34E-04	0.00E+00	5.82E+14	2.80E-02	6.25E-02	-1.51
76	Se	0.09	1.63E-02	0.00E+00	1.29E+16	6.21E-01	1.29E-01	3.88
77	Se	0.08	1.65E-02	0.00E+00	1.29E+16	6.21E-01	1.29E-01	5.32
80	Se	0.50	4.29E-02	0.00E+00	3.23E+16	1.55E+00	3.23E-01	-17.54
82	Se	0.09	5.71E-02	0.00E+00	4.20E+16	2.02E+00	4.19E-01	32.75
85	Rb	0.72	4.03E-07	0.00E+00	2.86E+11	1.37E-05	5.00E-01	-22.20
87	Rb	0.28	4.12E-07	0.00E+00	2.86E+11	1.37E-05	5.00E-01	22.20
87	Sr	0.07	0.00E+00	0.00E+00	0.00E+00	0.00E+00	0.00E+00	-7.02
88	Sr	0.83	2.13E-05	0.00E+00	1.46E+13	7.01E-04	1.00E+00	17.40

Table 3 (continued)

Mass No.	Element	Natural a/o	Change (Reacted-Fresh) (in micro-grams)	Fresh MS Atoms	Reacted MS Atoms	Difference % Metal (atomic)	SIMS a/o	Difference in a/o (SIMS-Natural)
89	Y	1.00	3.37E-05	0.00E+00	2.28E+13	1.10E-03	1.00E+00	0.00
93	Nb	1.00	8.13E-05	0.00E+00	5.27E+13	2.53E-03	1.00E+00	0.00
95	Mo	0.16	1.20E-04	0.00E+00	7.62E+13	3.66E-03	3.33E-01	17.63
96	Zr	0.03	7.85E-05	0.00E+00	4.93E+13	2.37E-03	1.00E+00	97.20
98	Mo	0.24	1.24E-04	0.00E+00	7.62E+13	3.66E-03	3.33E-01	9.53
100	Mo	0.10	1.26E-04	0.00E+00	7.62E+13	3.66E-03	3.33E-01	23.70
107	Ag	0.52	1.22E-01	7.32E+15	7.61E+16	2.47E+00	5.70E-01	5.17
108	Pd	0.27	3.27E-03	0.00E+00	1.83E+15	8.78E-02	2.73E-01	0.57
109	Ag	0.48	9.90E-02	6.68E+15	6.14E+16	1.87E+00	4.30E-01	-5.17
110	Pd	0.12	8.89E-03	0.00E+00	4.87E+15	2.34E-01	7.27E-01	60.93
111	Cd	0.13	2.33E-02	0.00E+00	1.27E+16	6.08E-01	1.12E-01	-1.60
112	Cd	0.24	5.38E-02	0.00E+00	2.89E+16	1.39E+00	2.56E-01	1.50
113	Cd	0.12	2.37E-02	0.00E+00	1.27E+16	6.08E-01	1.12E-01	-1.10
113	In	0.04	0.00E+00	0.00E+00	0.00E+00	0.00E+00	0.00E+00	-4.28
114	Cd	0.29	6.33E-02	0.00E+00	3.35E+16	1.61E+00	2.96E-01	0.70
115	In	0.96	4.86E-05	0.00E+00	2.55E+13	1.22E-03	1.00E+00	4.30
116	Cd	0.08	4.87E-02	0.00E+00	2.53E+16	1.22E+00	2.24E-01	14.82
117	Sn	0.08	8.85E-04	0.00E+00	4.56E+14	2.19E-02	1.48E-01	7.20
118	Sn	0.24	2.45E-03	0.00E+00	1.25E+15	6.02E-02	4.07E-01	16.74
119	Sn	0.09	7.87E-04	0.00E+00	3.99E+14	1.92E-02	1.30E-01	4.38
120	Sn	0.33	1.47E-03	0.00E+00	7.41E+14	3.56E-02	2.41E-01	-8.73
121	Sb	0.57	5.05E-03	0.00E+00	2.52E+15	1.21E-01	1.00E+00	42.80
124	Sn	0.06	4.69E-04	0.00E+00	2.28E+14	1.10E-02	7.41E-02	1.47
125	Te	0.07	5.82E-03	0.00E+00	2.81E+15	1.35E-01	3.75E-01	30.51
126	Te	0.19	3.91E-03	0.00E+00	1.87E+15	8.99E-02	2.50E-01	6.30
128	Te	0.32	5.96E-03	0.00E+00	2.81E+15	1.35E-01	3.75E-01	5.70
135	Ba	0.07	5.39E-05	0.00E+00	2.41E+13	1.16E-03	9.26E-02	2.67
137	Ba	0.11	6.93E-05	0.00E+00	3.05E+13	1.47E-03	1.17E-01	0.43
138	Ba	0.72	4.71E-04	0.00E+00	2.06E+14	9.88E-03	7.90E-01	7.31
151	Eu	0.48	1.74E-05	0.00E+00	6.94E+12	3.34E-04	3.33E-01	-14.47
152	Sm	0.27	2.46E-05	0.00E+00	9.74E+12	4.68E-04	2.14E-01	-5.27
153	Eu	0.52	3.52E-05	0.00E+00	1.39E+13	6.67E-04	6.67E-01	14.47
154	Sm	0.23	9.12E-05	0.00E+00	3.57E+13	1.72E-03	7.86E-01	55.87
155	Gd	0.15	3.92E-04	0.00E+00	1.53E+14	7.33E-03	9.09E-01	76.21
156	Gd	0.21	3.95E-05	0.00E+00	1.53E+13	7.33E-04	9.09E-02	-11.41
163	Dy	0.25	2.90E-05	0.00E+00	1.07E+13	5.16E-04	1.00E+00	75.00
165	Ho	1.00	3.42E-05	0.00E+00	1.25E+13	6.00E-04	1.00E+00	0.00
172	Yb	0.22	5.24E-05	0.00E+00	1.83E+13	8.82E-04	1.00E+00	78.20
206	Pb	0.24	2.67E-03	0.00E+00	7.82E+14	3.76E-02	2.67E-01	3.07
207	Pb	0.23	2.69E-03	0.00E+00	7.82E+14	3.76E-02	2.67E-01	4.07
208	Pb	0.52	4.75E-03	0.00E+00	1.37E+15	6.57E-02	4.67E-01	-5.63

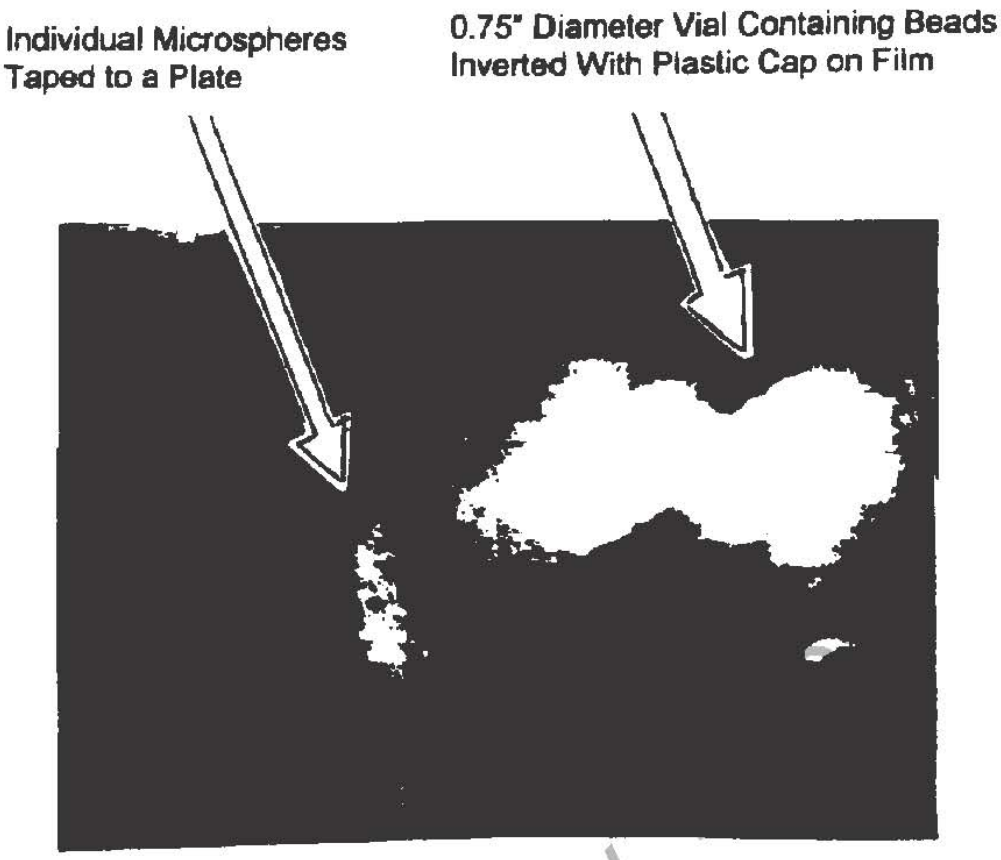

Fig. 6. Nickel microsphere exposure on Kodak ASA 3000 Polaroid film.

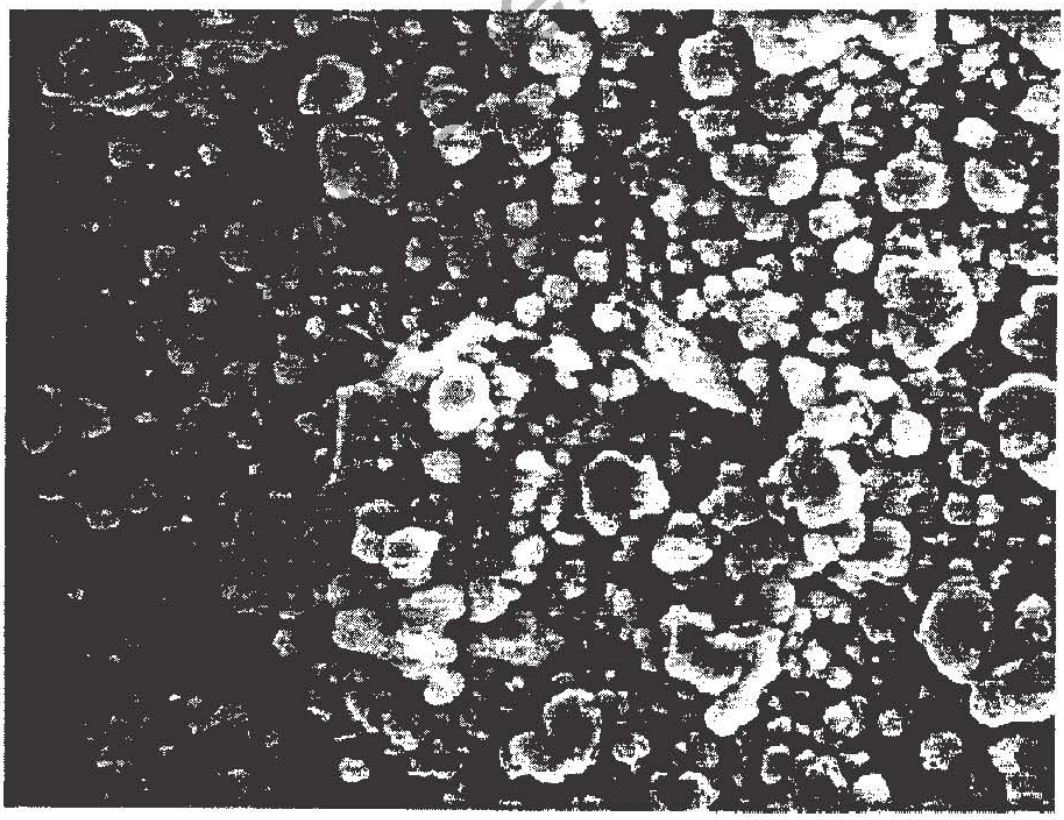

Fig. 7. SEM photograph of debris on filter paper.

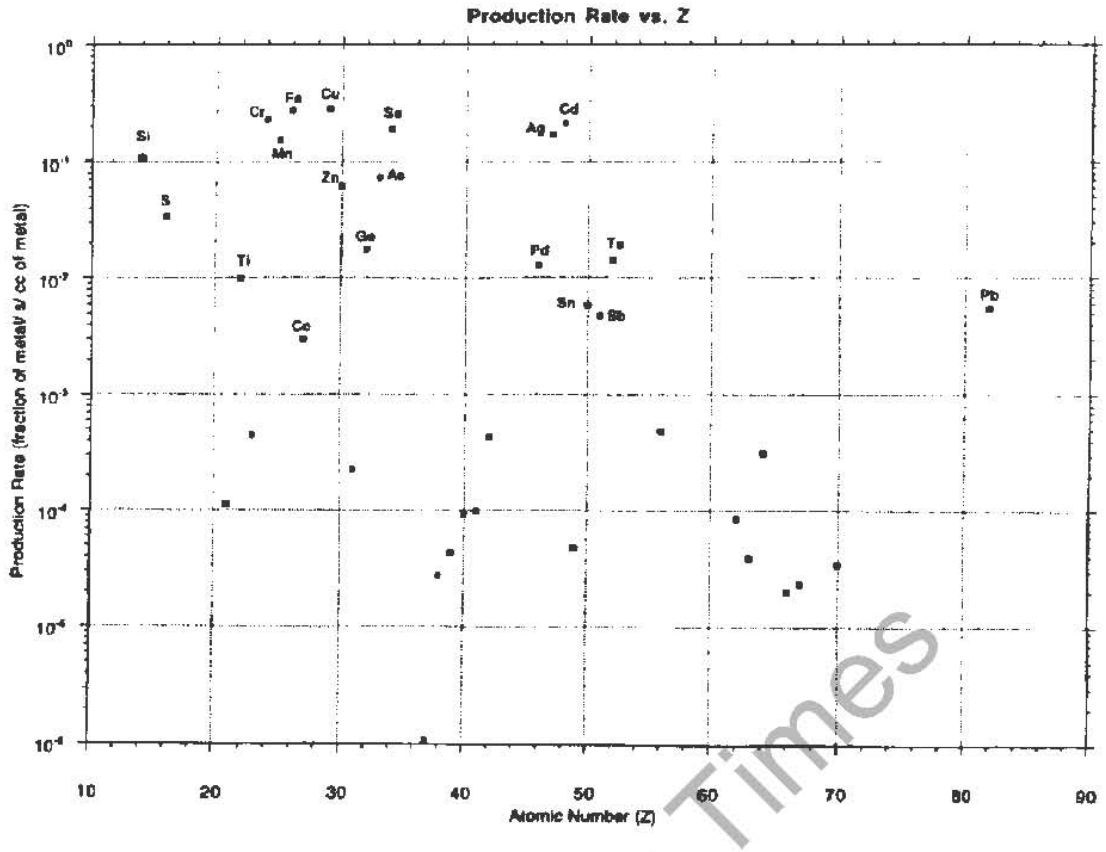

Fig. 8a. Production rate expressed as fraction of metal/ s/ cc of metal vs. atomic number, Z.

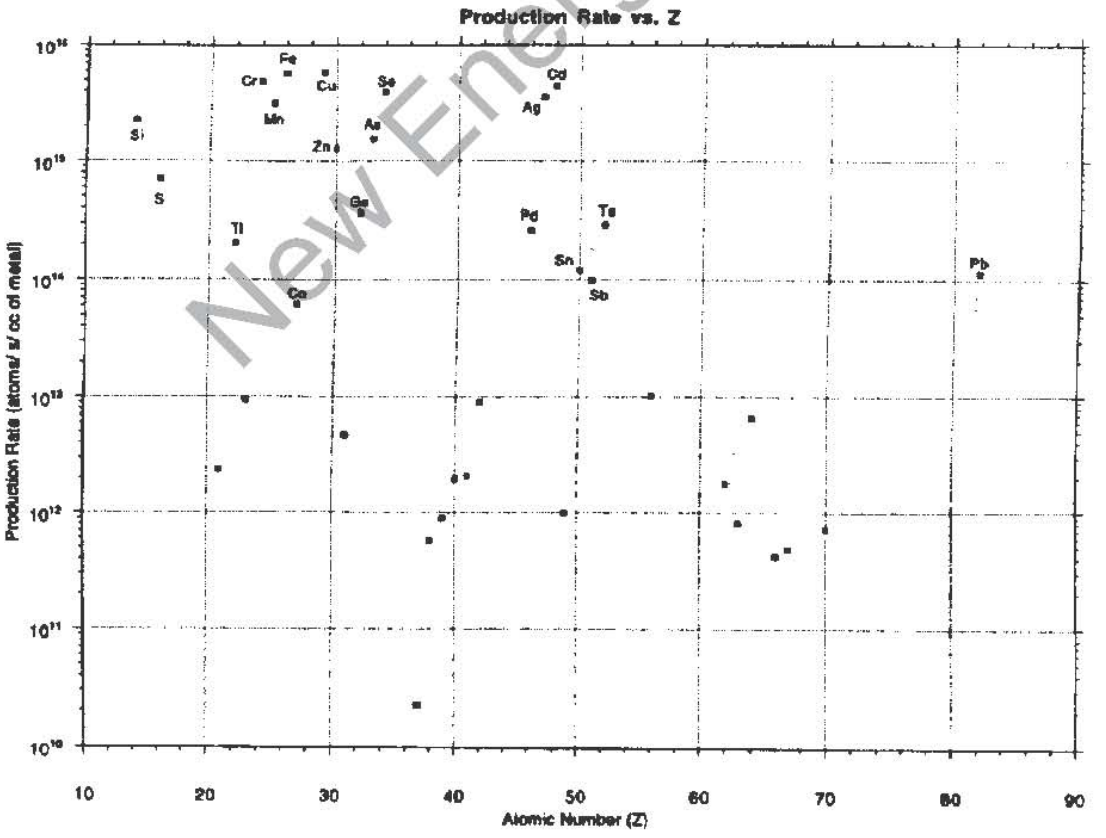

Fig. 8b. Production rate of atoms/ s/ cc of metal vs. atomic number, Z.

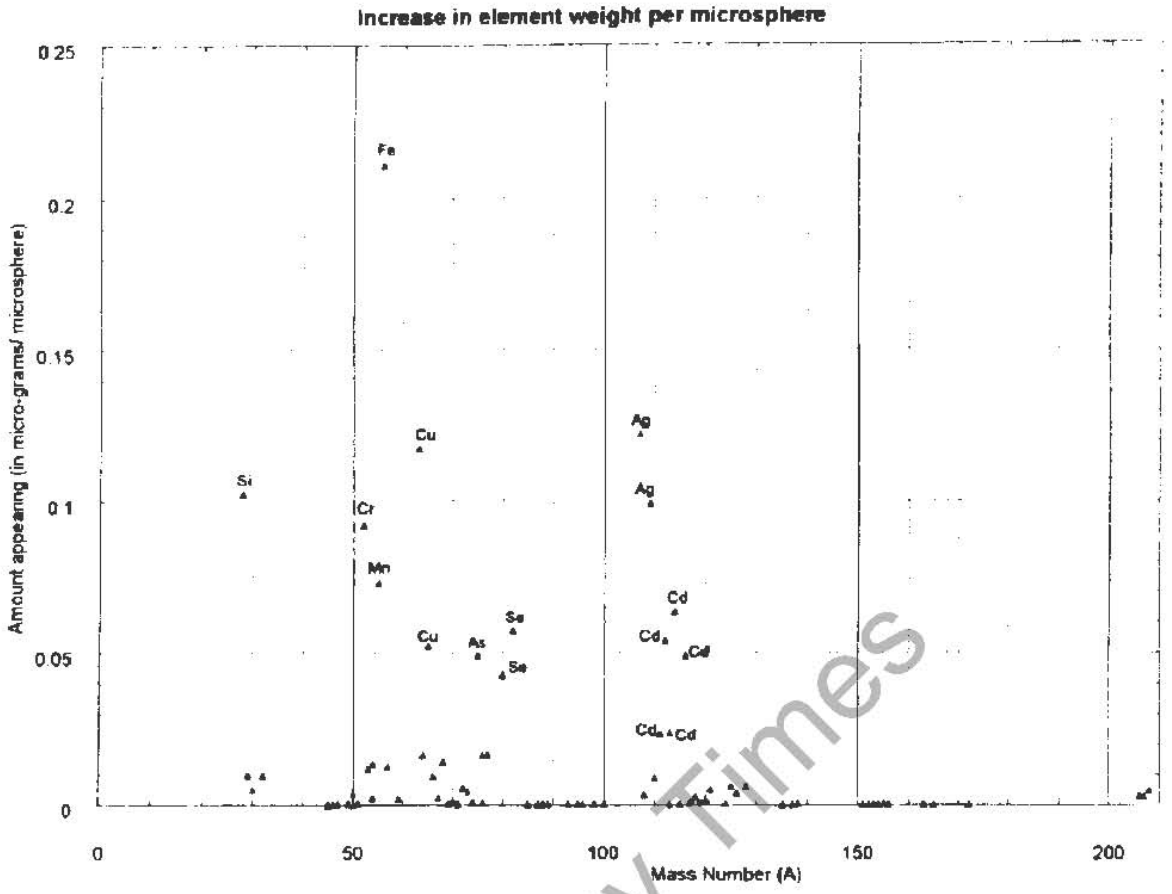

Fig. 9a. Increase in element weight per microsphere.

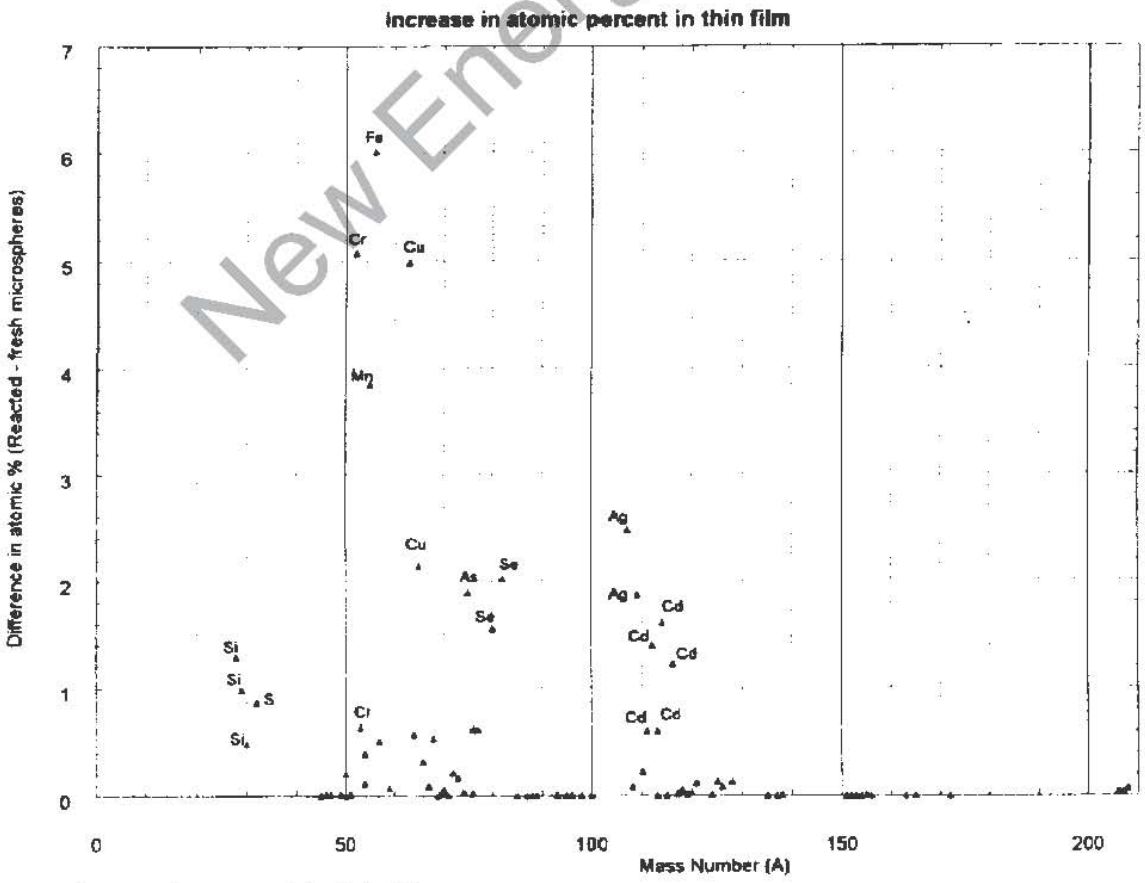

Fig. 9b. Increase in atomic percent in thin film.

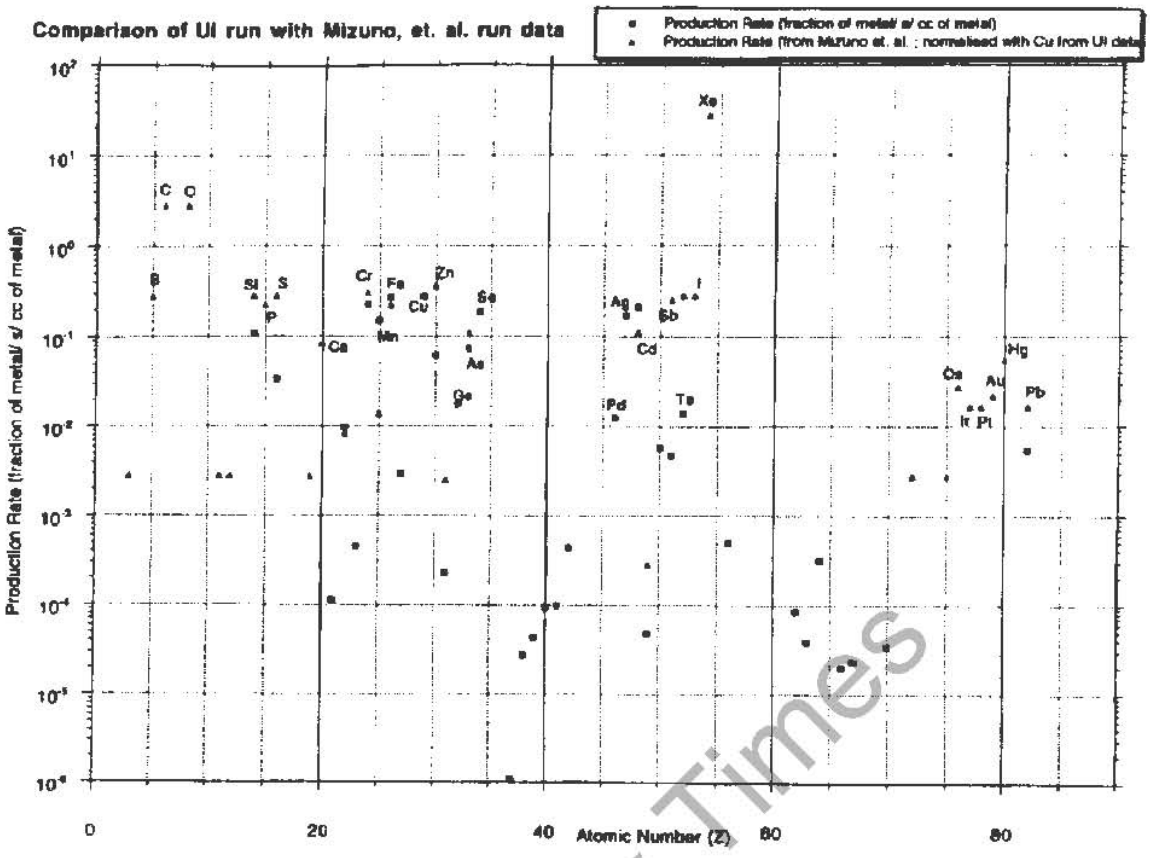

Fig. 10. Comparison of present production rate data with Mizuno et al.

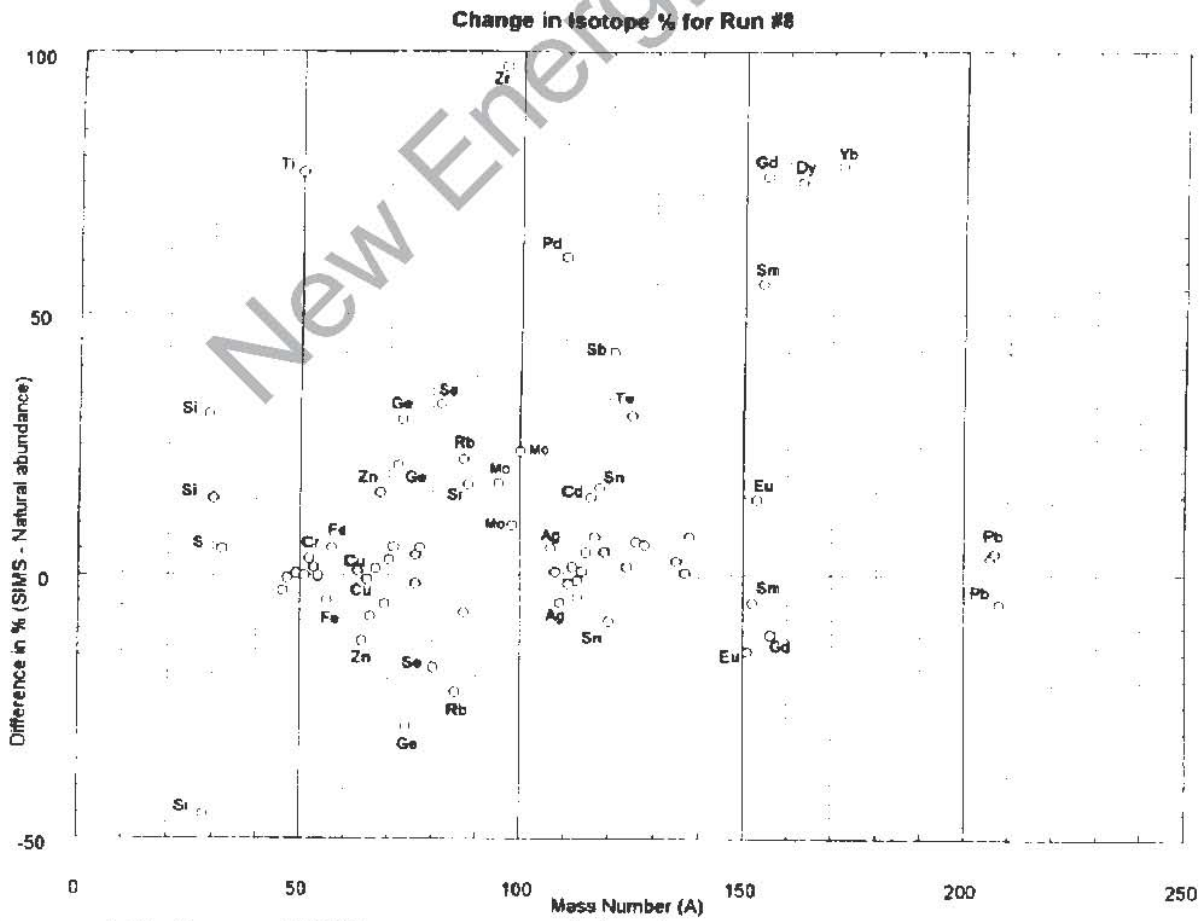

Fig. 11. Isotope shifts (percent SIMS - percent natural abundance) vs. mass number, A.

ISOTOPIC CHANGES OF THE REACTION PRODUCTS INDUCED BY CATHODIC ELECTROLYSIS IN Pd

Tadahiko Mizuno[1], Tadayoshi Ohmori[2], Michio Enyo[3]

ABSTRACT

It was confirmed by several analytic methods that reaction products with mass numbers ranging from 6 to 220 are deposited on palladium cathodes subjected to electrolysis in a heavy water solution at high pressure, high temperature, and high current density for one month. These masses were composed of many elements ranging from hydrogen to lead. Isotopic distributions for the produced elements were radically different from the natural ones.

INTRODUCTION

Since the announcement that, successfully a large amount of heat generation had occurred by simple electrolysis in a heavy water solution using a Pd electrode, nuclear reactions in a solid electrode at ordinary temperatures have been reported by many experimenters. Especially, the phenomena attracts much attention because of the generation of energy. However, this phenomenon is still not well accepted among researchers because of poor reproducibility and control and moreover the lack of the knowledge for the mechanism. What is urgently needed now is to obtain precise and quantitative relationships between potential nuclear reactions and their corresponding reaction products.

Many claimed that if nuclear reactions have been induced by electrochemical reaction occurring in solid electrodes, there must be clear evidence such as the evolution of radioisotopes and radiation. Moreover, the evolution rates of the reaction products should be quantitatively explained in terms of the proper nuclear reaction mechanisms. But such claims could be upheld if the reaction mechanism consisted of proper theories. However, there is no proof that the conventional mechanism explains the observed reactions.

It is difficult to detect the emission of radiation and radioisotope if the mechanism is different from the standard ones. In this work, evidence which indicates the occurrence of some nuclear reactions is presented, in the form of isotopic changed elements in and on the cathode surface. These products have been obtained with a mechanism which had not induced any detectable radiations. The anomalous isotopic distribution of these elements shows they do not come from contamination. For example, natural chromium is 4.3% Cr50, 84% Cr52, 9.5% Cr53 and 2.4% Cr54. But the chromium found in the cathode was 14% Cr50, 51% Cr52, 2.4 % Cr53 and 11 %Cr54. Natural isotopic distribution varies by less than 0.003% for chromium. We represent that the reaction mechanism

[1] Dept. Nucl. Engr., Facul. Engr., Hokkaido Univ., Kita-ku, North 13, West 8, Sapporo, 060 JAPAN, Tel:81-11-706-6689, Fax:81-11-706-7835, E-mail: mizuno@hune.hokudai.ac.jp

[2] Catalysis Research Ctr., Hokkaido Univ., Kita-ku, North 11, West 10, Sapporo, 060, JAPAN, Tel:81-11-706-2620,Fax:81-11-709-4748

[3] Hakodate Nat. Col. Technol., Tokura-cho 14-1, Hakodate, 042, JAPAN, Tel:81-138-59-1376, Fax:81-138-59-4410, E-mail:presiden@cc.hakodate-ct.ac.jp

was completely different from the accepted nuclei formation process. However, we attempt to explain the process which produced these anomalous products by the mechanism within the framework of the proper theory [1].

EXPERIMENTAL

Palladium rods used were of high purity (99.97% min.) supplied by Tanaka Noble Metals, Ltd. Impurities in the sample were as follows; B: 110, Si: 10, Ca: 9, Cr: 10, Cu: 6, Ti: 5, Ag: 44, Mg: 1, Pt: 20 and Au: 23 ppm, respectively. Nothing more was detected by atomic absorption photospectroscopy. The Pd rod was evacuated in a $5x10^{-5}$ Torr of vacuum at 473 K for $6x10^5$ sec to begin. Heavy water was supplied by Showa Denko, Ltd. It is 99.75% pure and includes 0.077 micro Ci/dm^3 of tritium. The heavy water was purified once in a quartz glass distiller. Reagent grade lithium hydroxide was obtained from Merck, Ltd. Impurities in the reagent were specified as follows; Li_2CO_3: 2% max, Cl: 0.05%, Pb: 20, Ca: 200, Fe: 20, K: 200 and Na: 200 ppm and the other impurities were under detectable limit by the atomic absorption analysis. The anode and recombiner catalyst were, respectively, a high purity (99.99%) Pt plate and a Pt mesh. The Pt metal is specified to contain impurities as follows; Rh: 18 ppm; Si, Cr and Pd: 2 ppm; Au, Ag, B, Ca, Cu and Fe: less than 1 ppm. Other impurities were under the limits of detection.

Electrolysis was performed in a closed cell made of stainless steel. The cell has another inner cell made with 1 mm thick Teflon; the height and diameter are 20 cm and 7 cm, the volume is 770 cm^3. The details have been described elsewhere [2]. Before the electrolysis experiment, electrolyte was pre-electrolyzed with other Pt mesh electrodes at 1 A and 150° C for 6×10^5 s (7 days) in the cell with the upper cover closed. After, the Pt electrode was removed and the Pd rod sample was attached at the terminal part. Electrolysis experiments were performed at a current density of 0.2 A/cm^2, total current of 6.6 A (33 cm^2 x 0.2 A/cm^2) at 105°C for 2.76×10^6 s (32 days). After the electrolysis rod was washed by Mill Q water (Mill Q-lab; Japan Millipore Ltd.) and covered by a Teflon tube. The analysis samples were prepared by cutting the rod into 1 cm lengths and again cut into two half-moon-shaped masses by a diamond cutter. The sample electrodes were supplied to element detection after removing the Teflon coat, washed by the Mill Q water for energy dispersive X-ray spectroscopy (EDX), Auger electron spectroscopy (AES), secondary ion mass spectroscopy (SIMS) and electron probe microanalyzer (EPMA). EDX measurements were done by 20 keV of electron irradiation and varying the scanning area; the energy spectra were measured by Silicon Li drift detector. The range of analysis energy was zero to 20 keV; the interesting range was divided into 1024 channels of energy width. The resolution power of energy was 150 eV at 5.9 keV, practically that was 200 eV. Peaks were calibrated using high purity of C, Al, Si, Ti, Cr, Mn, Fe, Co, Zn, Sr, Nb, Mo, Pd, Ag, Sn, Ce, Hf, W, Pt, Au and Pb. AES analyses were performed to obtain the depth distribution of the elements by ANELVA AAS-200; the ion irradiation energy and the current are 3 keV and 2.5 A respectively. EPMA-8705 of Simazu LTD. was used to obtain the elements distribution on the samples. The IMA-3 of Hitachi Co. analyzed for SIMS measurement; O_2^+ ions were irradiated on the sample as a spot diameter of 100 micro meters square having primary energy of 12 keV and 100 nano-Amperes of ion current. Resolution for the mass was m/e=10,000. Mass numbers were calibrated by high purity metals of Li, B, C, Al, Si, Ca, Ti, Cr, Mn, Fe, Co, Ni, Cu, Zn, Sr, Nb, Mo, Pd, Ag, Cd, Sn, Ce, Hf, W, Os, Pt, Au and Pb; no isotopic changes existed in the calibration measurements over the natural deviations.

RESULTS

EPMA analyses were done first to obtain the elements' distributions on the sample surface. There were no detectable depositions on the Pd before electrolysis. And there also no detectable depositions on the surface in case of the current density kept under 0.2 A/cm^2. Moreover, no deposition was seen if the current density was kept up to 0.2 A/cm^2 with no change. Many elements have deposited on the surface and distributed irregularly; these concentrations were changed with samples. The elements that have commonly been detected were C, O, S, Cl, Si, Ca, Ti, Cr, Mn, Fe, Co, Ni, Cu, Zn, Mo, Pd, Sn, Pt, Hg and Pb for all the samples. The amounts for Ca, Ti, Cr, Cu, Pt, Hg and Pb were abundantly present and differed more than 3 times at the surface place compared with

C, Cl, Si, Mn, Co, Ni, Zn and Sn which existed rather uniformly. These changeable elements were also fluctuating with sample lot as 3 times deviations. It means that uncontrollable factors such as surface conditions are of main importance for the reaction.

Depth distributions of the several elements were decided for one micro meter by the AES measurement. Carbon and Oxygen atoms occupied 40 atomic percentages respectively and Cr, Fe, Ca and Cd elements were detected as few atomic percentages; Oxygen concentration once increased in the bulk layer about 65% and gradually decreased with depth; carbon atom concentration gradually decreased with depth but other elements kept almost uniform.

Several elements were detected in the Pd electrode by the EDX method; the measurements were taken to determine the rough concentration for the elements because in the SIMS measurement the mass peaks have a possibility to contain other molecular peaks. Fig. 1 shows typical results before and after electrolysis. Several peaks of Pt, Cr and Fe are clearly seen; these amounts were comparably with Pd bulk peak. And less amounts for Sn, Ti, Cu and Pb elements were also clearly observed. The EDX analyses were repeated on various places of the sample; the deviation for the EDX counts sometimes reached to 10 times in various places. This change was depended on the scanning area. Deviation was 10 times for 10 micro meter square scanning areas but it decreased 2 times for 100 micro meters square. It can be suggested that the reactions had occurred in quite restricted places.

The amounts for the evolved elements were finally estimated as detected by SIMS measurement; a typical result obtained for the Pd surface electrolyzed by 0.2 A/cm^2 of current density is shown in Fig. 2. Mass number for 1 to 210 were detected and most of the masses have more than several hundred count numbers; it can be estimated for the counting errors were within few percentages. However, while there were only 1, 12, 16, 102, 104, 105, 106, 108 and 110 of mass number peaks existed in the before-processed Pd sample. The EDX, AES and EPMA methods were complimentary used to correspond a mass Spectra to a certain atom and decide their isotopic distributions. The procedure is described as follows: (1); the mass number were decided in the first from light mass number. (2); the mass number were adjusted with the EDX and AES spectra. (3) the large count number of mass peaks was confirmed by the existence of their molecular ion and oxide ion peaks. (4) the final mass spectra were estimated by multiplying the factors of counting correction to the original count of each mass. Fig. 3 shows the factor when the O_2^+ ion was irradiated for the analysis. The factor shows very high and low value at the inert gases and alkali metals respectively.

The ratios of atomic number for the mass were finally estimated with the above mentioned procedures. The ratios were shown in Fig. 4 normalized with the total mass set as one. Typical counts by EDX and SIMS ranged from 10^2 to 10^6 and were 10 to 100 times higher than the background counts. Thus, the presence of Ca, Ti, Cr, Mn, Fe, Co, Cu, Zn, Cd, Sn, Pt and Pb was clearly confirmed. These elements are mostly grouped in four ranges of mass numbers: lightest elements under 50 mass number, light elements from 50 to 80; middle elements 100 to 140; and heavy elements from 180 to 208. The ratio of the mass numbers from 102 to 110, which correspond with Pd atom, is under 1% of total even if it was bulk substance; the large ratio of existence for Oxygen and Xenon pull down their values. The reason for these high ratios can be considered that the many gas atoms may be released and successively contribute to the counting rate from the spot place heated up by ion bombardment.

AES and SIMS measurements were also made after bombardment by Ar^+ and O_2^- ions, thus removing surface layers, but the element concentrations at 1 micro meter below the electrode surface were decreased to 60%, 10% and 1% at the surface at 5 microns depth and 10 microns depth. Many holes and cracks having 1 to 10 microns of opening size were observed in the bulk layer; The same elements, having almost the same concentration, were also found at the inner surface. The SIMS analysis showed other elements; As, Ga, Sb, Te, I, Hf, Re, Ir, Br and Xe. These elements, except Xe, were difficult to detect by AES and EDX because the peaks were very close and sometime overlapped with others and these were lower than the detection limits by the measurements. Xe atoms

are naturally difficult to detect by EDX method because such gas atoms easily escape during ion bombardment from the spot area. The SIMS count numbers ranged from 10^3 to 10^6 where the background counts were as low as ~10, so we have confidence in these results. In Fig. 4 we show the peak intensities normalized with the total peak. The intensity of Xe was 10 times larger than Pd; it may be that the gas was released by bombarding with O_2^- ions which caused a temperature rise at the sample.

No peak except Pd has been observed after pre-electrolysis on the Pd surface. Pt and Pd concentrations in the electrolyte after experiment were 10 and 15 ppm respectively by atomic absorption measurement and no other elements excepts for Li was observed. Total amount for the elements existed in 1 micro meter depth of Pd surface were calculated as follows; C: 0.37, S: 0.67, Ca: 0.55, Ti: 0.86, Cr: 7.0, Mn: 0.005, Fe: 0.17, Co: 0.0057, Ni: 0.0157, Cu: 0.026, Zn: 0.80, Mo: 0.005, Pd: 4.77, Cd: 0.105, Sn: 0.069, Pt: 0.025, Hg: 0.0375 and Pb: 0.021 atomic percentage. The total deposited elements on the Pd and the calculated summation for the impurity in the electrolyte and Pd samples are plotted in Fig.5. Here, the total impurities except for Ca are less than the deposition amounts; especially, Mn, Ti, Cd and Hg were not present as an impurity.

Large differences in isotopic distributions compared with the natural distributions were observed by the SIMS method for Cr, Cu, Zn, Br, Xe, Pd, Cd, Hf, Re, Pt, Ir, Pb and Hg. The typical concentrations and their ratios for Chromium isotopes are shown in Fig. 6 for an example; the concentrations except Cr52 decreased exponentially with depth but Cr52 has a peak at 0.5 microns and they showed large shift in isotopic ratios: all the ratios are shown with the ratios of Cr52 which exist in natural most abundant. The reasons that we represented such the existence ratios for isotopes instead to show the results calculated by the ratios to the total existence were to avoid misunderstanding to some change of the isotopic distribution probably caused from mixing with others elements; for this chromium case the mixing may be raised with the existence of iron atom if there are Cr and Fe, may be Cr54 and Fe54 peaks overlapped together even if we employ such the high resolution SIMS measurement of m/e=10000 still the mass difference between Cr54 and Fe54 is only 0.0000135. That means it is impossible to divide their two isotopes by the SIMS measurement having the resolution power. However, we can see large deviations for isotopic existence with natural ones, that means, these are higher than Cr52, i.e., Cr52 is less than others, in the figure where the natural isotope existence is plotted at the 3 microns depth position. These isotopic distribution changes occurred mainly within the layer of most outer surface in 1 microns and their ratios approached normal values toward the inner bulk layer.

In Fig. 7, Pd is shown to have large shifts in abundances. Their concentrations are represented with the ratio to Pd106 which exists in natural as most abundant. Their atomic concentration increased with depth. This means the concentration of other deposition relatively decreased. Especially, amounts of Pd104 and 110 are higher value than the natural ones that values are shown at 3 microns depth in the figure.

In Fig. 8, Lead was seen. The Pb fluctuations are larger than Cr and Pd because their counting rates were one or two orders less. Their concentrations are represented with the ratio to Pb208 which exists in natural as most abundant. Their atomic concentrations show constant except 208 which increased with depth. The isotopic distributions for Pb206 and 207 are lower value than the natural ones that values are shown at 3 microns depth Figure 8.

Neutron intensity and the energy measurements were carried out simultaneously, in parallel. The neutron evolution rate was sporadic and weak, as previously reported [3], with levels of ~0.4 counts per second. No gases such as He, O_2 and Ar were detected during electrolysis experiment. Excess heat generation was less reproducible, but was detected and the value was the order of 10^7 joules [4].

DISCUSSION

Essentially the same phenomenon was confirmed five times with high reproducibility at high cathodic current density, above 0.2 A/cm^2. Current density ranged from 0.2 to 0.6 A/cm^2. Different isotope distributions were obtained, depending on the current density. This will be described more fully in an upcoming paper. It can hardly be imagined that all of the elements found were impurities in electrolyte, electrode or cell. Even if we suppose that all impurities in the system accumulated in the cathode, the amount would be 10 to 100 times smaller than the total amount we detected. Furthermore, it is simple impossible to explain the shifts in the isotopic distribution. Hence, it must be concluded that some novel reactions occurred, resulting in the reactants which were found abundant in the electrolyte and electrode material. We assume the cathode palladium was the starting material for these reactions, but it is possible that impurities and other cell components such as Li, D_2O, Pd, Pt, K, Na, Ca, B, C, Ag and Fe may have provided the starting material for the nuclear reactions.

The palladium surface became rough and porous after several weeks of electrolysis, probably due to hydrogen attack. The current may have increased in such roughened surface areas, which would in turn cause a larger reaction and a higher concentration of the reaction products. Enyo [5-7] reported that the effective hydrogen pressure at the hydrogen evolving electrode depends upon the hydrogen atom recombination process which follows the water discharge process; the total hydrogen overpotential η_t is represented by addition with two of components by $\eta_t = \eta_1 + \eta_2$; where η_1 and η_2 are arisen from discharge and recombination process. The η_1 is a slow step compared with η_2 of Tafel step for the normal palladium surface. But the claim can be held at a completely flat and uniform surface. The values of η_1 and η_2 are only estimated as averaged over the whole surface. The division of the overpotential between these two steps may be important. It was suggested that at Pd electrodes in alkaline solution the effective hydrogen pressure may rise as high as 10^6 atm [8,9]. There may be further increases at local points on a heterogeneous surface. One may even speculate that the hydrogen isotope nucleus sometimes closely approaches the medium nucleus [10]. An estimate by Nernst Equation indicates that 5×10^4 atm of pressure may be realized at 140 mV of overpotential at the electrolysis current density of 0.2 A/cm^2 on a flat palladium surface [11]. Furthermore, the pressure distribution depends on the roughness of the surface, because local current density and the partition of overpotential components may vary with roughness.

There are several reports [12-14] of evolution of elements by electrolysis. However, only a few [15,16] demonstrated shifts in isotopic abundance. For a gold electrode [17], which also generated various elements by cathodic electrolysis, different isotopic distributions were seen. In this case also, the reaction sites were unevenly distributed on the surface. Typically, the active points may have occupied about 10^{-6} cm^2 areas and numbered 10^4 to 10^5 per cm^2 at the surface. Thus, the current is likely to be concentrated at localized points 10 to 100 times higher than average. Moreover, the rate control may be changed at the parts by the condition of electrode surface, the recombination process becomes slow step compared with the discharge process; the over potential caused from the recombination process can be a considerable part of the over potential. Total cell voltage reaches sometimes more than 1Volt at 0.2A/cm2 of cathodic current density in alkaline solution. The major overpotential may be occupied by the discharge process at a flat and uniform part of the Pd surface, however, at the top of the Pd part where are rough surfaces, the major part of the overpotential may be occupied by recombination process. Then, the overpotential due to recombination process becomes more than 0.3V if the process occupied 2 times bigger than the usual if the current density reached more than 1V. We can conclude the statistical hydrogen pressure exceeds more than 10^{10} atm at the parts of Pd electrode.

Hydrogen gas and the electrode atom are compressed and changed like a metal solution under the such high pressure. The distance between their atoms were approached and entered through the electron shield. The hydrogen atoms can occupy the orbit according their spin quantum numbers. More electrons take the higher orbit and it occurs some possibility that can induce proton and neutrons into enter heavy nucleus under the above mentioned conditions [18]; two, four, eight and ten hydrogen and deuterium atoms can enter at the moment in

the heavy nucleus. If the reactions start from palladium as the electrode material, fusion and fission may take place simultaneously. Several possible reactions might be considered:

$$^{108}_{46}Pd + 2^{2}_{1}D \rightarrow {}^{108}_{46}Pd^{4}_{2} \rightarrow {}^{116}_{48}Cd$$
$$^{108}_{46}Pd + 4^{2}_{1}D \rightarrow {}^{108}_{46}Pd^{8}_{4} \rightarrow {}^{116}_{50}Sn$$
$$^{108}_{46}Pd + 8^{2}_{1}D \rightarrow {}^{108}_{46}Pd^{16}_{8} \rightarrow {}^{124}_{54}Xe$$
$$^{102}_{46}Pd + 8^{2}_{1}D \rightarrow {}^{102}_{46}Pd^{16}_{8} \rightarrow {}^{118}_{54}Xe \rightarrow {}^{118}_{50}Sn + 4ß^{+}$$
$$^{104}_{46}Pd + 8^{2}_{1}D \rightarrow {}^{104}_{46}Pd^{16}_{8} \rightarrow {}^{120}_{54}Xe \rightarrow {}^{120}_{52}Te + 2ß^{+}$$
$$^{105}_{46}Pd + 8^{2}_{1}D \rightarrow {}^{105}_{46}Pd^{16}_{8} \rightarrow {}^{121}_{54}Xe \rightarrow {}^{121}_{51}Sb + 3ß^{+}$$
$$^{106}_{46}Pd + 8^{2}_{1}D \rightarrow {}^{106}_{46}Pd^{16}_{8} \rightarrow {}^{122}_{54}Xe \rightarrow {}^{122}_{52}Te + 2ß^{+}$$

Here, left-hand sides in the equations are the reactants, right-hand sides are the products and the middle are the intermediate states that are unstable due to containing excess protons and neutrons; the bottom subscript at the right-hand side of the intermediates represents the proton number and the top superscript represents the total nuclear number which is connected with nucleus as the hollow atom. It can be assumed that these particles will stay in a stable orbit according to their quantum spin number as the same concept with electron orbits. The connecting nuclei are caught into medium nuclei by the force of high external pressure.

Other reactions have to be assumed because many light elements were observed. They may be as follows:

$$^{102}_{46}Pd + 2^{2}_{1}D \rightarrow 2\,{}^{51}_{23}V + {}^{4}_{2}He$$
$$\rightarrow {}^{50}_{22}Ti + {}^{52}_{24}Cr + {}^{4}_{2}He$$
$$\rightarrow {}^{48}_{20}Ca + {}^{57}_{26}Fe + {}^{4}_{2}He$$

Generally, one can write the fission reactions as follows:

$$^{102}_{46}Pd + 2^{2}_{1}D \rightarrow {}_{n}A + {}_{46-n}B + {}^{4}_{2}He$$

In the case of platinum deposited from the aug. electrode to the Pd electrode surface, some reactions may be involved, such as:

$$^{196}_{78}Pt + 2^{2}_{1}D \rightarrow {}^{196}_{78}Pt^{4}_{2} \rightarrow {}^{200}_{80}Hg$$
$$^{196}_{78}Pt + 4^{2}_{1}D \rightarrow {}^{196}_{78}Pt^{8}_{4} \rightarrow {}^{206}_{82}Pb$$

They may induce fission reactions as follows:

$$^{194}_{78}Pt + 2^{2}_{1}D \rightarrow {}^{136}_{54}Xe + {}^{58}_{26}Fe + {}^{4}_{2}He$$
$$^{195}_{78}Pt + 2^{2}_{1}D \rightarrow {}^{136}_{54}Xe + {}^{59}_{26}Fe + {}^{4}_{2}He$$
$$\downarrow$$
$${}^{59}_{27}Co + ß^{-}$$
$$^{196}_{78}Pt + 2^{2}_{1}D \rightarrow {}^{136}_{54}Xe + {}^{60}_{26}Fe + {}^{4}_{2}He$$
$$\downarrow$$
$${}^{60}_{28}Ni + 2ß^{-}$$

Atomic numbers of 20, 28, 50 and 82 are called magic numbers. Here, Xe136 nuclei are abnormally increased, and hence the number of neutrons changes to magic number 82, and especially stable nuclei are selectively produced. In this way, the isotopic distributions of the products after electrolysis can be explained in terms of the difference of binding energy of the nuclei.

It must be admitted that these reactions have no solid, detailed theoretical basis yet, but in broad terms this can explain most of the elements which were observed. One may also imagine that as such transmutation reactions were presumably taking place during the electrochemical process, they are likely to be connected with other phenomena such as hydrogen embrittlement and local corrosion.

CONCLUSION

Anomalous evolution of various elements in palladium electrodes was confirmed after high current density cathodic electrolysis under high temperature and pressure for a long time. The following conclusions were drawn:

(1) The mass number of the evolved elements was distributed roughly in four groups: less than 20, 20 to 28, 46 to 54 and 72 to 82, with the amounts, respectively, 10 %, >50 %, 10 % and <5% compared to palladium.

(2) These evolved elements were found on the surface, and also in the bulk of the electrode in amounts 10 to 100 times smaller.

(3) **Many evolved elements accumulated in holes and cracks on the electrode which formed during electrolysis.**

(4) Some of the evolved elements have isotopic distributions drastically different from natural ones, especially for Cr, Fe, Cu, Ze, Br, Xe, Pd, Cd, Hf, Re, Pt, Ir and Hg. The layer showed large change of isotopic concentrated in 1 micro meter of the Pd surface.

(5) Gaseous Xe was noteworthy because it was so abundant. Xenon is particularly unlikely to be a contaminant because metals do not absorb noble gases, and because the cathode was degassed in a vacuum at 473°K for 20 hours.

(6) The elements in the bulk layer changed in concentration with depth and showed shifts of isotopic distribution.

(7) Light elements such as O, C, Ca, Na, Mg and Al showed small isotopic shifts.

(8) Ni and Co were also confirmed but their isotopic distribution could not be measured because their SIMS peaks overlapped with those of other elements and isotopes.

(9) The isotopic distributions of Pd and Pt were also shifted.

(10) We conclude that nuclear reactions must have occurred during the electrochemical process.

ACKNOWLEDGMENT

The authors wish to acknowledge the support of the Institute of Applied Energy and The Thermal & Electric Energy Technology Foundation.

REFERENCES

1. Tadahiko Mizuno, Tadayoshi Ohmori, Kazuya Kurokawa, Tadashi Akimoto, Masatoshi Kitaich, Koichi Inoda, Kazuhisa Azumi, Shigezo Shimokawa and Michio Enyo, "Anomalous Isotopic Distribution of Elements Deposited on Palladium Induced by Cathodic Electrolysis," *Denki Kagaku*, vol 64, no 11 (1996).

2. Tadahiko Mizuno, Tadashi Akimoto, Kazuhisa Azumi and Michio Enyo, "Diffusion Rate of Deuterium in Pd during Cathodic Charging," *Denki Kagaku*, vol 60, no 5, p 405 (1992).

3. Tadahiko Mizuno, Tadashi Akimoto and Norio Sato, "Neutron Evolution from Annealed Palladium Cathode in LiOD-D_2O Solution," *Denki Kagaku, vol* 57, no 7, p 742 (1989).

4. Tadahiko Mizuno, Tadashi Akimoto, Kazuhisa Azumi and Norio Sato, "Tritium Evolution during Cathodic Polarization of Palladium Electrode in D_2O Solution," *Denki Kagaku*, vol 59, no 9, p 789 (1991).

5. Tadanori Maoka and Michio Enyo, "Hydrogen Absorption by Palladium Electrode Polarized in Sulfuric Acid Solution Containing Surface Active Substances, II," *Electrochimica Acta*, vol 26, no 5, pp 615-619 (1981).

6. Tadanori Maoka and Michio Enyo, "The Overpotential Components on the Palladium Hydrogen Electrode," *J. Electroanal. Chem.*, vol 108, pp 277-292 (1980).
7. Michio Enyo, "Kinetics of the Elementary Steps of the Hydrogen Electrode Reaction on Pd in Acidic Solution," *J. Electroanal. Chem.*, vol 134, pp 75-86 (1982).
8. Tadahiko Mizuno and Michio Enyo, "Sorption of Hydrogen on and in Hydrogen-Absorbing Metals in Electrochemical Environments," Modern Aspects of Electrochemistry, vol 30 (1996), Ed., J.O'M. Bockris and C. White, Plenum Pub. Corp.
9. M. Enyo and P. C. Biswas, "Hydrogen Absorption in Pd Electrode in Alkaline Solutions," *J. Electroanal. Chem.*, vol 335, pp 309-319 (1992).
10. C. E. Rolfs and W. S. Rodney, "Cauldron in the Cosmos," Theoretical Astrophysics Series, The Univ. of Chicago Press, pp 96-112 (1988).
11. Moshe H. Mintz, "Mixed Mechanisms Controlling Hydrogen-Interface Mechanism," *J. Alloys and Compounds*, vol 176, pp 77-87 (1991).
12. J. O'M. Bockris and R. Sundaresan, "Electrochemistry, Tritium and Transmutation," (Table 2), Cold Fusion Source Book (ed. by H. Fox), Intern'l. Symp. on Cold Fusion & Adv. Energy Sources, Minsk, Belarus, May 1994.
13. Y. Kucherov, A. Karabut, I. Savvatimova, "Calorimetric and Nuclear Products Measurements at Glow-Discharge in Deuterium," Scientific Industrial Association, LUCH, Podolsk, Moscow Region, Russian Federation, (1995); reviewed by M. Swartz, *Cold Fusion Times*, vol 1, no 4, p 10.
14. M. I. Martinov, A. I. Meldianov and A. M. Cherepovski (Kurchatov Atomic Energy Inst.), "Investigation of Anomalous Nuclear Events in Metals Saturated with Deuterium", Cold Nuclear Fusion, Ctr., of Intersectorial Science, Engineering and Venture, Non-conventional Technologies, Moscow, 84-91 (1993), Abstracts review; *Fusion Facts*, vol 5, no 5, p 20, November 1995.
15. Tadayoshi Ohmori and Michio Enyo, "Excess Heat Evolution during Electrolysis of H_2O with Nickel, Gold, Silver and Tin Cathodes," *Fusion Technology*, vol 24, pp 293-295 (1993). [see also in this issue.]
16. R. T. Bush and R. D. Eagleton, Frontiers of Cold Fusion, Universal Academy Press, pp 405-408 (1993).
17. Tadayoshi Ohmori, Tadahiko Mizuno, Nodasaka and Michio Enyo, "Nuclear Transmutation Forming Several Metals from Gold during Light Water Electrolysis;" to be published in *International Journal of Hydrogen Energy*.
18. A. C. Mueller and B. M. Sherrill, "Nuclei at the Limits of Particle Stability," *Annul. Rev. Nucl., Part Sci.*, pp 529-583 (1993).

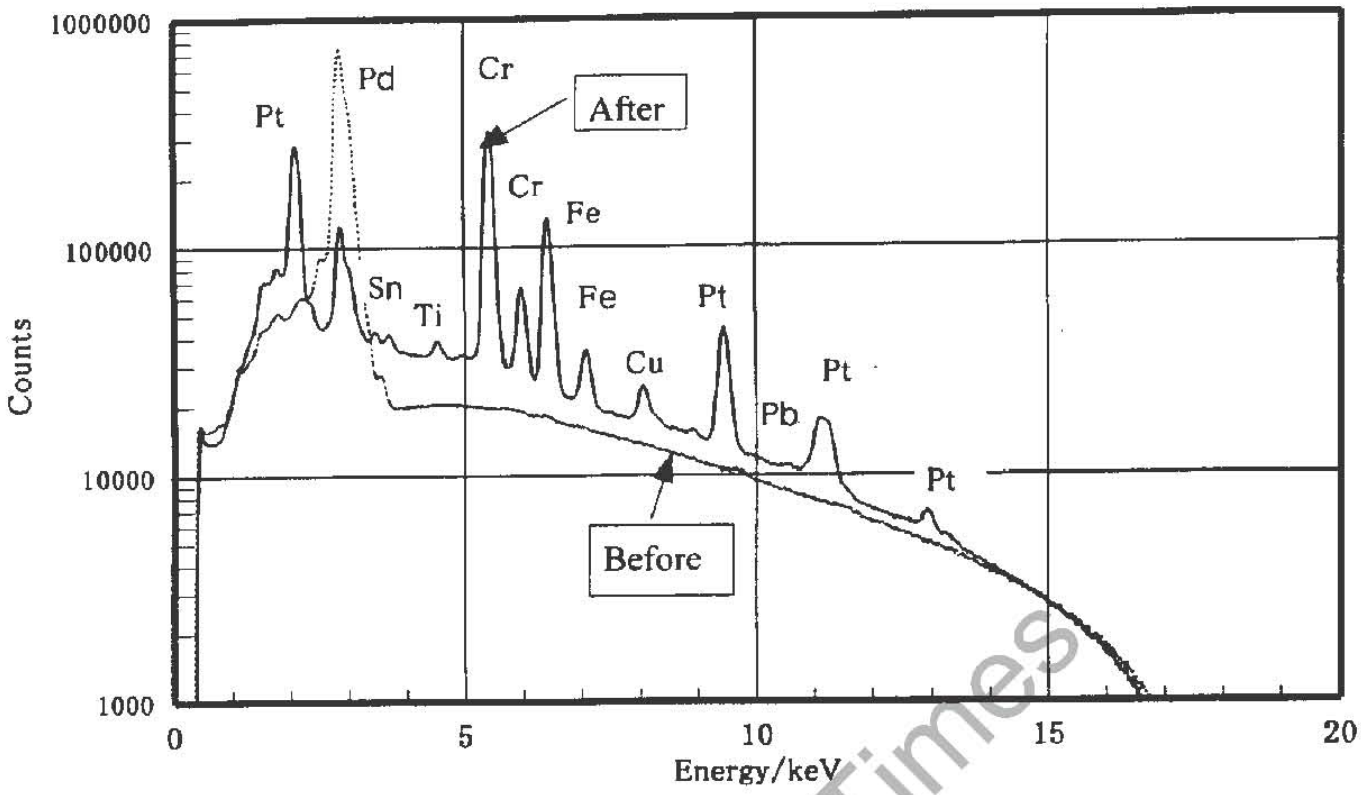

Fig. 1. EDX spectra from the Pd rod before and after the electrolysis.

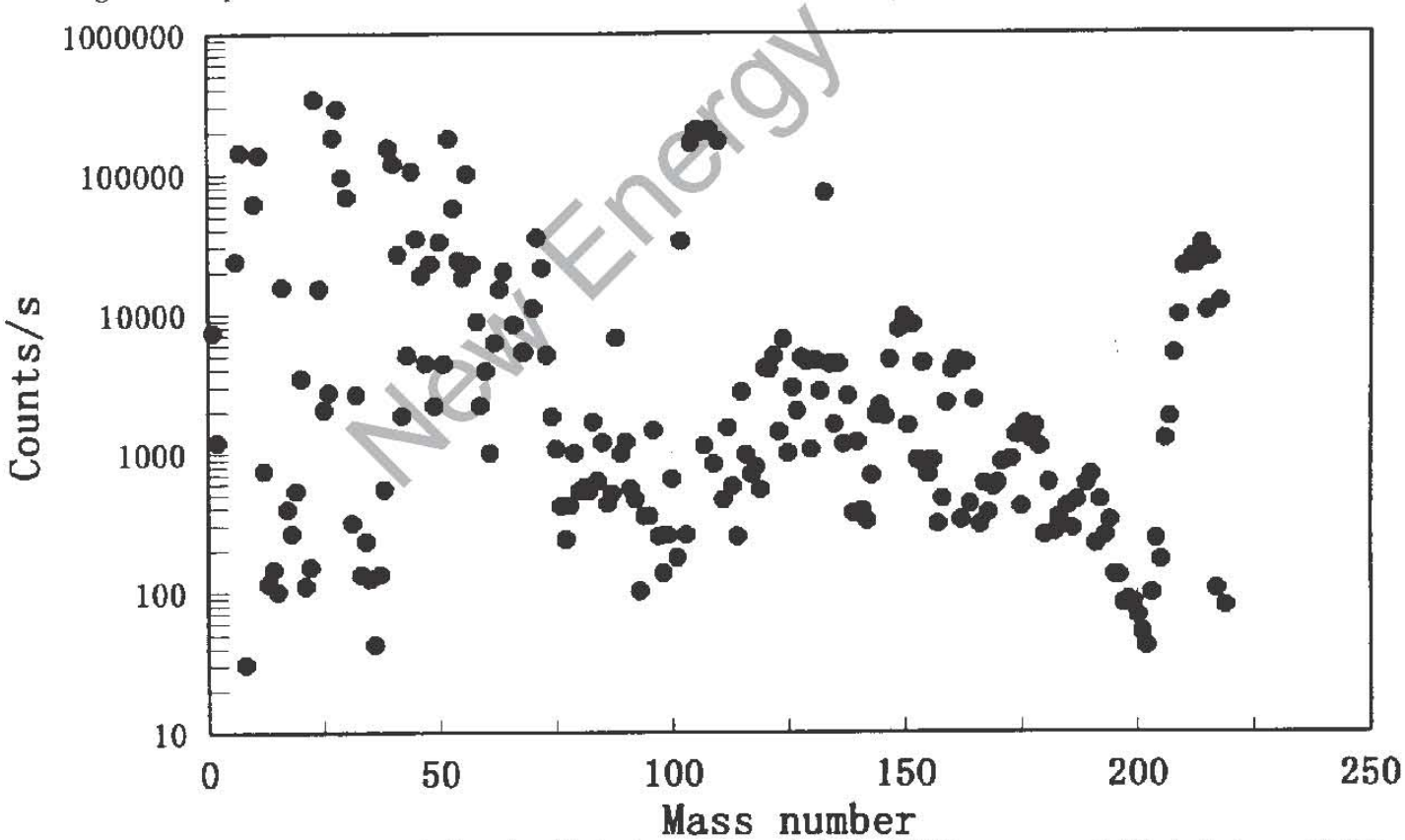

Fig. 2. Count rates for Pd electrode electrolyzed in the heavy water solution by SIMS measurement. (Electrolysis conditions; 1.0 mol LiOH-D_2O, 378 K, 0.2 A/cm^2 for 2.76 10^6 s)

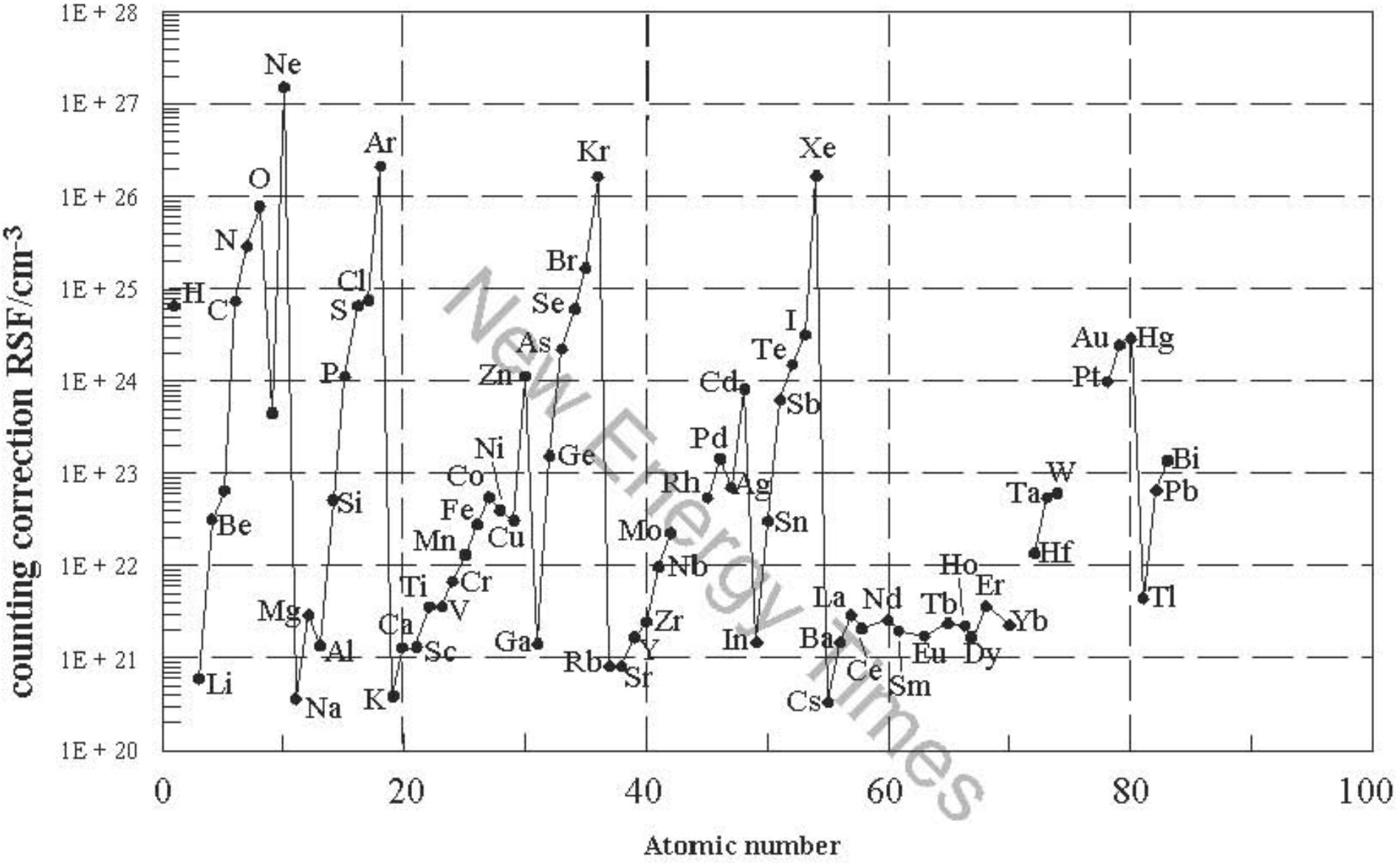
counting correction RSF/cm-3
1E + 28
1E + 27
1E + 26
1E + 25
1E + 24
1E + 23
1E + 22
1E + 21
1E + 20
0
20
40
60
80
100
Atomic number
H
C
N
O
Ne
Li
Be
Na
Mg
Al
Si
P
S
Cl
Ar
K
Ca
Sc
Ti
V
Cr
Mn
Fe
Co
Ni
Cu
Zn
Ga
Ge
As
Se
Br
Kr
Rb
Sr
Y
Zr
Nb
Mo
Rh
Pd
Ag
Cd
In
Sn
Sb
Te
I
Xe
Cs
Ba
La
Ce
Sm
Eu
Nd
Tb
Dy
Ho
Er
Yb
Ta
W
Hf
Au
Pt
Hg
Tl
Pb
Bi
New Energy Times

Fig. 3

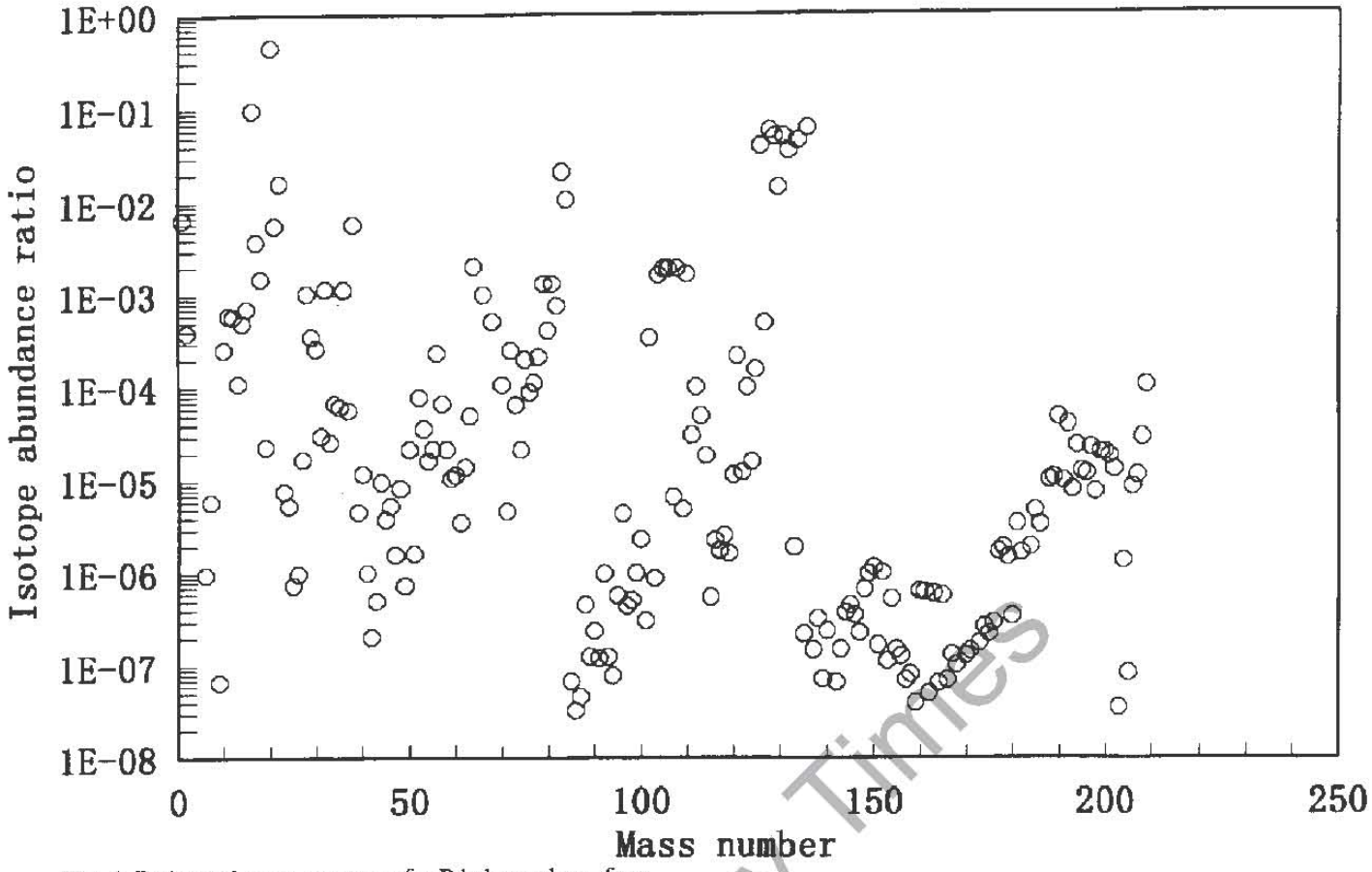

Fig. 4. Estimated mass spectrum for Pd electrode surface.

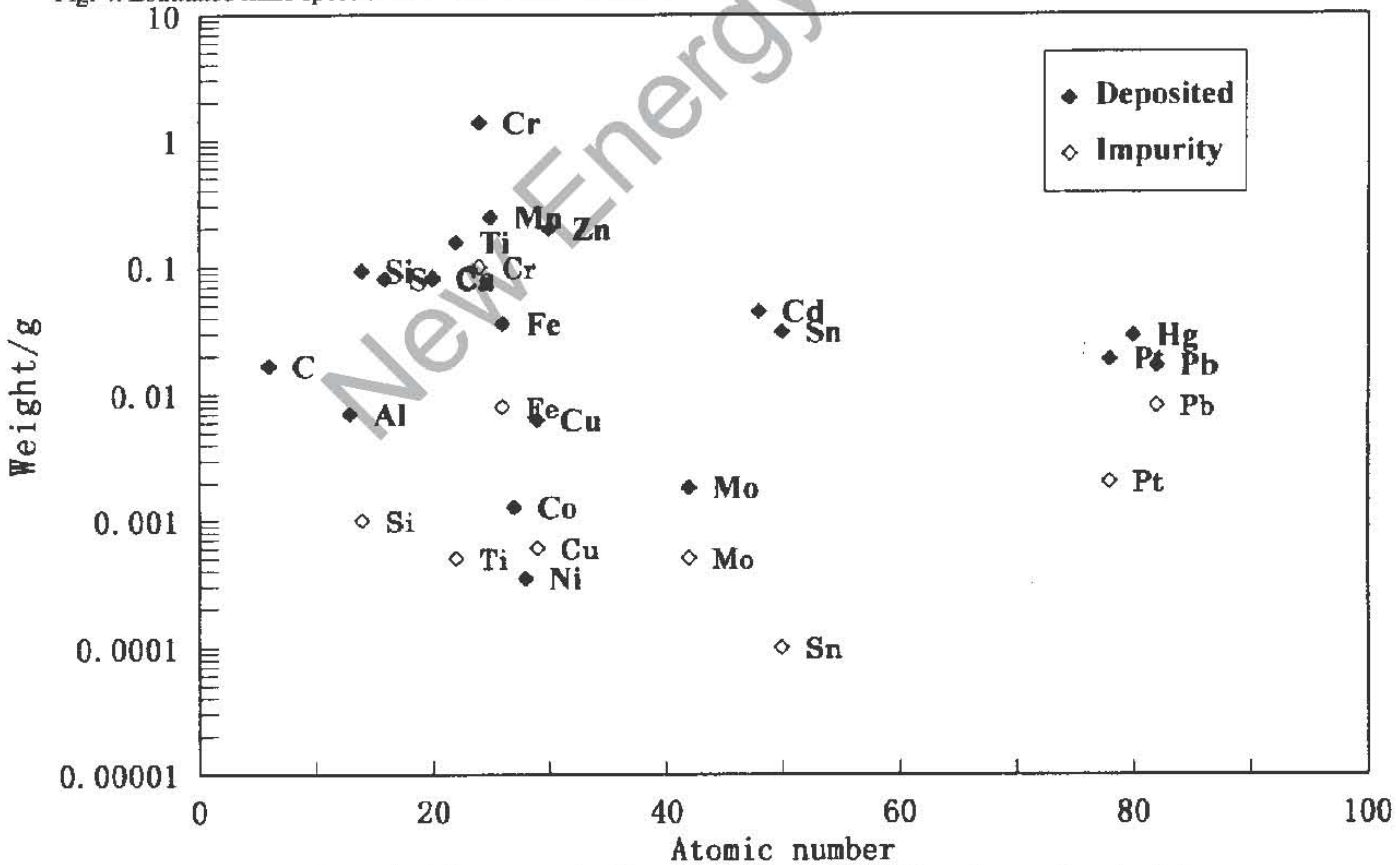

Fig. 5. Total amounts of deposited elements on the Pd and impurities estimated from the sample and solution.

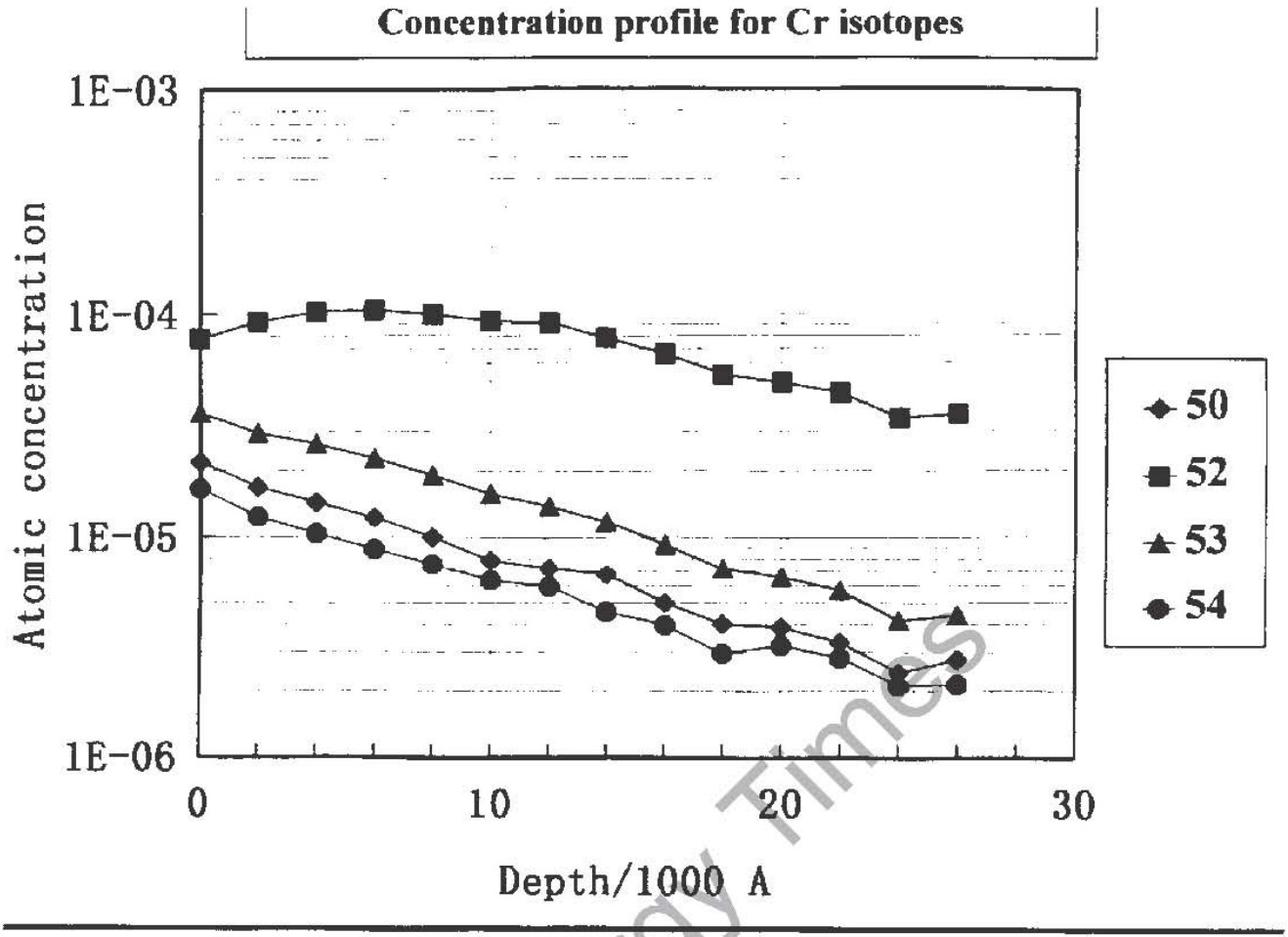

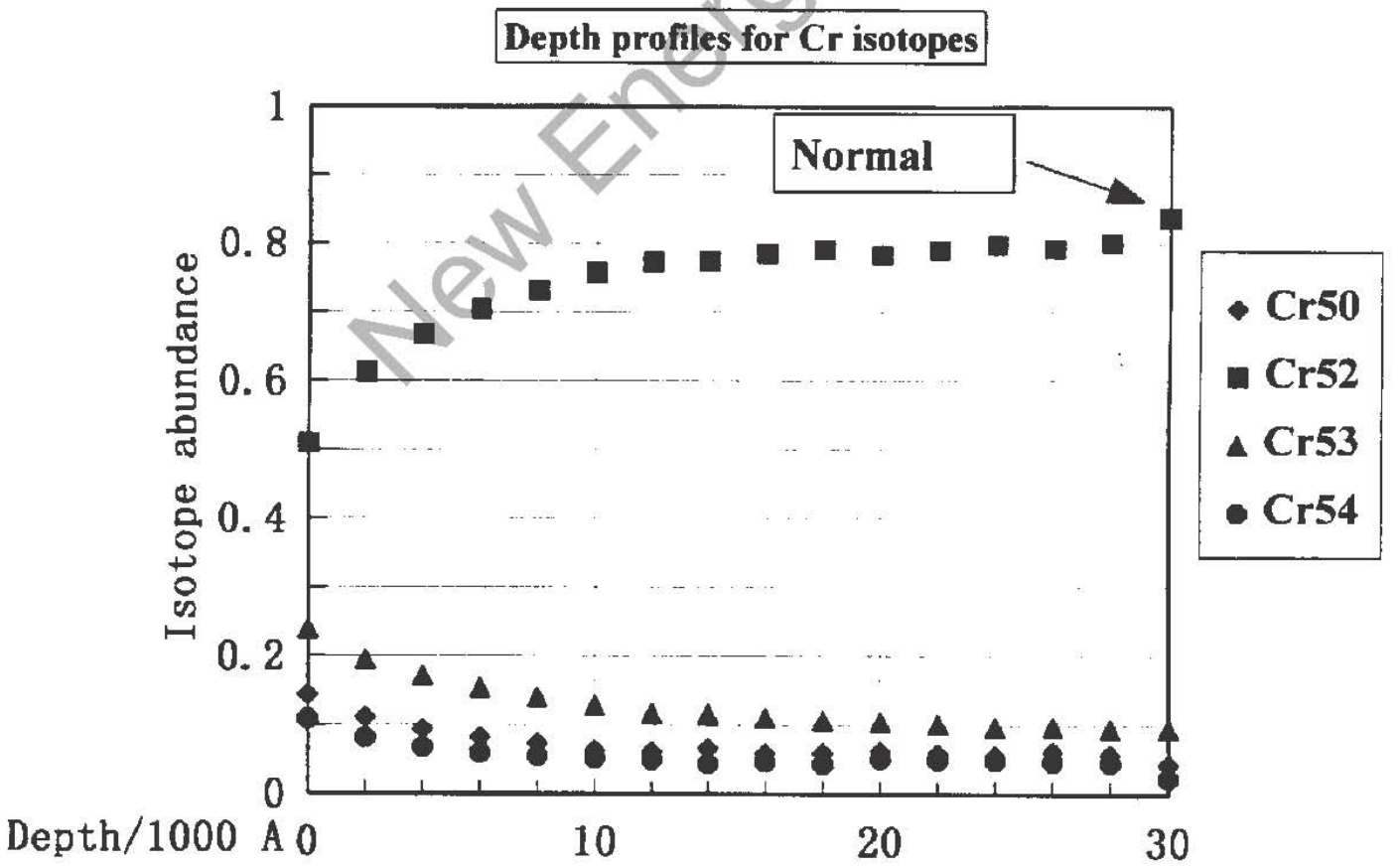

Fig. 6. Profiles for Chromium isotope concentrations (above)and the depth profiles for the isotopic ratios with Cr52 (bottom) in Pd.

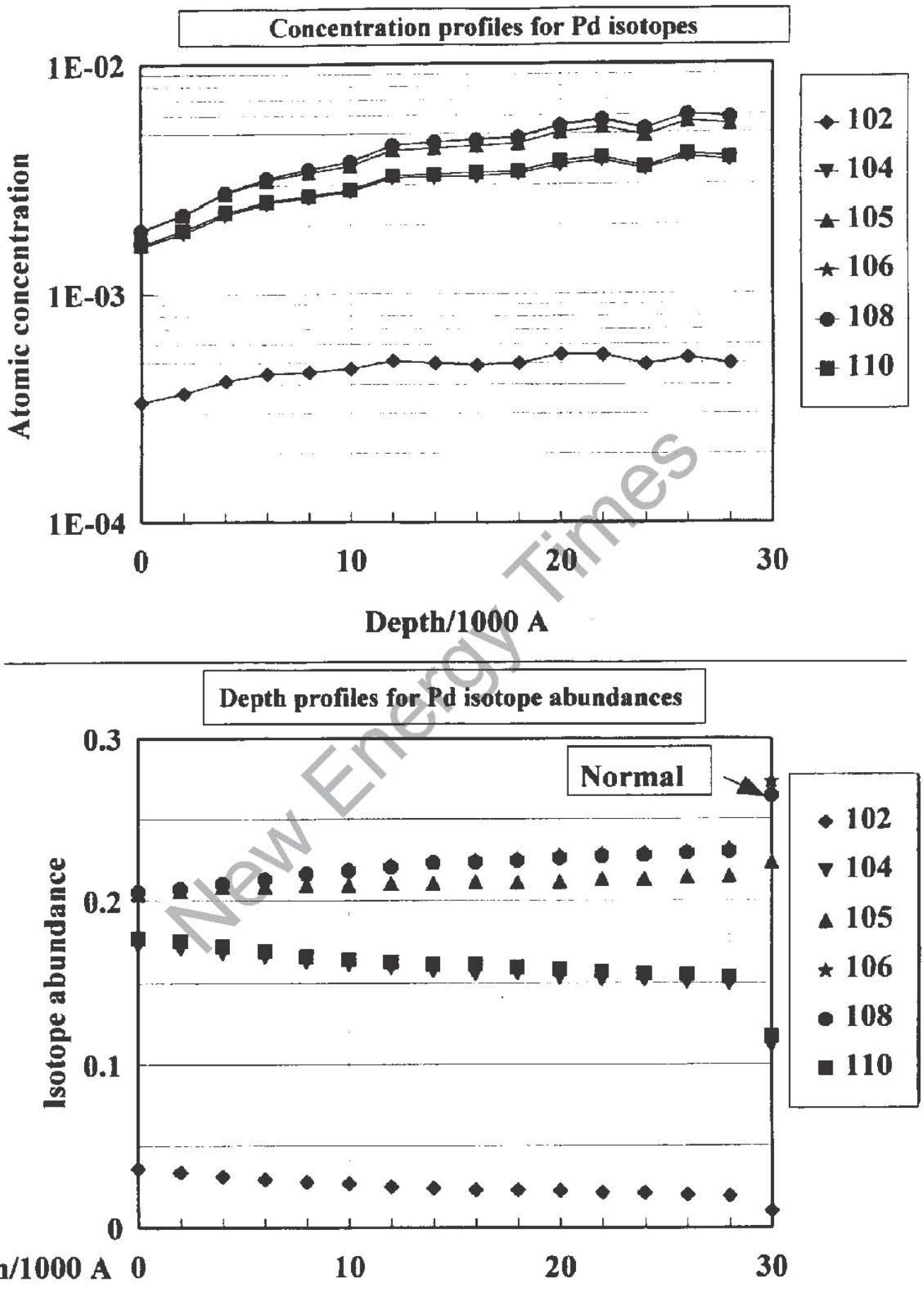

Fig. 7. Profiles for Palladium isotope concentrations (above) and the depth profiles for isotopic ratios with Pd106 (bottom) in the sample as compared with natural isotopic distribution.

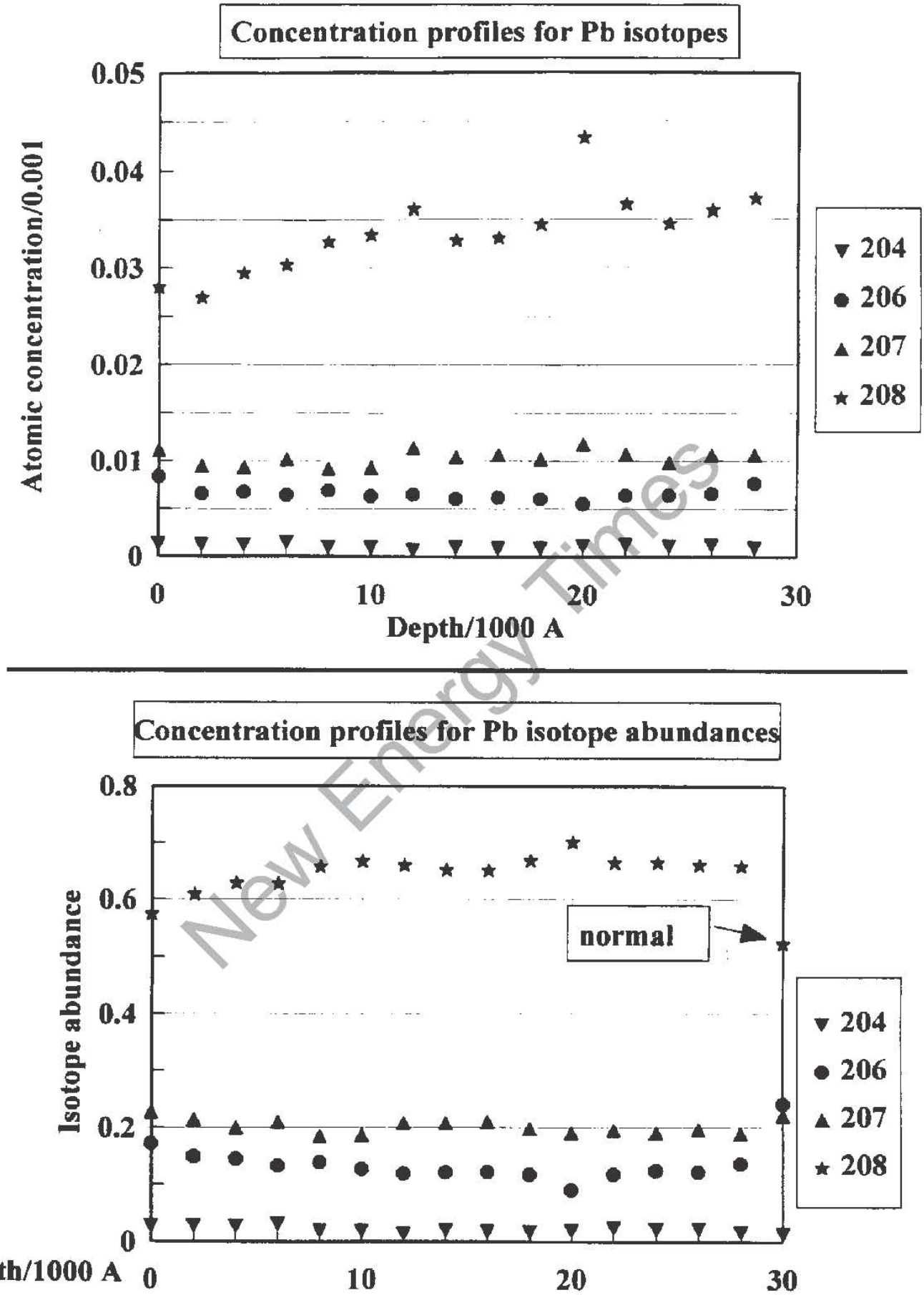

Fig. 8. Profiles for Lead isotope concentration (above) and the depth profiles for isotopic ratios with Pb208 (bottom) in the sample as compared with natural isotopic distribution.

Fig.9 Changes of Isotope abundance for deposition on Pd

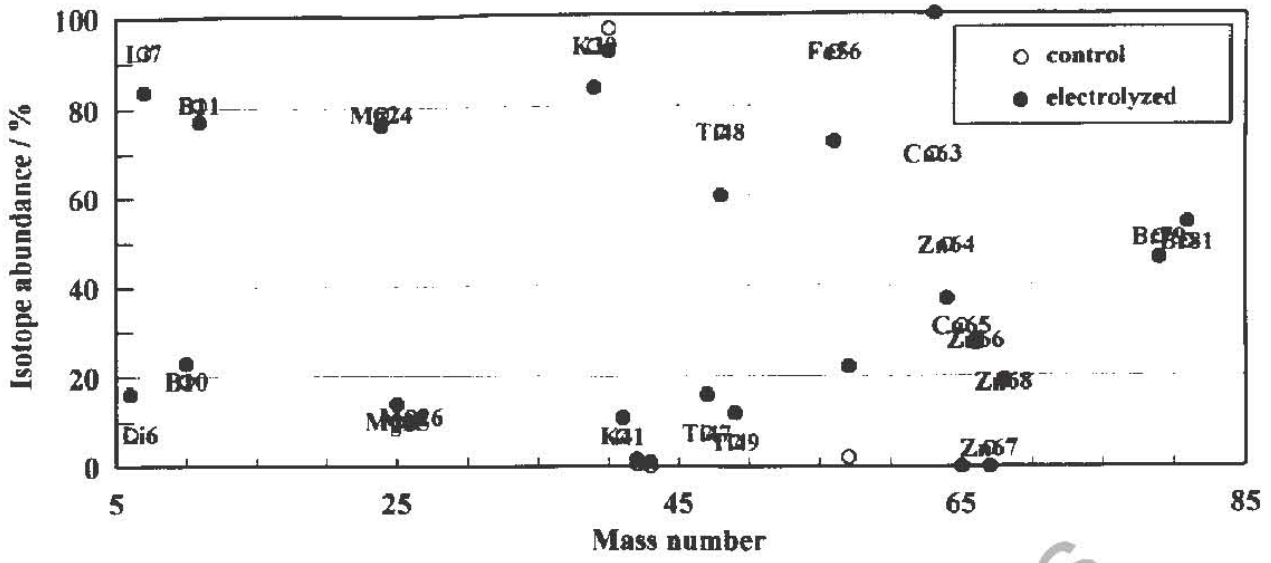

Fig.10 Changes of Isotope abundance of deposition on Pd

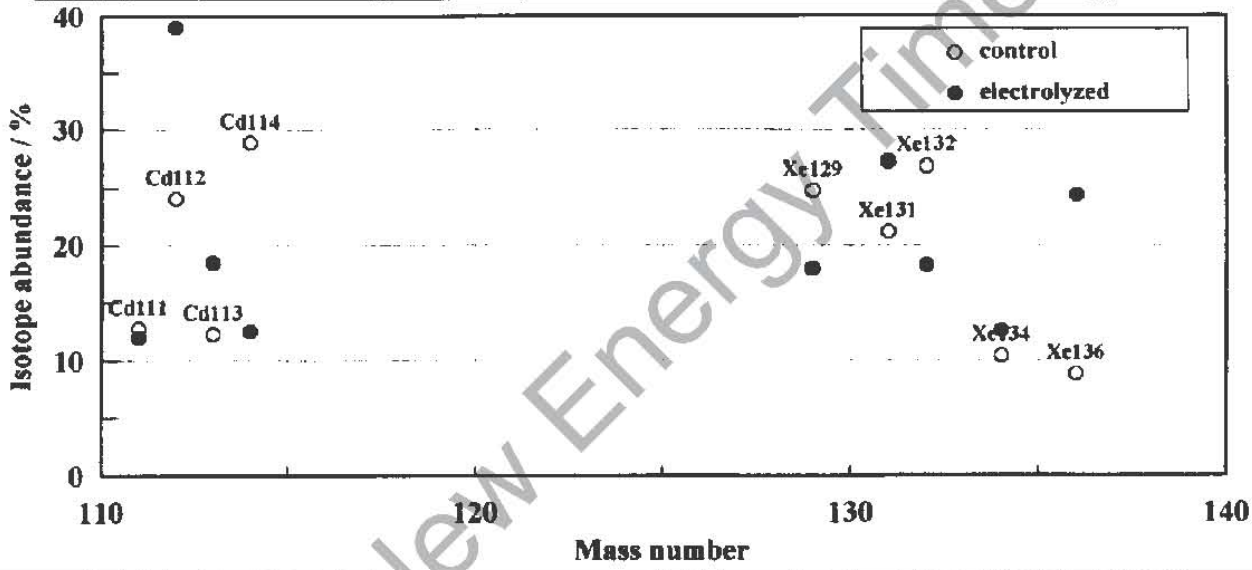

Fig.11 Changes of isotopic abundance of deposition on Pd

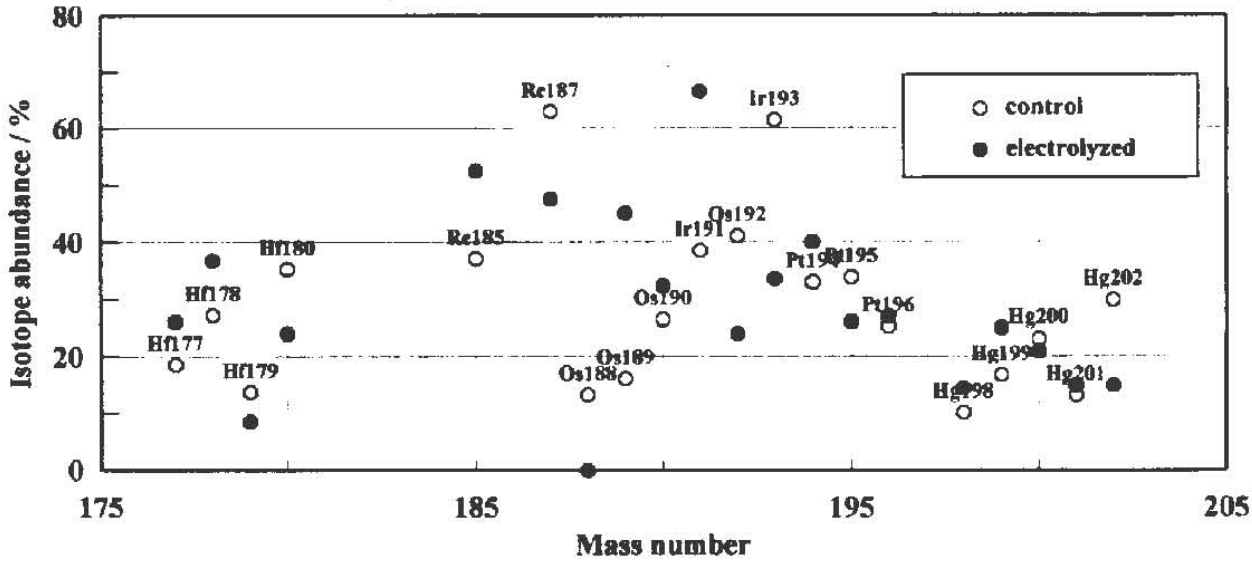

EXCESS HEAT AND UNEXPECTED ELEMENTS FROM ELECTROLYSIS OF HEAVY WATER WITH TITANIUM CATHODES

R. Kopecek and J. Dash[1]

ABSTRACT

Excess heat was produced at the rate of about 1.2 watts during electrolysis of heavy water with a titanium cathode weighing 0.0625 g. Analysis of the electrodes before and after electrolysis with a scanning electron microscope (SEM) and an energy dispersive spectrometer (EDS) revealed that new surface topographical features with concentrations of unexpected elements (S, K, Ca, V, Cr, Fe, Ni, and Zn) formed during electrolysis.

INTRODUCTION

Previously, we reported on our findings of excess heat and unexpected elements from electrolysis with palladium cathodes and an electrolyte containing either D_2O and H_2SO_4 or H_2O and H_2SO_4 [1]. We now present results of similar experiments using titanium cathodes and an electrolyte containing D_2O and H_2SO_4.

EXPERIMENTAL METHODS AND RESULTS

Pure titanium foil (0.25 mm thick, 99.99 + % Ti) was spot-welded to platinum lead wire and made the cathode in an electrolytic cell with a platinum anode and 15 ml of electrolyte containing 0.01 mol fraction H_2SO_4 (reagent) and 0.99 mol fraction D_2O (99.9 atom % D). Recombination catalyst (platinized Al_2O_3) was suspended above the electrolyte, and the cell was sealed. An identical cell containing a platinum cathode was connected in series. This cell was used as a control to measure heat effects by comparison with the titanium-cathode cell. An automated data acquisition system monitored cell voltages, six thermocouples attached to each cell (Fig. 1), and the ambient temperature. Constant current was used during the experiments.

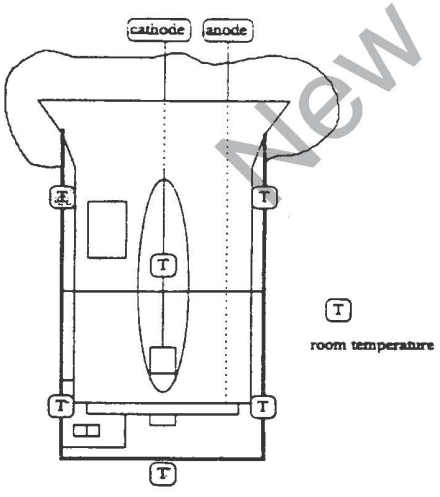

Fig. 1. Placement of thermocouples on the outsides of the control and experimental cells.

Using constant current of 0.55 A resulted in a current density of about 2 A per square cm on the titanium cathode. This current was passed for about 33.5 hours. The resulting power input and temperature-time data for each cell are shown in Fig. 2. It should be noted that the control (C) cell was taken out of the circuit after about 23 hours due to excessive loss of electrolyte.

Fig. 2a shows that the temperature of the titanium (D) cell exceeded that of the platinum control (C) cell. Fig. 2b shows that the power input to the C cell clearly exceeded the power

[1] Physics Dept., Portland State Univ, Box 751, Portland, OR 97207

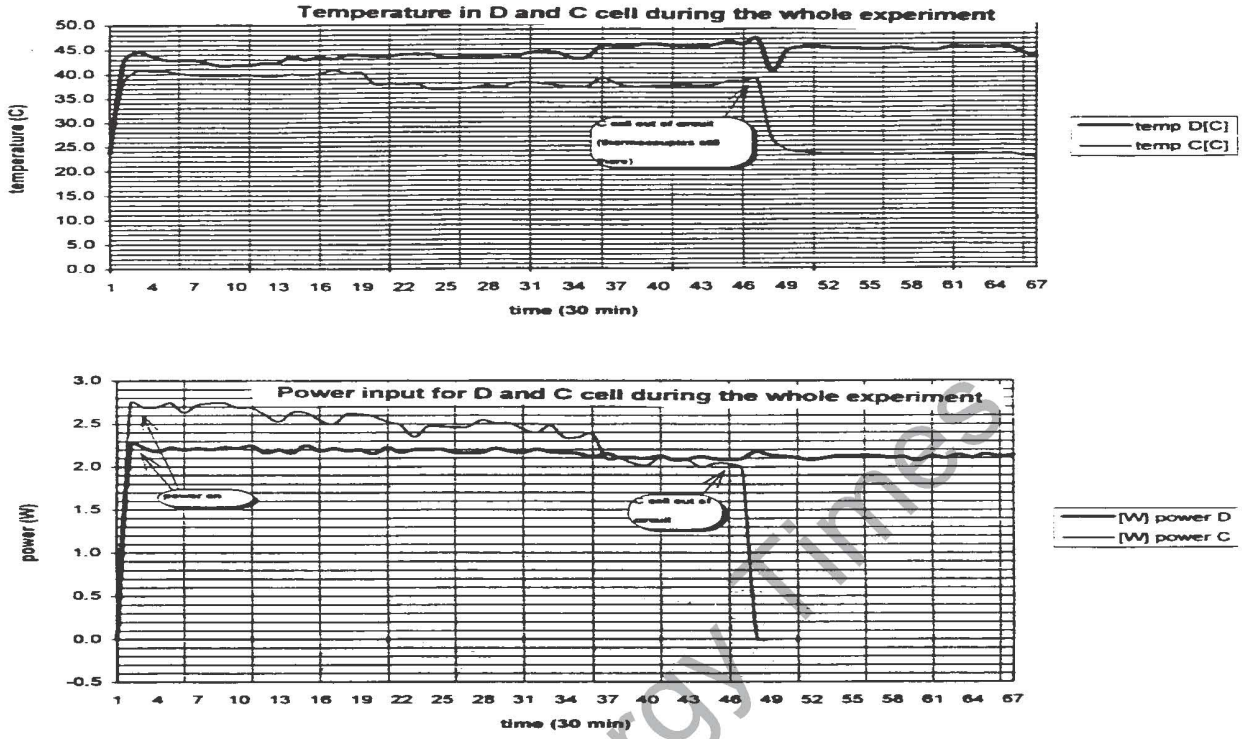

Fig. 2. (a) Temperature and (b) power versus time for the platinum-cathode control (C) and titanium-cathode (D) cells.

input to the D cell during the first 18 hours. Excess heat may have been produced by the D cell. This can be calculated by considering the power input, the heat produced by the combination of titanium with hydrogen isotopes, losses due to escape of gases through the tops of the cells, and the heat loss to the surroundings due to the thermal gradient between the cells and the surroundings.

The following equations give the rate of enthalpy change in each cell:

C (control) cell: $dH(C)/dt = IV(C) - dH(C_{esc})/dt - R\Delta T(C)$

D cell: $dH(D)/dt = IV(D) + dH(TiD)/dt + dH(XS)/dt - dH(D_{esc})/dt - R\Delta T(D)$,

where H(C) and H(D) are each the enthalpy of the C and D cells, respectively, H(TiD) is the enthalpy released by formation of TiD, $H(C_{esc})$ and $H(D_{esc})$ are each the enthalpy which escapes from its respective cell due to incomplete recombination, H(XS) is the excess enthalpy produced in the D cell, I is the constant current which

passed through both cells, V(C) and V(D) are the cell voltages, R is the rate of heat loss by each cell to the surroundings, and $\Delta T(C)$ and $\Delta T(D)$ are the temperature differences between each cell and ambient.

At steady state, which was reached in about 45 minutes, the enthalpy gain equals the enthalpy loss for each cell, so each equation can be set equal to zero. The enthalpy lost due to escape of gases is determined from the weight lost by each cell. For the C cell, this was 285 calories for the whole experiment (23 hours for the C cell), which gives $dH(C_{esc})/dt$ equal to 0.0034 calories per second. The average power input to the C cell during one hour at steady state IV(C), was 0.644 calories per second. Then the first equation is solved for R, using $\Delta T(C)$ of 16.5 C. This gives R equal to 0.0388 calories per degree C. This is used in the second equation.

About 40 calories is produced by conversion of the entire titanium cathode to TiD, so dH(TiD)/dt is about 0.0003 calories per second. I V(D) is 0.525 calories per second, $dH(D_{esc})/dt$ is 0.0012 calories per second, and $\Delta T(D)$ is 20.6 degrees C. Solving for dH(XS)/dt gives 0.28 calories per second , or 1.15 watt.

Geiger-Mueller counters were used to monitor radiation from the C and D cells throughout the experiment, and LiF chips sealed in plastic were in each cell during the experiment. The counters showed slightly higher amounts of radiation coming from the D cell, but the standard deviation was too high to have confidence in this data. The LiF chips showed no significant difference from background.

The titanium cathode was examined before and after electrolysis with SEM and EDS. Before each examination, the electrode was cleaned ultrasonically several times, each time for 5 minutes with deionized water. Fig. 3 shows that there are many changes in the surface topography. Those regions labeled a through h in Fig. 3b were examined in detail at higher magnification. A typical result is shown in Fig. 4, which is an enlargement of area e in Fig. 3b. This shows that cracking occurred along the edge of the sample. The protrusion labeled (a) gave the EDS spectrum in Fig. 5a, and point (b) gave the EDS spectrum in Fig. 5b. The protrusion shows the presence of many elements of both higher and lower atomic number than titanium. The concentrations of these elements is far higher than can be expected from the composition of the original material. In contrast to this, Fig. 5b shows that point b in Fig. 4 is almost pure titanium. Spectra similar to Fig. 5a were found in the other areas indicated in Fig. 3b.

In another, similar experiment, the current density during electrolysis was about 0.5A per sq. cm instead of 2A per sq. cm. The excess heat was about 0.5 watt for a titanium electrode from the same lot, of about the same mass. This electrode was also examined before and after electrolysis with SEM and EDS. The comparison of images is given in Fig. 6.

The double-headed arrow in Fig. 6b shows a feature which was not present on the titanium cathode before electrolysis. A portion of this feature is shown enlarged in Fig. 7. The bright spots (a) and (b) were used for the EDS spectra in Fig. 8.

DISCUSSION OF RESULTS

The results obtained with thin foil titanium cathodes are similar to those we obtained with thin foil palladium cathodes, using H_2SO_4 - D_2O electrolyte [1], in that excess heat and and unexpected elements are obtained reproducibly in both cases. A significant difference is that excess heat is observed from the very beginning of electrolysis when a titanium cathode is used, whereas there is an incubation time when a palladium cathode is used. The duration of the incubation period depends on the thickness of the Pd foil. At 0.025 mm it is about one hour, and at 0.1 mm it is about one day. The magnitude of the excess heat seems greater for titanium than for palladium under equivalent conditions.

The EDS spectra in Fig. 5a and Fig. 8a indicate the presence of chromium and vanadium. It is likely that both of these spectra contain both Cr and V because of the overlap of V Kbeta with Cr Kalpha. The chemical analysis provided by the supplier gave 0.910 ppm V and 1.150 ppm Cr, whereas Fig. 5a and Fig. 8a show concentrations of these elements more than four orders of magnitude higher. The feature which gave the spectrum in Fig. 5a may have been an inclusion which extruded above the surface due to swelling caused by hydride formation. **But the spectrum in Fig. 8a came from a surface eruption, similar to those where silver was observed on palladium [1].** Evidence of time-dependent changes in the silver spectrum which could indicate the changing of silver to cadmium was also presented [2].

REFERENCES

1. J. Dash, G. Noble, and D. Diman, "Surface Morphology and Microcomposition of Palladium Cathodes after Electrolysis in Acidified Light and Heavy Water: Correlation with Excess Heat," *Trans. Fusion Tech.*, vol 26, part 2, p 399 (1994).

2. S. Miguet and J. Dash, "Microanalysis of Palladium after Electrolysis in Heavy Water," *J. New Energy*, vol 1, no 1, Jan. 1996, pp 23-7.

ACKNOWLEDGEMENT

We are indebted to Prof. R. J. O'Brien for helpful suggestions concerning thermal analysis.

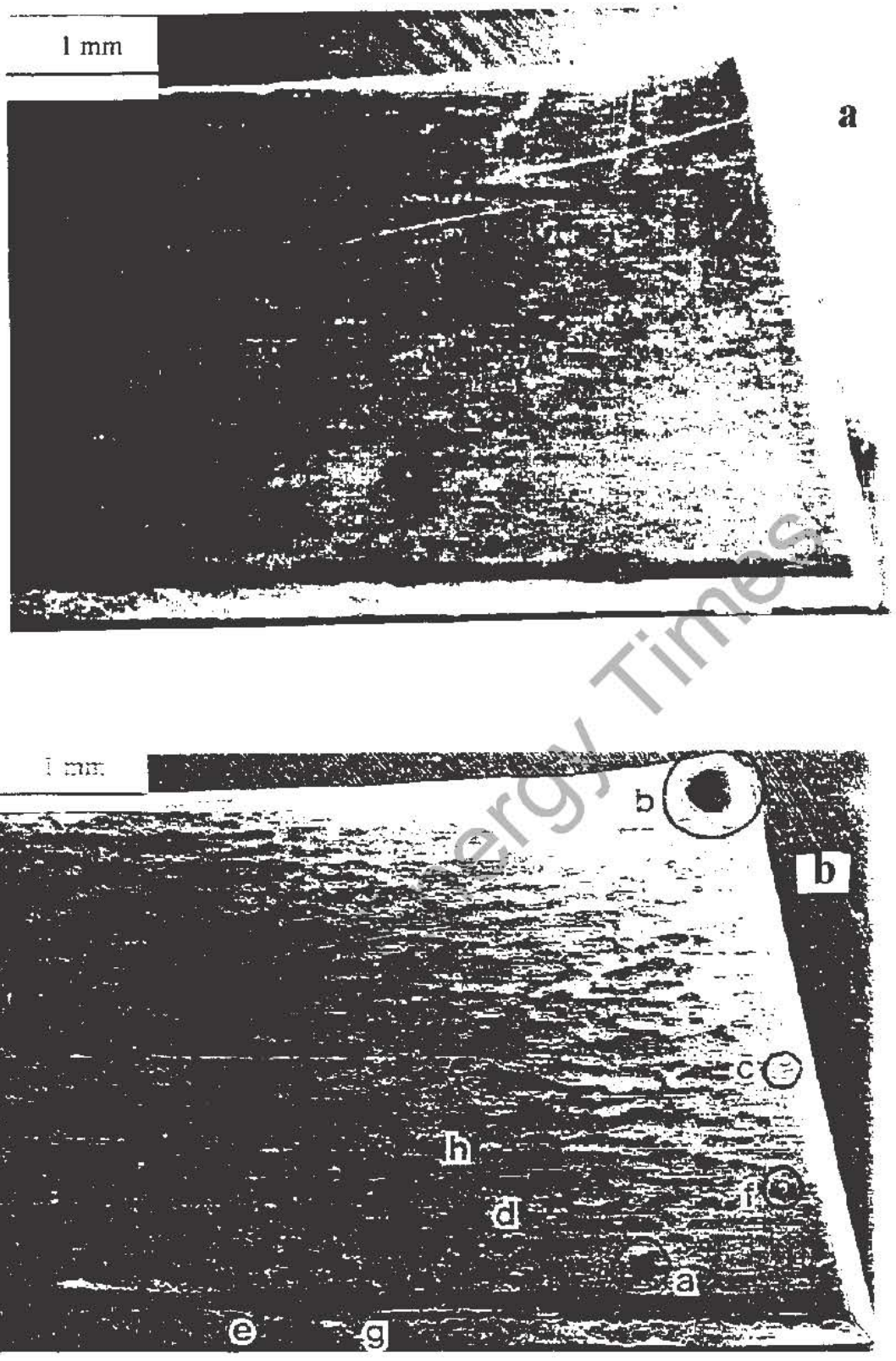

Fig. 3. Titanium cathode before (a) and after (b) electrolysis.

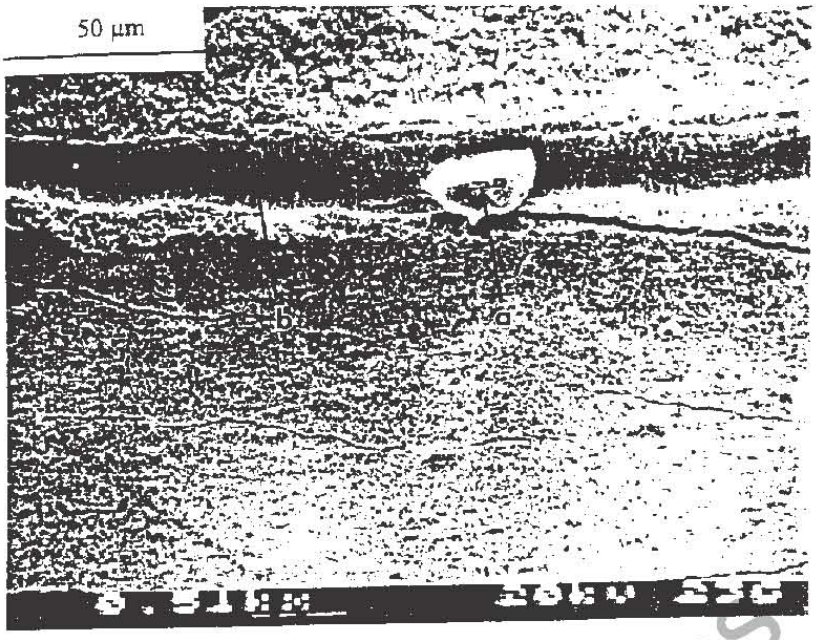

Fig. 4. Enlargement of region (e) in Fig. 3.

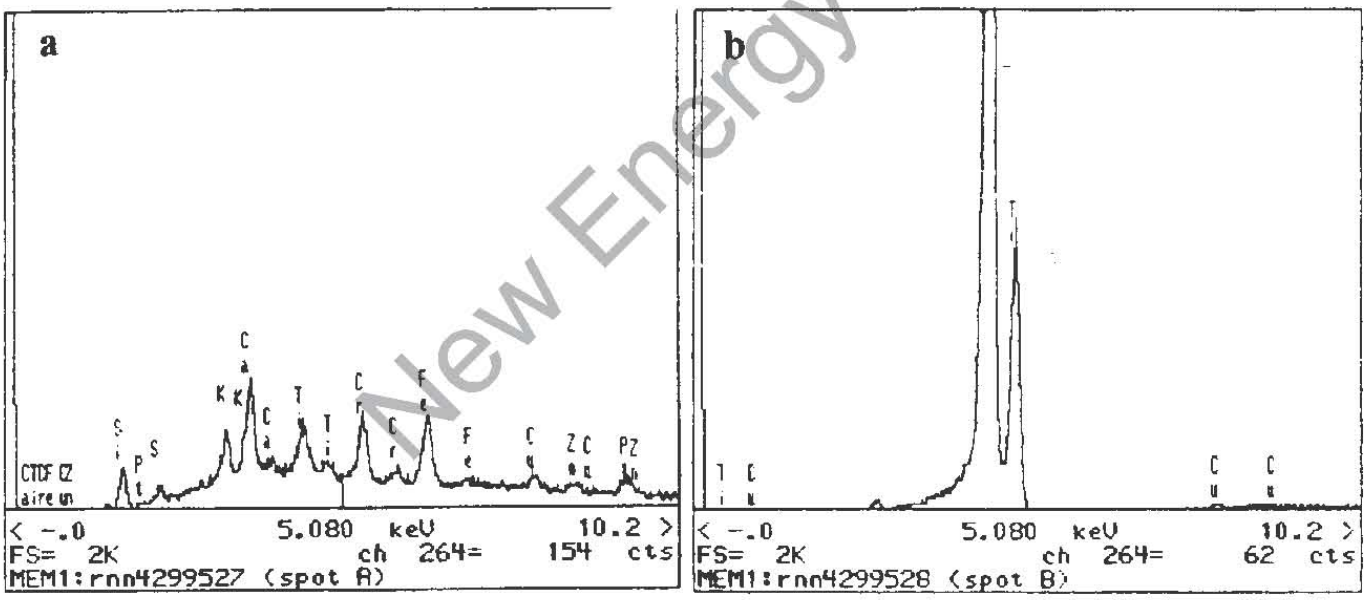

Fig. 5.(a) EDS spectrum from spot (a) in Fig. 4, and (b) EDS spectrum from spot (b) in Fig. 4.

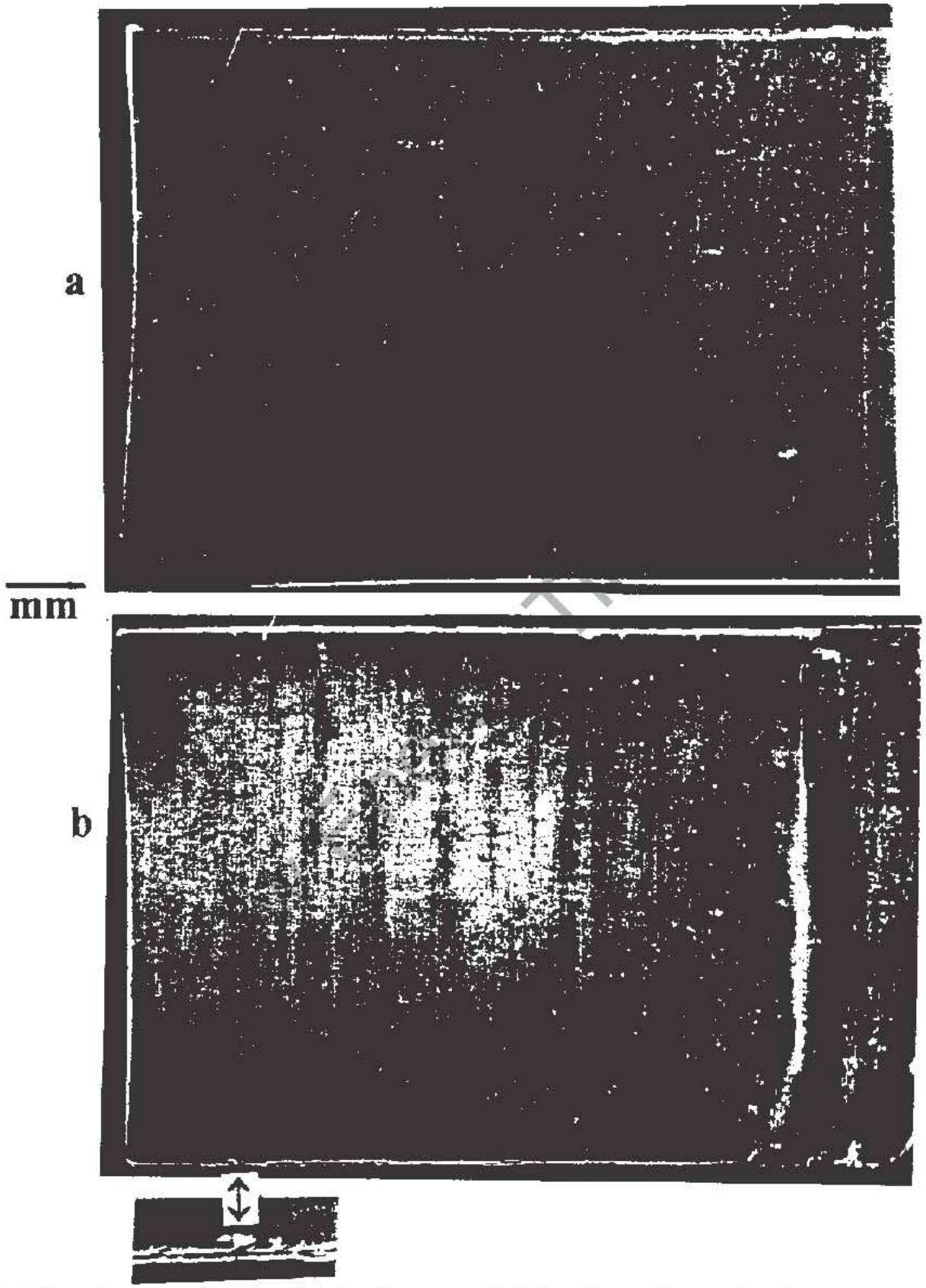

Fig. 6. Titanium cathode (a) before and (b) after electrolysis, using 0.5 A/sqcm. The arrow shows a new feature and its enlargement.

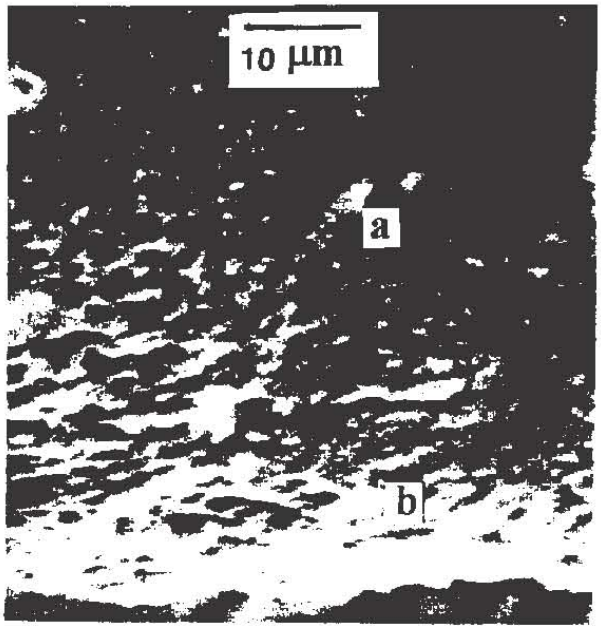

Fig. 7. Enlargement of the new feature shown in Fig. 6.

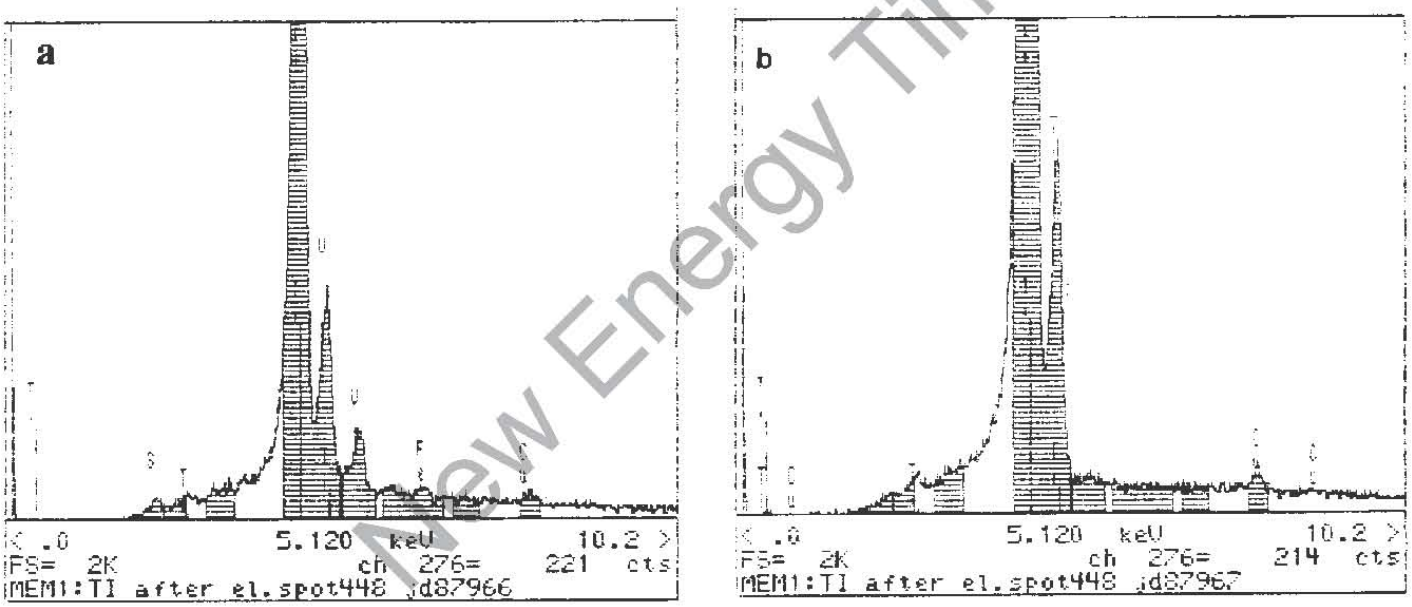

Fig. 8. EDS spectra (a) and (b) from points (a) and (b), respectively, in Fig. 7.

NUCLEAR AND THERMAL EVENTS ASSOCIATED WITH Pd + D CODEPOSITION

S. Szpak and P.A. Mosier-Boss[1]

ABSTRACT

In the Pd+D codeposition process, palladium is electrodeposited in the presence of evolving deuterium. This process favors the initiation and propagation of nuclear and thermal events through a rapid absorption of deuterium to yield high D/Pd atomic ratios. This process results in the formation of non-equilibrium electrode structures that become the seat for localized gradients. Evidence for tritium production, X-ray emanation and generation of localized heat sources, with emphasis on experimental methodology, is provided. The active role of the electrode/electrolyte interphase in the development of these events is examined.

1.0 INTRODUCTION

The main obstacle in accepting that nuclear and thermal events can, and do, occur during electrochemical compression of the Pd/D system was, and still is, their poor reproducibility. The lack of sound theoretical guidance is the primary reason for this difficulty. An experimental approach to resolve this situation rests with the construction of the "performance envelope," *i.e.*, the listing of all factors contributing to the initiation and propagation of these events. In particular, one must consider changes that take place as the concentration of deuterons rises to be *ca* 100 molar with even higher concentration of electrons (*ca* 1000 molar) [1]. Consequently, in an attempt to construct the "performance envelope" one must examine the state of the Pd/D system as the D content increases, with emphasis on interfacial and transport phenomena.

1.1 Triggering conditions.

A review of published material indicates that the triggering conditions fall into three categories: (i) high D/Pd atomic ratio, with D/Pd > 0.85, (ii) metallurgical aspects of the electrode material, such as grain size, number and kind of defects, the presence of voids and fissures, *etc*., and (iii) electrochemical aspects, *eg*, the structure of the electrode/electrolyte interphase.

2.0 THE Pd+D CODEPOSITION PROCESS.

The codeposition process is a process of palladium electrodeposition from a Pd^{2+} salt solution onto a substrate which does not absorb deuterium, *eg*, Au or Cu [2]. The applied cell current or potential are adjusted to deposit the Pd film in the presence of evolving deuterium. The advantage offered by the codeposition process rests with the morphology of the Pd electrode. The Pd electrode exhibits a "carpet-like" appearance, *ie*, the structure that assures locally a non-uniform distribution of current density and/or overpotentials as well as a very rapid and high absorption of deuterium [3]. Simultaneous evolution of gas bubbles introduces an additional component, namely, a source of random distribution of localized gradients (electrical, mechanical and chemical).

[1] Naval Command, Control and Ocean Surveillance Center, RDT & E Division, San Diego, CA. Author to whom correspondence should be addressed: E-mail address bossp@nosc.mil

3.0 RESULTS

The effectiveness of the codeposition technique with regard to the generation of nuclear and thermal events was demonstrated during the initial phase of our investigation [2]. Early results confirmed excess enthalpy production and X-ray emission. The excess enthalpy was deduced from the temperature difference, namely, higher temperatures were measured on the working electrode than in the electrolyte. The X-ray emanation was recorded on a photographic film placed in close proximity to the Pd electrode. Also, the concentration of tritium in the electrolyte phase was found to be substantially higher than expected from the known value of the separation factor.

These qualitative results were questioned on grounds of not being realistic. Typically, radiographs were not considered to be proof of electromagnetic radiation because they might result from mechanical or chemical interactions. Higher temperatures of the Pd electrode were attributed to the presence of a resistive film rather than a heat source. To prevent such criticisms, we developed a quantitative treatment which we present here in the following order: tritium generation rates, X-ray spectra and the thermal events associated with the Pd+D codeposition.

3.1 Tritium generation rates.

Details of the experimental arrangement, analytical procedure and modeling are given in [3]. Here, only essential points are presented in the condensed form.

3.1.1 Experimental arrangement and error analysis. Experimental arrangement and the sampling profile are shown in Fig. 1a and Fig. 1b. The electrolysis was under galvanostatic control and the sampling routine allowed for the accurate determination of the electrolyte volume and composition at the beginning and end of each time period. Error analysis involved the assessment of the precision of measurements in electrolyte volume, sampling/addition time intervals, constancy of cell current and tritium analysis. The typical error of ± 1.2 dpm (in Fig. 2 and Fig. 3) is not the statistical error of counting but the cumulative uncertainty due to the propagation of errors as determined by procedure commonly used in the treatment of experimental data.

3.1.2 Modeling. In a closed system, the concentration of deuterium in the electrolyte phase is computed by solving Eqs. (1) and (2)

$$d(fm)/dt = \sum f_n r_n + q \tag{1}$$

$$dm/dt = \sum r_n \tag{2}$$

where f is the tritium mass fraction, m denotes the mass of electrolyte, r is the rate of mass change and q denotes the rate of tritium produced during the electrolysis and subsequently transferred out of the Pd electrode. The subscript n identifies the relevant process.

The solution of Eqs. (1) and (2) for an open system with $r_1 = 0$, $r_2 = 0$ and constant q over the time interval Δt, is

$$\frac{f(t)}{f(0)} = \left[\frac{m(0) - r(i)\Delta t}{m(0)}\right]^{s-1} + \frac{q}{f(0)(s-1)r(i)}\left\{1 - \left[\frac{m(0) - r(i)\Delta t}{m(0)}\right]^{s-1}\right\} \tag{3}$$

where s is the isotopic separation factor defined here as the T/D atomic ratio.

3.1.3 Tritium distribution. Tritium generation rates are estimated by curve fitting technique or by computer modeling in which an arbitrarily selected q-value is inserted into experimental data and computer matched to obtain agreement with the observed distribution throughout the duration of the experiment. The essential difference between the method employed here and elsewhere is in the determination of the numerical value of the separation factor, s. This number is usually taken from the literature and may, or may not, represent the kinetic and thermodynamic properties of the interphase pertinent to the experimental conditions. Here, the value of the separation factor is determined for each experimental run by selecting that value which best fits the recorded data.

Examples of tritium production and distribution paths are illustrated in Fig. 2 and Fig. 3. In particular, Fig. 2a shows two active periods (4/21 - 5/3 and 5/19 - 5/21) separated by two weeks of inactivity. The computed (solid circles) and experimental points (open circles) for the indicated sampling and current profile, suggest that tritium produced in the course of electrolysis, first entered the liquid phase with its distribution governed by the electrodic reaction with s = 0.68. By inserting in Eq. (3) the following production rates: $q_1 = 4 \times 10^3$, $q_2 = 3 \times 1O^3$, $q_3 = 3 \times 10^3$, and $q_4 = 7 \times 10^3$ atoms/second, an excellent agreement between calculated and observed (experimental) points is obtained., Fig. 2b.

A quite different path is illustrated in Fig. 3, where the tritium distribution favors the gas phase, *ie.* where the distribution is not governed by the electrodic reaction. A direct transfer to the gas phase suggests an intense reaction occurring within the subsurface layer(s) with tritium desorption followed by recombination of D_{ads}. The basis for this conclusion is the enrichment of the liquid phase only, *i.e.*, it follows the calculated concentration by Eq. (3) with the separation factor s = 0.67.

3.2 Detection of soft X - rays.

The radiograph obtained early in the investigation [2] suggested the presence of a weak source of the electromagnetic radiation, most likely soft X-rays. In support of this interpretation as well as to provide additional information, we employed two detectors operating simultaneously, *viz.*, the Si(Li) for the X-rays and the Ge for γ rays. The background radiation was continuously monitored by the NaI(TI) detector.

3.2.1 Experimental procedure. The experimental program consisted of three tasks: (i) the assessment of the background radiation over the period of several months, (ii) design of an experimental procedure capable of detection low level radiation and (iii) computer simulation. The detailed description can be found in [5].

3.2.2. Presentation of data. The overview of the radiation intensity (count rate) recorded by the Ge detector (spectral region: 15 - 3000 keV) during the D_2O electrolysis on Pd electrodes with two vastly different surface morphologies is presented in Figs. 4a and 4b for the "carpet-like" and smooth surfaces, respectively. It is seen that the count rate is somewhat higher on "carpet-like" surfaces. More interesting, however, are the initiation times. In the first case, no initiation time was required; in contrast, a few days of electrolysis were needed to observe the same effect on smooth surfaces.

Further confirming evidence of electromagnetic radiation is provided in Fig. 5 where two independently operated detectors simultaneously recorded statistically significant increases in radiation (see section labeled II). It is noteworthy that the external field (high overpotentials) is instrumental in producing higher density of events that generate the X-ray emission.

The X-ray intensity data show a remarkable similarity to the tritium production. In both cases, surface morphology dominates the behavior. In particular, on "carpet-like" surfaces reactions are immediate while longer times are required on smooth surfaces.

3.2.3 Spectrum synthesis/modeling. The X-ray data presented in Fig. 6 were interpreted as resulting from the superposition of weak peaks upon a featureless background, e.g., the sharp peak of Pd K_α superimposed upon the bremmstrahlung arising from the oscillating plasma of the cathodically polarized Pd/D system. In support of this conclusion, we created a synthetic spectrum, Fig. 7, consisting of the featureless spectrum of thorium oxide and added to it the X-ray spectrum of americium. The resulting composite is similar in appearance to that recorded, i.e., being consistent with the experimental spectrum.

3.3 Thermal events

An almost immediate occurrence of nuclear events in the course of codeposition (tritium production, X-ray emission) suggests a much simpler approach to the accurate determination of excess enthalpy production. Short initiation times indicate that the calorimeter with quasi-adiabatic walls might be suitable.

3.3.1 Cell/calorimeter modeling. The development of governing equations for an operating electrochemical cell employs the conservation laws (energy and mass) and adjusts the applicable walls and constraints in a manner that is consistent with the cell-design relevant experimental procedure [7]. Applying the conservation of energy (in the enthalpy representation), the time rate of the temperature change after its activation is

$$C^{(1)}dT^{(1)}/dt = Q^{(1)} - j_q^{(1-2)} - J_q^{(1-e)} \tag{4}$$

$$C^{(2)}dT^{(2)}/dt = Q^{(2)} - J_q^{(2-1)} J_q^{(2-e)} \tag{5}$$

where $C^{(1)}$ and $C^{(2)}$ are heat capacities of the electrolyte and bath, respectively; $Q^{(1)}$ denotes the time rate of heat generated in the electrolyte while $Q^{(2)}$ is the rate st which the heat is supplied to the bath in order to maintain equality of the temperature in the cell and the bath; the J_q's are the heat fluxes exchanged between the electrolyte, bath and environment. Employing for the thermal flux an expression of the form $J_q = k\Delta T$ and introducing new variables $\Delta T = T^{(1)} - T^{(2)}$ and $\theta = T^{(1)} - T^{(e)}$, after some manipulation combined with a reasonable assumption, (e.g., low $Q^{(1)}$) , we obtain an equation of the form:

$$\frac{d\Delta T}{a - b\Delta T} = dt \tag{6}$$

which, upon solution, yields information concerning best experimental design and procedure.

3.3.2 Survey of thermal events. An example of the excess enthalpy production within the polarized Pd/D system is shown in Fig. 8, where the excess enthalpy, $0.239C^{(1)}\Delta T^{(1)} - \int_{\Delta t} I(E_c - \epsilon E_h)dt$ (y-axis) is plotted against the enthalpy input, $\int_{\Delta t} IE_c dt$ (x-axis). In the absence of excess enthalpy production all points would fall on the x-axis while excess enthalpy places these points above the x-axis. Inspection of Fig. 8 reveals two distinct time intervals. Within the first time interval, the points are located below the x-axis because within this time period the faradaic efficiency is less than that part of the cell current which is used for the reduction of Pd^{2+} ions.

A review of data indicates that the rate of excess enthalpy production is not uniform in time or position. When the electrode surface is viewed with an infra red camera [8], we notice a chaotic appearance and disappearance of hot spots which subsequently merge to form larger oscillating islands. **These spots indicate intense, localized heat sources acting for very brief periods of time.**

4.0 Discussion.

While the excess enthalpy production was attributed to nuclear reactions, the direct evidence for nuclear activities was provided by tritium production and further supported by radiation of soft X-rays. The lack of data for two

or more signatures of nuclear activities, simultaneously collected under rigorously controlled experimental conditions, is the weakest link.

A review of observations made during, and following, the codeposition process, show a common thread, namely, unpredictable (with regard to time and position) initiation, uncontrolled periods of activity, and a common response to additives, e.g., Be^{2+} or Mg^{2+} ions. However, the most unusual behavior was noted when the polarized Pd electrode surface was viewed with an infra red camera. These observations point clearly to the importance of the dynamics of the interphase region and its role associated with the transport of deuterium from the adsorbed to absorbed state. In our discussion we examine the proposed models of the inter-phase, the nature of the driving force, and the possible interplay between the various species or their energetic states.

4.1 The interphase.

The interphase region is a layer separating two homogeneous phases: the metallic electrode and liquid electrolyte. For the thermodynamic consistency this layer is viewed as a non-autonomous phase [8]. The solution side of the interphase is well understood, the metallic part has only recently been subjected to comprehensive examination. In particular, the effect of catalytic poisons on the H-population of the interphase was examined with the emphasis on the hydrogen evolution reaction rather than on the interfacial transport. A number of models have been proposed [8-14]. All contain a common feature, namely the accumulation of hydrogen in the subsurface layer. Experimental evidence, e.g., immediate formation of the ß - phase indicates rapid absorption [15]. The entrance of hydrogen into the subsurface layer is associated with swelling resulting in a "modular-like" structure [12].

4.2 Driving forces.

A model that shows a qualitative agreement with experimental data was constructed [15]. This model predicts small asymmetry in loading and unloading; it does not, however, account for changes as large as actually observed [16]. Natural forces driving the deuterium evolution reaction as well as the transport into the Pd electrode interior is the chemical potential, $\mu = \frac{\partial U}{\partial n} | s,v$. The chemical potential of the adsorbed hydrogen and its role with regard to the hydrogen evolution reaction was recently discussed by Jerkiewicz et. al., [13,14] and that of dissolved hydrogen by Wagner [17] with further extension to include high hydrogen content, by Brodowsky [18]. It is the chemical potential of species populating the interphase that is of interest in formulating the "performance envelope." However, the difficulty is in the specification of the internal energy as a function of position within the interphase formed between the polarized Pd electrode with high D content and the electrolyte.

A more realistic model incorporating an active interphase is needed. An approach currently under considerations in this laboratory, is to examine the nature of the driving forces operating in the course of charging/discharging of the polarized Pd electrode.

4.3 Thermal instabilities.

Thermal events occurring during the electrochemical compression of the Pd/D system were, and are, discussed in terms of excess enthalpy produced over a period of time, often several days. Thus, they represent an average value and provide no information on the distribution of heat sources. **However, if the surface of the polarized Pd electrode is viewed with an infra-red camera, it reveals the presence of randomly distributed (in time and space) heat sources of short duration.** This observation is consistent with ideas advanced recently by Fleischmann et. al. [19], that of expressing the heat generation in terms of a number of time dependent variables, $Q = f[E(t), \theta(t), ...X(t)]$. Some of these variables can be controlled by an experimenter, others cannot ("hidden

variables"). Because these variables are interconnected, they can lead to the development of instabilities which, in turn, may or may not be modified by imposing feed-back controls. A much simpler picture can be presented if (i) events take place within the interphase (*ie* subsurface layers), (ii) that the interphase is a non-autonomous phase and (iii) that the adsorbed deuterium travels across the interphase. This is the direction that we contemplate at this time.

5.0 Concluding remarks

An alternate method for the examination of the Fleischmann-Pons effect is the use of the codeposition technique. Employing this method for the electrochemical compression of the Pd/D system, we established as follows:

(I) Emission of soft X-rays.

(ii) Tritium production at rates ranging from 10^3 to 10^4 atoms per second.

(iii) Excess enthalpy production with random distribution of reaction sites.

REFERENCES

1. C. Bartomoleo, M. Fleischmann, G. Larramona, S. Pons and J. Roulette, "Alfred Coehn and After: The α ß γ of the Palladium-Hydrogen System," *Fusion Technology*, vol 26, no 4T, Proceedings of ICCF 4, p 23 (1995).
2. S. Szpak, P.A. Mosier-Boss and J.J. Smith, *J. Electroanal. Chem..*, vol 302, p 255 (1991).
3. S. Szpak, P.A. Mosier-Boss and J.J. Smith, *J. Electroanal. Chem.*, vol 379, p 121 (1994).
4. S. Szpak, P.A. Mosier-Boss, R.D, Boss and J.J. Smith, *J. Electroanal. Chem.*, vol 373, p 1 (1994).
5. S. Szpak and P.A. Mosier-Boss, *Physics Letters A*, vol 210, p 382 (1996).
6. S. Szpak and P.A. Mosier-Boss, *Physics Letters A*, in press.
7. S. Szpak and P.A. Mosier-Boss, *J. Phys. Chem.*. submitted.
8. R. Delay, I. Prigogine and A. Bellemans, Surface Tension and Adsorption, Chapters XX and XXI, Longmans and Green, London (1966).
9. R.J. Behm, V. Penka, M-G Kattania, K. Christmann and G. Ertl, *J. Chem. Physics*, vol 78, p 7486 (1983).
10. R.V. Bucur and F. Bota, *Electrochim. Acta*, vol 28, p 1373 (1983).
11. R.V. Bucur and F. Bota, *Electrochim. Acta*, vol 29, p 103 (1984).
12. T. Ohmori, K. Sakamaki, K. Hashimoto and A. Fujishina, *Chemistry Letters* (Japan) (1991).
13. G. Jerkiewicz and A. Zolfaghari, *J. Electrochem. Soc.*, vol 143, p 1240 (1996).
14. G. Jerkiewicz, J.J. Brodzinski, W. Chrzanowski and B.E. Conway, *ibid.*, vol 142, p 3755 (1995)
15. S. Szpak, P.A. Mosier-Boss, C.J. Gabriel and J.J. Smith, *J. Electroanal. Chem.*, vol 365, p 275 (1994)
16. A.M. Riley, J.D. Seader, D.W. Pershing and C. Walling, *J. Electrochem. Soc.*, vol 139, p 1342 (1992)
17. C. Wagner, *J. Phys. Chem., A*, vol 193, p 386 (1944)
18. H. Brodowsky, *Ber. Bunsenges. Phys. Chem.*, vol 76, p 797 (1972)
19. M. Fleischmann, S. Pons, M. LeRoux and J. Roulette, "Calorimetry of the PD-D_2O System: The Search for Simplicity and Accuracy ," *Fusion Technology*, vol 26, no 4T, ICCF4, p 323 (1994)

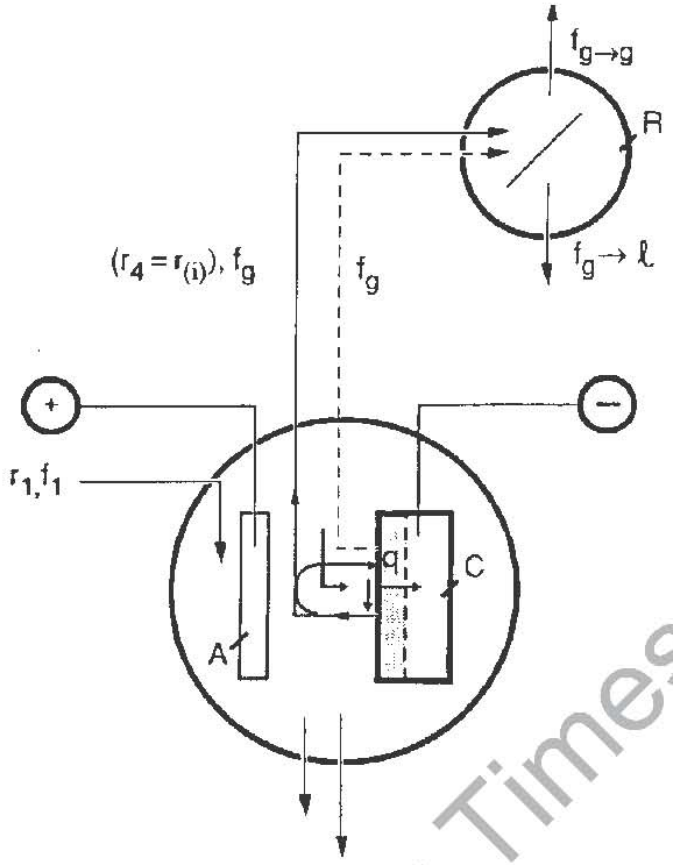

Fig. 1a - Mass balance on electrolyte.
r, rates of mass change (subscripts 1, 2, 3 and 4 indicate electrolyte addition, removal by sampling, evaporation and electrolysis, respectively); f, tritium mass fraction (subscripts g and l denote gas and liquid phases).

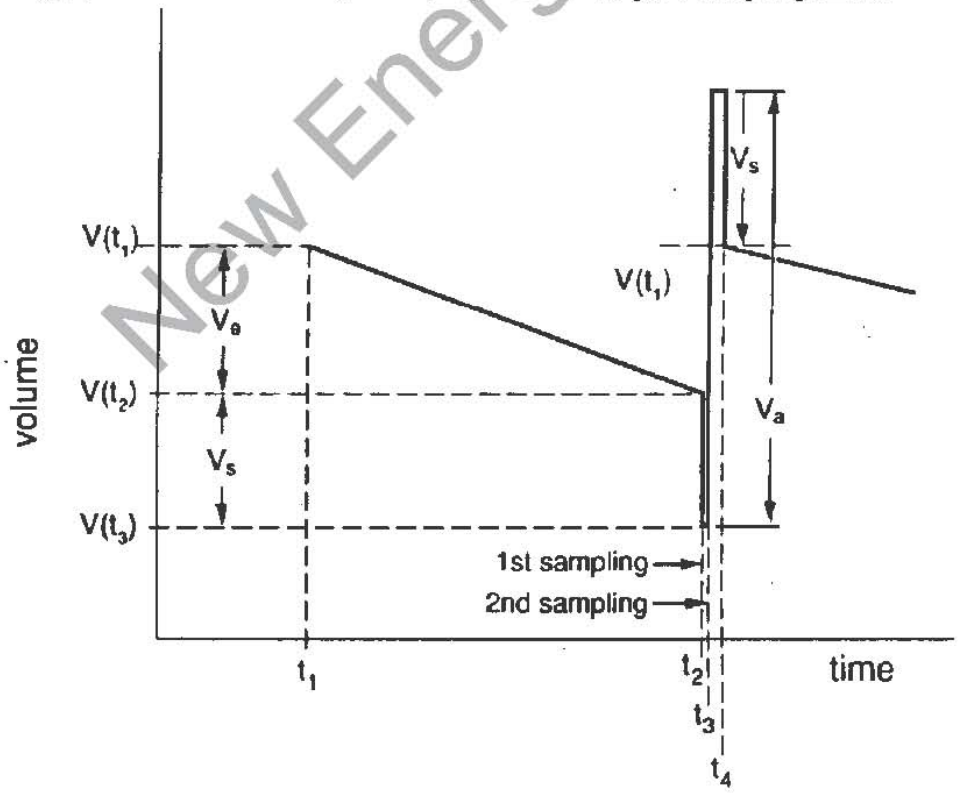

Fig. 1b - Sampling procedure for tritium generation in open cells. V_e is the volume lost by electrolysis: V_s is the sampling volume; V_a is the electrolyte volume added to restore prior conditions.

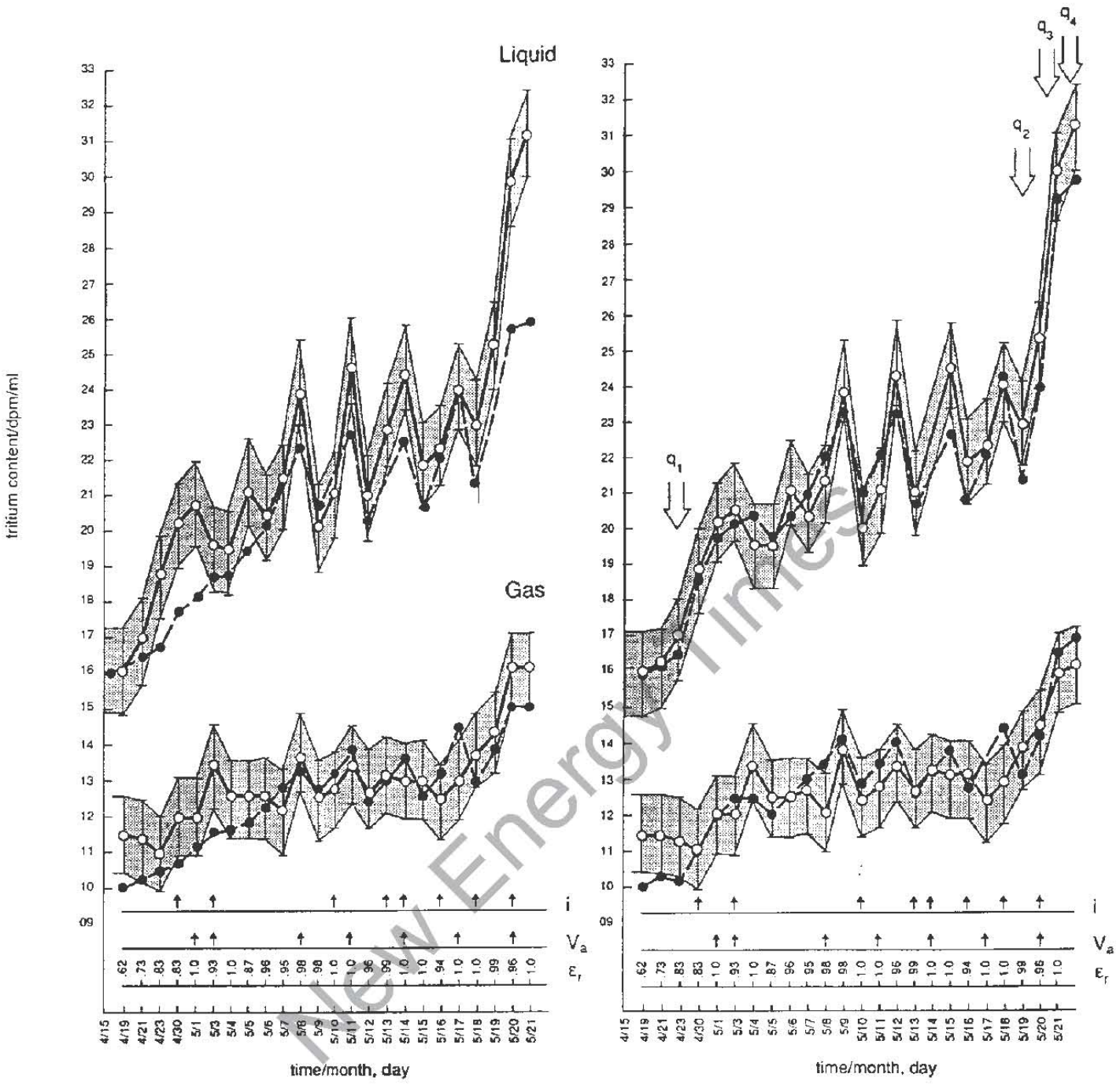

Fig. 2 - Tritium two-phase distribution. Electrode - Pd deposited from $Pd(NH_3)_2Cl_2$; Electrolyte - 0.3 M Li_2SO_4
a: recorded data; b: computer matched.

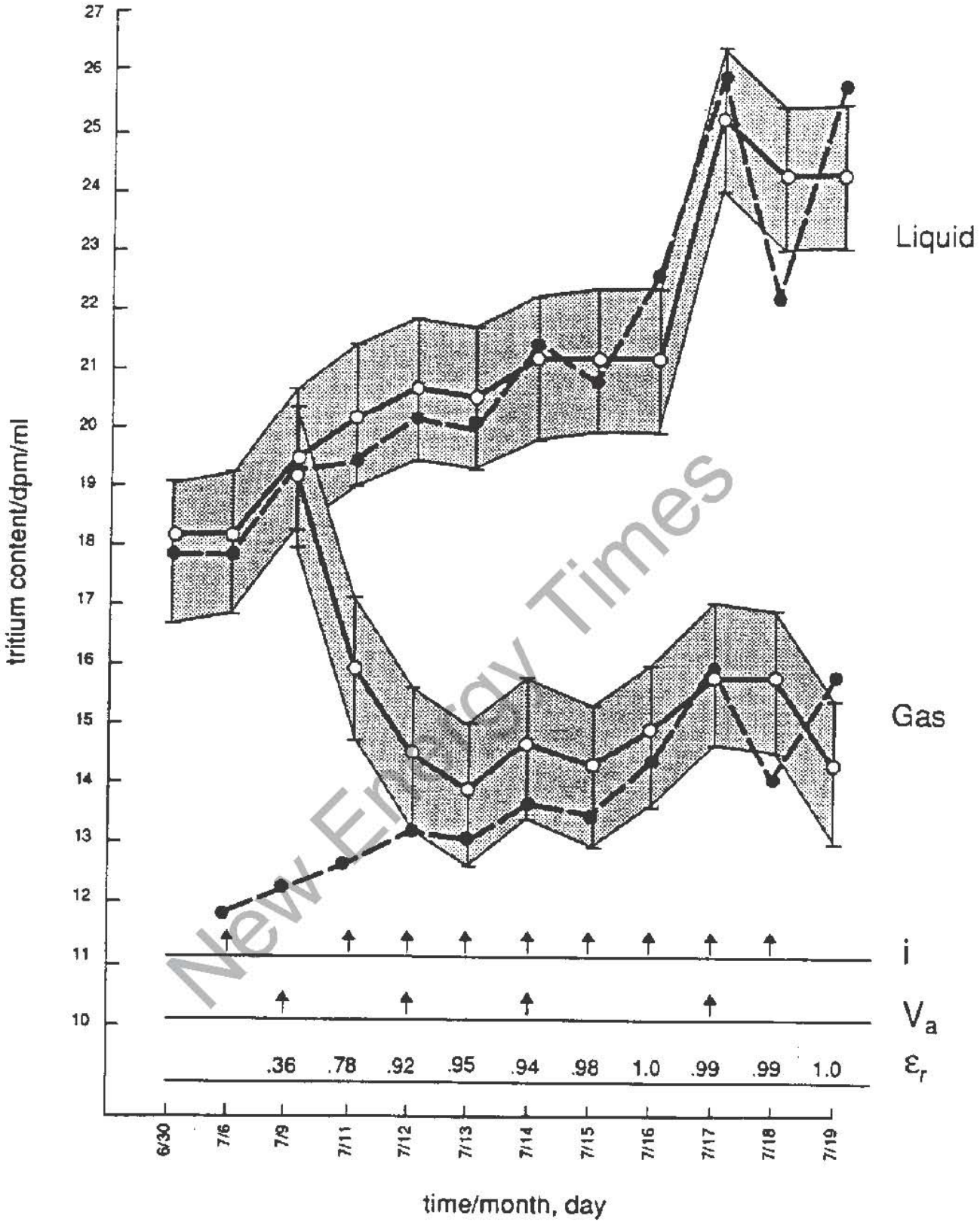

Fig. 3 - Tritium two-phase distribution during and after codeposition.
Electrolyte - 0.6 M LiCl.

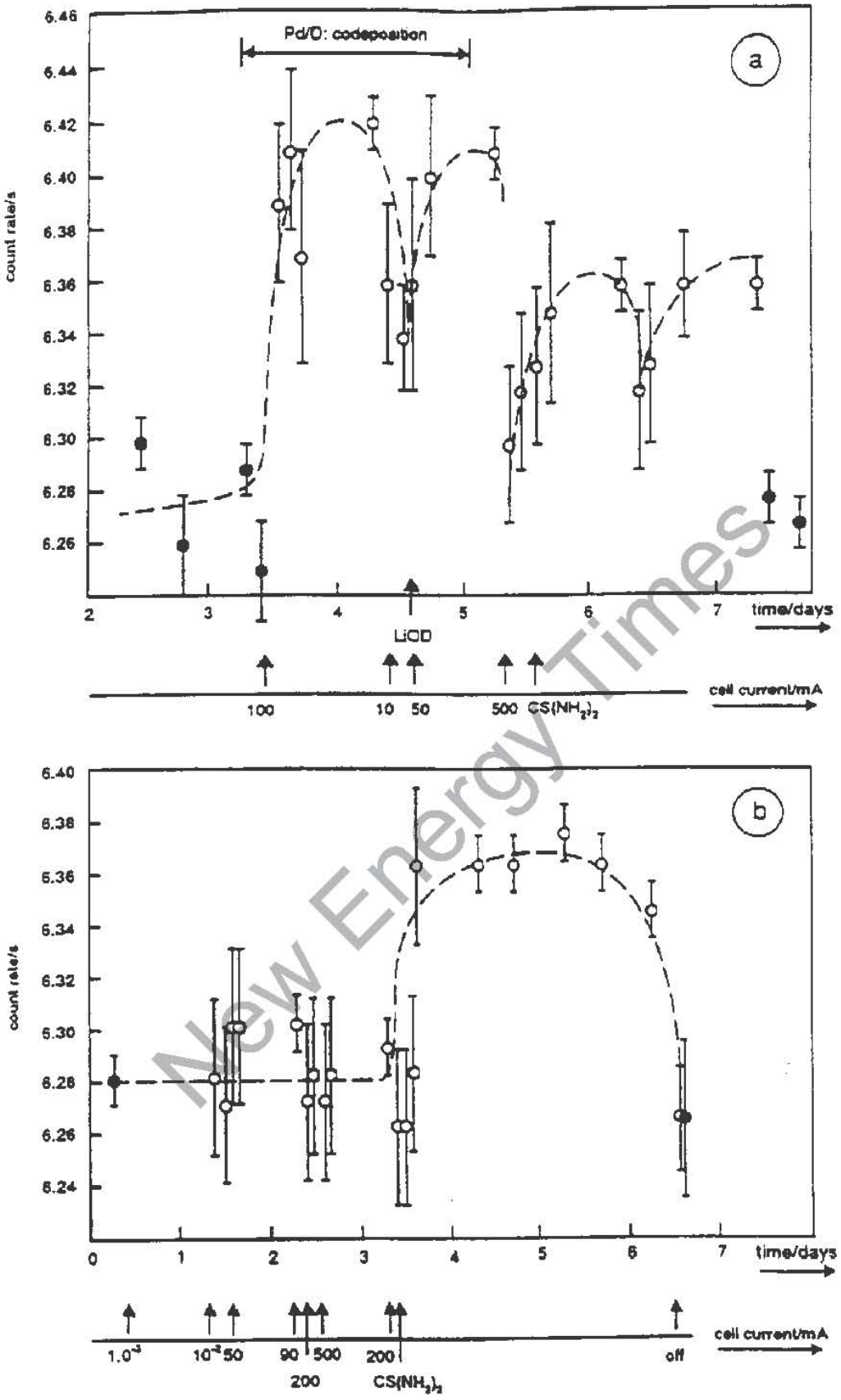

Fig. 4 - Electromagnetic flux emitted during cathodic polarization of the Pd/D system: Spectral region 15 - 3000 keV (indicated are cell current profile and additives): background - solid circles; operating cell - open circles.

Fig. 4a - Electrolyte - 0.003 M $PdCl_2$ - 0.3 M LiCi - D_2O; LiOD added after depletion of Pd^{2+} ions.

Fig. 4b - Electrolyte - 0.1 M LiOD.

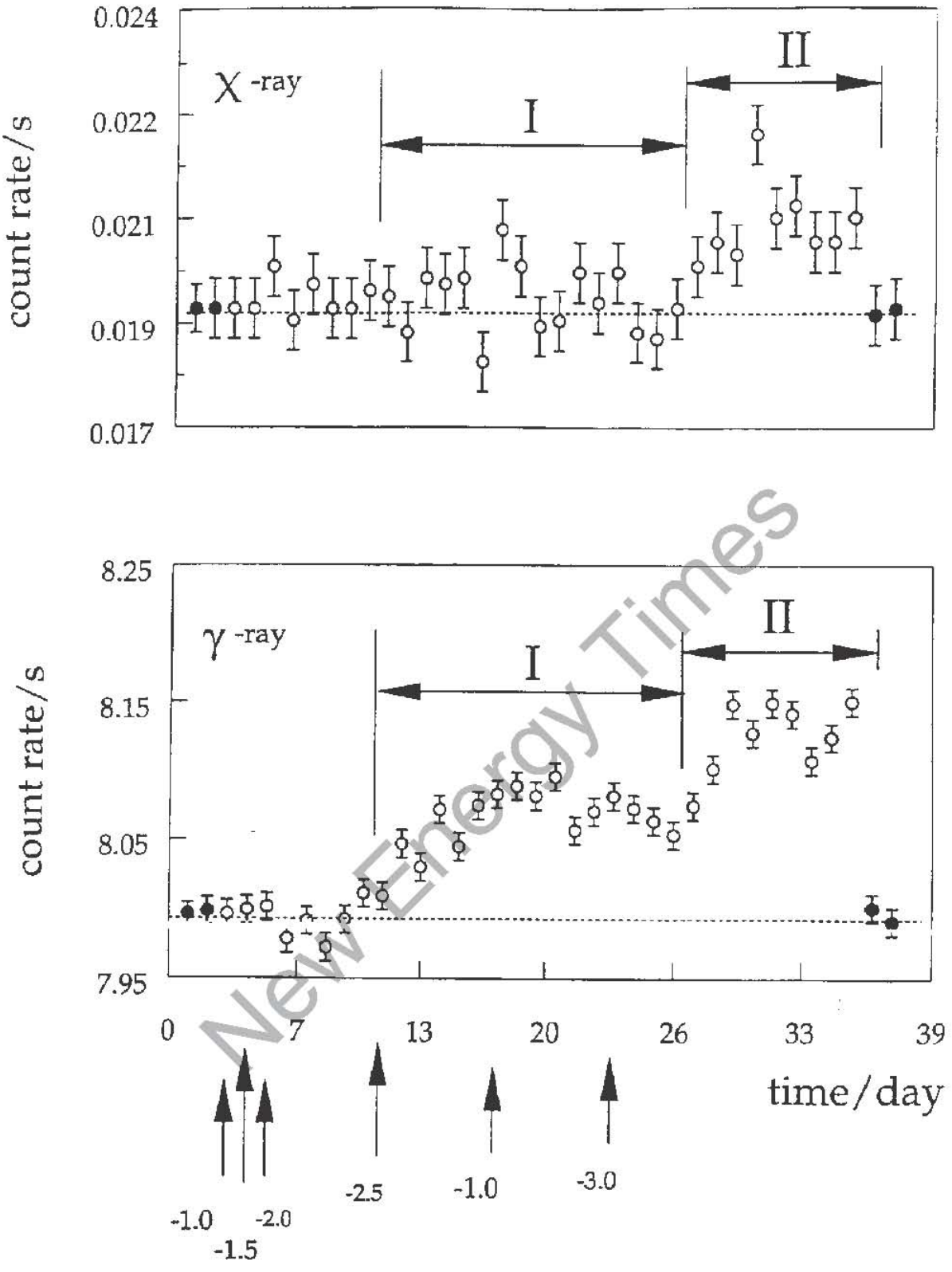

Fig. 5 - Electromagnetic flux emitted during cathodic polarization of the Pd/D system. upper - spectral region 7 - 40 keV; lower - spectral region 40 - 300 keV. Arrows indicate the applied overpotential (vs Ag/AgCl reference); background - solid circles: operating cell - open circles.

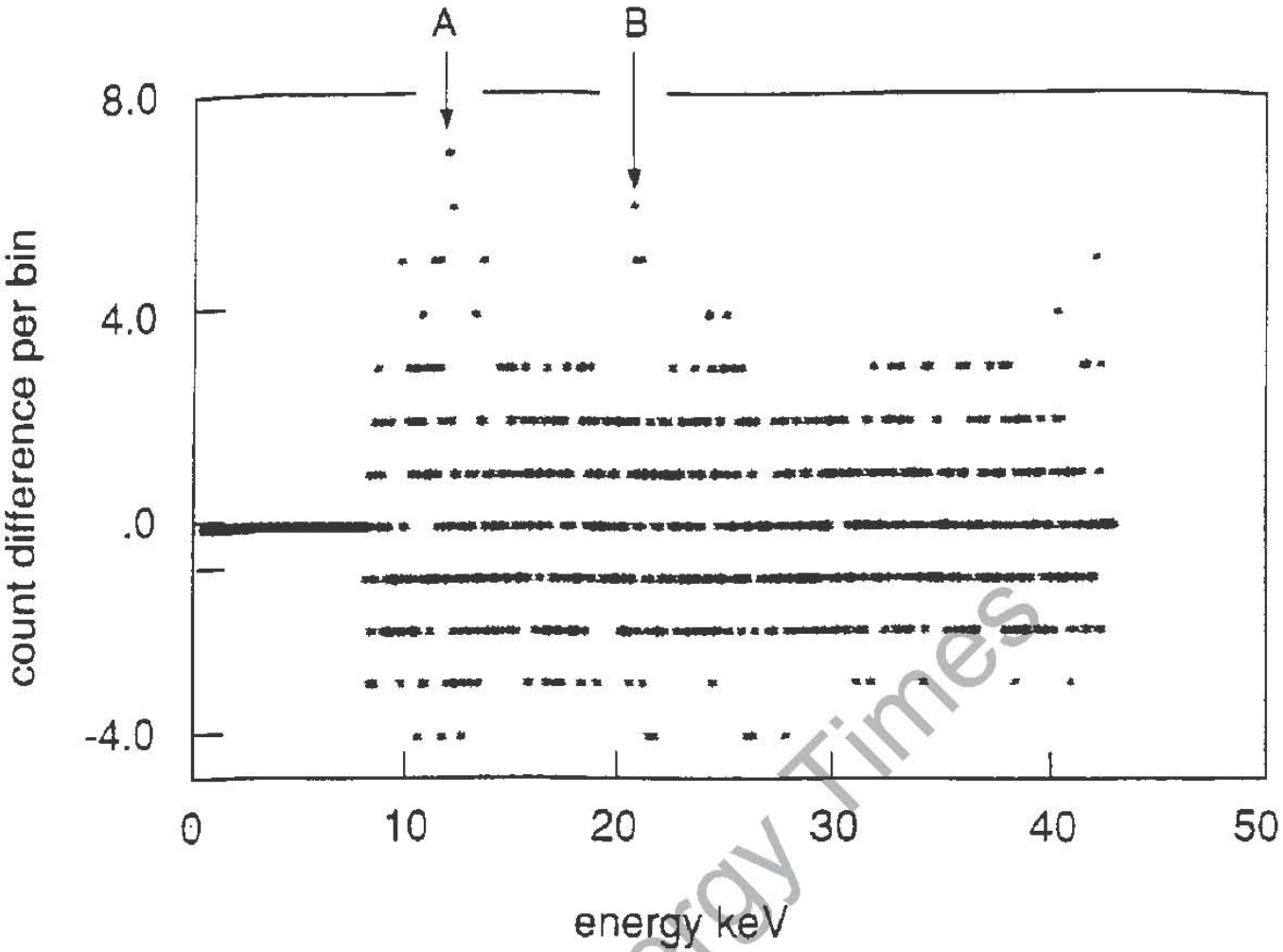

Fig. 6 - X-ray spectrum emitted during cathodic polarization of the Pd/D system. Spectral region 7 - 40 keV; background spectrum subtracted.

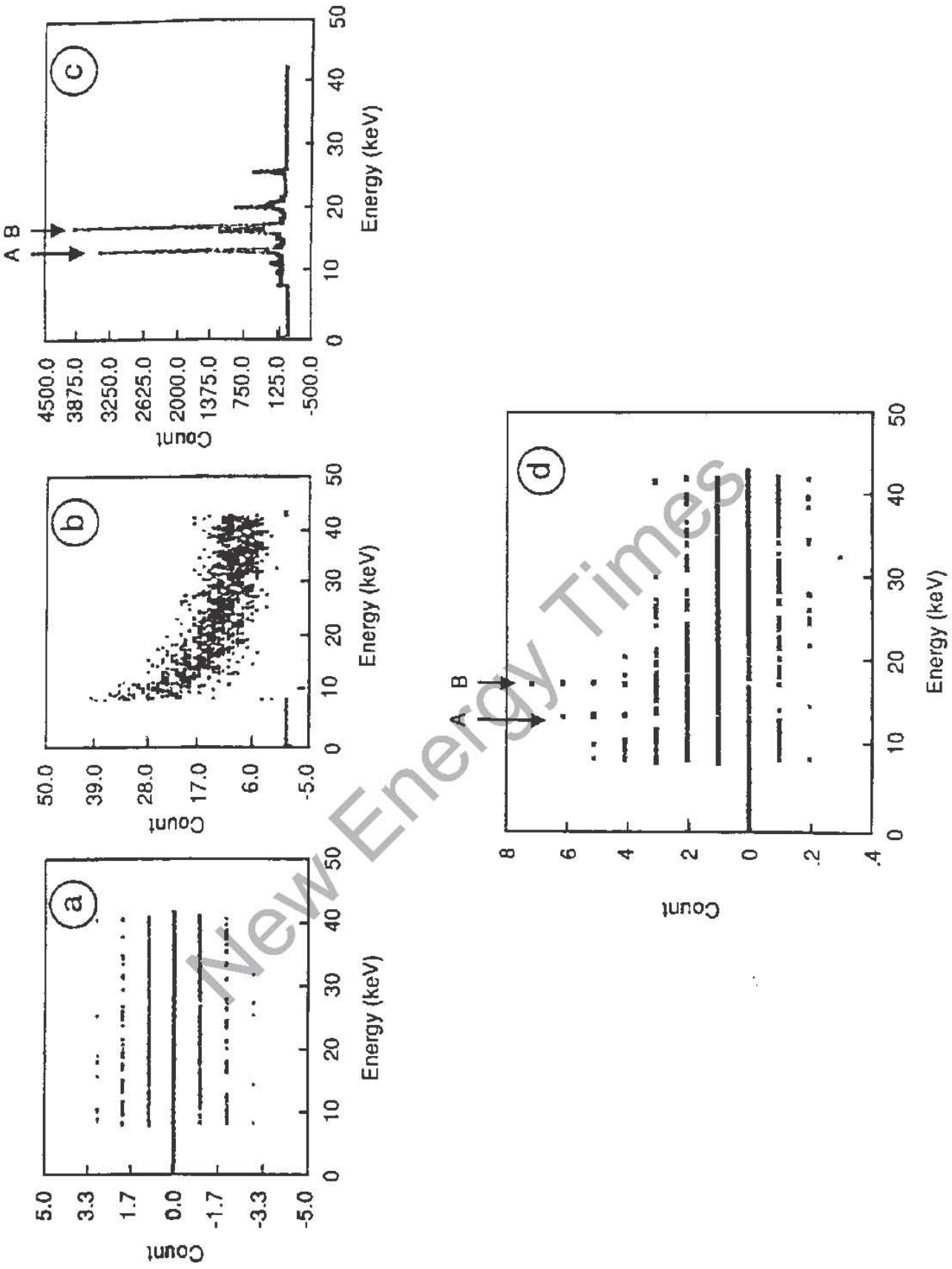

Fig. 7 - Computer simulation of the addition (superposition) of weak spectral lines to the broad distribution.
a. The difference of two background files (symmetric distribution about zero);
b - Energy distribution of the X -ray emanating from thorium oxide; c - X-ray spectrum of americium; d - Computer simulated energy distribution for a sum of 0.0015 Am spectrum and 0.02 ThO - 2 spectrum and a difference of two separate backgrounds, all normalized to a 24 hr period.

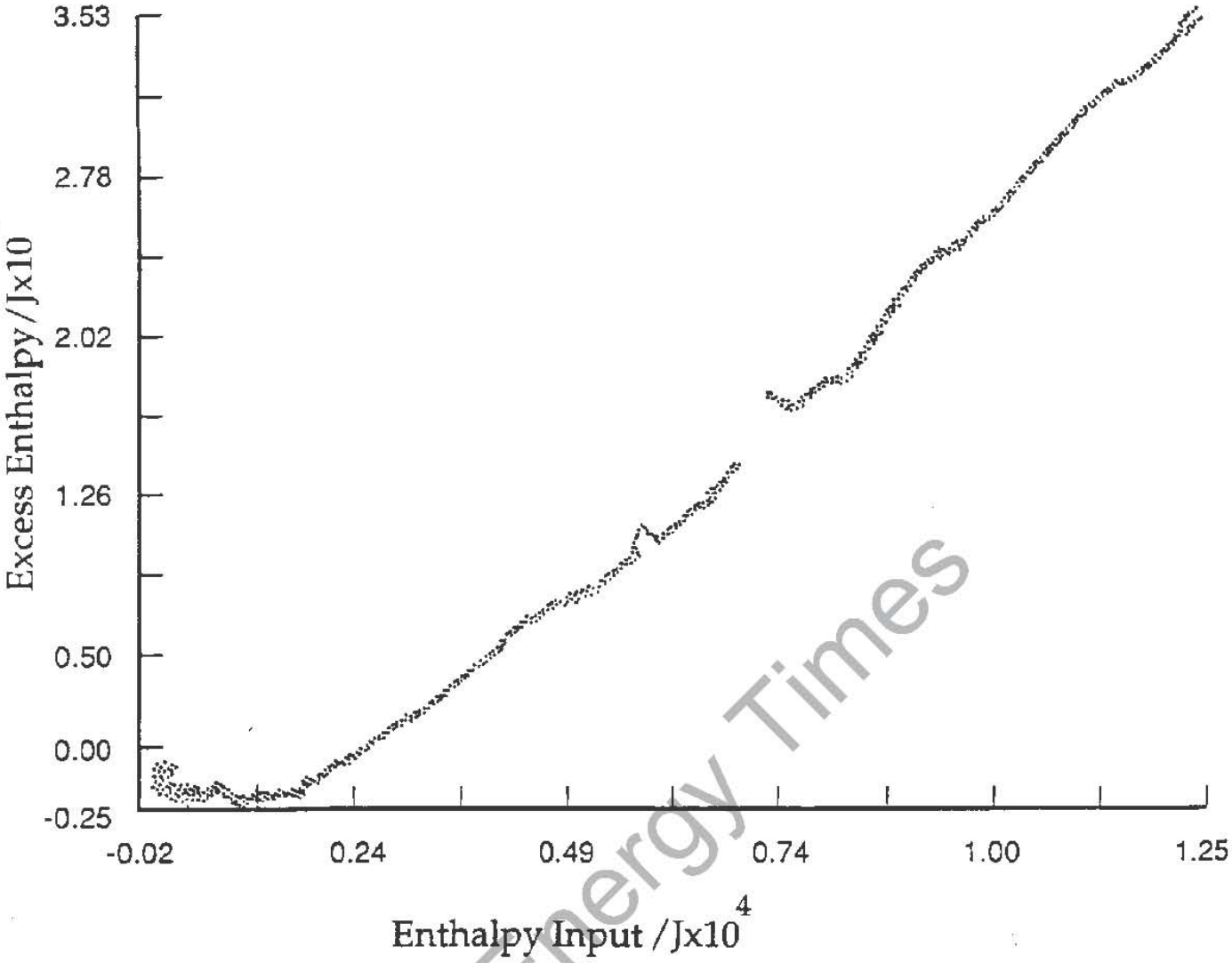

Fig. 8 Excess enthalpy generated in the course of codeposition.

POSSIBLE DEUTERIUM PRODUCTION FROM LIGHT WATER EXCESS ENTHALPY EXPERIMENTS USING NICKEL CATHODES

Mitchell Swartz
JET Energy Technology, Inc. [1]

ABSTRACT

Nickel cathodes that produced excess enthalpy during the electrolysis of light water solutions were examined serveral weeks later (metachronously) by electron emission spectroscopy. The absence of an obvious significant emitting ash might be consistent with a short-lived product, loss of the product, self-absorption, or low signal to noise, or a new fusion pathway leading to a stable ash. The latter may contribute to the excess heat as well as other researchers' reported transmutation reactions through a portion of the pathway leading to the production of *de novo* deuterons. If deuterium is a product of these reactions then its production levels, the inevitable separation factors, and present detection thresholds pose a significant challenge for its unambiguous identification.

INTRODUCTION -- EXPLANATIONS NEEDED

The deuteron is rarely, if ever, considered a possible product of cold fusion systems. Although examination of a large subset of the cold fusion literature (>840 abstracts [1]) revealed eighteen papers concerning tritium or triton production [2-19], a similar search revealed none discussing deuterium or deuteron production. This absence exists even though a pathway to its production might also explain the excess heat [20-27] and reported transmutations [3,25,26,28-30]. There must be a reasonable explanation for the excess heat and transmutation reactions. In light water nickel cold fusion systems, even purported transmutated products do not appear to be proportional to the expected ash required for the observed excess enthalpy. The anomalous branching ratio remains as problematic as the excess heat, and the lack of a theoretical model has been a major cause of the knee-jerk dismissal of this scientific field.

The coulomb barrier approach has been examined by many hypotheses but screening factors alone may not be sufficient to explain the observations, and thus the reaction pathway probably does not involve the classic collision of two particles. Several hypotheses exist including "shrunken" hydrogen [20], positron emission [31], and possible deuteron production [2]. In the case of helium produced from deuterium-loaded palladium, the Phuson theory [33] has been developed describing the multi-body reactions involving the loaded deuterons within the lattice of the fully loaded Group VIII transition metal electrode cathodically driven to ~1 kilomolar electron density. In the Phuson theory, the phonon clusters distribute energy between the excited state and the ground state, thereby conserving momentum within the palladium.

Because there does not exist a similar theory for nickel, due to the excess heat observed and the lack of a clear electron emission in these metachronous experiments, we elected to look more closely at deuterium, its production, its spin structure, and its possible role in these phenomena. This paper introduces a pathway that could yield *de novo* deuterons and explain the observed transmutation reactions. The hypothesis suggests that

energy may be transferred to the lattice through a phonon cloud (Phuson) as a non-bound virtual deuteron state collapses to the ground state configuration.

BACKGROUND -- DEUTERON STRUCTURE AND SEPARATION

Chemically, the hydrogen isotopes slightly differ in their equilibrium constants, enabling the difficult separation of deuterium oxide from ordinary water (Table 1). Although hydrogen was isolated as a distinct substance in 1766 by Cavendish, deuterium was separated electrolytically in 1932 by Urey, Brickwedde and Murphy after its spectroscopic identification one year earlier. The actual situation is complicated because of tritium and the fractional species (e.g., DTO). The fragile deuteron decomposes at temperatures cooler than our sun's core (~ million degrees Kelvin). So even though interstellar clouds and protostars contain deuterium (abundance D/H = ~1.9 {+/-0.5} 10^{-4}) evolved stars have essentially none [34-36]. Therefore, deuterium oxide (D_2O), although ubiquitous (D/H = ~1.5 10^{-4}) *in situ* within ordinary water, must be commercially refined and purified at considerable difficulty to obtain the several megaliters per year required for its use as a moderator for some nuclear reactors. The difficulty in refining deuterium arises for several reasons. The separation of the deuterium is highly endothermic, and most of the separation factors are small (Fig. 1). Deuterium is generally refined electrolytically following cascaded refiners using the slight difference in the free energies of formation of different hydrogen, nitrogen, or sulfer compounds (e.g., ammonia-hydrogen exchange and the Girdler-Sulfide system) [37].

In a deuteron, the constituent neutron and proton have an exceptionally large internucleon separation. The importance is the deuteron binding energy is only ~2.2 MeV in a well of about ~40-50 MeV. As a corollary, the deuteron has no bound excited states [38,39]. Since each nucleon has isospin +1/2, the deuteron has total isospin of either 0 or 1, and so there are four possible triplet and singlet states [40]. The deuteron ground nuclear state is the triplet $^3S_1$ state with the nuclear orbital angular momentum = 0, and the nuclear spins parallel. States with any nuclear orbital angular momentum of >0 show no signs of binding. The actual structure, and energy, of the deuteron ground state results from its three form factors (electric monopole {charge}, magnetic dipole, and electric quadrupole moments). The magnetic moment of the deuteron (μ_D = 0.8574) is not exactly the sum of its component parts (μ_H and μ_N), and the slight difference -- and the unusual electric quadrupole moment (Q = 0.282 e-fm^2) -- are both consistent with a more complex mixture of nuclear spin states in the deuteron ground state (suggested by Rarita and Schwinger) such as inclusion of some $^3D_1$ state [41,42]. There is a virtual ($^1S_0$) state located above the zero binding energy at +30 keV which has been confirmed by nuclear photoeffects and other phenomena [43].

EXPERIMENTAL - ABSENCE OF METACHRONOUS BETA EMISSION

Nickel cathodes produce excess enthalpy (heat) during electrolysis of light water solutions [27]. As a result of competing reactions [44-46], an optimum "notch" occurs in the power gain curve relative to input power [27]. Nickel electrodes were driven within their π-notch using ordinary water in combination with either platinum or gold anodes. We examined several electrodes that had demonstrated episodes of excess heat for their metachronous electron emission, at 12 to 24 weeks, using a modified Maestro-EEG system with solid state detector. Fig. 2 shows the control, the background, and the background subtracted from the sample's emission spectrum. There was apparently insignificant metachronous electron or ionizing radiation emission from the previously-driven nickel cathodes to herald an explanation for the excess enthalpy. The absence of an obvious emission signature to declare ash might be consistent with a short-lived product, or with inadvertant removal of the isotope from the surface during the interval between driving and examination of the samples, or with unintentional self-absorption of the emission signal, or with loss of the signal in the noise background, or even with an unconsidered pathway yielding a stable final product. Given the recent results of Lin [47] and Bockris, and Mizuno, it may be that the delay of several months prior to the metachronous measurement was far too long

and that emissons may have been in the range of 15-25 keV. Studies are underway to reexamine this experimentally. Nonetheless, we considered the latter possibility.

INTERPRETATION -- POSSIBLE PATHWAY

When the possible pathway mentioned above is considered, it is noted that it might contribute to the excess heat and to other researchers' reported transmutation reactions, through the production of *de novo* deuterons. We suggest a multistep pathway leading to deuteron production with the generation of an excited intermediate state (a virtual deuteron in light water with nickel, and -- as presented elsewhere -- an excited helium-4 nucleus in heavy water with palladium systems). Fig. 3 shows some of the relevant nuclear states.

The first step is the corollary of well-known neutron decomposition. Free neutrons have a theoretical lifetime of ~10 minutes but are observed to decay within circa three minutes via interaction with a proton. Taking the neutron lifetime as 918 seconds, we rewrite the basic beta decay equation, using backwards time, to give a proton and electron opportunity to react to an extremely rare occurance in a fully loaded, one kilomolar electron-loaded, fully-hydrided alloy. This gives a thermal neutron and neutrino.

$$p^+ + e^- \rightarrow n^0 + \nu^e$$

Could there actually be sufficient quantities of such putative ephemeral thermal neutrons available? Of the estimated 5 x 10^{21} nickel atoms in the cathode, perhaps the relatively active portion may extend to a depth yielding ~0.04% of the nickel lattice sites which actually are able to have a role and contribute. This constitutes about ~4 micromoles of nickel contributing lattice sites within the cathode. Thus, assuming full local hydridation, the amount of protons available is also in the range of 2 x 10^{18}. Given the neutron lifetime, there is a statistical likelihood of only 0.000987 contributing at any point in each second. With the putative active sites available, this would give ~2 x 10^{15} potential virtual neutrons per second. This does exceed the required event rate described below.

The second step, similar to the Phuson mechanism proposed for deuteron-laden palladium, involves a hypothesized intermediate precursor-product excited state. Here, the critical excited (and virtual) nuclear state (D^*) is energetically located above the non-bonding axis. The ground-state deuteron forms through a simultaneous cooperative reaction involving a cluster of phonons (the Phuson) linking the de-excitation of the excited virtual deuteron state. These phonons are critical because they account for the coupling, for the focusing of energy into the critical sites, and possibly even for the positive feedback that permits the reactions.
The D^* deexcitation enables the vicinal phonon ensemble to compete effectively and permit fusion reactions to proceed in the fully loaded metals with energy transfer to the phonon cloud. If such nuclear-phonon cloud pathway was not available then the tiny population of D^* would saturate and end all such reactions. Only in the fully loaded material are the virtual levels continuously drained leading to their replenishment. When nuclear-phonon cloud pathways are not available then the tiny population of D^* immediately saturates to an insignificant level.

Our calculations suggest that in order to conserve momentum and energy not all the ~2.2 MeV binding energy would be available. The four-vector relates the momenta (p_i; i = x,y,z) and energy (E), and begins in the center of mass frame-of-reference at the primary reaction site within the hydrided metal. Although several approximations have been made, the energy of the reaction actually available to the Phuson cluster appears to be closer to 1.4 MeV per transition; somewhat less than the binding energy. Because each watt requires ~6.24 10^{12} MeV per second, one impact of this correction is that this putative pathway would require 2.8-4.5 10^{12} events per second (Fig. 4).

Assuming a distribution of phonon energies in the range of 30-50 eV, there would be 2.8-7.3 x 10^7 phonons in the phuson cluster (the cooperative phonon group linked to the excited state). Thus, this would require the involvement of about 5-44 million lattice sites, and therefore about ~170-350 lattice sites in any direction radial from the prime reaction site. Now, any putative deuteron production releases energy on the ~1-2 MeV scale at a single location, but with a possibility for spreading the released energy among these lattice sites that can be coupled during the deexcitation time of D^*. The interaction radius [r_{DE}] is determined by the speed of light, c, so the number of lattice cells involved in a single event, coupled through the Phuson deexcitation pathway, assuming isotropicity, is

$$N_{sites}(r_{DE}) = \frac{[c * \tau_{DE}]^3}{[V_{unitcell}]}$$

The uncertainty principle can estimate the lifetime based upon the "energy bandwidth" of the energy involved. For the excited state of deuterium located at +30 keV, the energy width of the virtual state must be on the order of a fraction of that, which would be consistent with an adequate lifetime of the excited state. The ensemble of phonons, with consideration of the available lattice sites, is thus sufficient to account for energy transfer to the lattice during the deexcitation D^*.

LIMITS OF DEUTERON DETECTION

Several experiments are suggested based upon the Phuson theory. First, if deuterium is an ash, and if there are no secondary reactions (e.g., to convert the generated deuterium to helium-4), then there will be an ultimate limit to the amount of energy which can be obtained by loading nickel with a fixed volume of light water. Per mole of hydrogen converted (in ~9 cubic centimeters of ordinary water) this would theoretically generate a maximum energy of ~10^{11} joules. Second, if the putative thermal neutron production does occur, then there is a maximum excess rate of heat production available based upon that factor, too. This would limit the rate of generation of the desired product. The observed π-notches could be consistent with this.

Third, the rate of generation of *de novo* deuterium per megajoule, if any, is miniscule and would create only a few percentage change in a background of ordinary water (Fig. 4). Such small production levels, and the inevitable separation factors (Fig. 1) refining further possibly already present deuterium, together pose significant challenges for the unambiguous identification of deuterium. Reexamination of vibrational spectroscopic data [48] (Fig. 5) indicates that small amounts of deuteron production remain below the present selectivity and sensitivity of the system. However, other spectroscopies that may offer potential for *in situ* examination include infrared absorption analysis, neutron reflectometry and, nuclear resonance broadening (NRB) and elastic-recoil-detection-analytic (ERDA) techniques. Some techniques penetrate subsurface structures to examine the magnetic properties of, and the impact of nonequivalent occupied sites within, the hydrided metal.

Fourth, if Phusons are involved, then given the requirement for sufficient lattice recruitment, any observed isotopic changes in transmutation systems may occur in greatest amounts below the lattice surface, and at depths which are the order of the interaction radius. Fifth, if the putative thermal neutron pathway exists, then there may also be the potential for nickel (and other elements) to be transmutated to higher isotopes of the same element with the unstable isotopes becoming, for the nickel, the stable isotopes of copper and cobalt.

ACKNOWLEDGMENTS

The author is grateful to Drs. Michael Staker, Peter Hagelstein and Russ George for their discussions involving the possibility of deuteron production in some of these reactions, to Prof. Louis Smullin who performed the β-

emission collections, and also to Jeff Driscoll, Steven Olasky, Dr. Stephen Baer, and Prof. Keith Johnson for some of the equipment used to make these experiments possible, and to Gayle Verner and **JET Energy Technology** and its staff for their support and assistance during this study, and to the staff at Fusion Information Center for their assistance with the preparation of this manuscript.

REFERENCES

1. D. Britz, "*CNF bibliography updates and archive retrieval*", URL http://www.kemi.aau.dk/~britz. Of the eighteen papers dealing with tritium production, four were theoretical, and fourteen were experimental. Of the experimental papers, 78% were positive, although because of repeated authors this should be ~72%. 2. V.A. Alekseev, et al., *Tech. Phys. Lett.*, vol 21, p 231 (1995).
3. R.T. Bush, R.D. Eagleton, *J. Fusion Energy*, vol 9, p 397 (1990).
4. J. Chene, A.M. Brass, *J. Electroanal. Chem.*, vol 280, p 199 (1990).
5. C-C. Chien, D. Hodko, Z. Minevski, J.O'M. Bockris, *J. Electroanal. Chem.*, vol 338, p 189 (1992).
6. C-C. Chien, T.C. Huang, *Fusion Technol.*, vol 22, p 391 (1992).
7. T.N. Claytor, D.D. Jackson, D.G. Tuggle, "Tritium Production from Low Voltage Deuterium Discharge on Palladium," *Cold Fusion Times*, vol 4, p 3 (1996).
8. M. Fleischmann, S. Pons, G. Preparata, *Nuovo Cimento*, vol 107 A, p 143 (1994).
9. D. Hodko, J.O'M. Bockris, *J. Electroanal. Chem.*, vol 353 (1993).
10. Y.E. Kim, *Fusion Technol.*, vol 19, p 558 (1991).
11. G.H. Lin, R.C. Kainthla, N.J.C. Packham, O. Velev, J.O'M. Bockris, *Int. J. Hydrogen Energy*, vol 15, p 537 (1990).
12. G. Mengoli, et al., *J. Electroanal. Chem.*, vol 304, p 279 (1991).
13. G. Mengoli, et al., *J. Electroanal. Chem.*, vol 322, p 107 (1992).
14. S.R. Rajagopalan, *Curr. Sci.*, vol 58, p 1059 (1989).
15. K.A. Ritley, et al., *Fusion Technol.*, vol 19, p 192 (1991).
16. C.D. Scott, et al., *Fusion Technol.*, vol 18, p 103 (1990).
17. E. Storms, C. Talcott, *Fusion Technol.*, vol 17, p 680 (1990).
18. H. Wiesmann, *Fusion Technol.*, vol 17, p 350 (1990).
19. L.L. Zahm, et al., *J. Electroanal. Chem.*, vol 281 (1990).
20. R.L. Mills, S.P. Kneizys, "Excess Heat during the Electrolysis of an Aqueous Potassium Carbonate electrolyte and the implications for cold fusion," *Fusion Technol.*, vol 20, pp 65-81, (Aug. 1991).
21. V.C. Noninski, "Excess Heat during the Electrolysis of a Light Water Solution of K_2CO_3 with a nickel cathode," *Fusion Technol.*, vol 163 (1991).
22. R. Notoya, Y. Noya, T. Ohnishi, "Tritium Generation and Large Excess Heat Evolution by Electrolysis in Light and Heavy Water-potassium Carbonate solutions with Nickel Electrodes," *Fusion Technol.*, vol 26, pp 179-183 (1993); R. Notoya, "Alkali-Hydrogen Cold Fusion Accompanied by Tritium Production on Nickel," *Transactions of Fusion Technol.*, vol 26, pp 205-208 (Dec. 1994).
23. T. Ohmori, M. Enyo, "Excess Heat Evolution During Electrolysis of H_2O with Nickel, Gold, Silver, and Tin Cathodes," *Fusion Technol.*, vol 24, no 3, pp 293-295 (1993).
24. T. Matsumoto, "Cold Fusion Observed with Ordinary Water," *Fusion Technol.*, vol 17, pp 490-492 (1990); T. Matsumoto, "Cold Fusion Experiments with Ordinary Water and Thin Nickel Foil," *Fusion Technol.*, vol 24, pp 296-306 (1993).
25. R T. Bush, R D. Eagleton, "Evidence for Electrolytically Induced Transmutation and Radioactivity Correlated with Excess Heat in Electrolytic Cells with Light Water Rubidium Salt Electrolytes," *Transactions of Fusion Technol.*, vol 26, pp 431-441, (Dec. 1994); Robert T. Bush, "A Unifying Model for Cold Fusion," *Transactions of Fusion Technol.*, vol 26, pp 434-354 (Dec. 1994).
26. M. Srinivasan, A. Shyam, T.K. Shankarnarayanan, M.B. Bajpai, H. Ramamurthy, U.K. Mukherjee, M.S. Krishnan, M.G. Nayar and Y. Naik, "Tritium and Excess Heat Generation During Electrolysis of Aqueous Solutions of Alkali Salts with Nickel Cathode," Frontiers of Cold Fusion, Ed. by H. Ikegami, *Proceedings of the Third International Conference on Cold Fusion,* October 21-25, 1992, Universal Academy Press, Tokyo, pp 123-138 (1992).
27. M. Swartz, "Consistancy of the Biphasic Nature of Excess Enthalpy in Solid State Anomalous Phenomena with the Quasi-1-Dimensional Model of Isotope Loading into a Material", accepted in *Fusion Technol.*, for January 1997 issue.

28. T. Ohmori, T. Mizuno, M. Enyo, "Production of Heavy Metal Elements and the Anomalous Surface Structure of the Electrode Produced During the Light Water Electrolysis of Gold Electrode," 6th Int'l. Conf. on Cold Fusion, Oct. 1996, Toya, Hokkaido, Japan.
29. R. Notoya, T. Ohnishi, Y. Noya, "Nuclear Reactions Caused by Electrolysis in Light and Heavy Water Solutions," 6th Int'l. Conf. on Cold Fusion, Oct. 1996, Toya, Hokkaido, Japan.
30. B.F. Bush, J.J. Lagowski, M.H. Miles, "Nuclear Products Associated with the Pons and Fleischmann Effect: Helium Commensurate to Heat Generation, Calorimetry, and Radiation," 6th Int'l. Conf. on Cold Fusion, Oct. 1996, Toya, Hokkaido, Japan.
31. Russ George, personal communication.
32. Michael Staker, personal communication.
33. M. Swartz, "Phusons in Nuclear Reactions in Solids", accepted in *Fusion Technol.* for March 1997 issue.
34. J. Craig, D.N. Schramm, M.S. Turner, "Big Bang Nucleosynthesis and a New Approach to Galactic Chemical Evolution," *Astrophysics Journal*, vol 459, pp L95-98 (1996).
35. M. Rugers, C.J. Hogan, "Confirmation of High Deterium Abundance in Quasar Absorbers," *Astrophysics Journal*, vol 459 (1996).
36. Following the Big Bang (τ = ~1 second into the expansion), the temperature lowered to a few hundred MeV, and nucleons (baryons or ordinary matter) generated other elements, mainly helium ($24^{+/-1}$% throughout the universe at that time, and ~30% in our sun now, where additional helium has since been created). Although nucleosynthesis forms helium efficiently at high baryon density, the less efficient pathways generate deuterium. The D/H ratio then becomes the best indicator of initial baryon density. As a result of the destructionof deuterons due to their relative fragility, back corrections have been made to deduce an initial pregalactic deuterium abundance of 0.01% percent relative to protons.
37. This heavy water distillation machinery for commercial deuterium production involves towers of 35 meters height with a 9 meter diameter operating in countercurrent exchange mode. These towers must perform at high pressure in anticipated severely corrosive environments (> 6 mm allowance). In the GS system, hot hydrogen sulfide (70% H_2S) rises through falling water in a series of cascades; providing enrichments of ~30-40%. The GS system uses final enrichment of electrolytic means so as to produce 99.75-99.8% deuterium oxide (reactor grade heavy water). The ammonia hydrogen exchange system requires an additional catalyst. The high temperature is used since the forward reactions toward material deuteration (from the contamination levels in the water) are then favored. These reactors contain toxic, flammable, and corrosive substances. (Cf. H.K. Rae,
"Separation of Hydrogen Isotopes," ACS Symposium, Series 68, Washington D.C., 1978.)
38. A.I. Akhiezer, A.G. Sitenko, Tartakovskii, V.K., Nuclear Electrodynamics, Springer-Verlag (1993).
39. Byron. P. Roe, *Particle Physics at the New Millenium*, Springer (1996).
40. M.A. Preston, P.K. Bhaduri, Structure of the Nucleus, Addison-Wesley Publishing Co., Reading, MA (1975).
41. Povh, Rith, Scholz, Zetsche, Particles and Nuclei, ISBN 3-540-59439-6, Springer (1995); Kaplan, Irving, Nuclear Physics, Addison-Wesley, MA (1962); H. Kopfermann, E.E. Schneider, Nuclear Moments, Academic Press (1958).
42. Some use the Sachs formula to reveal several possible states, and other analyses (Feshback-Lomon) indicate a mixing of 4.3% or slightly more D state. The electric form factor of the deuteron suggests a 6-7% D-state contribution, but additional meson-exchange current to make this slightly less, ~4.3-5%. The meson exchange current enables electromagnetic transitions between T = 0 and T = 1 states, such as in the photodisintegration of the deuteron. Although the mixture is only a few per cent, the tensor force further contributes to the total binding energy of ~2.23 MeV.
43. G.A. Jones, The Properties of Nuclei, Clarendon Press, Oxford (1987); Nilsson, S.G., Ragnarsson, I., Shapes and Shells in Nuclear Structure, Cambridge U. Press (1987).
44. M. Swartz, "Quasi-One-Dimensional Model of Electrochemical Loading of Isotopic Fuel into a Metal", *Fusion Technol.*, vol 22, no 2, pp 296-300 (1992).
45. M. Swartz, "Generalized Isotopic Fuel Loading Equations," Cold fusion Source Book, International Symposium on Cold Fusion and Advanced Energy Systems, Ed. Hal Fox, Minsk, Belarus (May 1994).
46. M. Swartz, "Isotopic Fuel Loading Coupled to Reactions at an Electrode," Proceedings: Fourth International Conference on Cold Fusion, Vol 4, p 33 (1994); Swartz, M., "Isotopic Fuel Loading Coupled to Reactions at an Electrode," *Fusion Technol.*, vol 26, no 4T, pp 74-77 (December 1994).
47. G.H. Lin., Bockris, J. O'M., "Anomalous Radioactivity and Unexpected Elements Upon Heating Inorganic Mixtures," *Cold Fusion Times*, vol 4, no 4 (1996); Mizuno, T., Ohmori, T., Enyo, M., "Anomalous Isotopic Distribution in Palladium Cathodes after Electrolysis," *Cold Fusion Times*, vol 4, no 4 (1996).
48. M. Swartz, "Systems to Monitor and Accelerate Electrochemically Induced Nuclear Fusion Reactions," U.S. Patent Application 07/371,937 (June 27, 1989).

49. Compilations, including Handbook of Chemistry and Physics, C. Hodgeman et al. CRC (1961, 1973); S. Parker, "Encyclopedia of Science and Technology, McGrawHill, NY; R.B. Heslop, P.L. Robinson, Inorganic Chemistry, Elsevier, Ampsterdam, 1967; and T. Claytor (personal communication).

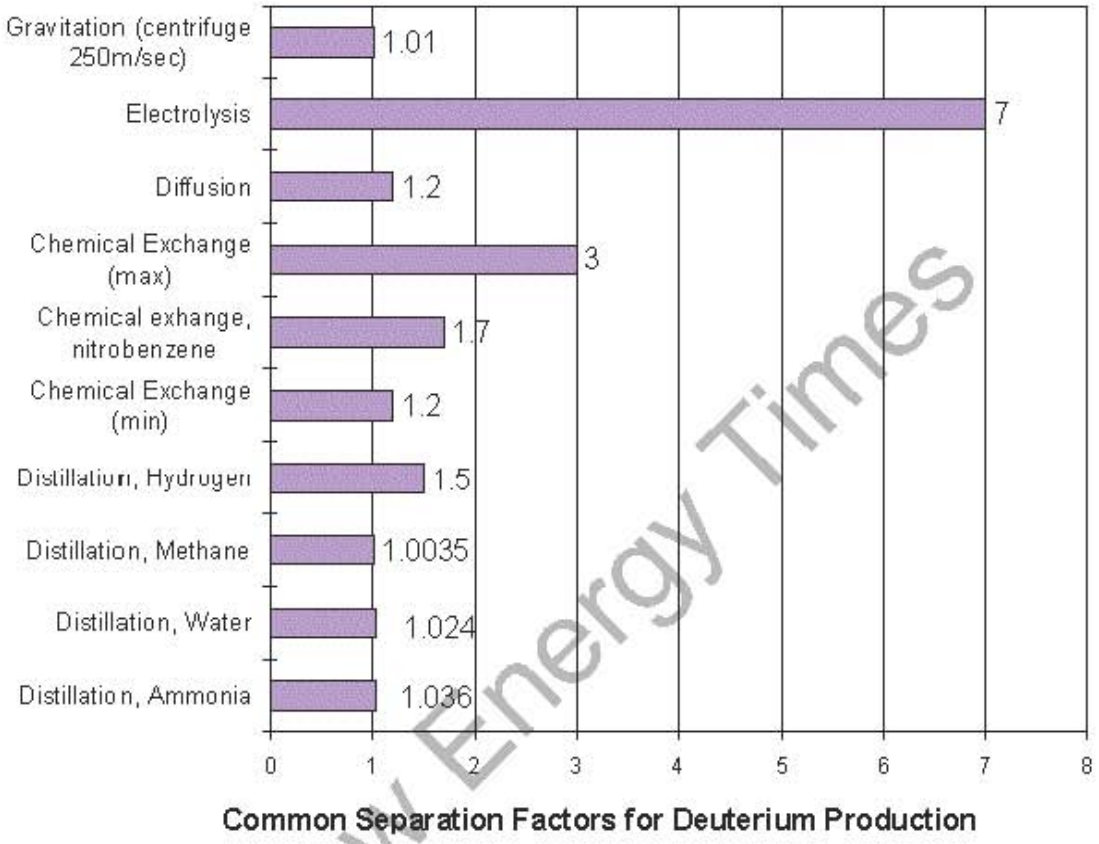

Fig. 1. Common Separation Factors for Deuterium Production

This Figure shows the separation factors for refining deuterium from ordinary water. The values range from a maximum for electrolysis to those values characteristic of evaporation or centrifugation.

Table I

HYDROGEN ISOTOPE PROPERTIES (ref. 49)			
Baryon/Nucleon	Proton	Deuteron	Triton
Mass (amu)	1.0078	2.0142	3.0160
Electric monopole charge	1+	1+	1+
Magnetic dipole moment	2.7928	0.8574	2.9789
Electric quadrupole moment (nuclear magnetons)	0	0.282 e-fm^2	0
Isospin (parity) J	1/2+	1+	1/2+
Binding energy	0	2.224 MeV	6.461 MeV
Lifetime	stable	stable, fragile	12.3y
Decomposition product	not applicable	not applicable	18.59 keV beta
Diatomic gas	Hydrogen	Deuterium	Tritium
Molar volume of solid cm^3	28.3	23.5	
Triple Point (deg K)	13.92 K - 13.96 K	18.58 K - 18.72 K	20.6 K
Heat of vaporization at triple point Joules/mole	910.9	1268.2	
Melting point (deg K)	13.95	18.65	
Boiling point (deg K)	20.38 - 20.4	23.5	
Latent heat of fusion (melt) Joules/mole	117.2	197 - 217	
Heat of dissociation KJoules/mole	437.5	439.2	
Water (ignores HDO, HTO, etc.)	H_2O	D_2O	T_2O
Background concentration	1	0.000156	1/10^{17}
Molecular weight (C^{12} scale)	18.015	20.028	
Surface tension (20C)	72.75 dynes/cm	67.8 dynes/cm	
Temperature of Maximum density	3.98 C	11.23 - 11.6 C	
Dielectric constant (25 C)	78.54	78.25	
Absolute viscosity (20 C)	10.09 millipoises	12.6 millipoises	
Melting point (deg C)	0	3.82	
Boiling point (deg C)	100.00	101.42	
Specific gravity (20 deg C)	0.9982	1.106	
Heat of fusion Joules/mole	6008.2	6317.8	
Heat of vaporization Joules/mole	43,840	44,936	
Solubility NaCl (25 C) gms/100 g	35.9	30.9	
Autopyrolysis constant [D_3O+] {OH-] 25 C	1.00 10^{-14}	3.00 10^{-15}	
pH	7.00	7.26	
Cost	rain, snow	1$/L(gas) $100 - $1000/L (liq)	~ $30 K/gm
World production	-	~ 1-3 10^8 L/year	< 10^2 Ci/yr
World capacity	-	10^{13} tons on surface	

Fig. 3. Metachronous Emission of Nickel Cathodes

This Figure shows Emission Spectrograms of a control, of the background, and of a nickel cathode which had previously demonstrated excess heat (~52 kilojoules, 0.35 cm^3, 28 cm^2, 15 weeks prior to examination).

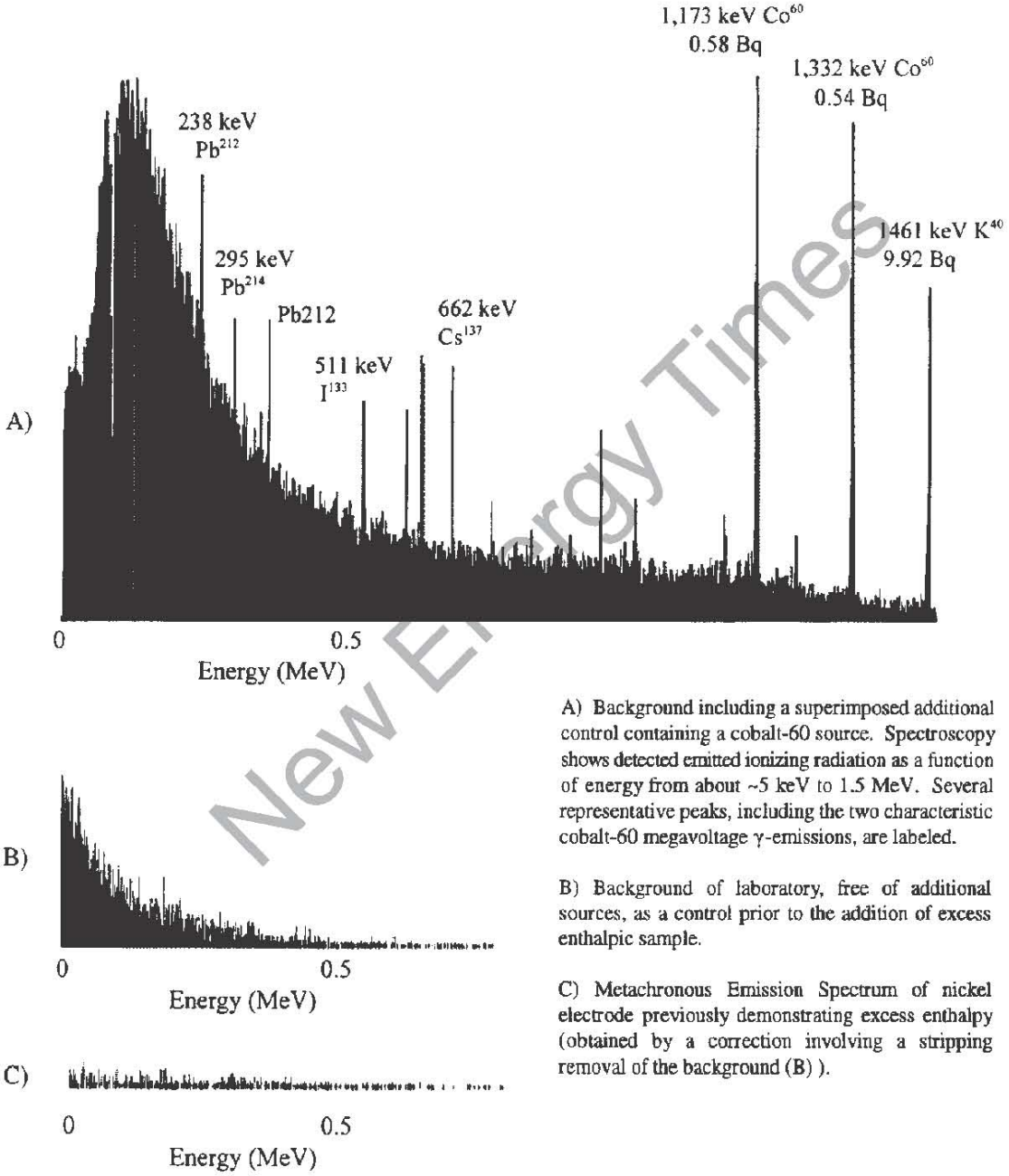

A) Background including a superimposed additional control containing a cobalt-60 source. Spectroscopy shows detected emitted ionizing radiation as a function of energy from about ~5 keV to 1.5 MeV. Several representative peaks, including the two characteristic cobalt-60 megavoltage γ-emissions, are labeled.

B) Background of laboratory, free of additional sources, as a control prior to the addition of excess enthalpic sample.

C) Metachronous Emission Spectrum of nickel electrode previously demonstrating excess enthalpy (obtained by a correction involving a stripping removal of the background (B)).

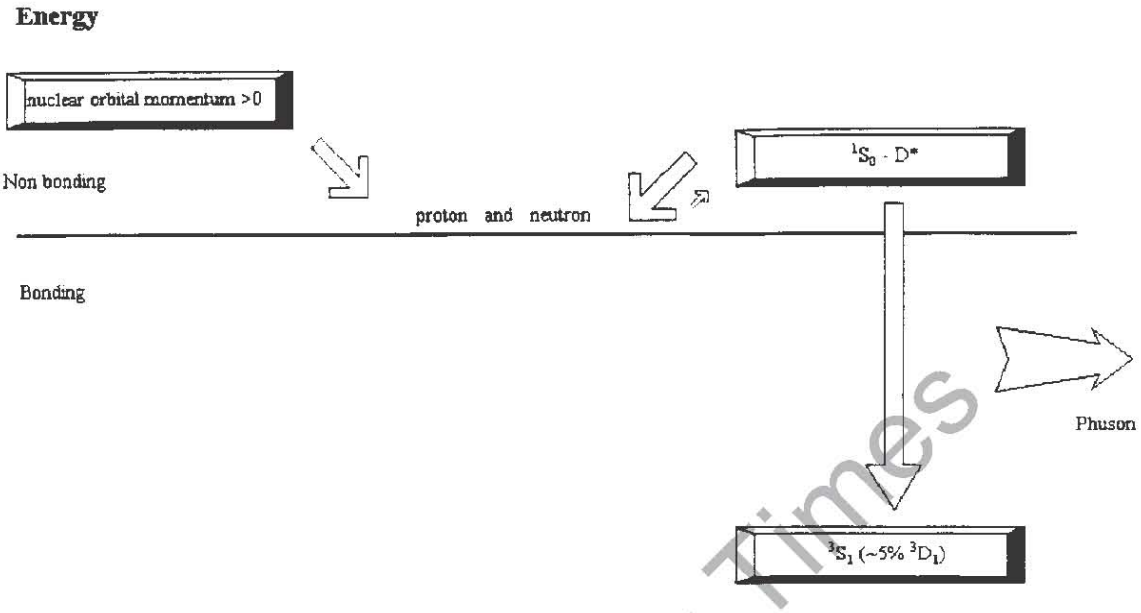

Fig. 3. Spin Manifolds of the Deuteron

This Figure shows the pathway leading to possible deuterium production. It does not include the preceeding generation of the neutron as discussed in the text. Shown are three of the "states" available to an interacting proton and neutron. The vertical axis is energy and is not quantitative. If there is any nuclear orbital angular momentum then the non-binding "state" on the upper left is not achieved for reasons discussed in the text. If the nuclear orbital angular momentum is zero, the manifold on the right can be entered. The singlet state above the axis (~30 keV) is a virtual state observed in incident beam studies. The state on the bottom right is the well-known ground state of the deuteron, which is mainly a $^3S_1$ state. The hypothesis is that there may be leakage from the virtual state to the ground state with Phuson coupling to the solid hydrided lattice cathodically loaded with electrons.

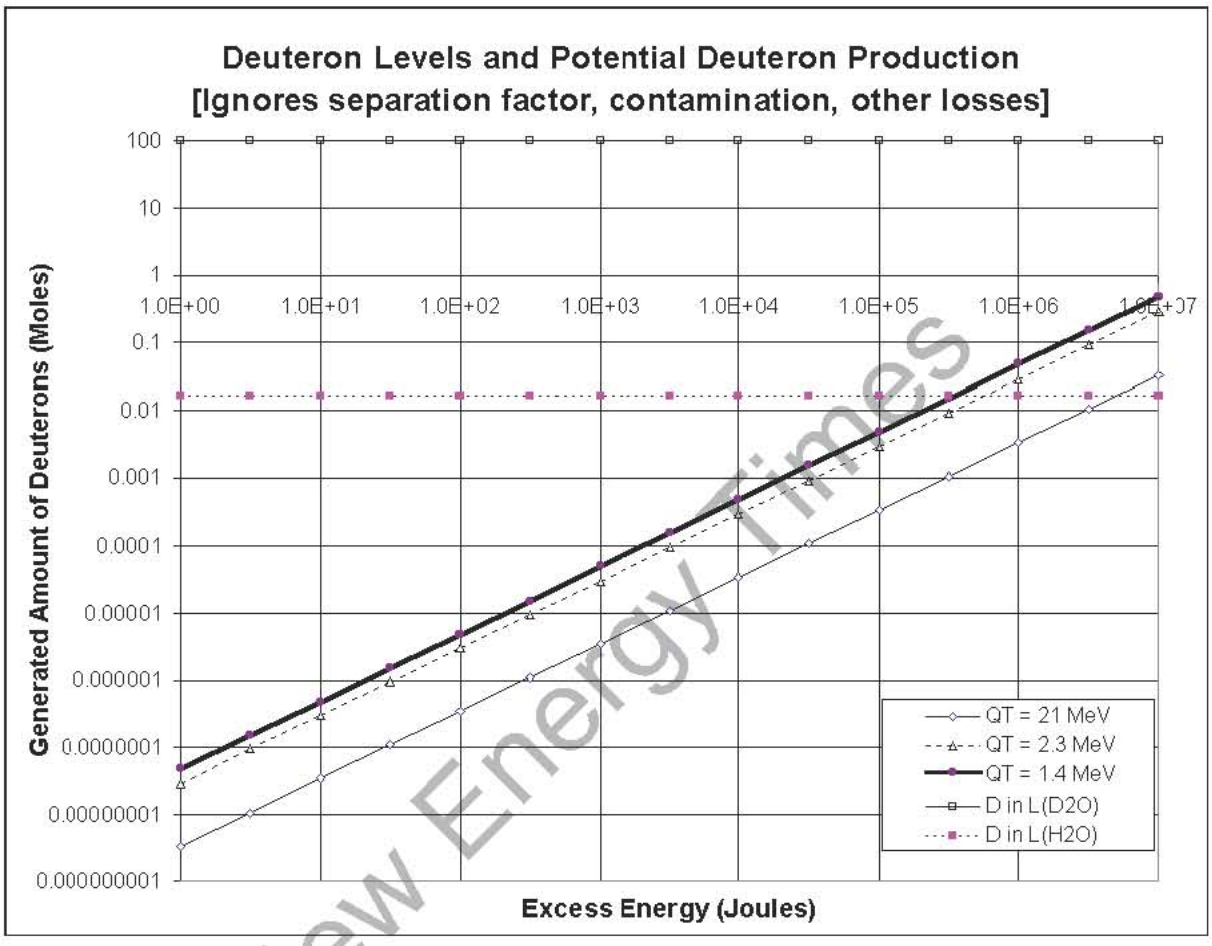

Fig. 4 Putative Production Rates of Deuterium Would Present Detection Challenges

This Figure shows the quantity of deuterium present in, or generated *de novo* in, water as a function of excess energy. The three rising curves show the amount of expected deuteron ash which would be produced if that reaction did occur and did only account for the observed excess heat. Each curve represents a different derived energy for each single event nuclear reaction. The event (binding) energy of 21 MeV does not hold for deuterium, but is representative of what occurs for other final states such as helium. Q_T of 2.3 is what might be expected for the binding energy of the deuteron. The curve representing "Q_T" of 1.4 (thick diagonal line) is derived from the calculations which correct for momentum transfer to the Phuson cluster (see text). Also shown for comparison is the quantity of deuterons contained in a liter of light, and heavy, water.

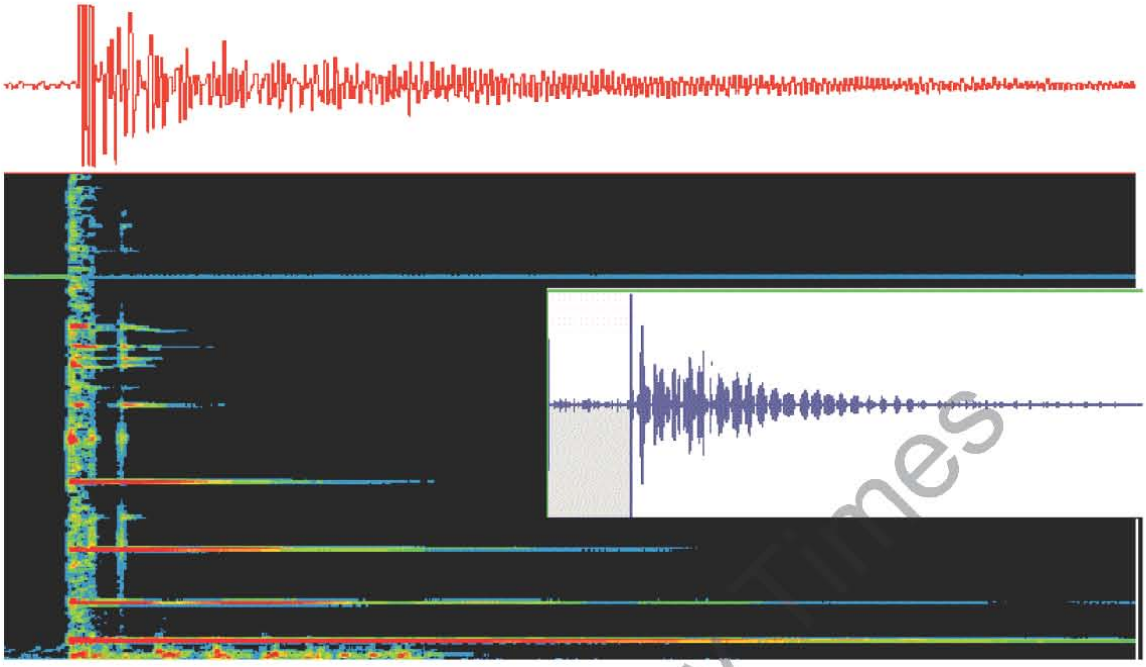

Fig. 5. Vibration Spectroscopy of Nickel Cathode

This figure shows a Vibration Spectrogram of a loaded nickel cathode. The cathode (Sample 92-505b/Ni-B2) surrounded with 20 ml of ordinary water, during its electrical polarization with a platinum anode, is struck with a single mechanical pulse at t = 0. The vibrational modes of the electrode, and their damping, can be used to determine loading, but because of separation issues may be insensitive to any putative deuteron production. Two recorders were used to pickup the data (top and inset), and the fast fourier transform is also shown as a frequency versus time plot. The solid bar three-quarters of the way up the calibration signal at $17{,}390^{+/-53\ Hz}$. The lowest evanescent normal mode, the most irregular of the group, is believed to be a circular mode around the relatively large annular electrode. The sampling rate was ~100 kHertz.

ELECTRO-NUCLEAR TRANSMUTATION: LOW-ENERGY NUCLEAR REACTIONS IN AN ELECTROLYTIC CELL

Robert Bass, Rod Neal, Stan Gleeson, & Hal Fox[1]

ABSTRACT

A special electrolytic cell and power supply have been designed to promote low-energy nuclear reactions (electro-nuclear transmutations). Using electrical power ranging up to 1,000 watts, it has been experimentally determined that various high-mass parent elements can be fissioned into somewhat equal daughter products. The experimental evidence for nuclear reactions is based on the difference between input samples and processed samples as determined by commercial mass-spectrometer analysis (providing the same results at two University labs and one commercial lab), by SEM spectroscopy, and by gamma-ray emission spectroscopy. Although other new elements are produced, the bulk of the fission elements appear to be mass fractions consistent with the conservation of the initial elemental atomic number. For example, tungsten can be fissioned into cadmium and iron. Thorium has been fissioned into mercury and neon. Up to seventy percent of a parent element has been fissioned with a few hours of processing time. Further development work is planned, especially for application to the stabilization of radioactive slurries. It is important that these preliminary results be independently replicated and verified.

A. INTRODUCTION

Rod Neal and Stan Gleeson have discovered, tested, and improved a low-energy mechanism for promoting nuclear reactions in elements of relatively high atomic numbers. The process is essentially electrolytic in that a power source (less than 1,000 watts) is connected to specially-prepared electrodes in an electrolytic cell. During this development work, the inventors have used aqueous solutions of various metallic salts as the electrolyte.

The results of the experimental process appears to be essentially a fission process although some nuclear fusion has been observed. Depending on the process control parameters (voltage, current, wave form, temperature, molarity, etc.), the fission products for a specific ionized high-mass parent element generally consist of two daughter elements. The daughter elements may be of about equal masses (such as tungsten → two rubidium) or of disparate masses (such as thorium → mercury + neon).

Although the mass spectrometer results show the presence of several new elements in the processed solution, the predominant elements are essentially the same daughter products. It is not, as yet, known if the process rate of transmutation is relatively uniform throughout the process time. The experimental approach used in experiments covered by this report is essentially a batch process. A carefully measured amount of an element to be processed (usually as a water-soluble salt in distilled water) is prepared as the electrolyte. The process is operated for a measured time period. The end product results appear to indicate that even though the molarity of the target element is changing during the process time period, the predominant nuclear reaction(s) remains the same.

Experimental data indicates that different process control parameters affect the nuclear reactions. For example, at some parameter settings the daughter products of the parent thorium are mercury and neon. Under other

[1] Fusion Information Center, P.O. Box 58639, Salt Lake City, UT 84158

process parameters the parent thorium can produce some other pair of elements. A complete catalog of the effect of changes to process parameters on the nuclear reactions is being compiled.

Similar experimental observations of nuclear reactions have been reported by Bockris and Minevski [1] and by Mizuno, et al. [2]. However, the electrolytic reactor designed and used by Neal and Gleeson is significantly different than the experimental work previously reported [1,2]. No theory has been developed to explain the observed phenomena — and it appears that the experimental findings are not consistent with any standard model of the atom and its nucleus. The purpose of this paper is to present selected experimental evidence, discuss the implications of the Neal-Gleeson Process, and report on further planned activities.

B. EXPERIMENTAL OBSERVATIONS

DESCRIPTION OF THORIUM TESTS

Thorium Nitrate, $Th(NO_3)_4$, was chosen because it is **very soluble** in water. Thorium, in nature, consists of about 100% $_{90}Th^{232}$ which is mildly radioactive with a half life of 1.4×10^{10} years. The entire chain of radioactive thorium decay is:

$$_{90}Th^{232} \rightarrow {}_{88}Ra^{228} \rightarrow {}_{89}Ac^{228} \rightarrow {}_{90}Th^{228} \rightarrow {}_{88}Ra^{224} \rightarrow {}_{86}Rn^{220} \rightarrow {}_{84}Po^{216} \rightarrow {}_{82}Pb^{212} \rightarrow {}_{83}Bi^{212} \rightarrow {}_{84}Po^{212} \text{ or } {}_{81}Tl^{208} \rightarrow {}_{82}Pb^{208}.$$

If the thorium nitrate were absolutely 100% pure and freshly constituted one could assume that there would be no decay products. However, the radioactive decay products are continuously produced by the **radioactive decay** of thorium. The amount of each daughter product in a prepared sample is a function of previous purity of the thorium and the shelf life of the product. The following table provides information on half-lives, decay modes, and energies of emitted particles:

TABLE I. THORIUM DECAY DAUGHTER PRODUCTS

Element	Half-Life	α (MeV)	ß (MeV)	γ (KeV)
Thorium-232	1.4×10^{10}y	4.01, 3.95	--	59(w)
Radium-228	5.76 y	--	.039, .015	14(w)
Actinium-228	6.15 h	--	1.2, 2.1	911, 969, 338
Thorium-228	1.91 y	5.42, 5.34	--	84, 216, 132, 166
Radium-224	3.66 d	5.69, 5.45	--	240
Radon-220	55.6 s	6.29	--	550
Polonium-216	0.145 s	6.78	--	805(w)
Lead-212	10.6 h	--	.331, .569	239, 300
Bismuth-212	60.6 m	6.05	2.25	40, 727
Polonium-212	298 ns	8.78	--	--
Thallium-208	3.05 m	--	1.8, 1.28, 1.52	2615, 583, 511
Lead-208	stable			

SOURCES: Lapp et al., [3], Hunt [4].

The use of gamma-ray spectroscopy is an appropriate choice because all of the daughter products of thorium emit gamma rays except for polonium-212 which has a half-life of 298 nanoseconds. **The assumption is made that the total emission of gamma-rays is an acceptable measure of the amount of radiation in a sample prior to processing. It is further assumed that the same gamma-ray total emissions after processing is an**

acceptable measure of radioactivity. If we observe an experimental procedure in which the radiation of container, electrodes, and gaseous effluent (if any) are the same before and after processing, then we assume that the changes in radioactivity of the electrolyte are an appropriate measure of the before-and-after amounts of radioactivity.

Typical Test Procedure: A measured sample of naturally radioactive thorium nitrate was dissolved in 700 ml of water. 350 ml of the solution was poured into the electrolytic cell. After the desired processing time (usually less than three hours) the electrolytic contents were poured into a flask and water was added to make-up liquid lost due to the processing. If necessary, acid is added to the processed-sample residue to ensure that any precipitates are dissolved into the **post-processing sample**.

A 10 ml control sample was taken from the initial thorium nitrate solution. A 10 ml sample was taken from the processed sample after the make-up water was added. These samples were submitted for testing to determine the amount of thorium reduction.

Test Results 1: Quoting the commercial laboratory's report: "Sample A was used as a standard. A Thorium line was generated with a blank, 0.5 g/l of Sample 4-22 [laboratory calibrating sample], and 1.0 g/l of Sample A [before-processing sample]. Using this line, the after-processing sample, Sample B [post-processing sample], had a Thorium content of 0.23 times that of sample A, a 77% reduction in Thorium." [Words in square brackets are additions by the authors.]

Note: The commercial testing laboratory used Atomic Emission Spectroscopy (ICP). The above test results are indicative of one of the best achievements in the amount of thorium reduction produced by the processing. By proper observation of the radioactivity of container, electrodes, and evolved gases on a **before-and-after** basis (all were essentially background), it is assumed that the thorium was changed into some other element or elements. This simple analysis was done to determine the amount of reduction in thorium. Another **before-and-after** sample from another experiment was submitted for gamma-ray spectroscopy. Here are the results of this second set of samples:

Test Results 2: The before-processing sample (Sample A) was analyzed using gamma-ray spectroscopy and the number of counts (gamma-ray emissions from sample A) were recorded for 50 energy levels (ranging from 77 KeV to 2614 KeV) and later tabulated. The after-processing sample (Sample B) was then analyzed using the same procedure and the counts were recorded and tabulated.

Most of the gamma-ray energy levels in the report are identified as various emissions from the daughter products of thorium. For this set of samples, the thorium reduction percentage had not been determined. The initial thorium in Sample A was present in Sample B in a substantially lesser amount. The testing laboratory's comments were: "The ratio column [**after processing** divided by **before processing**] indicates the percentage of gamma-ray counts remaining (not the reduction) for each of the daughters of thorium. **The reduction of gamma-ray counts for each of the daughters of thorium varies dramatically.**"

Authors' Analysis: The total radioactivity of the samples was determined by adding all of the gamma-ray counts from all fifty energy levels for both samples. One would expect that the ratios of **before-and-after** would be the same for all energy levels that correspond to the daughter products of thorium. This was not the case. The total counts for the **before-processing** sample A totaled 5,567,687 counts. The total counts for the **after-processing** sample B totaled 2,234,490 counts. The ratio of **after-processing** to **before-processing** is 0.401. **Therefore, it can be stated that the total radioactivity (as measured by gamma-ray counts) of the processed material was reduced by about 60 percent.** This is a dramatic achievement for a low-energy electrolytic process. However, there was considerable disparity in the ratios of the various gamma-ray emission energy levels. This

disparity in the ratios of the various thorium daughter isotopes suggests that unknown nuclear processes are involved. This experimental observation deserves further study.

Test Results 3: This test ran for four hours. About 0.8 grams of thorium nitrate was processed with 40 drops being added at the start, 30 more drops after one hour, and 30 more drops of thorium nitrate after two hours. **Before** and **after** samples were submitted for gamma-ray spectroscopy. The total counts for the unprocessed sample was 270,741 counts and the total counts for the **after-processing** sample was 117,003. Assuming that no thorium decay products were lost from the electrolyte, these measurements show that the radioactivity (as measured by gamma-ray counts) was reduced by 56.8 percent. A retest, using the same samples, was conducted at a later time. The total before-counts were 335,840; the after-counts were 153,285; the amount of reduction was 54.4%.

Authors' Interpretation: Because there is a close agreement between the reduction in thorium and the reduction of radioactivity of the thorium daughter decay products, it is **assumed** that the Neal-Gleeson Process has about the same capability to change both thorium nuclei **and the nuclei of the daughter products** into other elements which are not radioactive. Other experiments have been conducted on stable elements with before-and-after samples submitted for tests made with mass spectrometer equipment. In these tests new elements were found in the **after-samples** that were not present in the **before-samples** —elements that also were not originally present in the electrodes or container walls.

While it is readily admitted that these experimental results are highly unexpected according to our current models of nuclear reactions, the implications of these results strongly suggest that additional independent replications of this experiment be conducted. Assuming that successful replications are independently performed and similar results are achieved, there are reasons to believe that this newly-discovered electro-nuclear process can be adapted to the amelioration of radioactivity in radioactive liquids.

C. AMELIORATION OF RADIOACTIVE SLURRIES

One of the important potential applications of the **Neal-Gleeson Process** is the reduction of radioactivity in radioactive slurries. For example, at the Hanford Site, Washington state, there are 177 tanks of radioactive slurries, 67 of which are assumed to be leaking [5,6]. The 66 million gallons of slurries contained in these tanks are the byproduct of over fifty years of processing. Initially, the Hanford Site was established to separate uranium-235 from other uranium isotopes by a gaseous-diffusion process. Later, experimental nuclear reactors were established at the site for further research and development of nuclear processes.

While it is important to properly handle any type of radioactive materials, the most dangerous are the high-mass elements that tend to breakdown by self-induced nuclear reactions. Although most of the radioactive decay processes involve beta decay, the higher mass elements often decay by the emission of alpha particles and a few elements decay by spontaneous fission with neutrons emitted. The listed byproducts of nuclear decay are beta particles; alpha particles (essentially an ionized helium-4 nucleus); gammas (high-energy photons); and a few neutrons. All of these can be characterized as ionizing radiation and can be hazardous to living organisms.

The emission of beta particles can be contained easily as these electrons have little mass and can be stopped by a thin sheet of material. The emission of alpha particles (helium-4 nuclei), especially at high energy levels, and the high-energy gamma emissions are the more dangerous and predominant radiation from the radioactive slurries. These ionizing radiations traveling through living tissue can cause tissue damage by impinging on the structure of living cells and can lead to cancers and death. The leading long-term cause of death in the Chernobyl aftermath has been some of the long-lived radioactive isotopes of cesium and strontium (especially cesium-137 and strontium-90) because these elements are stored in bone tissue where they act as long-term sources of tissue-damaging radiation.

A careful study of the type of nuclear byproducts of the Neal-Gleeson Effect will show that elements having atomic numbers of 1 through 40 (hydrogen through zirconium) are generally stable. If isotopes of these elements are radioactive, the radioactive decay processes are almost all beta decay and the half-life of such radioactive isotopes are short (generally in seconds or minutes). In contrast, the elements of high atomic numbers 66 through 96 (dysprosium through californium) have many radioactive isotopes. The radioactive decay processes are often alpha particles or spontaneous fission with some production of neutrons. The half-life of many of these radioactive isotopes range from 1 to 1,000 years.

A process which can cause the higher atomic number elements to be split into smaller elements appears to be a desirable method by which certain radioactive elements can be handled. **It is highly desirable to be able to select process-control parameters so that only stable daughter nuclei of the parent elements are produced.** In this manner, the radioactivity of today's highly dangerous radioactive slurries can be ameliorated.

CONTINUOUS FLOW PROCESSING

It would be highly desirable to be able to take a batch of radioactive material, process the material, and remove 100 percent of the radioactive elements. At the current state of the art, this desirable condition may not be feasible. The best result that has been demonstrated experimentally is the reduction of about seventy percent of the initial amount of a high atomic number parent element.

The results of further experiments (nuclear reactions occurring with elements of high atomic mass) will be used to design a system to remove a high percentage of radioactive materials. If not all of these heavier elements are transformed into fission products with one pass through the Reactor Cell, it will be necessary for there to be a removal of stable elements and the return to the Reactor Cell of the remainder of the slurry being processed.

Two such processes are depicted in the following Fig. 1:

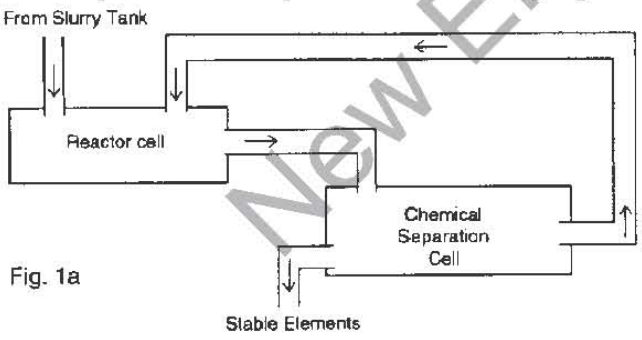

Fig. 1a

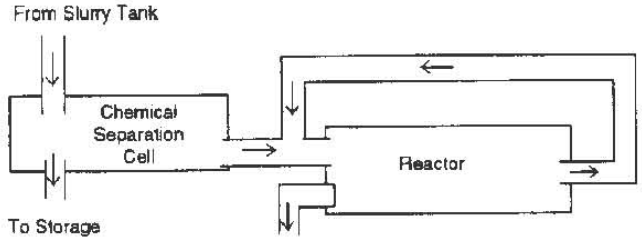

Fig. 1b

In Fig. 1a, the input of the parent elements (which could be a radioactive slurry) into the Reactor Cell would be controlled to maintain a desired volume of material in the reactor cell. The output of the reactor cell would flow into a chemical separation process. In this operation the stable elements that were formed would be removed by a selected chemical process. (It is believed possible to design the reactor cell process to ensure that the new elements created would be easy to remove in the Chemical Separation Process.) One output from this process would be the removal or output of stable elements. The remainder of the processed slurry would be fed back into the Reactor Cell for reprocessing.

In actual operation, this process in the Reactor Cell is energy intensive and therefore, a considerable amount of heat is generated with the result that steam is produced. At least part of the heat produced is assumed to be produced by exothermic nuclear reactions. The production of steam serves to maintain a reasonably high degree of molarity of the parent element in the process stream.

It is desirable to select the process control parameters so that, if possible, one of the daughter products of the nuclear reactions is a stable isotope of a gas. The other daughter product (experimental evidence indicates predominate pair production) is a stable isotope of an element easy to remove by simple chemical reactions in the Chemical Separation Process. In addition, one of the process design goals is to be able to treat a variety of radioactive trans-uranic heavy elements and still be able to chemically separate the stable products with simple chemical or electrochemical processes. The alternative is to make a chemical separation prior to processing the slurry in the Reactor Cell as depicted in Fig. 1b. However, this type of chemical processing is a more complex and expensive process. Until further properly conducted experiments are performed, the most beneficial method is yet to be determined.

NUCLEAR REGULATORY LICENSE

For the processing of radioactive slurries in the U.S., it will be necessary for the operational entity to qualify for and be licensed by the U.S. Nuclear Regulatory Commission. Careful engineering considerations must be given to the following aspects of the processing of radioactive slurries:

1. It is expected that the primary radioactive materials to be processed will be various isotopes of thorium, uranium, and plutonium.

2. Experimental data needs to be obtained on slurries containing each of these three elements when processed separately and also when processed in combination.

3. The processing of a variety of isotopes of the same element is expected to be more complicated than the processing of a single stable element. For example, Bismuth (atomic number 83) and Thorium (atomic number 90) have only one naturally-occurring isotope. In contrast, Platinum (atomic number 78) has seven stable isotopes.

4. In radioactive slurries, the number of isotopes for a specific element is expected to be numerous. Therefore, the end result may be a wider range of daughter products. For example, Uranium (atomic number 92) has three naturally-occurring isotopes and eleven isotopes with half-lives ranging from 1 day to many years.

5. A careful experimental and theoretical study should be performed concerning the possible daughter elements that can be produced by the Neal-Gleeson process and the change in radioactivity between **before** and **after** radioactive samples.

6. The energy-intensive nature of this low-energy nuclear reactor should not be deemed a deterrent to the consideration of on-site processing of radioactive materials. This point is especially true in view of the existing laboratory demonstrations of several new-energy devices that are expected to greatly reduce energy costs.

7. A cost-benefit analysis should be made for the **on-site amelioration of radioactive slurries** as compared to the enormous costs of packaging, transporting, and storing the same materials. (One of the latest proposals for packaging, transporting, and storing radioactive slurry is to encase a volume of slurry in a hydraulic cement that hardens under water. One of the potential failure modes of such a concrete tank is the gradual breaking of mineral bonds in the cement by long-term radioactive emission of gamma rays and by neutron bombardment.)

8. Practical engineering design must include methods of replacing electrodes in the Reactor Cell. Obviously, the Reactor Cell will be highly radioactive when full of radioactive slurry. The Reactor Cell will be less radioactive when drained of slurry but still sufficiently hazardous to require some type of robotic or automatic method of electrode replacement.

9. It must be determined to what extent vapors from the Reactor Cell or from the Chemical Separation Cell are radioactive and what methods are required to contain or handle such vapors.

10. It is obvious that the processes described for the processing of radioactive slurries can be applied to stable elements having high atomic numbers. Therefore, there is expected to be a great deal of experimental work performed with stable elements and an increased understanding of the processes involved before working with radioactive slurries. However, the ease of replication and the relatively short processing time (typically one to three hours) should permit rapid accumulation of experimental data.

D. CONCLUSIONS

The discovery and development of the **Neal-Gleeson Process** for the electro-nuclear transmutation of heavy elements appears to be a major scientific discovery. However, the process must be replicated by independent third parties (currently in process). When replicated, it is expected that the process will be developed as a cost-effective contribution to the elimination of the major hazards associated with the amelioration of high-level radioactive wastes.

ACKNOWLEDGEMENTS: The inventors, Rod Neal and Stan Gleeson, acknowledge the considerable financial support of Don and Virgil Holloman; the scientific support of Robert Bass, Robert Bush, Robert Eagleton, and Samuel Faile, the months of professional help and encouragement of this work by Hal Fox, and the inspiration from others.

REFERENCES

1. J.O'M. Bockris & Z. Minevski, "Two Zones of **Impurities** Observed After Prolonged Electrolysis of Deuterium on Palladium," *Infinite Energy*, vol 1, no 5&6, 1996, pp 67-69, 2 tables, 3 figs, 8 refs.
2. T. Mizuno, T. Ohmori & M. Enyo, "Anomalous Isotopic Distribution in Palladium Cathode after Electrolysis," *J. New Energy*, Summer 1996, vol 1, no 2, 5 figs, 17 refs.
3. R.E. Lapp & H.L. Andrews, Nuclear Radiation Physics, (1992), Prentice-Hall, Inc., Englewood Cliffs, New Jersey.
4. S.E. Hunt, Nuclear Physics for Engineering and Scientists, ©1987, Ellis Harwood, Ltd., Market Cross House, Cooper Street, Chichester, West Sussex, P019 1EB, England.
5. Radioactive Tank Waste Remediation Focus Area, Technology Summary, U. S. Dept. of Energy, Environmental Management, Technology Development, June 1995, DOE/EM-0255, illus. (Available from NTIS, Springfield, VA 22161, 703-487-4650.)
6. Nuclear Wastes: Technologies for Separations and Transmutation, Committee on Separations Technology and Transmutation Systems, National Research Council; published by National Academy Press, Washington, D.C. ©1996 by the National Academy of Sciences. [The essence of this large volume report is that there was no process known to the committee that would be more economical than geologic storage of radioactive wastes. **Now there is.**]

For further information contact Rod Neal or Stan Gleeson, 9772 Princeton-Glendale Rd., Cincinnati, OH 45246; 513-874-4943.

COLD FUSION EXPERIMENTS, THEORY, AND MANAGEMENT AT THE NAVAL RESEARCH LABORATORY

David J. Nagel
Naval Research Laboratory
Washington, D.C.

ABSTRACT

As a matter of responsibility to the public, which ultimately funds it, the Naval Research Lab. has actively conducted and monitored attempts to make "cold fusion" phenomena reproducible and understandable. This presentation will survey these activities.

Experiments: We performed six different experiments, either new or copies of others, explicitly aimed at "cold fusion" and related phenomena. These will be summarized and some views of others reported "cold fusion" experiments will be presented.

Theories: NRL and associated scientists have published theoretical work on two "cold fusion" motivated studies, namely ion band states and phonon-driven hydrogen isotope diffusion. A broad review of "cold fusion" theories is now underway.

Management: Numerous presentations have been made by the author to government agencies and other groups to provide information and stimulate programs. These include the OSTP, DARPA, DSWA, (ex-DNA), ONR, IDA, and the Philosophical Society of Washington. results of these interactions will be summarized briefly.

TRITIUM PRODUCTION FROM PALLADIUM AND PALLADIUM ALLOYS

T.N. Claytor, M.J. Schwab, and D.G. Tuggle
Los Alamos National Laboratory
Los Alamos, New Mexico

ABSTRACT

A number (22) of pure palladium samples and palladium alloys have been loaded with a deuterium or hydrogen plasma in a system that allows the instantaneous measurement of tritium. By carefully controlling the high pressure plasma conditions, the plasma can be constrained to only contact palladium surfaces and to only lightly sputter the palladium. Long run times (up to 200 h) result in an integration of the tritium and this, coupled with the high intrinsic sensitivity of the system(~ 0.1 nCi/l), enables the significance of the tritium measurement to be many sigma (> 10). In addition to the real time tritium measurement, the deuterium gas can be combined with oxygen, at the end of a run, resulting in water samples that were counted in a scintillation counter. The results of these confirmatory measurements of the tritium in these water samples agree quantitatively with the decrease in tritium as measured by the ion sensor. However, surprising concentrations (up to 1.5×10^6 dpm/ml) of tritium were found in several samples that had been exposed to a hydride inhibitor. We have continued to investigate the effect of hydrogen additions on the output of tritium in these types of experiments and find that hydrogen additions always suppress tritium production. We will show the difference in tritium generation rates between batches of annealed palladium, as received palladium and the palladium alloys (Rh, Co, Cu, Ni, Be, B, Li, Hf, Hg and Fe) of various concentrations to illustrate that tritium generation rate can vary greatly from alloy to alloy as well as within a specific alloy, dependent on concentration. Other metals (Pt, Hf, Ni, Nb, Ta, V, W, Zr) have also been run in the system as background samples or to determine if tritium could be detected in the gas analysis system. In nearly all cases they have produced results very close to background drift rates.

ISOTOPIC DISTRIBUTIONS OF HEAVY METAL ELEMENTS PRODUCED DURING THE LIGHT WATER ELECTROLYSIS ON GOLD ELECTRODE

T. Ohmori, T. Mizuno, and M. Enyo[1]

ABSTRACT

Some 100 μ g of fine black porous deposits comprised mainly of Au, Hg, Pt, Fe, Si and F were obtained during the cathodic electrolysis on Au electrodes in 0.5 M Na_2SO_4 and Na_2CO_3 light water solutions for 20-30 days at a current densities > 300 mA/cm^2. The isotopic distributions of these elements other than Au, Pt and F as determined by SIMS analysis were found to deviate from their natural isotopic abundance. The structure of Au electrode surface after the electrolysis revealed very unusual aspects.

INTRODUCTION

We have observed the production of some 10 μ g of Fe with an unusual isotopic abundance (^{57}Fe: 14.5 - 25%) on/in Au electrode during the cathodic electrolysis for 7 days at a current density of 100 mA/cm^2 [1]. More recently, it was found that when the current density was increased up to 200 - 300 mA/cm^2, some 100 μ g of fine black porous powders were deposited at the bottom of the electrolytic cell from the Au electrode, the main constituting elements of the deposits were Hg, Pt, Fe, Si and F other than Au and, in addition, a small amount of Os was detected in some cases. The isotopic distributions of Hg, Fe and Si contained in the deposits were evidently different from their natural values. This fact suggests strongly the occurrence of some nuclear transmutation reactions. In this report we will describe the experimental procedures and results, and propose some possible reaction schemes.

EXPERIMENTAL

The electrolytic cell used was made of fused quartz. The working electrodes were cold worked Au plates (about 2.0 cm^2 in area; 0.1 mm thick; 99.99% purity; Ag: 21 ppm; Pd: 3 ppm; Cu: 1 ppm; Fe, Si, Rh, Pt: < 1 ppm; no detectable Hg, Os and Zn), whose surfaces were scraped with a cleaned glass fragment to make the strained surface. The roughness factor of the electrode determined from the double layer capacitance [2] was around 2.0. The counter electrode was a 1 x 7 cm, 80 mesh Pt net (99.98% purity; Rh: 18 ppm; Pd, Cr, Si: 2 ppm; no detectable Hg, Os and Zn). The electrolytes used were Na_2SO_4 and Na_2CO_3 from Merck (supra-pure grade; Fe, Zn < 0.01 ppm; no detectable Si, Hg, Os and F for Na_2SO_4; Si < 0.5 ppm; Fe, Hg < 0.05 ppm; Zn < 0.01 ppm; no detectable Os and F for Na_2CO_3). The volume of the electrolyte solution used was 100 ml and the concentration was adjusted at 0.5 M. The electrolysis was carried out galvanostatically for 20 - 30 days at a constant current ranging from 1 to 3 A. Before the electrolysis, the working electrode was kept at RHE potential by passage of H_2 gas into the cell. During the electrolysis , MilIi Q water was supplied every 24 hours to maintain the total solution amount constant. The deposits obtained were washed with MilIi Q water and placed on Ni or Zr plates and the constituent elements of the deposits were analyzed by means of SIMS, AES and EDX. The AES measurement was made with use of an ANELVA ASS-200 Auger electron spectrometer with 3.0 KeV of beam energy and 2.5 Å of filament current. The EDX measurement was conducted with use of an EG &

[1] Ohmori -- Catalysis Research Center, Hokkaido University, Sapporo, Japan.
Mizuno -- Faculty of Engineering, Hokkaido University, Sapporo, Japan.
Enyo -- Hakodate National College of Technology, Hakodate, Japan.

GORTEC EEDS-II. The SIMS measurement was carried out with use of a HITACHI IMA-3 ion micro analyzer by O_2^+ ion irradiation (100 nA primary ion current, 12 KeV accelerating voltage) from Hitachi Instruments Engineering Company, Ltd.

RESULTS AND DISCUSSION

ANALYSIS OF THE DEPOSITS

Fig. 1 shows the pictures of the deposits placed on a Ni substrate and their SEM image. The deposits are very porous with a lot of fine pores of nm order, and look like pumices. As a typical example, the relative concentrations of the constituent elements of the deposits and electrodes before and after the electrolysis with mass numbers ranging from 1 to 200 estimated from the analysis of SIMS spectra (1st scan) are shown in Fig. 2 (a-d). In this case, the electrolysis was performed in Na_2CO_3 solution for 30 days at a current density of 500 mA/cm^2. We can see from this figure that the major component is Au, besides that, considerable amounts of Hg, Pt, Fe, Si, and F are contained in the deposits and on/in the electrode after electrolysis. In addition, Zn also looks to be present, however the SIMS spectra in that region are possible to be overlapping with TiO_2^+, SO_2^+ and TiF^+ so that the quantitative estimation of Zn would be difficult. The considerable amount of C detected here is probably due to some contamination. From the comparison of these results, it is clear that the contents of Hg, Pt, Fe, and F are much higher in the case of the deposits or of the electrode after electrolysis than in the case of the electrode before electrolysis and, especially, the contents of Hg, Pt, and F are much higher in the deposits.

The presence of Hg and Pt was also confirmed by AES and EDX measurements. Fig. 3 and Fig. 4 show AES and EDX spectra of the deposits, respectively. EDX spectra shown here was those of the deposits obtained by the electrolysis in Na_2CO_3 for 20 days at a current density of 800 mA/cm^2. In AES spectra, both Hg and Pt signals are detected in the vicinity of the surface. Inspection of the EDX spectrum of the deposits, on the other hand, we can see only Au signals with Pt shoulders (the widths were a little expanded). However, when subtracting the spectrum of pure Au from the spectrum of the deposits, two pairs of Hg and Pt signals appear in the energy ranges from 9 to 10 and from 11 to 12 keV. The fact that the major constituent element of the deposits is Au suggests strongly that the deposits were produced at Au electrode during the electrolysis.

ISOTOPIC ABUNDANCE

The isotopic distributions of Hg contained in the deposits and on/in the electrode after electrolysis and the isotopic distributions of Fe, and Si contained in the deposits obtained by SIMS analysis are shown in Fig. 5, Fig. 6, Fig. 7, Fig. 8 from 1st to 15th scans. The data of Fe and Hg on/in the electrode were obtained by the electrolysis in Na_2CO_3 at a current density of 500 mA/cm^2 and the datum of Hg in the deposits was obtained in Na_2CO_3 at a current density of 800 mA/cm^2. The datum of Si was obtained by the electrolysis in Na_2SO_4 at a current density of 800 mA/cm^2. The isotopic distributions of these elements reveal significant deviation from their natural isotopic abundance. Thus, for Hg, Fig. 5 and Fig. 6, the isotopic content of ^{200}Hg is 35 - 50%, evidently higher than its natural value of 23.13%, while the content of ^{202}Hg, which being the major component in nature, is reduced from its natural value of 29.80% down to 15-20%. The content of ^{200}Hg has a tendency to increase in the inner part of the deposits or electrode, and the contents of ^{199}Hg and ^{204}Hg in the deposits tend to increase in the surface part. The contents of other isotopes change to some extent. We can see from these results that there is not much difference in the change of the isotopic distribution between Hg in the deposits and on/in the electrode.

For Fe, Fig. 7, the content of ^{57}Fe increases significantly as in the case of Fe produced on Au electrode after electrolysis [1], however, in this case, its ratio (^{57}Fe/^{56}Fe) is much higher, exceeding 50% especially in the vicinity of the surface. This ratio has a tendency to decrease in the inner part of the deposits.

The content of Si in the deposits was increased significantly by the electrolysis in Na_2SO_4 at a large current density (eg. 800 mA/cm^2), and, in that case, the color of the deposits changes from black to white gray. The signal of Si was clearly observed also by EDX measurement. As seen from Fig. 8, the content of major isotope, ^{28}Si, in the deposits is decreased down to about 58% from its natural value of 92.2% in the vicinity of the surface. On the contrary, the contents of ^{29}Si and ^{30}Si were increased. The extent of the decrease in the content of ^{28}Si of the deposits prepared in Na_2CO_3 at a current density of 500 mA/cm^2 is a little smaller, the content near the surface being 70-75%. These results show that considerable large amounts of ^{29}Si and ^{30}Si are produced preferentially by the electrolysis in Na_2SO_4 at a large current density, eg. 800 mA/cm^2. As reported already, the isotopic distribution of Si present on/in Au electrode after electrolysis in 0.5 M Na_2SO_4 at a current density of 100 mA/cm^2 was nearly equal to the natural isotopic abundance [3], and in fact, the isotopic distribution of Si present on the Au electrode after the electrolysis in Na_2CO_3 for 30 days at a current density of 500 mA/cm^2 remains to be equal to natural isotopic abundance. Such Si is considered to be fine glass powders produced when scraping the electrode. Therefore, there would be no doubt that ^{29}Si and ^{30}Si are produced at Au electrode through some process occurring when the deposits are produced.

SURFACE STRUCTURE OF AU ELECTRODE AFTER ELECTROLYSIS

It was found that a lot of craters with various sizes are created and developed along the scraped lines of the Au electrode surface during the electrolysis, for example, in Na_2CO_3 at a current density of 500 mA/Cm^2 for 30 days. **Each crater has a deep hole**. The size of the largest one reaches about 20 μm diam. and 30 μ m height. Typical SEM images of the craters are shown in Fig. 9(a-b). From the appearance of the crater, one can imagine that some micro explosion took place at that place. Their outside walls consist of very fine porous substances, very alike to the structure of the deposits shown in Fig. 1(b). In addition, the major element of the deposits was found to be Au from the EDX analysis. Hence, it is very likely that the deposits were spewed out from these craters as the ashes as a result of some partial micro explosion, probably caused by some micro nuclear reactions. The walls inside the crater are constituted by a lot of fine hexagonal crystallites which are assignable Au(111). These crystallites may be considered to be produced by the reconstruction of Au polycrystals owing to the elevated heat evolved locally by the micro explosion. As already described above, we did not detect as much Hg, Pt on/in Au electrode after electrolysis as in the deposits. Perhaps, SIMS analysis was not pin-pointed at the wall of the crater precisely.

REACTION SCHEME

The amount of deposits obtained by the electrolysis conducted in this experiment was 0.5 - 1 mg. The content of Hg in the deposit can be estimated at least at several percent from the result of AES, EDX and SIMS measurement, from which the total amount of Hg produced yields some 10 μ g. On the other hand, even in 100 ml of the electrolyte solution of 0.5 M Na_2CO_3 containing 0.05 ppm of Hg as an impurity, the amount of Hg which must be contained in the deposits as an impurity would be at most 0.35 μ g. In addition, we detected considerable amounts of F by SIMS measurement in every deposits obtained, the amount of which being somewhat larger than the amounts of Hg or Si obtained by the electrolysis at current densities < 500 mA/cm^2. The element, F, would be scarcely present in the environment as long as we do not add it artificially. Hence, it is not understandable that such amount of F is introduced into the electrolytic cell as an impurity. The deviation of isotopic content of Hg, Fe and Si in the deposits strongly suggests that these elements were produced by some nuclear transmutation reaction.

As to the reaction scheme, although it is still far from the completion, we presume on the basis of the results obtained that the nuclear transmutation start by the following reaction,

$$^{197}Au + n^{1}H \rightarrow {}^{198\text{-}204}Hg. \quad (1)$$

The Hg atoms thus produced have very high energies, being unstable, then decompose partly to produce Pt, e.g. by the following reaction,

$$^{200}Hg \rightarrow {}^{196}Pt + {}^{4}He \quad (2)$$

and occasionally, to produce Os by

$$^{196}Pt \rightarrow {}^{192}Os + {}^{4}He. \quad (3)$$

However the change of the isotopic distribution of Pt is not significant so that the reactions (2) and (3) would not occur pronouncedly (most of Pt present on the deposits is considered to come from the counter electrode.).

On the other hand, we presume that Si and F are produced from Fe, by the following reactions,

$$^{56}Fe \rightarrow {}^{28}Si + {}^{20}Ne + 2\,{}^{4}He \quad (4)$$

$$^{57}Fe \rightarrow {}^{29}Si + {}^{20}Ne + 2\,{}^{4}He \quad (5)$$

$$^{56}Fe \rightarrow {}^{29}Si + {}^{19}Ne + 2\,{}^{4}He \quad (6)$$

$$^{19}Ne \rightarrow {}^{19}F + \beta^{+} \quad (6')$$

$$^{57}Fe \rightarrow {}^{30}Si + {}^{19}Ne + 2\,{}^{4}He \quad (7)$$

$$^{19}Ne \rightarrow {}^{19}F\ \beta^{+}. \quad (7')$$

The reaction scheme of producing Fe is unambiguous yet, however, at present stage, we presume as follows,

$$^{198\text{-}204}Hg \rightarrow {}^{56\text{-}57}Fe + {}^{141\text{-}144}Xe \quad (8)$$

The Xe atoms thus produced are unstable which would cause further fission reaction to produce some elements with smaller atomic numbers.

It is very mysterious why such transmutations take place by the electrolysis of light water at a room temperature. It is known that there are small amount of H active sites on Au [4-5] where the hydrogen evolution reaction occurs exclusively by slow recombination mechanism [6-8]. Therefore, at the place where such sites are concentrated (perhaps, it corresponds to the lattice defect), the concentration of H would remarkably increase with increasing hydrogen overpotential, and, in addition, **a considerable amount of micro cracks would be created with high loading of H. As a result of this, extremely strong electric field would be possible to be formed locally at that place.** Under such a condition, some H atoms would have a chance to acquire extremely high kinetic energy and become accessible to Au nuclei enough to cause the nuclear transmutation even instantaneously.

The study of this field is still a starting stage and our concepts concerning the reaction scheme would be far from the completion. In spite of this, there is hardly any doubt that the nuclear transmutation reaction occurs in the electrolysis system at a room temperature from the experimental results obtained here. To elucidate this problem, much more extensive information would be needed.

REFERENCES

1. T. Ohmori and M. Enyo, "Iron Formation in Gold and Palladium Cathodes," *J. New Energy*, vol 1, no 1, pg 15. (1996)
2. T. Ohmori, *J. Electroanal. Chem.*, vol 157, pg 159 (1983).
3. T. Ohmori, M. Enyo, T. Mizuno, Y. Nodasaka and H. Minagawa, *Fusion Technology* (1996) in press.
4. M. Breiter, C.A. Knorr and W. Voelkl, *Ber. Bunsenges. Phys. Chem.*, vol 59, pg 681 (1955).
5. F.G. Will and C.A. Knorr, *Ber. Bunsenges. Phys. Chem.*, vol 62, pg 378, (1958).
6. T. Ohmori and M. Enyo, *Electrochimica Acta*, vol 37, pp 2021 (1992).
7. S. Schuldiner and J.P. Hoare, *J. Phys. Chem.*, vol 61, pg 705 (1957).
8. A.T. Kuhn and M. Byrne, *Electrochimica Acta*, vol 16, pg 391 (1971)

(a)

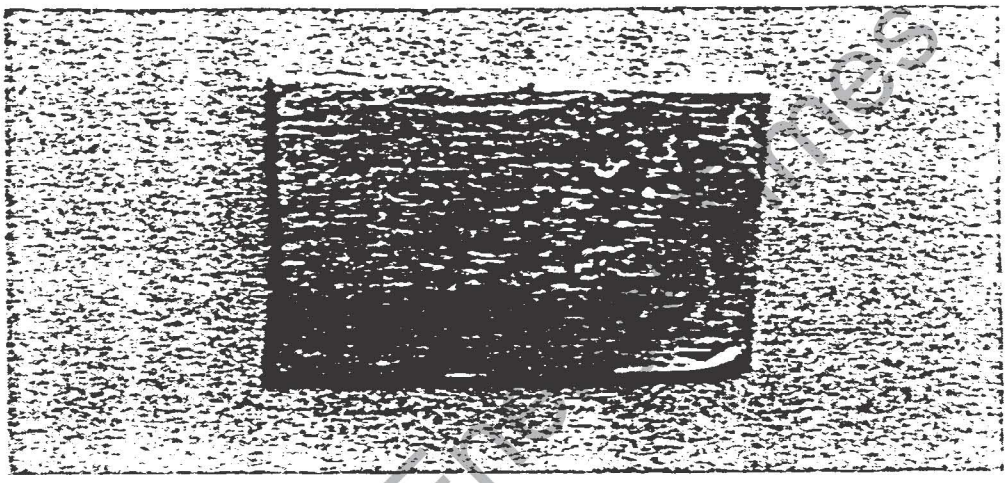

(b)

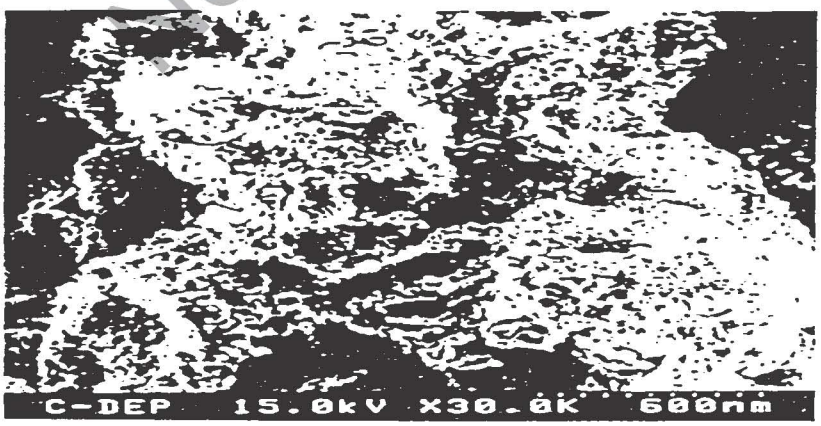

Fig. 1.
(a) Deposits placed on a Ni plate (dark spots mostly distributed at the right hand side) and (b) their SEM image (x 30,000).

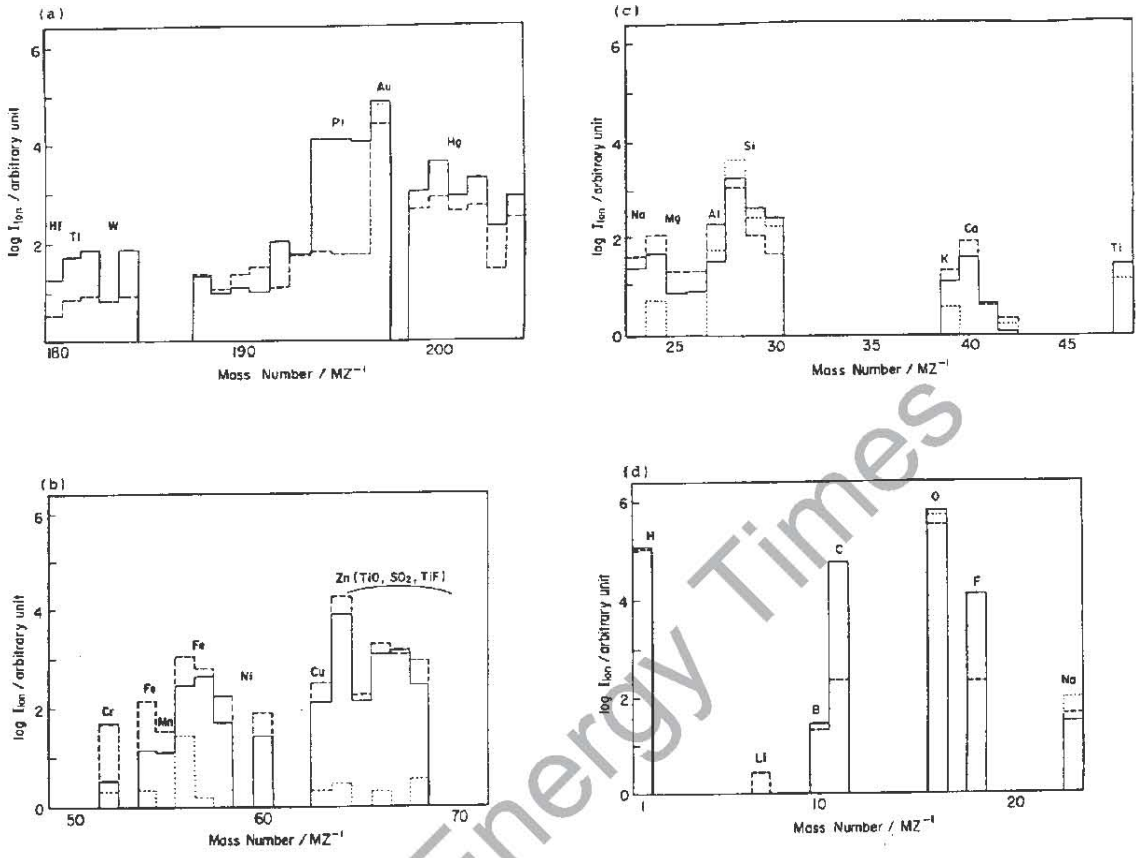

Fig. 2
Relative concentration of the constituent elements of the deposits and of Au electrodes before and after electrolysis. (a) elements with mass number from 180 to 204, (b) elements with mass numbers from 50 to 70, (c) elements with mass numbers from 23 to 48, (d) elements with mass numbers from 1 to 23, (solid line) deposits, (dashed line) electrode after the electrolysis and (dotted line) electrode before the electrolysis. Electrolysis was performed in 0.5 M Na_2CO_3 solutions for 30 days at a current density of 500 mA/cm^2.

The value of Zn is that estimated by assuming that all spectra in that mass number range are only attributed to Zn.

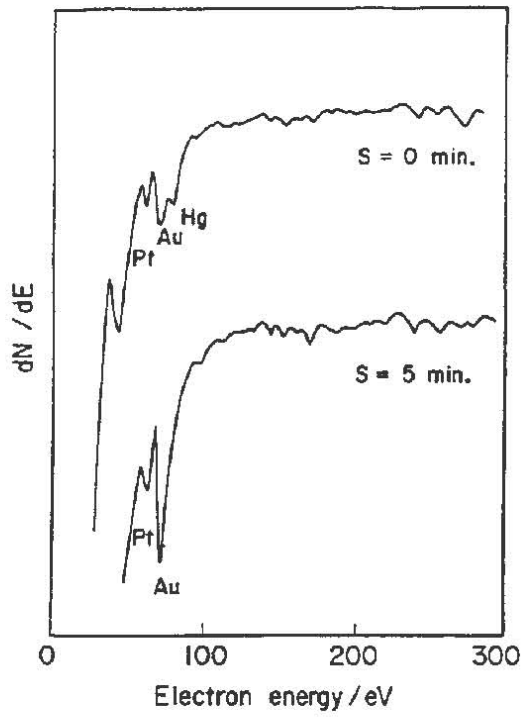

Fig. 3
Typical AES spectra of the deposits, where S means the sputtering time. The deposits were prepared by the electrolysis in 0.5 M Na_2CO_3 solution for 30 days at a current density of 500 mA/cm^2.

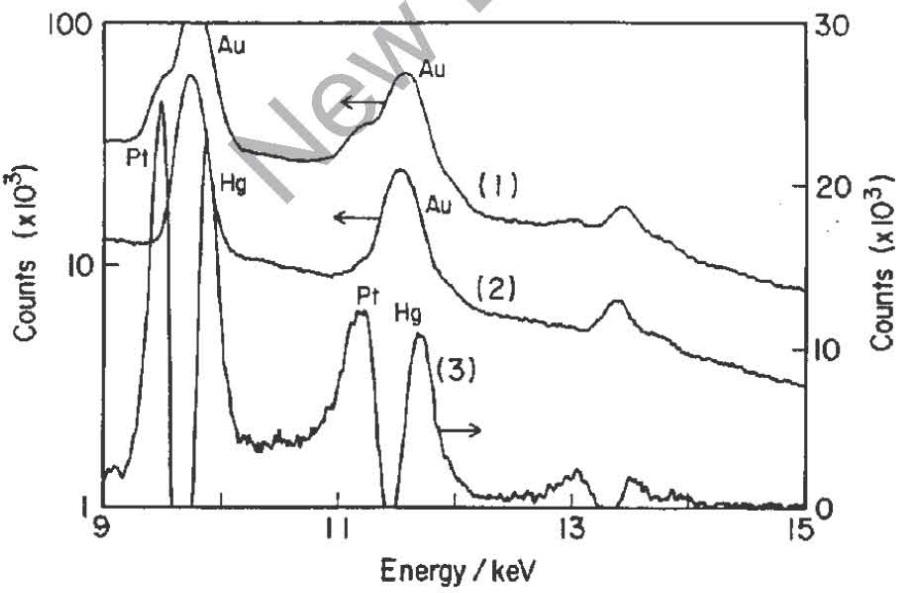

Fig. 4
Typical EDX spectra of the deposits and pure gold and difference spectrum between two spectra. (1) spectrum of the deposits, (2) spectrum of Au electrode before electrolysis and (3) difference spectrum. The deposits were prepared by the electrolysis in 0.5 M Na_2CO_3 for 20 days at a current density of 800 mA/cm^2.

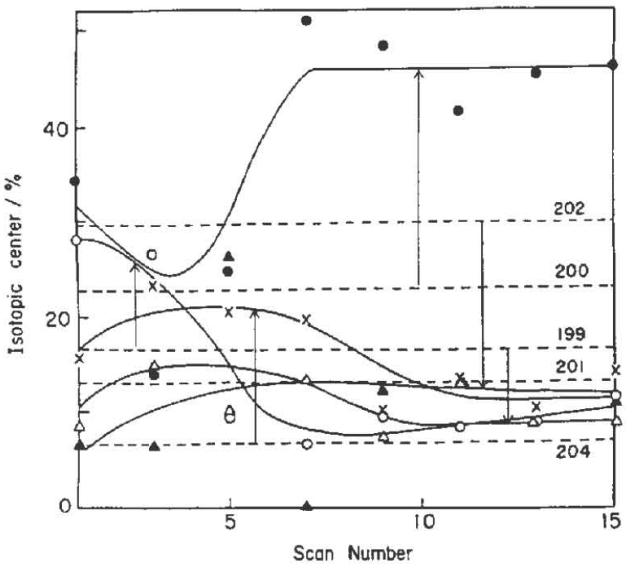

Fig. 5
Isotopic distribution of Hg containing in the deposits, (○) ^{199}Hg, (●) ^{200}Hg, (Δ) ^{201}Hg, (▲) ^{202}Hg and (X) ^{204}Hg. Dashed lines show the natural isotopic abundance levels of individual isotopes. The deposits were prepared by the electrolysis in 0.5 M Na_2CP_3 for 20 days at a current density of 800 mA/cm^2. In this calculation the isotopic content of ^{198}Hg was regarded as natural isotopic abundance.

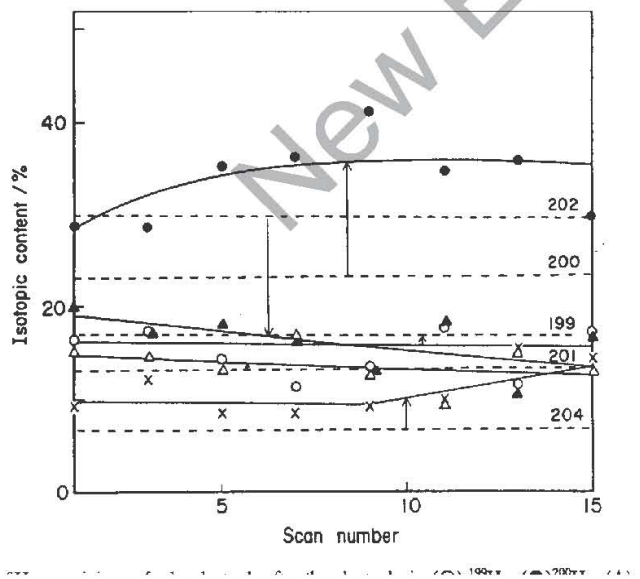

Fig. 6
Isotopic distribution of Hg containing on/in the electrode after the electrolysis, (○) ^{199}Hg, (●) ^{200}Hg, (Δ) ^{201}Hg, (▲) ^{202}Hg and (x) ^{204}Hg. Dashed lines show the natural isotopic abundance levels of individual isotopes. The electrolysis were made in 0.5 M Na_2CO_3 for 30 days at a current density of 500 mA/cm^2. The deposits were prepared by the same procedures in the case of Fig. 5.

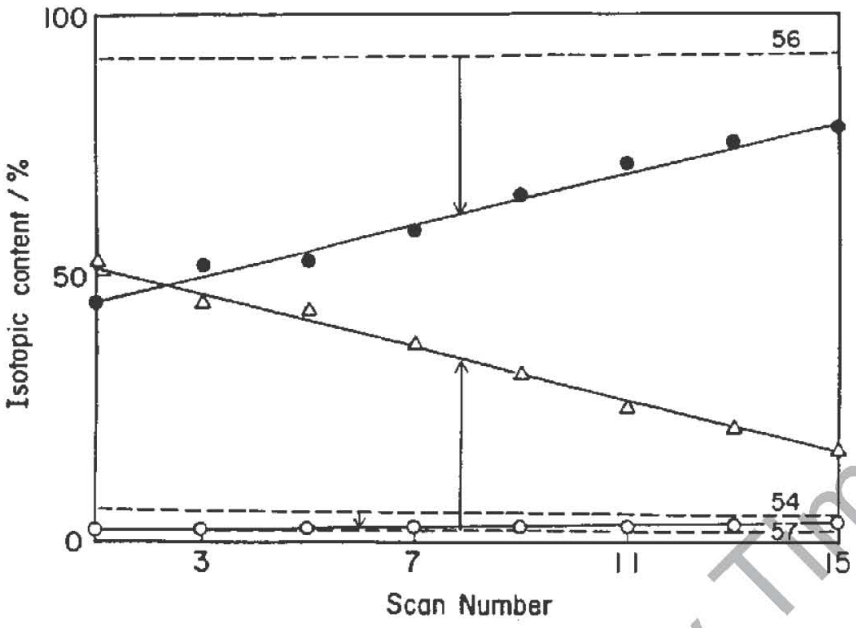

Fig. 7
Isotopic distribution of Fe containing in the deposits, (○)^{56}Fe and (●)^{57}Fe. Dashed lines show the natural isotopic abundance levels of individual isotopes. The deposits were prepared by the electrolysis in 0.5 M Na_2CO_3 for 30 days at a current density of 500 mA/cm^2.

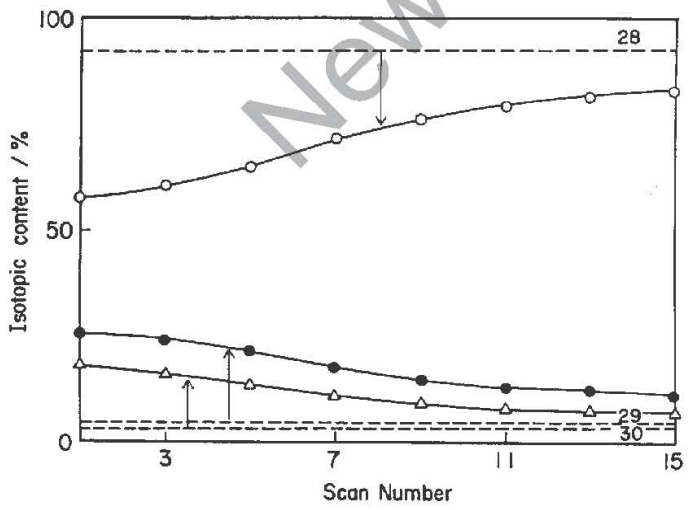

Fig. 8
Isotopic distribution of Si containing in the deposits, (○)^{28}Si, (●)^{29}Si and (Δ)^{30}Si. Dashed lines show the natural isotopic abundance levels of individual isotopes. The deposits were prepared by the electrolysis in 0.5 M Na_2SO_4 for 30 days at a current density of 800 mA/cm$_2$.

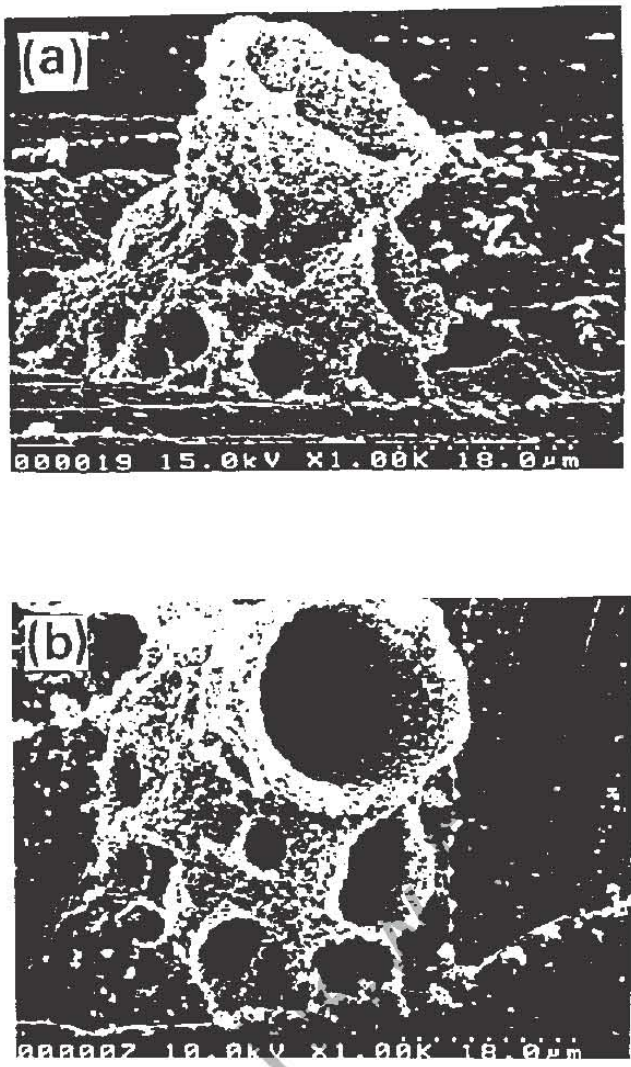

Fig. 9
SEM images of the Au electrode after the electrolysis in 0.5 M Na_2CO_3 for 30 days at a current density of 500 mA/cm^2, (a) image from upside (x1,000), (b) image from horizontal side (x1,000).

ANOMALOUS RADIOACTIVITY AND UNEXPECTED ELEMENTS AS A RESULT OF HEATING INORGANIC MIXTURES

G.H. Lin and J. O'M. Bockris [1]

ABSTRACT

This paper reports anomalous radioactivity and unexpected elements observed in 1992 at the Texas A&M University as a result of igniting a mixture of inorganic compounds. The details of the experiments and the analysis in our laboratory and other private laboratories are presented.

INTRODUCTION

Rutherford [1,2] at Cambridge in 1919 achieved the first "artificially induced transmutation" by bombarding nitrogen with alpha particles from radium to produce oxygen. This achievement rounded high energy physics but it also created a mind set; breaking a nucleus needed a million times more energy than is given out in a chemical reaction.

The first reported cold transmutation in modern times is that of Ramsay et. al., who claimed the transmutation of other elements into helium and neon, reported by J.J. Thomson [3]. Thomson did a similar experiment as that of Ramsay, but he was uncertain whether the liberation of rare gases upon bombardment in a discharge tube is due to the fact that the gases are earlier absorbed from air or whether they are formed by means of transmutation. Kervran, in 1955, did some systematic studies in biological systems where he described the conversion of Na to K [4]. George Oshawa, et al. [5] and Michio Kushi [6] in 1964, made a series of experiments on the transmutation of elements. These experiments were performed at normal temperature and pressure through electrochemical methods. The experiments described by Oshawa et al. for the production of Fe from C and O allow one to reproduce the experiments and has been repeated recently [7,8,9]. Many recent reports [10] are now appearing in the literature which suggest low energy nuclear conversion of elements.

The recovery of precious metal (noble metals) using fire assaying has been used for a long time and a number of variations of this technique have been proposed. Some methods have given more precious metals then others. It has been suggested that recovery of more gold from the ores by use of different fire assaying technique is the result of transmutation at chemical temperatures of other elements to gold instead of by means of a greater efficiency in extraction.

In this paper, we report experimental results on anomalous radioactivity and appearance of small quantities of unexpected elements achieved by rapidly igniting a mixture of inorganic compounds. The details of the experiments and the results analyzed in our laboratory and in other private laboratories are presented.

[1] Dept. of Chemistry, Texas A&M Univ., College Station, TX 77803

EXPERIMENTAL RESULTS

A. Anomalous Radioactivity

A decay of β- radiation after igniting a chemical mixture has been observed [11].

The experiment was performed on April 14, 1992. The chemical composition of the mixture used are listed as follows:

C	100 g	(Johnson Matthey, 300 mesh, 99.5 %)
KNO_3	300 g	(Baker, 99.2%)
S	30 g	(Spectrum)
SiO_2	30 g	(EM Science, 60-200 mesh)
FeS	40 g	(Chempure)
Hg_2Cl_2	10 g	(Fisher, 99.98%)
PbO	10 g	(Johnson Matthey, 99.99%)

The chemicals were weighed separately, and then mixed together. The mixture was ignited in a hood. The burn lasted about 60 sec. The product was ground in a mortar with a pestle after cooling down. Samples from both the original mixture and the product were examined.

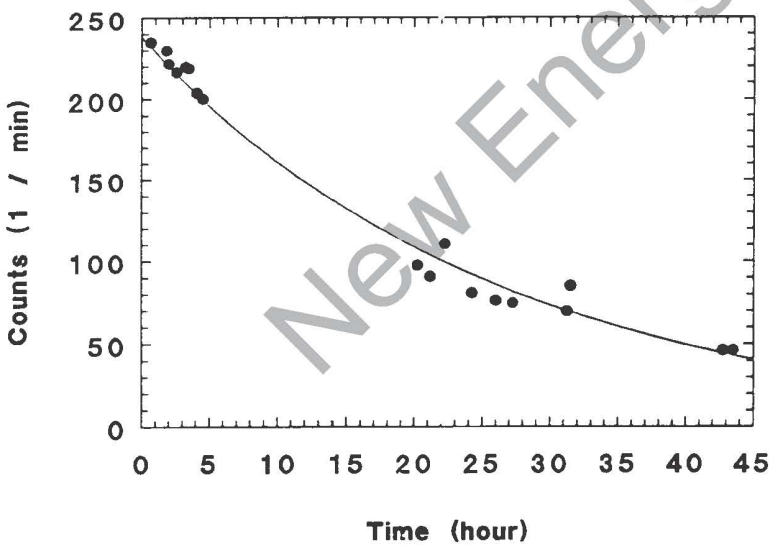

Fig. 1. β counts as a function of time.

Radioactive emission from the samples was detected by means of a β detector (Model 44-1, Ludlum Measurements, Inc.), and recorded by a multichannel pulse height analyzer (Model 800, The Nucleus Inc.) and a data system (Model ZVM-123-A, Zenith). The β detector was covered by a black box to shield it from the room light.

The β counts of the product were higher than those of the raw material, about 1.4 times greater. The β counts of the raw material were stable. On the other hand, decay of the β radiation from the product was observed. The β count of the product (background counts subtracted), as a function of time is shown in Fig. 1. An exponential β decay was observed, and a half life time of 17.7 hours was calculated.

Several other experiments were performed. Not every experiment gave the same results, i.e., conditions for the reproduction of the experiment are not yet well defined.

B. Unexpected elements

Six experiments, named thermal 1 to thermal 6, were performed in Texas A&M University from April 30, 1992 to June 15, 1992. The experimental results are summarized briefly in Table I. The concentration factor has been considered in the table and the following text.

Table 1. Summary of Experimental Results

Experiments	Main Results
Thermal 1	Two times increase of Pt was observed. One fire assay experiment showed the existence of visible Au.
Thermal 2	250-450 ppm of gold present in the product. An increase in Pd was observed, too.
Thermal 3	The weight of precious metal after cupelling from the chemical mixture with Hg was 3-4 times heavier than that without Hg.
Thermal 4	A large amount of gold, about 1700 ppm (with respect to the mineral sand) was found.
Thermal 5	The gold concentration in the product was about 178 ppm (with respect to the raw material).
Thermal 6	No gold was found in either experiment (with and without Hg in the raw material).

(1). Thermal 1 experiment was fired on April 30, 1992. The weight of chemicals in the experiment was 1671 g, and the chemical composition of mixture is listed below:

C	300 g	(Johnson Matthey, 300 mesh, 99.5 %)
KNO_3	900 g	(Baker, 99.2%)
S	80 g	(Spectrum)
SiO2	120 g	(EM Science, 60-200 mesh)
$FeSO_4$	100 g	(Chempure)
Cd	30 g	(Johnson Matthey, 325 mesh, 99.5%)
Hg_2CI_2	100 g	(Fisher, 99.98%)
PbO	50 g	(Johnson Matthey, 99.99%)
Ag	4.99 g	(Johnson Matthey, 100 mesh, 99.95%)
$AgNO_3$	6.2 g	(Johnson Matthey, 99.998%)
Ni	20 g	(Johnson Matthey, Grade I)
Pd	9.78 g	(Engelhart)

Twenty two gram of the raw chemical mixture (before firing) were sent out for analysis, and 1649 g. of the mixture were fired using a propane-oxygen torch. The mixture after ignition burned with a yellow flame and the reaction was completed in 3-4 minutes. The total product after firing was 783.4 g.

Both the raw material and product were sent to Bondar-Clegg in Ottawa and the CSIRO Laboratories in Melbourne, Australia for analysis. Bondar-Clegg used a fire assay and an ICP method. The CSIRO used ICP

and atomic absorption. The remaining product was analyzed by our research team in Texas A&M University by using a fire assay method.

The produced precious metals after cupelling were analyzed by different methods, including XPS, EDS, X fluorescence, X-rays, ICP, and neutron activation.

Both the result from Bondar-Clegg and CSIRO showed no gold, and the analysis results by our team with different methods also showed no gold, except for a specific fire assay run, where visible gold was found by EDS and 148 ppm of gold (with respect to the raw material) was observed by ICP measurement.

The results from Bondar-Clegg and from CSIRO showed twice times increase in Pt in the product. The X rays experiment in Texas A&M University also showed a Pt signal. Neutron activation in Texas A&M showed a small signal for Au and Ir.

(2). Thermal 2 experiment was fired on May 22, 1992. The total weight of the chemicals in the thermal 2 experiment was 1715 g, and the chemical composition are listed on following:

C	300 g	(Johnson Matthey, 300 mesh, 99.5%)
KNO_3	900 g	(Baker, 99.2%)
S	80 g	(Spectrum)
SiO_2	120 g	(EM Science, 60-200 mesh)
$FeSO_4$	100 g	(Chempure)
Cd	20 g	(Johnson Matthey, 325 mesh, 99.5%)
Hg_2CI_2	100 g	(Fisher, 99.98%)
PbO	50 g	(Johnson Matthey, 99.99)
Ag	4.9 g	(Johnson Matthey, 100 mesh, 99.95%)
CaO	20 g	(Baker, reagent)

There are two main differences between thermal 2 and thermal 1. The first is that CaO was used to replace Ni. The second is that Pd was not used.

The total weight of the chemical mixture was 1715 g, and 1655 g was used for the firing. The weight of the product was 849 g.

Both the raw material and product were sent to three labs (Bondar-Clegg in Ottawa, Chemex in Nevada, and Mintek in South Africa) for analysis. The remaining products were treated by means of a fire assay method and analyzed in our laboratory in a similar way as was thermal 1.

Chemex used a fire assay - ICP technique. The gold composition increased from 0.3 ppm (with respect to the raw material) to greater than the detection limit in the product (detection limit is 100 ppm). Bondar-Clegg used a fire assay - DCP technique. The gold concentration increased from 0.12 ppm to 450 ppm (with respect to the raw material) in the product. Mintek used four different methods to analyze the samples. The gold concentration increased from 4 ppm in the raw material to 420 ppm. An interesting feature is that an increase of Pd was observed in all the three analyses. The increases of Pd were from 0.5 ppm to 1.3 ppm by Bondar-Clegg, from 0.4 to 2.1 ppm by Chemex, and from 0.3 ppm to 1.3 ppm by Mintek.

The analytical results in our laboratory were the following. Three sets of experiments were performed. The first set used 126 g of product, and 0.4 ppm (with respect to the raw material) of gold was detected. The second set use 131 g of product powder, 253 ppm gold was detected. The third set used 481 g of product, 240 ppm of gold was obtained.

(3). The next experiment, thermal 3, used mineral sand instead of pure chemicals. Thermal 3 used a mineral (mineral 1), which contained no gold and silver. The total weight of chemicals in the thermal 3 experiment was 770 g, and the chemical composition are the following:

Mineral 1	100 g	(Action Mining)
PbO	20 g	(Johnson Matthey, 99.99%)
C	150 g	(Johnson Matthey, 300 mesh, 99.5%)
KNO_3	450 g	(Baker, 99.2%)
S	30 g	(Spectrum)
Hg_2CI_2	20 g	(Fisher, 99.8%)

Thermal 3 was fired on May 27, 1992. On the same day, another comparison experiment was fired, which had the same chemical composition but contained no mineral.

Thirty grams of thermal 3 product and a comparison product were treated. The fire assay treatment from thermal 3 products contained 3 mg of precious metal (50 ppm), compared to 0.8 mg of bead (13 ppm) from a comparison sample.

No further analysis for the thermal 3 product was performed.

(4). Thermal 4 had the same chemical composition as thermal 3 except that mineral sand 2 instead of mineral sand 1 was used. The mineral sand 2 contains 1.6 ppm of Au and 4.8 ppm of Ag. The experiment was fired on May 30, 1992.

The total weight of the mixture was 770 g. The product powder was 360 g. Part of the product, 100 g, was treated by the fire assay method. A quite large amount of visible gold, about 47.3 mg, was obtained, which was equivalent to 1700 ppm of gold (with respect to the mineral sand).

(5). Thermal 5 was a repetition of the thermal experiment 2. The total weight of the chemical matrix was 1615 grams. The weight of the homogenized powder after ignition was 841 g. The fire assay -ICP method gave 178 ppm of gold (with respect to the raw material).

(6). Thermal 6 experiment had two independent parts. The first part was the same as thermal 4, and the second part containing all the chemicals but no Hg_2Cl_2. The two parts were done in the same experimental conditions. Both parts were fired on June 8, 1992.

However, the fire assay method gave no gold in either part of thermal 6 experiment.

C. Other Thermal Experiments

Eleven experiments, thermal 7 to thermal 17, were run from June 1992 to January 1993. The recipes of these experiments were the same as thermal 2. No gold was detected in these later experiments except in one specific run (thermal 10) in which 0.3 ppm (with respect to the initial weight of chemical mixture) of gold was detected by fire assay plus ICP technique. The β counts were also recorded. No significant changes were observed except in a specific run (thermal 13), where an exponential β decay with a half life time of 23 hours was observed.

DISCUSSION

Four experiments showed an enhancement of gold by 1-2 orders of magnitude above the maximum concentration of gold present in the starting material. These results were confirmed by multiple independent analyses using several different methods and executed by various organizations. However, it was not found possible to reproduce these results in later attempts.

Two β decay experiments showed a half life time of around 20 hours. However, these two runs did not give positive gold production. In 1995, Nominski [12] suggested that the apparent β decay of the burned product may have been caused by a layer of water adsorbed increasingly from the atmosphere. Thus, further investigation would be required for obtaining a definite conclusion as to the reality of the radioactivity.

The lack of repeatability of the results firstly obtained, does not permit a conclusion that the examined "gunpowder" method caused transmutation at low energies. There is a tradition among mining engineers that, by use of such explosive techniques, an order of magnitude increase in the noble metals extracted from ores otherwise classed as "low grade" can be achieved. However, three successful experiments used pure chemicals, not ores, as starting materials.

ACKNOWLEDGMENT

This work was supported by William Telander in an initiative called the Philadelphia Project.

The thermal 1 recipe was supplied by J. Champion. The authors thank Mr. Champion for discussion of the recipes of thermal 2 to thermal 4 and for much other discussion of the mode of carrying out the experiments.

The authors thank Dr. Bhardwaj, Dr. Monti and Dr. Minevski for their help in the experiments.

REFERENCES

1. E. Rutherford, "Collision of α-Particles with Light Atoms," *Nature*, vol 103, (1919), pg 415.
2. E. Rutherford and J. Chadwick, "The Disintegration of Elements by α-Particles," *Nature*, vol 107. (1921). pg 41.
3. J.J. Thomson, "On the Appearance of Helium and Neon in Vacuum Tubes," *Nature* vol 90, (1913). pg 645.
4. C.L. Kervran, Biological Transmutation, Beckman, N.Y. (1971).
5. G. Oshawa, *East-West Institute Magazine*, March 1995.
6. M. Kushi, Private communication to J. O'M. Bockris, May 1992.
7. R. Sundaresan and J. O'M. Bockris, "Anomalous Reactions during Arcing Between Carbon Rods in Water," *Fusion Technology*, vol 26, (1994), pg 261.
8. P. Sing, et. al., "Verification of the George Oshawa Experiment for Anomalous Production of Iron from Carbon Arc in Water," *Fusion Technology*, vol 26, (1994), pg 266.
9. T. Nakamura, et. al., *Chemistry Express*, vol 8, (1993), pg 341.
10. J. O'M. Bockris, R.T. Bush, G.H. Lin, and R.A. Monti, "Do Nuclear Reactions Take Place under Chemical Stimulation?" *J. of New Energy*, vol 1, no 1 (1996), pg 5.
11. G.H. Lin, R. Bhardwaj, and J.O'M. Bockris, "Observations of β Radiation Decay in Low Energy Nuclear Reactions," *J. Sci. Exploration*, vol 9, no. 2, pg 5, (1995).
12. V.C. Nominski, J.L. Ciottone, and P.J. White, "Experiments on Claimed β-particle Emission Decay," *J. Sci. Exploration*, vol 9, no. 3, (1995), pg 1.

INVESTIGATION OF REPORTS OF THE SYNTHESIS OF IRON VIA ARC DISCHARGE THROUGH CARBON COMPOUNDS

T. Grotz[1]

ABSTRACT

Recent research [1,2] has investigated the transformation of carbon to iron under certain experimental conditions. Reports by Pulver [3] and Oshawa [4] of iron formation in carbon by exposure to an electric arc are the subject of this report. Iron formation was originally proposed as a result of the reaction in air of carbon and oxygen to form silicon, then nickel and finally iron as follows;

$$_2C^{12} + _8O^{16} \rightarrow {}_{14}Si^{28} \rightarrow {}_{28}Ni^{58} \rightarrow {}_{26}Fe^{56}$$

Particles of magnetic material attracted to a magnet were given as proof of a transformation. Duplication of this experiment under more controlled conditions with analysis of the iron content of the of the carbon sample before exposure to an electric arc discharge lead to the conclusion that the iron found in the sample may be due to other factors than originally proposed.

INTRODUCTION

This series of experiments was conducted to confirm reports of iron formation in carbon when the latter is subjected to an arc discharge in air. The description of an experiment conducted by Frederick Pulver [3] formed the basis for the investigation. Pulver had heard from Michio Kushi of the experiment done by George Oshawa [5] and associates, circa 1960, to show the transmutation of carbon to iron. The experiment was based on the theory that the transmutation effect can be classified according to the eastern philosophical principles of yin and yang [6]. The experiment consisted of stirring carbon from a "laboratory vial of pure carbon powder" [7] with a carbon rod on a copper plate, across which was connected a variable a.c. power supply as shown in Fig. 1. The carbon was initially tested for iron content by placing a sample on a clean white piece of paper and passing an Alnico™ magnet under the paper to observe the motion of any iron particles present. No particles were attracted to the magnet. The carbon was then stirred with the carbon rod and subjected to arcing and heating for 10 - 15 minutes. After allowing the carbon to cool, it was again tested for magnetic particles by placing the sample on the paper and passing a magnet underneath. As reported by Pulver [8] "...there were small (sand grain size) particles which were definitely magnetic, which followed the magnet around." Pulver's' recreation of the experiment yielded the same results as predicted and previously obtained by Oshawa.

Because there was no stated iron content of the sample before and after the experiment and because the magnetic particles were not analyzed for iron content, a series of experiments was conducted to more closely examine the phenomenon.

[1] Wireless Engineering, Inc., 760 Prairie Avenue, Craig, Colorado 81625

EXPERIMENT

EXPERIMENTAL SETUP

As shown in Fig. 1, the experiments required the use of a 220 VAC voltage source and current regulator. A series of adjustable chokes totaling 15 mH was used as a current regulator. The current was adjusted to a maximum of 40 amps during the process of stirring the sample with a 12.79 mm diameter x 128.18 mm long carbon rod on a copper plate. The carbon rod was obtained from Wale Apparatus. Typical iron content for is given at 100 ppm. Before processing, each sample was poured over a 1 inch square by 1/2 inch neodymium iron boron magnet to remove any magnetic material that might be present in the sample. Charcoal, activated carbon, and coal were used as sources for carbon in the experiment. No detectable magnetic material was found in the samples before processing.

Charcoal, (activated powder)

The first experiment was conducted using 10 g of fine mesh charcoal manufactured by Mallinckrodt. No data concerning iron content is available from the manufacturer. Heavy metal content was listed on the label as 0.002%, chloride (Cl) 0.02%, sulfate (SO_4) 0.02%, and uncarbonized constituents as passes test.

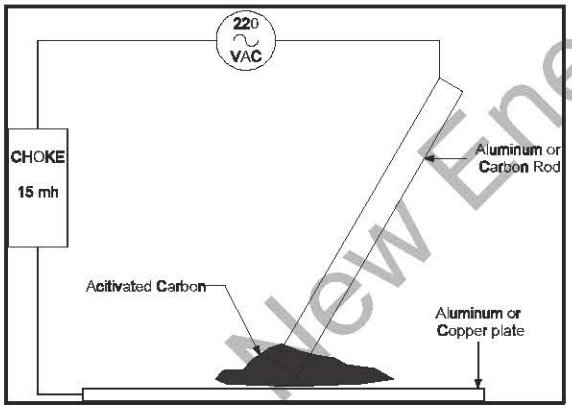

Fig. 1 Diagram of Electrical connections.

After stirring the charcoal for 15 minutes and allowing 10 minutes for the sample to cool, a 1/2" diameter x 1.4" thick neodymium magnet was used in an attempt to pull magnetic material from the carbon. No magnetic material was obtained from the carbon. No transformation was evident as described by Pulver.

Activated Carbon

A bag of activated carbon of the type commonly used in fish tank filters was obtained from a pet supply store. The activated carbon was divided in half and ground into # 8 and # 60 mesh lots. Ten grams of #60 mesh carbon was stirred for 10 minutes with a five minute pause and then stirred again for 10 minutes. Using the 1/4 inch diameter neodymium magnet, 0.12 g of magnetic material was pulled from the sample. Immediately after the last arc was struck, the temperature of the tip of the carbon rod was measured to be 136°C.

Ten grams of #8 mesh activated carbon was processed in the same manner. Using the same magnet, 1.20 g of magnetic material was removed from the sample.

Further processing of the sample in 10 minute intervals for a total of 40 minutes yielded an additional 0.34 g of magnetic material for a total of 1.54 g. Before the additional processing, the weight of the carbon rod was 28.59 g. After processing the rod was weighed again and found to have retained the same weight of 28.59 g.

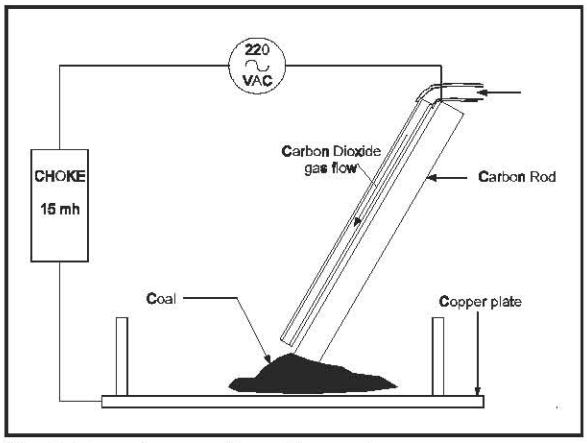

Fig. 2 Experiment with coal as carbon source.

Copper and Aluminum plates and rods.

In an attempt to rule out the possibility that the carbon rod and the copper plate might somehow be contributing to the phenomenon, a 6061T6 aluminum plate 100 mm x 65 mm x 6.32 mm and a 12.71 diameter x 128.60 mm rod of 6061T6 alloy was used to repeat the experiment. Aluminum alloy 6061T6 has an iron content of not more than 0.007 % by weight After processing for 10 minutes 0.23 g of magnetic material was pulled from the sample. Further processing was discontinued due to the formation of slag on the tip of the aluminum rod which had a tendency to melt during the discharge.

Coal used as a Source of Carbon.

An alternate form of carbon for the experiment in the form of sub-bituminous coal was also tested for magnetic material formation. Coal of this type is used in fossil fuel electrical generation plants and typically contains 40 - 60% carbon. In order to prevent the coal from igniting during the arc discharge process, the sample was bathed in a stream of CO_2 as shown in Fig 2.

The mineral analysis of the coal is typical for coal mined in northwestern Colorado. An ash analysis yields the following typical percentages.

phosphorous pentoxide	1.35	potassium oxide	1.14
silicon dioxide	53.06	sodium oxide	0.28
ferric oxide	1.16	sulfur trioxide	6.71
aluminum oxide	19.18	barium oxide	0.65
titanium dioxide	0.63	strontium oxide	0.19
manganese dioxide	0.05	undetermined	4.82
calcium oxide	9.14		
magnesium oxide	1.64	Total percent	100

Both #8 mesh and # 60 mesh coal were used in the arc discharge experiment. Each sample of 10 g was stirred for 10 minutes. Because the 60 mesh coal would not conduct an arc, 5 g of the Mallinckrodt charcoal was added to the mixture to facilitate a discharge. After cooling, there was no detectable magnetic material in the samples using the magnetic separation method previously described.

ANALYSIS OF THE RESULTS

Ash analysis of the activated carbon was performed by Standard Laboratories in Casper, Wyoming. The iron oxide (Fe_2O_3) by ash analysis was determined to be 3.81%. Iron makes up 70% by weight of iron oxide. The percentage by weight of iron in the ash is then;

0.70(3.81%) = 2.67% iron content in the activated carbon

In 10 g of the activated carbon sample there would be;

0.0267(10 g) = 0.267 grams of iron

The experiment that yielded the most magnetic material was analyzed by The Colorado Assay Company, Denver, Colorado. The total iron in the 1.50 g sample sent in for analysis was found to be 1.485%

0.01485(1.50 g) = .022 g of iron removed from the sample (processing time of 40 min.)

An experiment was conducted to determine the iron, nickel, and silicon content of the activated carbon before and after processing, and the content of iron, nickel, and silicon in the magnetic material pulled from the processed activated carbon. Table I shows the results.

This amount of iron is an order of magnitude less than that which occurs naturally in the sample. Because of this result, an analysis of possible iron contamination from the rods or other sources was not considered The excess weight of the material moved after processing appears to be due to magnetic material that is part of or encased in particles of carbon. Using an Alnico™ magnet to pull magnetic material out of the sample resulted in removal of very fine particles that closely resembled iron filings. The particles removed using the neodymium magnet resembled grains of sand as described by Pulver.

Table I

% Content of elements	Fe	Ni	Si
Before processing	3.8	< 0.01	4.01
After Processing	0.33	< 0.01	2.82
Magnetic material removed from Activated Carbon	2.48	< 0.01	4.62

Additionally, it was noted that there was a great variability in the amount of material removed vs. time under process. In Fig. 3 it can be seen that after 40 minutes of process there was slightly less than a gram of magnetic material removed. The curve appears to reach an asymptote around 0.10 grams indicating that there is a point at which no more magnetic material may be removed from the sample using the arc discharge process. If the data reported by Sundaresan and Bockris are plotted in this manner, ingnoring a data point that seems to be abnormally high, (electrode three after 10 hours), a similar shaped curve results.

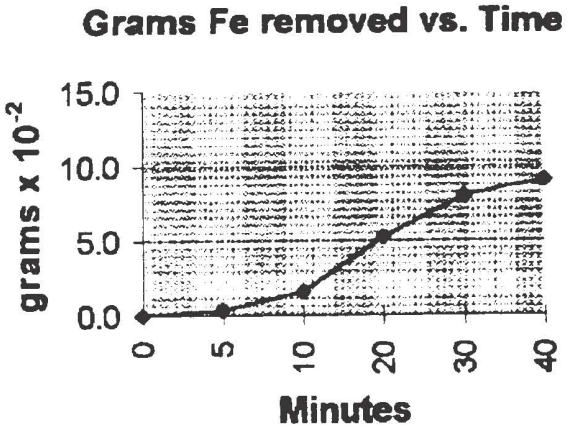

Fig. 3. Fe removed over time.

It is proposed here that the high current density of the arc discharge magnetizes magnetic material that exists within the particles of the activated carbon. This then allows separation of the magnetic material from the sample using a magnet. The #60 mesh samples may have had magnetic material broken down into a size that was too small to be magnetized by the current flow of the arc. The relationship between size of a particle containing magnetizable material and the ability of an electric arc discharge through the particle to magnetize the material is outside the scope of this report.

Because the #60 mesh samples of charcoal and activated carbon did not yield magnetic material, it may

have been that the "laboratory grade" carbon used by Pulver was much coarser in size.

In essence there are two contradictions to the original reports of transmutation of carbon into iron. First, the laboratory grade carbon by Mallincrodt did not produce magnetic material, although the laboratory grade carbon used by Pulver did. Second, when magnetic material was produced from carbon, the quantity that was removed was an order of magnitude less than occurs naturally.

It is however fortuitous that the theory of Oshawa sparked the experiments of Bockris, Sundaresan [1], Singh, et al [2], who have found anomalous formation of iron during arc discharge experiments.

FUTURE RESEARCH

Since the experiments described above were conducted, the author has learned of experiments conducted by C. Akbar at the Kushi Research Institute that indicate that voltage potential and current density are important in the formation of iron in chemically pure carbon [8]. This is in accordance with more detailed descriptions of the carbon to iron transformation experiments presented by Kushi and Akbar [9]. Future work will attempt to define the parameters around iron formation vs. voltage and current and if anomalous amounts of iron are formed at optimum conditions.

REFERENCES

1. R. Sundaresan and J.O'M. Bockris, "Anomalous Reactions During Arcing Between Carbon Rods in Water," *Fusion Technology*, vol 26, Nov. 1994.
2. M. Singh, M.D. Saksena, V.S. Dixit, and V.B. Kartha "Verification of the George Oshawa Experiment For Anomalous Production Of Iron In Water," *Fusion Technology*, vol 26, Nov 1994.
3. F. Pulver, in Biological Transformations, New Alchemy by Louis Kervran and George Oshawa, George Oshawa Macrobiotic Foundation (1971), pp 48-49.
4. M. Kushi and G. Oshawa, Kushi Institute Study Guide, vol 10 (1980), p 1.
5. M. Kushi and G. Oshawa, Kushi Institute Study Guide, vol 10 (1980), p 1.
6. M. Kushi, The Book Of Macrobiotics, p 140, Japan Publications, Inc. (1977), Tokyo, ISBN 0-87040-381-8.
7. Lewis Kervran and George Oshawa, Biological Transmutation, Natural Alchemy, Macrobiotic Found., G. Oshawa Pub. (1971), pg 47.
8. Louis Dervran and George Oshawa, Biological Transformations New Alchemy, George Oshawa Macrobiotic Foundation, (1971), pg 48.
9. C. Adbar, Kushi Institute, private communication.
10. M. Kushi and Edward Esko, "The Philosophers Stone," Michio Kushi's Guide to Alchemy, Transmutation, and the New Science, One Peaceful World Press, Becket, MA (1994).

OBSERVATIONS ON THE ROLE OF CHARGE CLUSTERS IN NUCLEAR CLUSTER REACTIONS

Ken Shoulders and Steve Shoulders[1]

ABSTRACT

Deuterium loaded palladium foils, produced by both electrolytic and ultrasonic processing, have been micro-analyzed for nuclear reactions. The characteristic strike marks of charge clusters, known as EVs, have been found to occur concurrently with nuclear reactions in micrometer-sized areas. In the electrolytic case, the reaction is attributed to charge clusters generated from mechanical energy, first stored and then suddenly released, from a brittle metal lattice through the mechanism of fracto-emission of electrons. For the acoustic case, EVs are generated by charge separation in a collapsing bubble. When areas previously free of low energy nuclear reactions are bombarded in either vacuum or air by externally generated charge clusters, nuclear reactions are produced at the bombardment site. Charge clusters are considered to function as a collective accelerator capable of injecting a large group of nuclei into a target with sufficient energy density to promote the nuclear cluster reactions observed.

I. BACKGROUND

Highly organized, micron-sized clusters of electrons having soliton behavior, along with number densities equal to Avagadro's number, have been investigated by K. Shoulders since 1980 [1] [2] for use in electronic systems. To facilitate daily discussion of the entity, a short Latin acronym has been adopted and the structure is called an EV, for *strong electron*. Their organizational properties have been theoretically studied and reported by P. Beckmann [3] and R. Ziolkowski [4]. The origin of an explosive emission process capable of producing this extreme state of matter has recently been described by G. Mesyats [5].

What is seen in the laboratory is an extremely energetic entity capable of being transformed into a wide range of action-producing variations. Measurements have been made showing there are no included ions to a limit of at least one ion per million electrons. The total number of electrons in a one micrometer diameter EV is 10^{11}. This number allows for inclusion of about 10^5 nuclides that would escape detection by measuring the charge-to-mass ratio of the structure in such a primitive way as time-of-flight. For all practical purposes, the entire ensemble of electrons and nuclides would be collectively accelerated to the velocity of electrons. This gives the effect of a very simple and efficient nuclear particle accelerator. Nuclides can be added to the basic EV to such a high level that the net charge becomes positive. Under this condition there is no valuable collective acceleration, although other interesting effects occur.

Over time, a number of observations have been made showing that the characteristically high energy density of EVs are enhanced further by interaction with certain target materials. The simplest observation method is to allow an EV to strike a metal electrode and note the magnitude of the plasma plume arising due to the explosive decomposition of the EV order. On some strikes there is copious X-ray production, very energetic plasma plumes and a "wildfire" effect to be discussed later. Conversely, other strikes cause a normally energetic micro plasma plume without the higher energy output. The cause for some of these differences, as seen on palladium foil, is the

[1] 1025 Freestone Ranch Rd., PO Box 243, Bodega, CA 94922-0243 Phone: (707)876-1880

subject of this paper. In the interest of brevity, we will use the term, NEV, to designate EVs containing nuclides. In the scenario being developed here, the NEV acts as an ultra-massive, negative ion with high charge-to-mass ratio. This provides the function of a simple nuclear accelerator.

It is not the intent of the observations presented here either to add or take away anything from the ongoing discussions of low-energy nuclear reactions. Rather, it is the intent to show a similarity between electrolytic, sonic, and gaseous discharge methods for producing the effects observed. However, it is difficult to explain the observations without some extraordinary means for introducing "foreign" material.

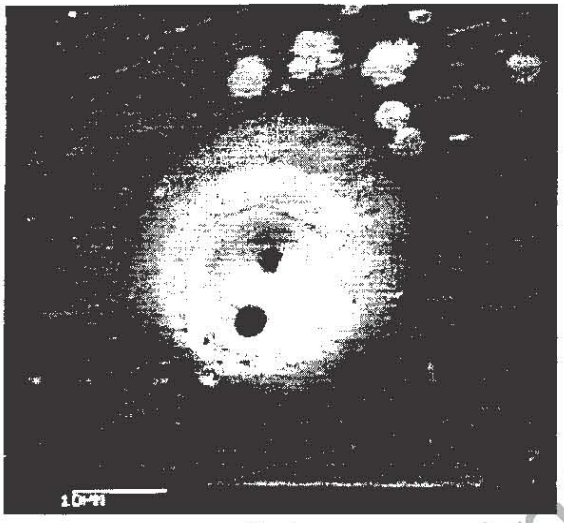

Fig. 1

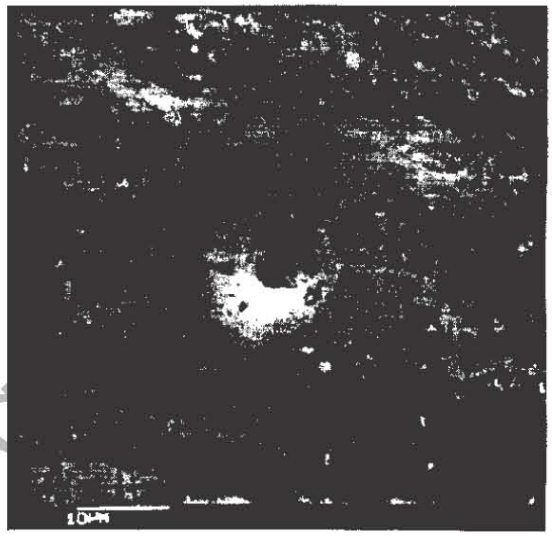

Fig. 2

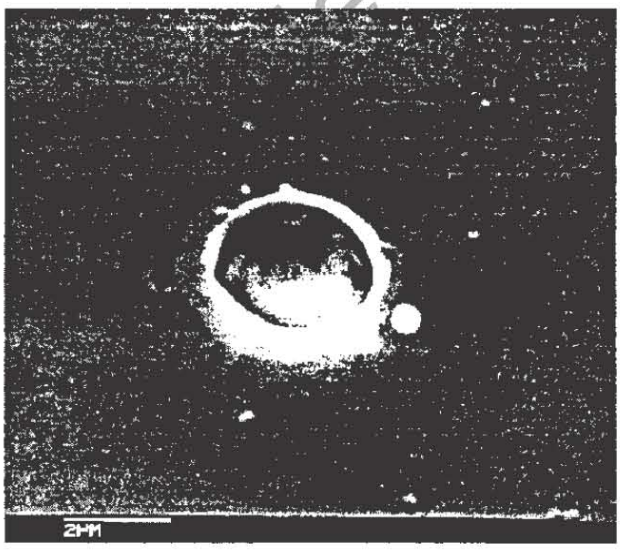

Fig. 3

II. STRIKE MARK INTERPRETATION

As a reference to what a normal EV strike on a metal foil target looks like, Fig. 1 shows an example produced on an aluminum target having a thickness of about 6 μm. In this case, the EVs were produced by a very simple external power source consisting of a hand-held Tesla coil applied in air. The backside of a typical strike on the same material is shown in Fig. 2. It can be seen that the energy of the strike is sufficient to penetrate the aluminum. Using a higher resolution, chromium film-on-glass type of witness plate, Fig. 3 shows more detail of the energy center for the same kind of strike without having much lateral thermal transfer through the target. The strike is about 3μm in diameter and this should serve as a reference for the core size of energy that is delivered to the Pd sample being investigated.

When higher melting point materials are struck in vacuum by an EV, the craters change in both size and shape. Fig. 4 is an example of a strike on a stainless

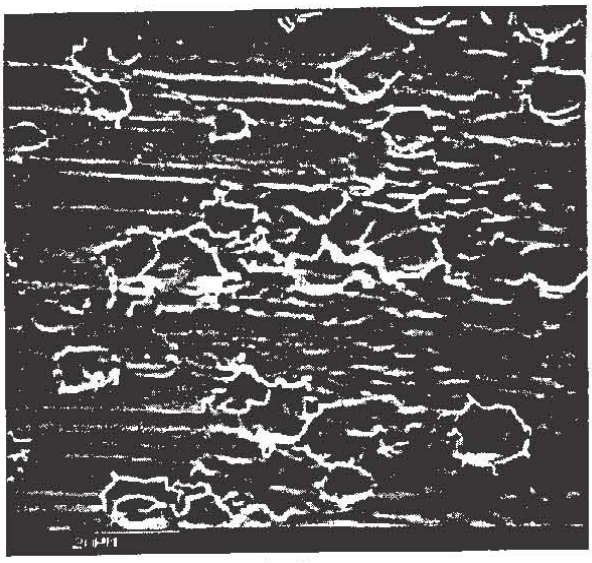

Fig. 4

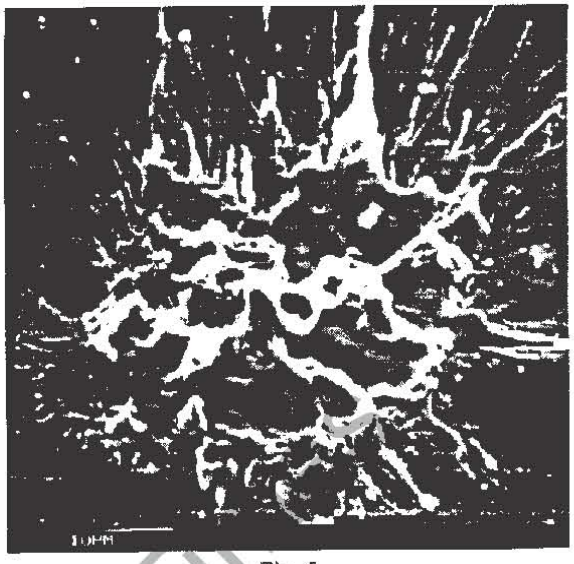

Fig. 5

steel metal foil 13 μm thick. The back side of the foil is shown in Fig. 5. Once again, there is adequate energy for penetration. The peculiar splash pattern of ejected material on the back side is caused by using an aluminum back-up plate to help suppress charge accumulation on the high resistance stainless steel foil. Without this plate, the negative charge density can be so high that the EV is unable to land and it will skip away to deposit energy elsewhere.

The arc literature has many examples of this type of strike mark, often called cathode craters, but there is difficulty in distinguishing between cathode and anode craters on bulk materials by appearance alone. This point is often complicated by not being able to tell which electrode is a cathode and which is an anode. Further exasperation results by studying work done on unipolar arcs where a laser beam strikes a surface having a single potential and produces a miniature thunderstorm of charge that, first, separates into positive and negative clouds, and then forms an EV destined for the electrode that appears positive to this newly-formed negative entity.

In fact, both cathode and anode craters do appear very much alike unless analyzed at high resolution. This analysis is not easy to do on most bulk materials, such as those used here. The craters seen on both sonically processed and electrolytically processed surfaces share the enigma of the unipolar arc. Cathode and anode marks are largely indistinguishable. Fortunately, for externally generated EVs, where the distance is large and filtering is possible, the polarity problem is largely overcome. The target is the anode.

III. PALLADIUM SAMPLE PREPARATION

Two samples of palladium, treated by different processes, were contributed from other laboratories. A sample was sent by John Dash of Portland State University. A slightly similar sample was used by Dash [6] in an early cold fusion paper showing nuclear conversion in micrometer-sized areas. The particular sample we received was about 100μm thick and had been electrolytically treated in heavy water, using sulfuric acid electrolyte, on 7-26-93. According to Dash, "the sample was immediately washed in deionized water and stored in a covered plastic dish."

A second sample, treated by ultrasonic process, was contributed by Roger Stringham of E-Quest Sciences. The sample was run in D_2O on April 29, 1996 in reactor M 11 B and was originally a foil 100 μm thick. The received

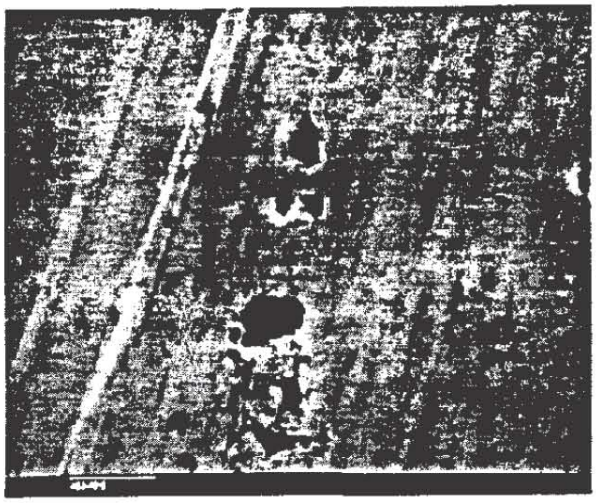

Fig. 6

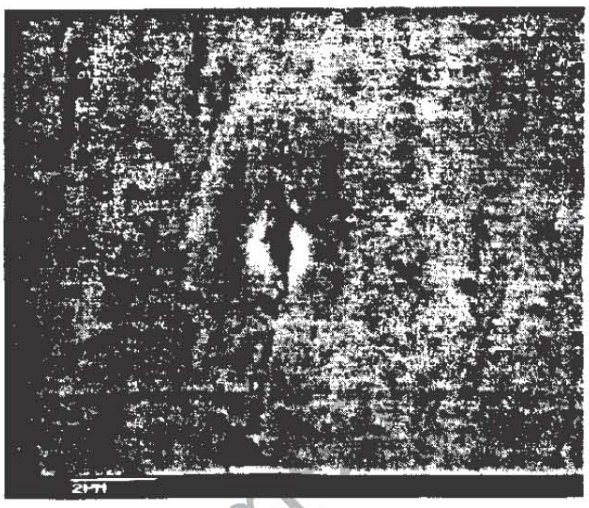

Fig. 7

sample consisted of bits of palladium that were energetically detached by cavitation from the main palladium foil and had fallen to the bottom of the ultrasonic apparatus. The samples analyzed were about ½ millimeter in extent across their diameter. They were tested in the as-received condition.

IV. TESTS ON THE DASH SAMPLE WITHOUT EXTERNAL STIMULATION

Initial tests on the surface morphology of the sample were done in the authors' laboratory using a SEM to see if EV strike marks could be located that would likely arise from fracto-emission. Such strike marks were found, although they differed slightly from standard EV marks produced using the aforementioned methods. A typical

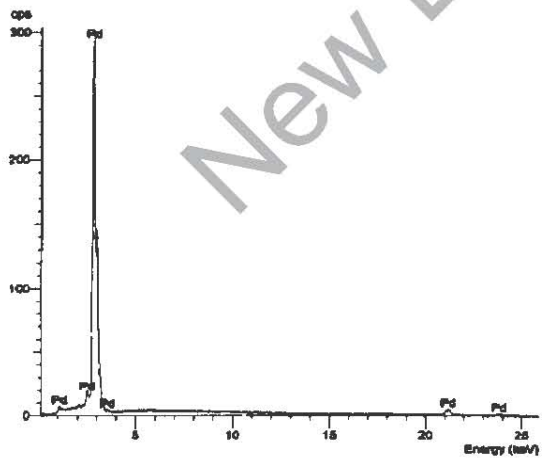

Fig. 8

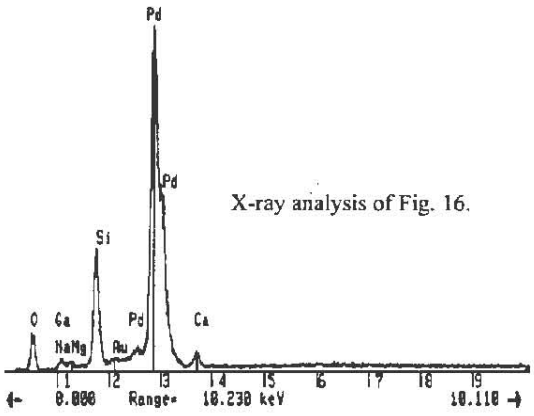

X-ray analysis of Fig. 16.

Fig. 9

example is shown in Fig. 6. Although the small bright mark in the center is somewhat characteristic of an EV strike, the one on the extreme right is more typical. This mark is magnified in Fig. 7. The size of the strikes are smaller than is usually seen by external EV generation methods and the brittle structure of the base Pd has altered their appearance slightly, sometimes producing a molten, elongated cavity aligned with some metallographic feature. In all likelihood, the main strike hit the large black area in Fig. 6 and was blown away with it. A slight,

light colored decoration of the lower edge of the crater shows the effects of evaporated material as the ejected fragment left.

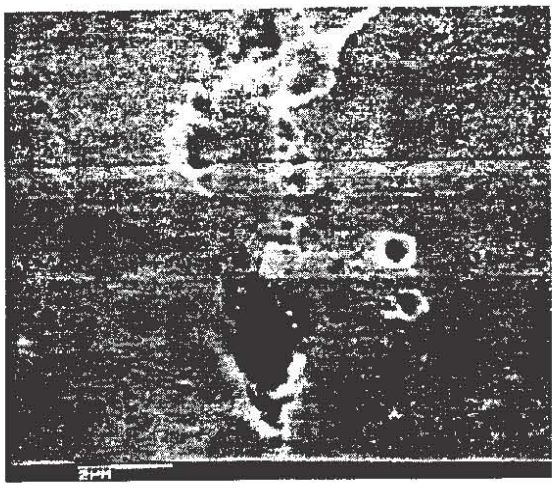

Fig. 10

The brittle nature of the material shown in Fig. 6 is apparent from the shape of the fracture lines. Also, there are melted regions showing that testify to an intense heating process. An X-ray microanalysis of almost any area of the surface that has not been subject to a disruptive process is shown in Fig. 8 and is basically pure palladium. On the other hand, an X-ray microanalysis of a typical fractured region, like that shown in Fig. 6, is shown in Fig. 9 and depicts quantities of Mg, Ca, Si, Ga and Au, along with the base Pd signature. Many examples similar to the one shown appear on the substrate, although, on this particular sample, they are widely separated. It is possible that these new materials were produced by nuclear reactions involving the two major materials initially present, namely, palladium and deuterium, although they could have conceivably migrated into the region along grain boundaries.

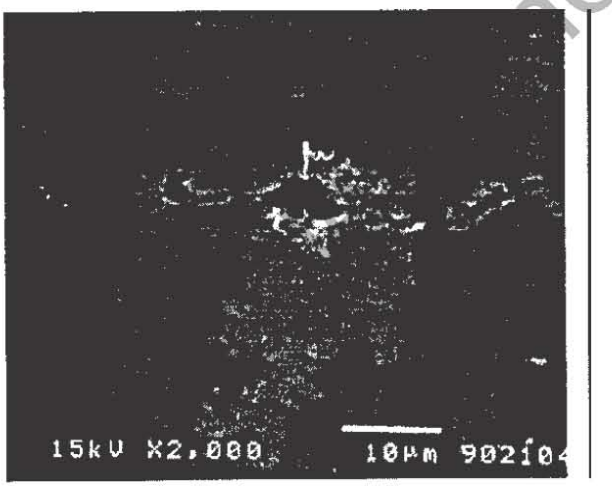

Fig. 11

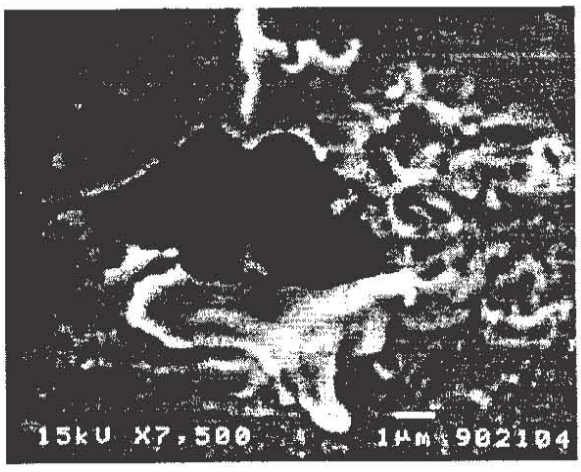

Fig. 12

Taking the nuclear reaction view, it is the authors' contention that the craters on the surface are caused by a locally created, fracto-emission site that then produces a NEV strike and that, in turn, this nuclear cluster input is responsible for the nuclear cluster reaction produced. A wide variety of crater shapes would be expected on such an active surface. That some of the most energetic strike marks would be carried away with the ejection of a brittle material chunk would be expected as well. In fact, brittle chunk ejection is the *sine quo non* of the surface. In this case, most of what remains to be seen would be the ineffective strikes. The ejection of incompletely-used nuclear fuel material is not a desirable trait, but it is commonplace in this sample. In the next section, an example will be shown of more complete retention of material using an external initiation method.

V. TESTS ON THE DASH SAMPLE WITH NEV STIMULATION

A primitive EV generator was used to bombard a localized region of the same sample just discussed. It consists of a hand-held Tesla coil of the type designed to locate vacuum leaks in glass apparatus. A region of the sample was masked off by a dielectric shield, and then, with the sample grounded, sparks were allowed to strike the

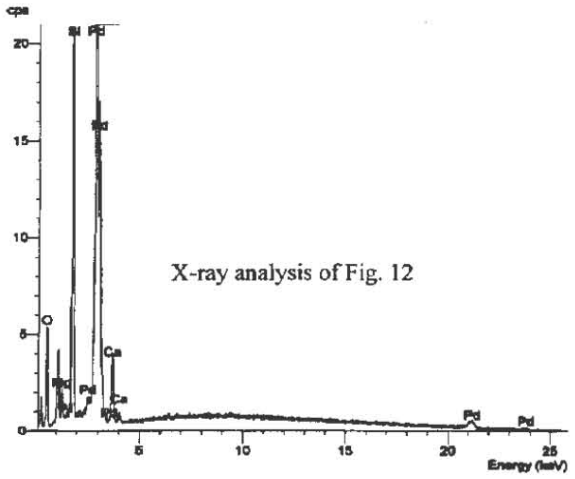

X-ray analysis of Fig. 12

Fig. 13

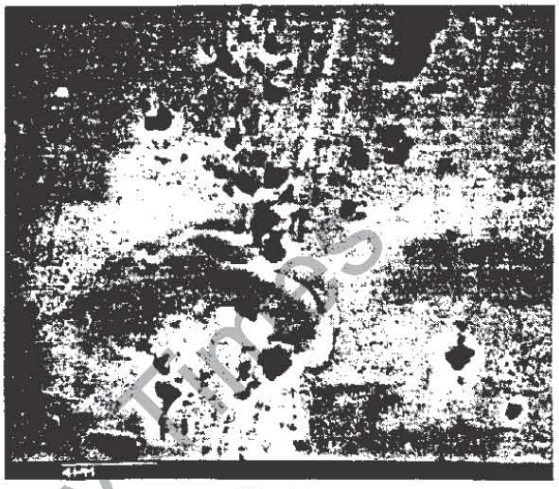

Fig. 14

surface from a distance of about 1 centimeter. Small flashes are produced wherever the spark terminates on the surface. This is the signature of an EV strike and it dependably produces the kind of marks shown in Fig. 1 and Fig. 3, provided there is no added energy from the surface itself.

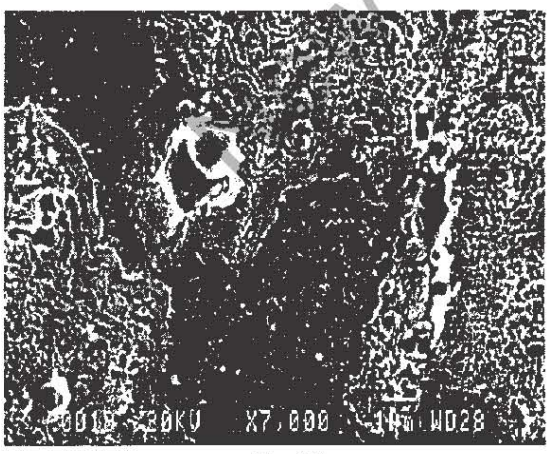

Fig. 15

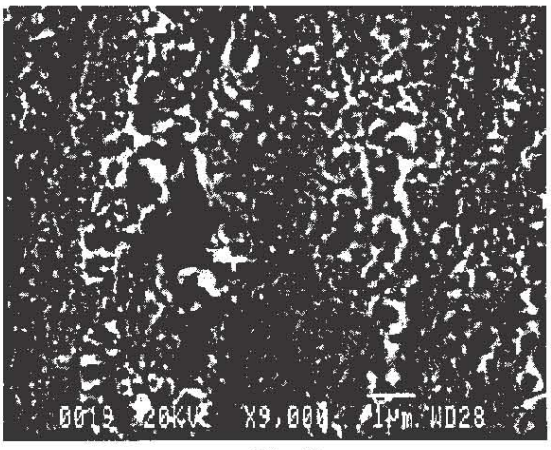

Fig. 16

Although the strike mark produced by the above method of generating an EV is very consistent on the standard witness plates discussed, there is no assurance as to the kind and number of nuclides loaded into the structure. When this EV loading is an important parameter of a nuclear reaction produced by a NEV, as it may be when working with deuterium loaded Pd, such a chance method of loading may be found insufficient for consistent work.

Occasionally, one of the strikes on the material being analyzed produces a result that is uncommon to the low energy EV strikes shown in either Fig. 1 or 3. An example of this shows in Fig. 10 on a region of the surface that includes a brittle fracture on a thin surface layer. This layer has been effectively peeled back by throwing molten material sideways along the path of propagation. Although the NEV strike may have initiated the process, continuation appears to be self-propagating due to locally added energy. This is the Hallmark of an exothermic process, and if the active material extends to a great depth, complete runaway can occur.
In the center region shown in Fig. 11, and magnified in Fig. 12, the X-ray analysis shown in Fig. 13 defines the production of either new material or something foreign included in the substrate along the boundary defined by the dark marks. Although an inclusion of dirt is easily suspected for the crack shown, no suspect material appears unless the region is involved in an energetic strike.

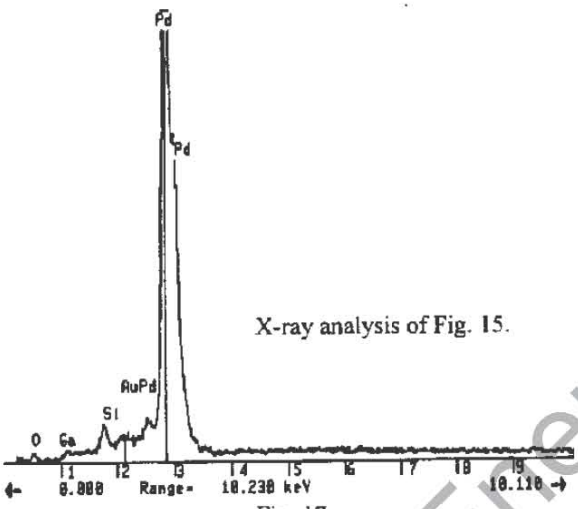

X-ray analysis of Fig. 15.
Fig. 17

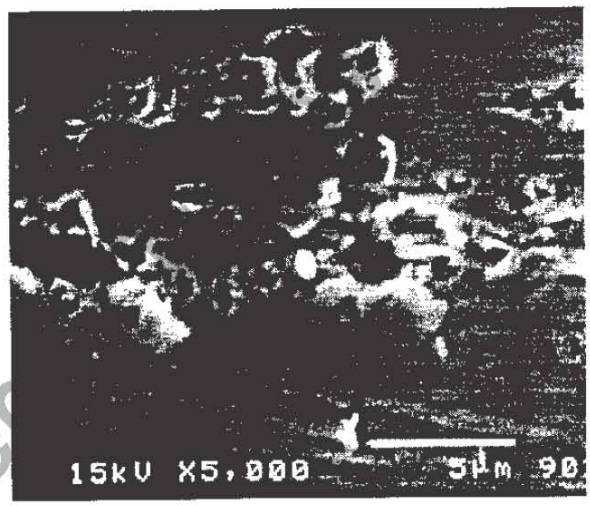

Fig. 18

The explosion in this region was produced by bombardment with an externally produced NEV and the strike mark can be clearly seen. In addition, there is some surface decoration showing that defines an energy release which has scoured the surface, producing a light colored region below the main strike. The cause of this "wildfire" will be discussed later.

In some regions there is an exception to the rule of ejecting a brittle piece of substrate material. Fig. 14 shows a strike region where gross melting occurred in a way that is also very uncommon for EV-only energy deposition on benign substrates. This melted region seems to have been moving sideways at the time it froze in place. Keeping the nuclear fuel bound to the surface, as it is here, is more desirable than losing it through brittle fracture chunks being thrown off. Unfortunately, electrolytic processing needs the brittle structure to serve as the nuclear initiator. Separation of the processes of initiation and fueling would be desirable.

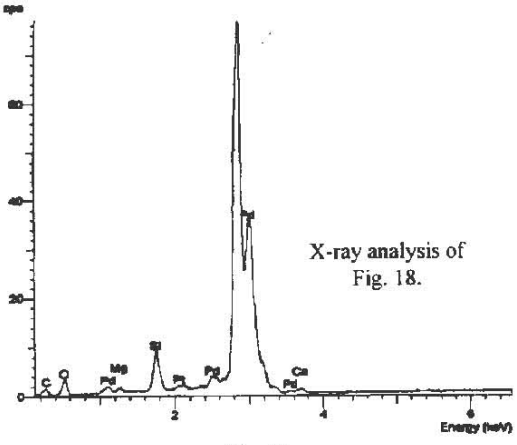

X-ray analysis of Fig. 18.
Fig. 19

An example of what appears as a "wildfire" propagation of energy shows in Fig. 15 and Fig. 16. This effect has also been seen on other than Pd surfaces, but it is quite pronounced here. The runaway process was triggered by

the arrival of an externally made NEV. The energy feeding the process seems to emanate from cracks formed in the brittle, top layer of Pd. This layer is about 0.1μm in thickness and extends over the entire surface. It would seem incumbent on this highly stressed layer to either peel or otherwise breakaway from the base material in an explosive fashion, producing fracto-emission of electrons. An input shock from an externally supplied EV would likely supply a trigger for this process.

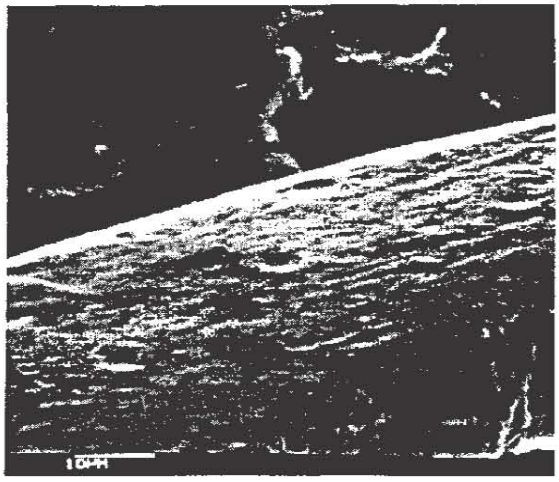

Fig. 20

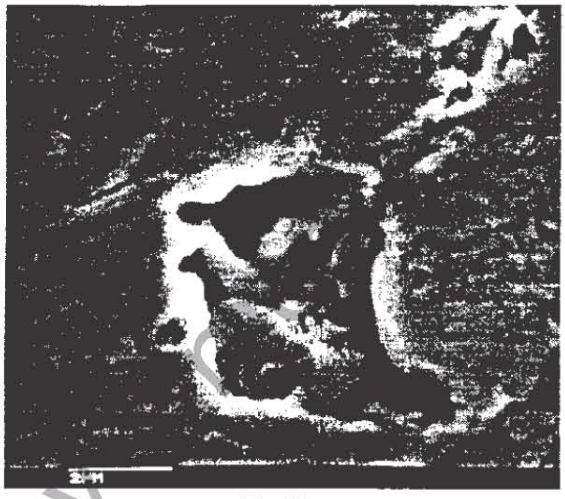

Fig. 21

The X-ray microanalyses of Figs. 15 and 18 are shown in Fig. 17 and Fig. 19 respectively. The analysis of Fig. 16 was done while centered on the large, dark crack on the left. Analysis for Fig. 15 was done on the crack on the right side. When the bright, melted area, slightly above center and left in Fig. 15 was analyzed, there was nothing but Pd showing. Apparently this area was below a critical threshold of energy density or size for nuclear cluster reactions.

Fig. 18 shows an area having a mixture of cracks, molten spheres of material and an EV strike that has been partially obliterated by other activity. There is a minimum amount of wildfire activity in this eruption. Fig. 19 is an X-ray analysis of the dark crater on the left side of Fig. 18. Small amounts of "foreign" material show here. With the limited analysis done, the source of this material is unknown.

Mechanical storage of energy is thought to be the source for the small EVs produced. It has been determined, both experimentally by the authors and theoretically by G. Mesyats [5], that the size of an EV structure is a function of the high specific energy delivered to the metal. Higher energy density produces smaller structures. The locally obtained energy from micrometer-size sources gives a higher input energy density than the best external power sources used for EV generation, usually limited to the one micrometer size range.

This wildfire process appears to have little value in the mode seen because it is below the threshold level for triggering the main nuclear cluster reaction we seek. So far, there have been no nuclear transitions observed that

are associated with wildfire action. Its principal function has been to more accurately point to mechanical, fracto-emission as the local source of stored energy to trigger a cluster nuclear reaction through the instrument of NEVs.

VI. TESTS ON THE E-QUEST SAMPLE

The ultrasonic processing method produces a different surface morphology from samples processed electrochemically. The ultrasonic method tends to wipe out its past surface history more rapidly than does the electrochemical method. It does this by both adding colloidal particles of the parent metal to the surface, and at the same time, removing material by mechanical shock. EV craters that would normally look very sharp on unmolested surfaces show a fuzziness characteristic of repeated pummeling. Nevertheless, Fig. 20 is a view that shows 4 classic EV witness marks, similar to those shown in Fig. 4, and characteristic of most bulk material surfaces having a high-melting point. Fig. 21 shows a crater produced in a protected region. Brittle fracture is evident here. There is evidence of melting shown deep down in the crater, signifying an energy production process at work that is not strictly surface related. In a private discussion, Roger Stringham has stated that the edges of such craters are usually the location of transmuted material. This is in accordance with what is found in electrolytically treated samples where it is easier to view the undisturbed residue of a reaction.

The origin of the observed strikes has not yet been clearly delineated in any theory known to the authors. However, work has been done on EVs produced under water by electrical methods, and the results give the same witness marks as those shown earlier from gaseous production methods. The fact that light shows as 50 ps flashes in the sonoluminescence process associated with cavitation, and that this corresponds to the time known to occur in EV formation processes, points to the possibility of sonically produced EV structures made through cavitation charge separation.

Fig. 22 shows a SEM photo taken of a foil prepared by R. Stringham and photographed by J. Dash and R. George. The micron mark in the photo has been restored by the authors and is only approximate. The most obvious thing that can be seen at this low magnification is the large impact craters generated by a few strikes from some unknown energy concentration process, probably having to do with momentum transfer from the fluid bath to the surface. These strikes both totally penetrate the foil and also knock out trumpet-shaped, brittle fragments on the reverse side of the strike. These strikes are more like driving a nail through the material and, according to the notions being presented here, would not likely yield nuclear reactions. In the nuclear cluster reaction theory, the energy density is the all-important parameter to maintain. Large, low-energy-density strikes represent a loss of energy gain in the process of nuclear conversion. The measure of energy density might be found most expeditiously by the number and type of nuclear transitions produced.

The main point to be made here is that marks are made on the ultrasonically processed surfaces that are very similar in both size and shape to those made by EVs under more controlled conditions. Examples of sonically bombarded surfaces taken from the literature show many classic EV-like witness marks.

VII. DISCUSSION OF OBSERVATIONS

The nuclear reactions produced in the observations made have many things in common, but the most outstanding of these is the clustering effect. All reactions found occur in regions of only a few square micrometers in extent. This is also the size realm of the NEVs used to either fuel or trigger the events. From this observation it is necessary to conclude that such nuclear reactions are fundamentally an intense event involving large numbers and not one of widely isolated events working individually at an atomic level.

From only a small set of observations, it is increasingly apparent that there is a threshold effect in which no new or "foreign" material is produced until the physical size of the stressed area is above about 1.5 μm in lateral extent. Additionally, the percentage of new material seems to increase as the size of the reaction grows. The

production of high atomic number elements also increases with reaction size. Before the observations made in the course of this work can be taken seriously, many more samples must be tested.

In the search for the validity of this threshold effect, one must consider that the energy density of the initiator sets the threshold size of the nuclear cluster reaction. High energy density in the initiator would produce small clusters, just as it does with high-energy, individual nuclei found in standard nuclear processes. The low energy density of our initiator process would be expected to give rise to larger clusters containing more events with the concomitant low energy by-products. NEV generation is a compression process that blends smoothly with other compression processes, like cavitation excitation, but the maximum density is limited by unknown factors.

From other work done in the area of high-charge-density effects, the timing of the events being studied here occur in scarcely more than a few tens of picoseconds. Even with this short interval of time, there is a series of steps leading to the final result we see in frozen images. For the self-triggered electrolytic process, first, there is a slow loading process that produces a brittle product. Next, there is a very rapid brittle fracture of sufficient magnitude and shape to give rise to a NEV that is loaded with whatever nucleons are most available. In the case considered here, it is likely that over 100,000 deuterons are included. These nuclei are then hurled, with the high energy density afforded by the EV compression process, into the parent material. This is done by a collective acceleration at a low-applied voltage, in the kilovolt range, but having the equivalent velocity of megavolts, due to the acceleration mechanism.

The theoretical basis for a controlled, micro volume, D-T thermonuclear process is described in a paper by V. Skvortsov and N. Vogel [6]. In the model, the authors interact a local, laser-produced, intense micro beam of heavy ions with condensed matter. The extreme state of matter produced, in the Gbar pressure range, is generated by interacting shock waves like those demonstrated in EV technology [7]. Functionally, the two processes are nearly identical with the NEV method being the easier of the two.

At this point in the reaction process there is a void of knowledge, but we will attempt an ad hoc explanation of the observed results. The most outstanding observation of "cold fusion" in general is that the by-products of the nuclear reactions produced have much lower energy than conventional "hot fusion" reactions. In our opinion, this is due largely to a *nuclear cluster reaction* having an unknown form of coherence .

As in any harmoniously coupled reactions, it is easier to dispose of excessively high peak energies by coupling them into an interlocked network of lower energy, coupled states. A supreme example of this is found in the Mössbauer effect whereby a solid lattice of atoms, acting in unison, takes up departing gamma photon recoil energy. In a like fashion, the most energetic components of our nuclear cluster reactions are transferred to multiple, lower energy states through group action. This can be a conversion process without loss. Carried to an extreme, a theoretical conversion could be made in which all of the energy in one class of nuclide is converted to another without any external indications. This super transmutation would be the equivalent of superconductivity and really not that much more surprising.

In the imperfect world in which our process is embedded, the debris of nuclear reaction is transformed into heat and some errant, energetic particles. It is the effect of nuclear cluster reactions, with their propensity for low levels of peak energy output that produce the most desirable properties and not whether the process is either cold, tepid, hot, low energy or high energy. The underlying merit of this unspecified process stems from the salient fact that some still unknown, coherent, group action lies at the root of it.

Electrolytic and sonic processes, occurring in solutions, are difficult processes for extraction of certain operating mechanisms. By bombarding surfaces in vacuum with externally generated NEVs, the brittle fracture requirements become null and nuclear fueling processes can be separately investigated in great detail. What is immediately apparent here is that any area on the surface becomes a willing site for nuclear reactions and concomitant isotopic conversion. However, there remains a requirement for cluster action in which billions of atoms cooperate to produce a more desirable end point.

With the crude method of generating a NEV used here, there can be no accurate determination of either the energy level or the number of nuclides included in the NEV. The critical size must lie between the limits of the successful 3 μm cluster used by the authors and the largest of the ineffective strikes seen, around 0.5μm in diameter.

There is also a contribution of energy from the substrate that cannot be accurately accounted for at this time. Taking advantage of the mechanically-stored energy is mostly a matter of supplying a mechanism for concentrating the available energy of the many small strikes that lie below the triggering threshold. Arranging for a particular fracture geometry would be one such method, but this technique is felt to be impractical because external NEV generation is much easier.

VII. CONCLUSIONS

It has been determined that the electrolysis of Pd in heavy water produces a brittle layer on the surface that fractures in a manner producing fracto-emission of electrons. These electrons are organized into concentrated electron structures containing nuclei, called NEVs, and then collectively accelerated into the surface where they produce a nuclear cluster reaction.

Sonically-treated Pd surfaces in heavy water are also subject to the same dense-electron and ion-cluster treatment that arises from charge separation in a collapsing bubble. A nuclear-cluster reaction is also produced from this process.

Deuterium loaded Pd foils, spark bombarded in air with an electron cluster, incidentally loaded with nucleons, produce nuclear cluster reactions.

Indications are that the cluster type of nuclear reaction is responsible for the limited number and mild nuclear reaction products escaping the reaction site that produced them.

In the limited work done here, there is the appearance of a threshold for the nuclear cluster reactions observed. The threshold is connected to a physical size for the eruption seen and is near 3 cubic micrometers of material. In addition, there seems to be a preferred production of heavier nuclides with increasing size of the disrupted area.

ACKNOWLEDGMENTS

The authors gratefully acknowledge the moral and financial support provided by Tom Shanks.

REFERENCES

1. K. R. Shoulders, EV-- A Tale of Discovery, Austin, TX (1987). A historical sketch of early EV work having: 246 pages, 153 photos and drawings, 13 references. Available from the author.
2. See U.S. Patents by K. R. Shoulders. 5,018,180 (1991) - 5,054,046 (1991) - 5,054,047 (1991) - 5,123,039 (1992), and 5,148,461 (1992).
3. Petr Beckmann, "Electron Clusters," *Galilean Electrodynamics*, Sept./Oct., Vol. 1, No. 5, pp. 55-58, 1990.
4. Richard W. Ziolkowski and Michael K. Tippett, "Collective Effect in an Electron Plasma System Catalyzed by a Localized Electromagnetic Wave," *Physical Review A*, vol. 43, no.6, pp. 3066-3072, 15 Mar. 1991.
5. G. A. Mesyats, "Ecton Processes at the Cathode in a Vacuum Discharge," Proceedings of the XVIIth International Symposium on Discharges and Electrical Insulation in Vacuum, Berkeley, CA, pp. 721-731, July 21-26, 1996.
6. Vladimir Skvortsov, Nadja Vogel, Andrei Lebedev, "The Dynamic of Matter Transition into Extreme States Initiated by High Power Micro Beam of Heavy Ions," Proceedings of the XVIIth International Symposium on Discharges and Electrical Insulation in Vacuum, Berkeley, CA, pp. 813-817, July 21-26, 1996.
7. For an example of shock wave depiction by surface decoration, see ref. 1, Fig. 2:14, page 2-22.

ADVANCED TRANSMUTATION PROCESSES AND THEIR APPLICATION FOR THE DECONTAMINATION OF RADIOACTIVE NUCLEAR WASTES

A. Michrowski [1]

ABSTRACT

There are deviations to the standard model of radioactive atomic nuclei decay reported in the literature. These include persistent effects of chemical states and physical environment and the natural, low-energy transmutation phenomena associated with the vegetation processes of plants. The theory of neutral currents is proposed by Nobelist O. Costa de Beauregard to account for the observed natural transmutations, also known as the Kervran reaction. "Cold fusion" researchers have also reported anomalies in the formation of new elements in cathodes. This body of knowledge provides the rationale for the observed and successful and developed advanced transmutation processes for the disposal of nuclear waste developed by Yull Brown involving a gas developed by him with a stoichiometric mixture of ionic hydrogen and ionic oxygen compressed up to 100 psi. Another procedure, still in experimental stages, involves the environmental interaction of non-Hertzian electromagnetic fields and targeted radioactive samples. In both methods, the radioactivity in samples decreases by up to 97% rapidly and at low cost.

INTRODUCTION

Since the discovery of natural radioactivity, it was generally believed that radioactive processes obeyed orderly, simple decay rate formulae and that nuclear processes operated completely independent of extra nuclear phenomena such as the chemical state of the system or physical parameters such as pressure or temperature. A solid body of scientific literature describes a small percentage variation of the order of 0.1 to 5% in the decay constant under a variety of chemical and physical conditions. [7, 8, 10, 12, 13, 23, 28]

The standard definition of half-life or half-decay time is the time taken by a given amount of a particular radioactive substance to undergo disintegration or decay of half of its atoms. Measured half-lives vary from less than a millionth of a second to billions of years in the case of Uranium. There are four modes of decay, three are named after the first three letters of the Greek alphabet, i.e., **alpha**, **beta,** and **gamma** and the fourth is the recently discovered **proton decay**.

CURRENT MODEL OF DECAY

By way of review, for the Bohr-Rutherford model of the atom, the nucleus is composed of the heavy particles or hadron or the proton and the neutron, and is surrounded by a cloud of electrons (or light particles or leptons) the number of which depends on the atomic number (for neutral atoms) and also the valence state (for ionized atoms). **Alpha** particles are Helium nuclei, $^{4}He^{2}$ consisting of two protons and 2 neutrons; **beta** particles are electrons (negative charge) and positrons (positive charge) and **gamma** rays which are in the short wave length of the electromagnetic radiation band; the proton is a hadron. **Alpha** particles and protons are strongly interacting particles as are all hadrons.

[1] President, Planetary Association for Clean Energy, Inc.,
100 Bronson Avenue, Suite 1001, Ottawa, Ontario K1R 6G8, Canada (613) 236-6265; fax: (613) 235-5876.

The current model of beta decay is that an inter nucleon neutron spontaneously decays into a proton and an electron (or beta particle and an anti-electron neutrino, $n^o \rightarrow p^{\cdot} + e^{\cdot} + \nu_e$). A neutrino is a zero-rest mass spin 1/2 particle which conserves momentum in the decay process. There are many pure beta emitters throughout the periodic table; Carbon ^{14}C and deuterium are two examples. Beta particles penetrate substance less deeply than gamma radiation but are hundreds of times more penetrating than alpha particles. Beta particles can be stopped by an inch of wood or by a thin sheet of aluminum foil, for example. The energy of most emitted alpha particles are stopped by a piece of paper and the most energetic gamma rays require a thick piece of lead or concrete.

Electromagnetic radiation emission from atomic processes can be in the x-ray energy range and nuclear in the x-ray and gamma ray energy range.

It is believed that all radioactive atomic nuclei decay spontaneously without prior cause at a specific and steady decay rate which differs for each radioactive isotope. Some precise measurements of half lives have been made which show deviations of the standard type decay curves which appear to depend on non-nuclear variable conditions in origin and structure.

Past measurements of variations in the decay constant $N = N_o e^{-\lambda \pi}$ with $T_{1/2} = 0.693/\lambda$ are based on crude instruments from some 70 years ago. Later, with more sophisticated electronics, the value of λ, of the decay of Beryllium ^7Be, was first shown in 1949 to deviate by 0.1% between atomic Be and molecular BeO. In 1965, the λ of Niobium, ^{90}Nb, is altered by 4% between the metal and the fluoride form, as discussed by **G. Emery. H.C. Dudley** reported on studies that have varied decay characteristics of twelve other radionuclides according to changes in the energy states of the orbital electrons, by reason of pressure, temperature, electric and magnetic fields, stress in monomolecular layers and other physical atomic conditions. [10]

The alteration of decay rates by non-nuclear processes may not be truly random and would seem to require a new theoretical model. As these decays occur, the term nuclear may need to be expanded to include reactions and processes involving the entire atom and even multi-atom crystal matrix forms rather than just mass-energy changes in only the nucleus. [19, 22, 23]

OBSERVED DEVIATIONS FROM ACCEPTED DECAY LAWS

Not too well known is a quite prodigious body of work on the persistent effects of chemical states and physical environment on the deviation from the accepted decay law of nuclear decay rates. Theoretical as well as experimental research has been conducted. [7, 8, 10, 12, 13, 23, 28] In 1947, **R. Daudel and E. Segre** predicted that under certain conditions a dependence of the decay constant on the chemical and physical environment of the nucleus should be observable; subsequent to these predictions such a dependence was experimentally observed (with **R.F. Leinzinger** and **C. Wiegand**) in the K capture decay of ^7Be and the internal conversion decay of the 99m isomeric state of Technetium.

During the decay process, the chemical environment of the nucleus is changed, thus altering the decay constant. R. Daudel pointed out that the isomeric decay constant of the 2-keV isomeric state transition in the Technetium isotope, ^{99m}Tc, arose from a change in the electron density near the nucleus. **J.C. Slater** suggested that the faster decay rate observed for the $RTcO_4$ compound form is due to a **greater squeezing** of the Tc atoms with the metal Tc-Tc bond distance of 2.7 Å. Note that the symbol Å refers to the distance measure of one Angstrom which equals 10^{-8} cm.

A good example of the effect of a chemical change in the nuclear environment during radioactive decay is for the intensity change of the 122-keV E2 gamma ray observed for the ^{90m}Nb isomeric state of Niobium. This effect on the decay rate for the 21-second transition was an order of magnitude greater and in the opposite direction than observed in ^{99m}Tc and was achieved at **Lawrence Berkeley Laboratory** by **J.O. Rasmussen** and his colleagues, **J. A. Cooper** and **J. M. Hollander** in 1965. [27]

In 1975, **Elizabeth A. Rauscher** lengthened beta emissions for ^{20}Si simply by surrounding it with specifically designed matrix material, thereby lengthening the decay rate by about 6% with only 15 minute exposure, demonstrating the impact of environmental conditions on radionuclides.

NATURAL TRANSMUTATION

Natural, low-energy transmutation phenomena have been observed for centuries. In 1799, the French chemist, **Nicolas Louis Vauquelin** noted that hens could excrete 500% more lime that they take in as food, suggesting a creation -- transmutation of Calcium Carbonate. Scientific literature notes many similar phenomena that occur in vegetation processes of plants as well where new elements and minerals inexplicably emerge. Nobel Nominee **Prof. Louis Kervran** replicated these numerous findings and advanced very far the understanding of natural, non-radioactive transmutations, acquiring in this pursuit a term for such transmutations, **Kervran reaction**, while engendering solid physics support from the Institut de Physique Theorique Henri Poincare physicist, Olivier Costa de Beauregard. He stated in 1974 that the theory of weak neutral currents accounts for the transmutations observed, with due respect for the physical laws of conservation. [9, 14, 15, 16] The theory of neutral currents gave its authors, Sheldon Glashow Abdus Salam and Steven Weinberg the Nobel Prize for Physics in 1979. De Beauregard proposed the following equations for biological transmutation:

Table 1. The Olivier Costa de Beauregard equations for biochemical transmutation

$$n \rightarrow p + e^- + \underline{\nu} \quad (1)$$

$$p + \nu \leftrightarrow p' + \nu' \quad (2)$$

$$p \leftrightarrow p' + \underline{\nu} + \nu' \quad (3)$$

These equations imply the conversion of a neutron (n) to a proton (p) by virtual exchange processes -- the neutral currents of Weinberg. These processes produce protons (p and p') of different energy levels and two neutrinos (ν and ν') of different energy levels. $\underline{\nu}$ represents the antineutrino and e^- the electron. In one state the proton will be bound to an atomic nucleus, and in the other state, it will be relatively free in a chemical binding.

IN VITRO TRANSMUTATION

Physicist Dr. Andrija Puharich was able to observe and photograph Kervran reactions *in vitro* by using a high-power dark-field microscope which was developed by the Canadian scientist, Gaston Naessens. Kervran reactions were documented by him to include the oxygen atom entering into a virtual nuclear reaction with p or n to yield ^{14}N or ^{19}F, by using an electrolytic process similar to that of Prof. Yull Brown, as disclosed by Puharich in his U.S. Patent 4,394,230, "Method and apparatus for splitting water molecules." [20, 21]

There exists as well the phenomenon of transmutative "digestion." L. Magos and T.W. Clarkson of the British Research Council Carshalton Laboratories noted disintegration of the radioactive isotope ^{203}Hg ingested by rats, a volatilization which they ultimately attributed to such bacteria as **Klebsiella aerogenes**. [17]

COLD-FUSION EXAMPLES

On June 19, 1995, Texas A&M University hosted a low-energy transmutation Conference, sponsored by the "father of electrochemistry," Professor Dr. John O'M. Bockris. Some of the papers which were presented noted anomalies in the formation of new elements in cathodes - definitely not sourced from contamination - which were involved in cold-fusion experiments. For example: Drs. T. Ohmori and Reiko Notoya, both of Hokkaido University, reported Iron formation in Gold and Palladium cathodes, Potassium changing into Calcium, Cs^{133}

producing an element of mass 134, and Na^{23} becoming Na^{24}; Dr. John Dash of Portland State University, reported spots of silver, cadmium and gold protruding in palladium electrodes in both light and heavy water cells; Dr. Robert Bush of California Polytechnic, Pomona, reported strontium on the surface of nickel cathodes.

LOW-TEMPERATURE TRANSMUTATION

Very pertinent is the long-term research by Dr. Georgiy S. Rabzi of the Ukrainian International Academy of Original Ideas who reported his analyses of the mechanism of low-temperature transmutation, which he has conducted since 1954. He passed out samples to attendees: a steel nut which acquired the color of copper and was reduced in size; magnetic stainless steel turned non-magnetic, asbestos which became like ceramic. No radioactivity had been observed in any of his experiments and he is convinced that radioactive wastes can be stabilized. [18]

These observations, originating from various domains of scientific research form a solid case of low level advanced transmutation -- with minuscule power and signal strength and sometimes without any, i.e. in nature alone.

ADVANCED TRANSMUTATION: DISPOSING OF NUCLEAR WASTE

Experimental results obtained by advanced transmutation have direct bearing on the problem of disposal of nuclear wastes.

The first relies on the interaction of nuclear wastes with ionic hydrogen and ionic oxygen gas known as Brown's Gas. Brown's Gas has been developed by a Bulgarian-born Australian national, Prof. Yull Brown. In his process, water is separated into its two constituents, hydrogen and oxygen in a way that allows them to be mixed under pressure and then burned simultaneously and safely in a 2:1 proportion. The proprietary process results in a gas containing ionic hydrogen and oxygen in the required proportions which can be generated economically and safely and be compressed up to 100 psi. [2, 5, 6]

Brown's Gas is a "cornerstone of a technological edifice" with many commercial and industrial applications.

At this time, Brown's Gas generators are mass produced in the Bautou, a major research city in the People's Republic of China by the huge NORINCO factory which also manufacturers locomotives and ordinances -- and services the nation's nuclear industry complex. Most of these generators (producing up to 4,000 liters/hour/2.4 liters of water at 0.45 MPa with power requirements ranging from 0.66 kW up to 13.2 kW) are marketed for their superior welding and brazing qualities, costing between $2,000 and $17,000. Some units have been used for the decontamination of radioactive materials since 1991. Brown's Gas generators produce between 300 and 340 liters of Brown's Gas per 1 kW energy DC current approximately and one liter of water produces about 1,866.6 liters of gas. A generator which produces 10,000 liters per hour has been built specifically for the reduction of nuclear waste. Prof. Brown first successfully de-radioactivated radionuclides of Cobalt 60 in his laboratory in Sydney, Australia with initial experimental results of about 50%. [28]

On August 24, 1991, Baotou's **Nuclear Institute #202** released a report, **The results of experiments to dispose of radiation materials by Brown's Gas** which establishes that experimentation on Cobalt 60 radiation source decreased radiation by about 50% or half-life of radiation. [4] Sometimes more radiation is decreased, a fact which requires further investigation of the possibilities for decreasing more of the radiation by treatments of single exposures to Brown's Gas flame, *lasting only a few minutes*, as in the samples described in the table below.

Table 2. De-radioactivation of Cobalt 60 by exposure to Brown's Gas flame for less than 10 minutes. 1991 experiments conducted by Baotou Nuclear Institute #220, People's Republic of China.

	First Experiment	Second experiment
Original Source Intensity	580 millirads/hour	115-120 millirads/hour
After Treatment	220/240 millirads/hour	42 millirads/hour

In another test conducted by Yull Brown before a public audience including U.S. Congressman Hon. **Berkeley Bedell** with committee responsibilities in this area of concern, the experiment ran as follows as reported by the press:

Using a slice of radioactive Americium ... Brown melted it together on a brick with small chunks of steel and Aluminum... After a couple of minutes under the flame, the molten metals sent up an instant flash in what Brown says is the reaction that destroys the radioactivity. Before the heating and mixing with the other metals, the Americium, made by the decay of an isotope of Plutonium, registered 16,000 cunes per minute of radiation. Measured afterward by the [Geiger Counter], the mass of metals read less than 100 counts per minute, about the same as the background radiation in the laboratory where Brown was working. [4]

This experiment indicated a reduction of radiation in the order of over 99% (to about 0.00625 of original level) --in less than 5 minutes, with minimal handling. The improvement in the de-radioactivation process from about 50% to nearly 100% has come only with persistent research over the decades by Brown and his colleagues. The Brown's Gas generating units that produced such effects are not expensive -- a far cry from the multi-million processes tabled by atomic energy agencies worldwide. They are powered by low energy requirements and require only small volumes of water, at most a few liters per hour as fuel. Furthermore, the training required for operation is minimal.

The Hon. Bedell has reported, "it has been my good pleasure to witness experiments done by Prof. Yull Brown in which it appeared to me that he significantly reduced the radioactivity in several nuclear materials. Under the circumstances, I believe it is very important for our federal government to completely investigate Dr. Yull Brown's accomplishments in this area." [11]

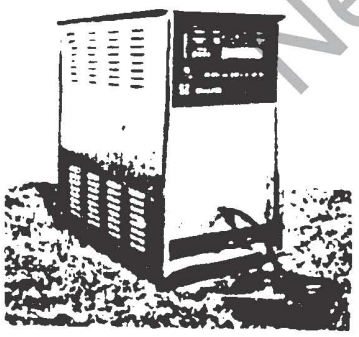

Fig. 1. A Brown's Gas generator manufactured in the People's Republic of China by NORINCO

On August 6, 1992, almost a year after the Chinese nuclear report, Prof. Yull Brown made a special demonstration to a team of 5 San Francisco field office observers from the **United States Department of Energy**, at the request of the Hon. Berkeley Bedell. Cobalt 60 was treated and resulted in a drop of Geiger readings from 1,000 counts to 40 -- resulting in radioactive waste residue of about 0.04 of the original level. Apprehensive that somehow the radioactivity might have been dispersed into the ambient environment, the official requested the **California Department of Health Services** to inspect the premises. The health services crew found no radioactivity in the air resulting from this demonstration nor from another repeat demonstration held for their benefit. [11] This sequence of experiments was monitored by the Hon. **Daniel Haley**, the legislator who established the forerunner **New York State Energy Research and Development Agency**.

Other demonstrations, measured with under more sophisticated protocol and instrumentation have been conducted before Japanese nuclear experts, including four scientists from **Toshiba** and **Mitsui**: Cobalt 60 of 24,000 mR/hr reduced with one treatment to 12,000 mR/hr. The Japanese scientists were so excited by what they saw that they

immediately purchased a generator and air shipped it to Japan. They sent Prof. Brown a confidential report of some of their results. Subsequently, they tried to obtain additional Brown's Gas generators directly from the People's Republic of China.

Prof. Brown, during his 27 years of studying water and its atomic structure and experimenting with the disassociation of water into its constituent parts of hydrogen and oxygen has noted that there are many variations of the atomic structures of the various waters dependent on the mixing of the three hydrogen isotopes (^{1}H - protium, $^{1}H^{2}$ - deuterium, $^{1}H^{3}$ - tritium) which combine into 6 combinations of hydrogen and the 6 oxygen isotopes ($^{8}O^{14}$, $^{8}O^{15}$, $^{8}O^{16}$, $^{8}O^{17}$, $^{8}O^{18}$, and $^{8}O^{19}$) – or practically, 36 types of water– 18 are stable and 18 have short life. Accordingly, because of all of these types of water, there could be 36 types of Brown's Gas, and even more with special modifications of the gas; at the moment only a few are under investigation. His studies have led to the observation that the anomalous behavior of water depends on the ability of water to modify energetics and physicochemical properties of the various permutations of the hydrogen/oxygen isotopes. As is known the lifetime, modes of decay, and thermal neutron capture cross-sections vary significantly between these isotopes; likewise, Brown has seen the various stages of his gas offer very different effects. He has found that he can modulate a number of suitable mixes for his technology, thus providing an engineering tool in decontamination of nuclear wastes [2].

INTERACTION WITH NON-HERTZIAN ENERGY

In the 1960's, the Canadian engineer, **Wilbert Brockhouse Smith**, a major player in advancing the technical aspects of radio and television broadcasting in Canada began experimenting with Caduceus coils and noted that this counter-winding set-up produced anomalous effects and proposed that other experimenters attempt to follow this new area of investigation. These coils became popularly known as the "Smith Coils" and he believed that they were producing, in summation, a "scalar" field – a non-Hertzian phenomenon. It is now known that similar non-Hertzian phenomena may also be obtained by mobius, and bi-filar coils which oppose their alternating currents by virtue of their unique geometry. The resultant of all electromagnetic energy is to sum to zero in accordance with Newton's third law, thereby orthorotating the zero-point-energy into our 3-space. [26]

A recent investigation by Dr. **Glen Rein** and **T.A. Gagnon**, assisted by **Prof. Elizabeth A. Rauscher** (Nuclear Physics, University of California, Berkeley and with Lawrence Berkeley Laboratory, **William Van Bise** – and with some support by Professor Emeritus (Material Sciences) **William A. Tiller** of Stanford University – involved a modified Caduceus coil. [24, 26]

The 8.2 ohms coil indicated no electromagnetic fields even though powered with only 3 mA, 5 watt amplifier/mixer. Yet, the field from this set-up was able to decrease ambient radioactivity associated with environmental isotopes from 0.5 mR/hour to 0.0015 mR/hr-- or by 97%. In contrast, Cobalt 60 increased its radioactivity from 150 to 250 mR/hour, in response to the non-Hertzian energy. Thus the same non-Hertzian energy field produced opposite effects on different radioactive isotopes. [26]

This type of experiment, which may have been highly dependent on the a mix of waveform signaling, involving superimposition of square waves containing specific repetition rates developed by **Dynamic Engineering** of Sacramento, California, indicates that research and development can determine the fine-tuning of special non-Hertzian procedures for the transmutation of specific isotopes.

Another non-Hertzian approach to advanced transmutation has been hypothesized by the nuclear scientist, **Tom E. Bearden** and involves the use of "Whittaker scalar interferometry" directed in such a way as to directly extract electromagnetic energy from the mass of the radioactive nuclei. [3]

In this system, the fundamental nuclear rates would be altered by way of "de-materializing" nuclei into constituent hidden (scalar) electromagnetic Whittaker energy. **E.T. Whittaker** was a prominent British mathematician who published two papers of interest in this matter: 1) a general analysis of force fields into constituent fields -- differentiated into "undulatory", wave-disturbance propagation, longitudinal in character; and 2) an analysis of electrons as being characterized by two scalar potential functions. [29, 30] His work successfully pre-dates the experimental work of **Y. Aharanov** and **D. Bohm** who demonstrated that in the total absence of electromagnetic force fields, the potentials remain and can interfere at a distance to produce real effects of charged particle systems. Force fields are actually effects generated from potentials. [1]

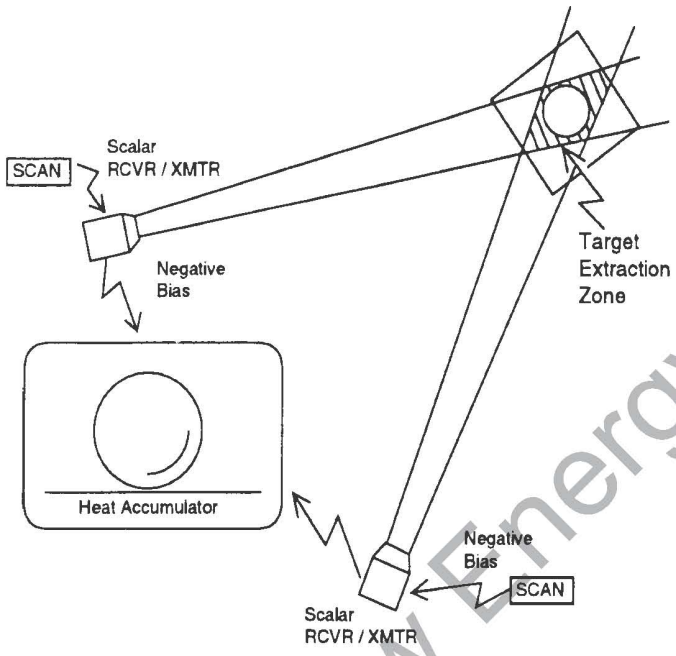

Fig. 2. Whittaker interferometer in endothermic mode for energy extraction from the mass potential of radioactive nuclei.

Fig. 2 shows the conceptual use of a Whittaker Interferometer in the endothermic (energy extraction, electrostatic cooling) mode, for use in direct extraction of the electromagnetic energy constituting the radioactive nucleus.

By exposing the atomic nucleus to an externally engineered Whittaker-structured potential with a deterministic internal electromagnetic wave pattern, the internal structure of the mass potential may be slowly altered, changing the targeted atomic nucleus by gradually inducing a direct alteration of its internal Whittaker electromagnetic bi-wave composition.

A process based on this hypothesis remains proprietary, pending patent application.

ACKNOWLEDGEMENTS

This paper has been possible by the advice and help of Tom E. Bearden, John O'M Bockris, Yull Brown, Olivier Costa de Beauregard, Hal Fox, Elizabeth A. Rauscher, Glen Rein, William A. Tiller, Tom Valone, William Van Bise.

REFERENCES

1. Y. Aharonov and D. Bohm, "Significance of Electromagnetic Potentials in the Quantum Theory," *Physical Review*, Second series. vol. 115, no 3, August 1, 1959. p. 485-491. [In the total absence of electromagnetic force fields, the potentials remain and can interfere at a distance to produce real effects of charged particle systems. Forced fields are actually effects generated from potentials. See: Whittaker's two papers and research by T.E. Bearden on radioactive neutralization.]

2. "Anomalous water," explained by Brown's Gas research, *Planetary Association for Clean Energy Newsletter*. vol. 6, no 4, July, 1993. pp 11-12.

3. T.E. Bearden, "A Redefinition of the Energy Ansatz, Leading to a Fundamentally New Class of Nuclear Interactions," Proceedings of the 27th Intersociety Energy Conversion Engineering Conference, San Diego, California, 1992. IECEC. clo American Nuclear Society, vol 4, pp 4.303 - 4.310.

4. Christopher Bird, "The Destruction of Radioactive Nuclear Wastes: Does Professor Yull Brown Have the Solution?" *Explore !*, vol 3, no 5, (1992), pg 3.

5. Yull Brown, "Welding," U.S. Patent 4,014,777, March 29, 1977, ["The invention also relates to atomic welding to which the mixture {of hydrogen and oxygen generated ion substantially stoichiometric proportions} is passed through an arc causing disassociation of both the hydrogen and oxygen into atomic hydrogen and oxygen which on recombination generate an extremely hot flame."]
6. Yull Brown, "Arc-Assisted Oxy/Hydrogen Welding," U.S. Patent 4,081,656, March 28, 1978.
7. R. Bruch, Elizabeth A. Rauscher, H. Wang, T. Tanaka and D. Schneider, *Bulletin of the American Physical Society*, vol 37, (1992), [Discusses nature of variable decay rates of the radioactive nuclides, and the basis for their interaction with electromagnetic and gravitational forces].
8. R. Bruch, Elizabeth A. Rauscher, S. Fuelling, D. Schneider, "Collision Processes of Molecules and Atoms." In: L. Byass, editor, Encyclopedia of Applied Physics, American Institute of Physics, 1993. [Discusses nature of variable decay rates of the radioactive nuclides, and the basis for their interaction with electromagnetic and gravitational forces].
9. Oliver Costa de Beauregard, "The Expanding Paradigm of the Einstein Theory." In: Andrija Puharich, editor, Iceland Papers, New York. Essentia Research Associates, (1979), vol 190, pp 161-189.
10. H.C. Dudley, "Radioactivity-Examined," CAEN Editors, April 7, 1975. [Review of deviation of radioactive decay rates].
11. Daniel Haley, "Transmutation of Radioactive Matreials with Yull Brown's Gas - 2500% Radioactivity Reduction," *Planetary Association for Clean Energy Newsletter*, vol 6, no 4, July, 1993. pp 8-9.
12. K. Harada and Elizabeth A. Rauscher, "Unified Theory of Alpha Decay," *Physical Review*, vol 169, (1968), pg 818.
13. K. Harada and Elizabeth A. Rauscher, "Alpha Decay of $Po^{212} \rightarrow Pb^{208}$, $Po^{210} \rightarrow Pb^{206}$, Treated by the Unified Theory of Alpha Decay," UCRL-70513, May, 1967.
14. C. Louis Kervran, "Biological Transmutations," Magalia, CA., Happiness Press, (1989), 163 p.
15. C. Louis Kervran, "Transmutation of the Elements in Oats: New Analyses," *Planetary Association for Clean Energy Newsletter*, vol 2, no 3, July/August 1980, pp 4-6.
16. C. Louis Kervran, "Transmutation à Faible Énergie," Paris Maloine, (1972).
17. L. Magos and T.W. Clarkson, "Volatilization of Mercury by Bacteria," British Journal of Industrial Medicine, October 1964, pp 294-8.
18. Georgiy S. Rabzi, "Mechanism of Low Temperature Transmutation," *J. Of New Energy*, vol 1, no 1, pp 46-55; Proceedings of Low-Energy Transmutation Conference, Texas A&M University, June 19, 1995.
19. Elisabeth A. Rauscher and R. Bruch, "S-Matrix Theory of Alpha Decay," [Book manuscript in progress.]
20. Andrija (Henry K.) Puharich, "Successful Treatment of Neoplasms in Mice with Gaseous Superoxide Anion (O_2) and Ozone (O_3) with Rationale for Effect," New York Essentia Research Associates. [Presented to Sixth Ozone World Congress. International Ozone Association, May 26-28, 1983, Washington.] 89 p. [Pages 5-7 discuss numerous *in vitro* biological transmutation or Kervran reactions.]
21. Andrija (Henry K.) Puharich, "Method and Apparatus for Splitting Water Molecules," U.S. Patent 4,394,230, July 18, 1983.
22. Elizabeth A. Rauscher, "Study and Application of the Modification of Nuclear Decay Rates by Changes in Atomic States," Tecnic Research Laboratories, Nevada, April, 1993, 28 p. [Protocol for design, test and implementation of decay rate change effects to nuclear waste materials].
23. Elizabeth A. Rauscher, "The Properties of Plutonium and Comparison to Other Metallic Elements," University of California, Lawrence Berkeley Laboratory, February 23, 1991. [Set basis for variable decay rates of the radioactive nuclides -- and their interaction with electromagnetic and gravitational forces].
24. Glen Rein, "Ability of Non-Hertzian Energy to Modulate Cobalt-60 Radioactivity," [Manuscript prepared for Canadian Environmental Assessment Agency presentation by the Planetary Association for Clean Energy], 1 sheet, (1995).
25. Glen Rein, "Utilization of a Cell Culture Bioassay for Measuring Quantum Fields Generated from a Modified Caduceus Coil," In: Proceedings of the 26th Intersociety Energy Conversion Engineering Conference, Boston, Massachusetts. IECEC, c/o American Nuclear Society, August, 1991, 4 pages. [Specific details regarding protocol and procedure used for modulation of radioactivity].
26. Wilbert B. Smith, "The New Science," Ottawa. The Planetary Association for Clean Energy, (1995), Keith Press, (1964), 72 p.
27. A.J. Soinski, Elizabeth A. Rauscher and J.O. Rasmussen, "Alpha Particle Amplitude and Phases in the Decay of ^{253}Es," *Bulletin of American Physical Society*, vol 18, (1973), p. 768. [Modulation of decay rate of radionuclides by extra nuclear environmental conditions].
28. "Yull Brown's Gas," *Planetary Association for Clean Energy Newsletter*, vol. 6, no 4, July, 1993, p. 10-11.
29. E.T. Whittaker, "On the Partial Differential Equations of Mathematical Physics," *Mathematische Annalen*, vol. 57, (1903), pp 333-355. [Demonstrates that a standing scalar potential wave can be decomposed into a special set of directional electromagnetic waves that convolute into a standing scalar potential wave. As a corollary, then, a set of bi-directional electromagnetic waves -- stress waves -- can be constructed to form such a wave in space. Whittaker's wave represents a standing wave of variation in the local curvature of vacuum.]

30. E.T. Whittaker, "On an Expression of the Electromagnetic Field Due to Electrons by means of Two Scalar Potential Functions," Proceedings of the London Mathematical Society, vol 1, (1904), pp 367-72. [Shows how to turn a standing scalar potential wave back into electromagnetic energy, even at a distance, by scalar potential interferometry, anticipating and greatly expanding the famous Aharonov-Bohm effect, predating the modern (Bohm) hidden variable theory of quantum potentials. Such a procedure could be developed to neutralize radioactive nuclei.]

LOW ENERGY NUCLEAR REACTIONS: EXPERIMENTAL EVIDENCE FOR THE ALPHA EXTENDED MODEL OF THE ATOM

Roberto A. Monti

SUMMARY

An up-to-date list of experimental tests constituting, in my opinion, a good validation for the alpha-extended model of the atom, is presented.

INTRODUCTION

In order to explain the experimental results of L. Kervran [1], in 1988 a new model of the atom was devised, characterized by the following features: 1) substantial asymmetry of the Coulomb electric and magnetic fields of electrons and protons; 2) existence of positions of stable electromagnetic equilibrium of electrons in the vicinity of nuclei; 3) the neutron is a particular "bound state" of a proton and an electron; 4) the nuclei are composite structures of hydrogen atoms of period 4 (alpha-extended model [2,5]); 5) physical and chemical properties of each atom depend on the various possible isomeric configurations.

In light of this new model, the periodic table of the elements has been reconstructed [2]. This model proved itself very useful not only in order to understand Kervran's low energy nuclear reactions but also to explain, in 1989, the "cold fusion" phenomena claimed by Fleischmann and Pons [3]. In 1990 a list of experimental tests was made of the Alpha-extended model of the atom [4]. These tests, repeated and extended, constitute now, in the author's opinion, a good validation for the Alpha-extended model.

1) The Periodic Table of the Elements (Fig. 1).
The reconstruction of the Periodic Table of the Elements according to the Alpha-extended model of the atom is very simple (Fig. 2, Fig. 3, Fig. 4).

The horizontal view of Fig. 1 shows clearly that the nuclei are periodic structures of period 4. The vertical view (Mendeleff order, in which only the two most abundant isotopes are listed) suggests immediately the "composite structures" of the nuclei.

Example: $n \cdot 4\alpha$ Reactions.

Group I A.

$^{7}_{3}Li$ $(\alpha + T_1)$
$\Downarrow + 4\alpha$
$^{23}_{11}Na$ $(5\alpha + T_1)$
$\Downarrow + 4\alpha$
$^{39}_{19}K$ $(9\alpha + T_1)$
$\Downarrow + 3 \cdot 4\alpha$
$^{87}_{37}Rb$ $(18\alpha + 3\alpha_o + T_1)$ $(4{,}8\ 10^{10}y)$
$\Downarrow + 3 \cdot 4\alpha$
$^{135}_{55}Cs$ $(27\alpha + 6\alpha_o + T_1)$ $(3\ 10^{6}y)$

Group O (Noble Gases).

$^{4}_{2}He$ (a)
$\Downarrow + 4\alpha$
$^{20}_{10}Ne$ (5α)
$\Downarrow + 4\alpha$
$^{36}_{18}Ar$ (9α)
$\Downarrow + 3 \cdot 4\alpha$
$^{84}_{36}Kr$ $(18\alpha + 3\alpha_o)$
$\Downarrow + 3 \cdot 4\alpha$
$^{132}_{54}Xe$ $(27\alpha + 6\alpha_o)$

2) Neutron synthesis and α_o group.
Neutron synthesis - which is the first step in atom building- was achieved by Borghi, starting from a cold plasma of protons and electrons [5].

The following steps: synthesis of Deuterium (D), Tritium (T_1), He3 (T_2), Helium 4 (α) and experimental evidence for the 4-neutron (α_o) group were already well documented in the scientific literature. As well as the production and decay of the nuclei from 11 α to 18 α and the "New Radioactivities" (reversible transition): [4]

$$\alpha_o \underset{2EC}{\overset{2\beta^-}{\rightleftarrows}} \alpha$$

3) Experimental evidence for low energy nuclear reactions: Nucleus + n · 3α; Nucleus + n · 4α.
At the end of 1989 I could get information about the reactions: Nucleus + n·3α; Nucleus + n·4α, which confirmed the reality of the "composite structure" of the nuclei [4]. The nuclear reactions indicated were the following: 2(C + O) → Fe; Na + O → K.

The first could be very easily reproduced. Consequently I tested it following methods 2 and 3. The report handed to me claimed the production, with the same methods, of 35 different elements. I noticed that all the stable isotopes of Si and Fe could be considered "composite structures" of C and O [4].

4) Further experimental evidence for the reactions: Nucleus + n · 3α and Nucleus + n · 4α.
a) Experiments at B.A.R.C.
In 1991 I gave a lecture at B.A.R.C. on low energy nuclear reactions. One year later M. Srinivasan gave me a preprint showing experimental evidence for the reactions: C + N → Al; C + O → Si; 2(C + N) → Cr; 2(C + O) → Fe; 2(C + O) → Ni [6].

b) Experiments at Texas A&M.
Immediately after this positive result Sundaresan and Bockris repeated test 2 [4], showing once more experimental evidence for the reaction: 2(C + O) → Fe [7].

4) Experiments by Champion and co-workers.
In 1992 I informed J. Champion about the experimental tests of Oshawa and I showed him how to use my Periodic Table of the Elements. Champion and co-workers repeated later (1994) method 3 [4], with the following results [8]:

a) Carbon - Iron - Carbon arc.
New elements produced: Zr, Mo, Ru, Ba, Sm, Yb, Hf, Os.

b) Carbon - Nickel - Carbon arc.

New elements produced: Mo, Ru, Pd, Ce, Ba, Nd, Sm, Hf, W, Os, Pt.

c) Carbon - Copper - Carbon arc.
New elements produced: Rh, Pd, Ag, Nd, Eu, W, Re, Ir, Pt, Au.

5) Cold fission.
The low energy nuclear reactions listed by Kervran were all reversible, in accordance with the Alpha-extended model.

I summarized all the biological low energy nuclear reactions indicated, together with a peculiar low energy nuclear reaction: the half-fission : $^{206}_{82}Pb \rightarrow 2^{103}_{45}Rh$, obtained by electromagnetic excitation of the lead nuclei.

Moreover "old" and "new" radioactivities showed a very good experimental evidence for "spontaneous cold fissions" followed by the transition:

$$\alpha_o \xrightarrow{2\beta^-} \alpha$$

6) Low energy nuclear fission of stable isotopes.
a) Experiments at Texas A&M and Engelhard laboratories.
to witness experimental tests suggested by J. Champion. The first of these tests told me immediately what was going on: I had already seen it in a drawing made 500 years before (Fig.1).

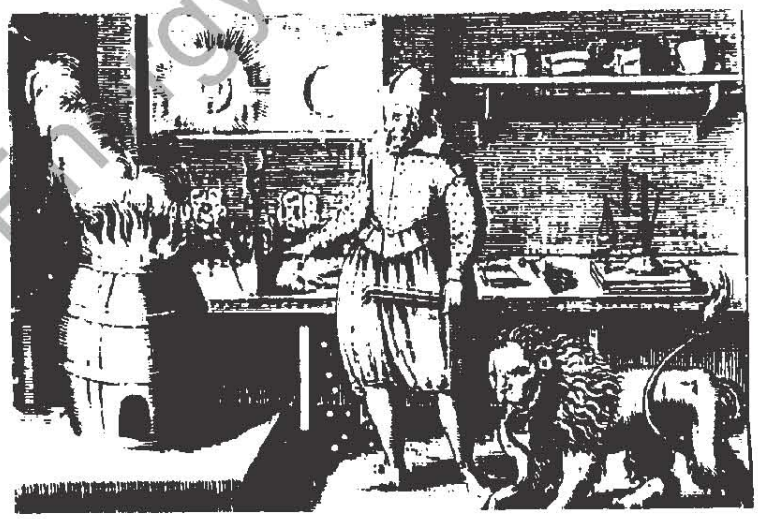

The same experiment, repeated at Engelhard Laboratories, showed conclusively the reactions:

$$^{201}_{80}Hg - \alpha \longrightarrow {}^{197}_{78}Pt \xrightarrow{\beta^-} {}^{197}_{79}Au$$

$$^{109}_{47}Ag - \alpha \longrightarrow {}^{105}_{45}Rh \xrightarrow{\beta^-} {}^{105}_{46}Pd$$

That is: the possibility to cause a decay of stable isotopes by means of "ordinary" chemical reactions [9].

b) Experiments by Champion and coworkers.
In 1995 J. Champion noticed that one of his "Hg cells", designed to make Platinum by electromagnetic excitation, was producing Ru at a rate 10 times bigger than that of Pt, giving further confirmation of the reality of the half-fission nuclear reactions indicated by Kervran [10]. It is easy, in fact, to notice that the half-fission of: $^{196}_{80}Hg$, $^{198}_{80}Hg$, $^{200}_{80}Hg$, $^{202}_{80}Hg$, $^{204}_{80}Hg$, results in: $^{98}_{44}Ru$, $^{99}_{44}Ru$, $^{100}_{44}Ru$, $^{101}_{44}Ru$, $^{102}_{44}Ru$.

The two remaining isotopes of Hg: 199 and 201, by the induction of an α decay, produce Pt and Au.

7) Low energy nuclear reactions of unstable isotopes.
The possibility to cause nuclear fission of stable isotopes by "ordinary" chemical reactions suggests immediately the possibility to cause the fission of unstable isotopes.

A series of experimental tests made in '93, '94, '95, '96, gave me very useful information [11]. In addition to what I have shown last year [12], I can say that the amount of thorium oxide in the "Thorium ash" was 78%. Consequently the "missing Thorium" after the reaction is ≈ 70%. Today (September 1996) I am waiting for definitive results from two National Laboratories.

8) Reactions Hg - Na.
In 1995 J. Champion showed in Colorado Springs (13) the possibility to obtain the following reactions:

$$^{198}_{80}Hg + ^{23}_{11}Na \xrightarrow{p} ^{197}_{79}Au + ^{24}_{12}Mg$$

$$^{198}_{80}Hg + ^{23}_{11}Na \xrightarrow{\alpha} ^{194}_{78}Pt + ^{27}_{13}Al$$

simply making an amalgam of mercury and sodium.

I repeated the same test after a few months in a condition of "sodium excess". The result was the production of the following elements: Si , K , Ca , Fe , Ti , Cr , Cu. The Periodic Table suggests immediately further tests of this kind (reactions: Hg - Li , Hg - K , Hg - Rb , Hg - Cs), which can be easily performed.

9) "Cold fusion" in metal lattices.
When Fleischmann and Pons published their experimental results about the "cold fusion" D + D in Palladium lattices [3] I had already published (in Italian) my new model of the atom and the Periodic Table [14].

Consequently it was easy, for me, to understand what had really happened and where Fleischmann and Pons were wrong. I explained these facts for the first time in the Erice conference (Italy, Spring 1989). In 1991 I gave the following written explanation at the Second ICCF (Como, Italy) (4):

a) Pd does not only act as a catalyst of the D + D reactions.
b) As a consequence of the nuclear reactions among Pd and LiOD The Palladium was "burning" like a match forming, at least within a thin layer, a plethora of new nuclei.

In order to limit the nuclear reactions I suggested to use monoisotopic electrodes and to analyze the atomic and isotopic composition of the electrodes **before** and **after** the reactions. In 1996 Mizuno et al. made this test, with the following results: Within a thin layer of 1micron they found: Cr, Fe, Cu, Pt, Ca, Ti, Mn, Co, Zn, Cd, Sn, Pb, Ga, As, Br, Sb, Te, I, Xe, Hf, Re, and Ir [15].

A similar test was made by Bockris and Minevskii, with the following results: Within a layer of 1micron they found: Mg(6.7%), Si (10.2%), Cl(3.0%), K(1.1%), Ca(19.9%), Ti(1.6%), Fe(10.5%), Cu(1.9%), Zn(4.2%), Pd(31.9%), Ag(1.9%), Pt(7.1%) [15]. The starting concentration of palladium was: 99.8%.

The various different reactions can be singled out using the Periodic Table and finding the exact isotopic composition of each new element.

10) Isomeric configurations of the atoms.
The Alpha-extended model allows each atom to "keep in storage" within its "rigid" tridimensional structure the "information" which determines its physical and chemical behavior.

In 1991 I suggested that the two allotropic forms of the Carbon atom (diamond and graphite) were a good example of this kind and that this example should be: "only the first of a long series. This opinion has recently been confirmed by the experimental results of S.K. Dixit. In the Rasasastra Department (Alchemy) of the Banaras Indu University it is normal practice to obtain different isomeric configurations of atoms and molecules, characterized by different physical and chemical properties, from the most 'common' configurations. The same

atom or molecule is given a specific name according to the various isomeric configurations which prove useful in the medical field" [4].

A few months later (October 1991) I could get information about the discovery of a **third** isomeric configuration of the Carbon atom: fullerenes, obtained by arcing Carbon in a Helium atmosphere [16].

Finally, in 1995, I was informed by D. Hudson about the discovery of new, peculiar, isomeric configurations of monoatomic transition elements, which he called O.R.M.E.S. (Orbitally Rearranged Monoatomic ElementS) [17]. These isomeric configurations are well known in Alchemic literature [18]. But, according to the Alpha-extended model of the atom (no "orbits"), the "right" name for these isomeric configurations should be: E.R.M.E.S. (Electronically Rearranged Monoatomic ElementS).

CONCLUSIONS

The experimental evidence listed above constitutes, in my opinion, a good validation for the Alpha-extended model of the atom.

REFERENCES

1. C.L. Kervran, "Proofs in Geology and Physics for Low Energy Transmutations," Giannone, Palermo 1983; "Proofs in Biology for Low Energy Transmutations," Giannone, Palermo 1986.
2. R. A. Monti, "Historico-Critical Analysis of Atom Models," Andromeda, Bologna 1988.
3. M. Fleischmann, S. Pons, *J. Electroanal. Chem.*, vol 261, p 301 (1989).
4. R. A. Monti, "Cold Fusion and Cold Fission: Experimental Evidence for the Alpha-Extended Model of the Atom," Communication to the Second I.C.C.F., Como, Italy 1991. An up-to-date copy is available at the second I.C.L.E.N.R.
5. D.C. Borghi, D.C. Giori, A. Dall'Olio (CEN, Recife, Brazil), "Experimental Evidence on the Emission of Neutrons from a Cold Hydrogen Plasma." See also Ref. 4.
6. M. Singh, M.D. Sakesena, V.S. Dixit, V.B. Kartha (BARC), "Verification of the George Oshawa's Experiment for Anomalous Production of Iron from Carbon Arc in Water," *Fusion Technology*, vol 26 (1994), p 226.
7. R. Sundaresan, J.O'M. Bockris, "Anomalous Formation of Iron from Carbon as a Result of Arcing in Water," *Fusion Technology*, vol 26 (1994), p 261.
8. J.E. Champion, "Explanation of Observed Nuclear Events Associated with Cold Fusion and Similar Low Energy Nuclear Reactions," June 1994.
9. R.A. Monti, "Experiments in Cold Fusion and Cold Fission," Communication to ICCF 4. Maui, (1993).
10. J.E. Champion, private communication, (1995).
11. R.A. Monti, "Transmutation of Radioactive Elements by Atomic Chemistry," private communication to J.O'M. Bockris (1993).
12. R.A. Monti, "Variations of the Half-Lives of Radioactive Eelements and Associated Gold Fusion and Cold Fission Reactions," *J. of New Energy*, vol 1, no 1, pp 119-125, Proc. 1st Int'l. Conf. on Low Energy Nuclear Reactions, College Station (TX), June 1995.
13. J.E. Champion, "Nuclear Change via Chemical Reaction; Modern Day Nuclear Change," Extraordinary Science Conference 1995 (videotapes); International Tesla Society. PO Box 5636, Colorado Springs, CO, 80931.
14. R.A. Monti, "Reconstruction of the Periodic Table of the Elements," *Seagreen N° 8*, Andromeda Bologna, Spring 1989, p 53.
15. H. Fox, "Implications of the Bockris-Minevskii and Mizuno et al. Papers," *Fusion Facts*, April 1996.
16. R.F. Curl, R.E. Smalley, "Fullerenes," *Scientific American*, October 1991, p 32.
17. D. Hudson, "Non-Metallic, Monoatomic Forms of Transition Elements," Keely Net, PO Box 870716, Mesquite (TX) USA 75187.
18. Ireneo Filalete, "Open Entrance to the Closed Place of the King (1645)," Phoenix. Geneva, Italy (1987).

PERIODIC TABLE

Colors:
Yellow = Maximum abundance
Orange = 2nd by abundance
Green = Stable Isotope
Light Blue = Unstable. $t_{1/2} > 1$ year
Pink = Unstable. $t_{1/2} < 1$ year

Constants

1 Mev = 1,0735355 10^{-3} u.m.a.

1 u.m.a. = 931,501567 Mev = 1,6605655 10^{-27} Kg

Elementary Constituents.

e = electron; m_e = 0,51100337 Mev.

p = proton; m_p = 938,27961 Mev.

P = Protium (p + e); m_P = 938,790601 Mev.

P_0 = neutron (pe) = n; m_n = 939,57304 Mev.

D = Deuterium; m_D = 1876,138974 Mev.

D_0 = n + p(k)e = (2n); m_{D_0} = 1876,138974 + 0,782439 = 1876,921413 Mev.

T_1 = Tritium; m_{T_1} = 2809,454646 Mev.

T_2 = Helium 3; m_{T_2} = 2809,436021 Mev.

T_0 = (3n); m_{T_0} = 2810,237085 Mev.

α = Alpha; m_α = 3728,431208 Mev.

α_0 = Alpha-zero (4n); m_{α_0} = 3729,996085 Mev.

Elements and their Mass (in Mev.) (14)

m_A = mass of the element of mass numver A; $m_A = A_{u,m,a,} + \Delta$; Δ = mass excess

$_0{}^1n$ = (pe) = (p) + (e) + 0,78242663 Mev. = 939,57304 Mev.

$_1{}^1H$ = (p + e) = P = 1 + Δ = 931,501567 + 7,289034 = 938,790601 Mev.

Fig. 1 - PERIODIC TABLE

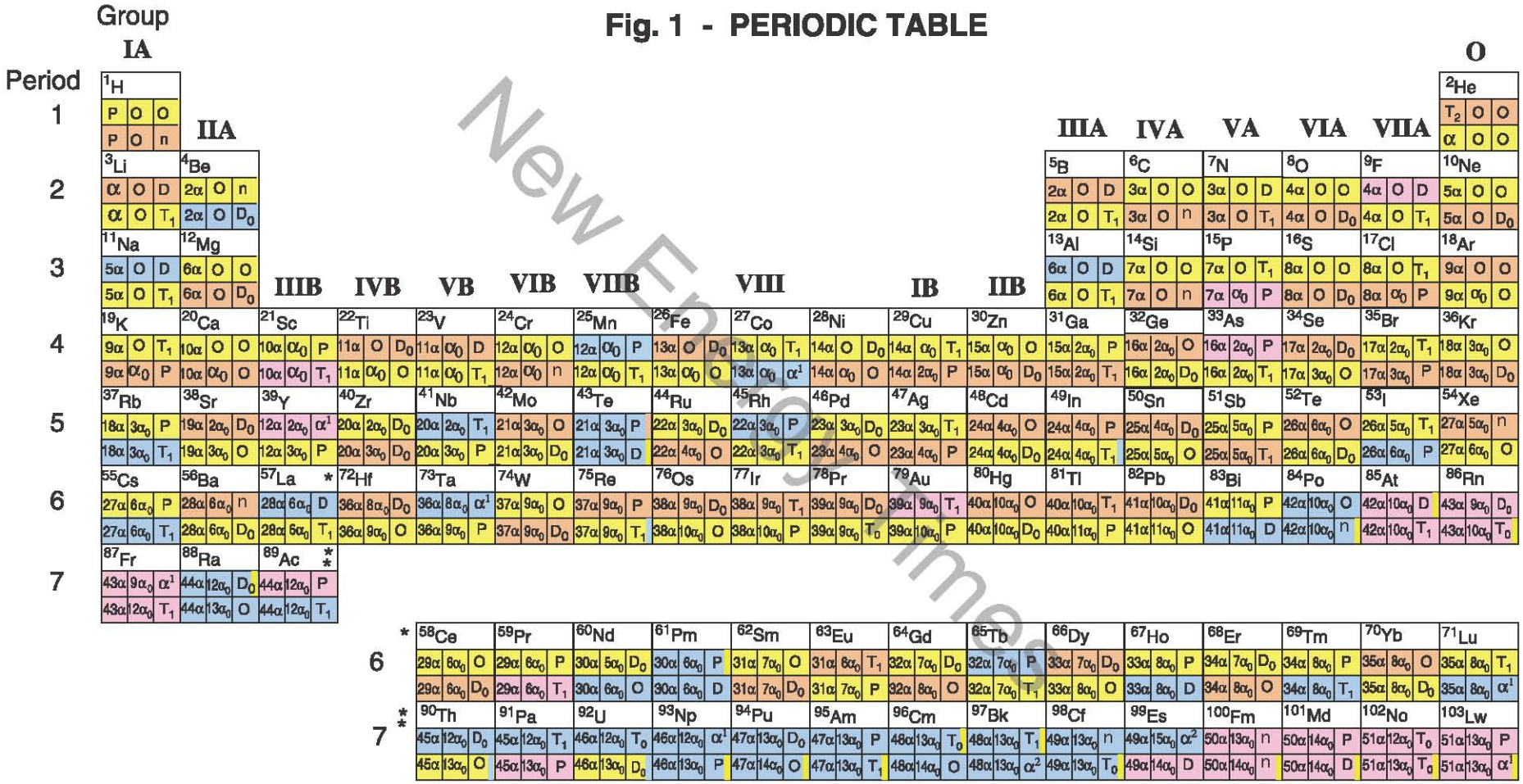

BLANK - BACK OF PERIODIC TABLE

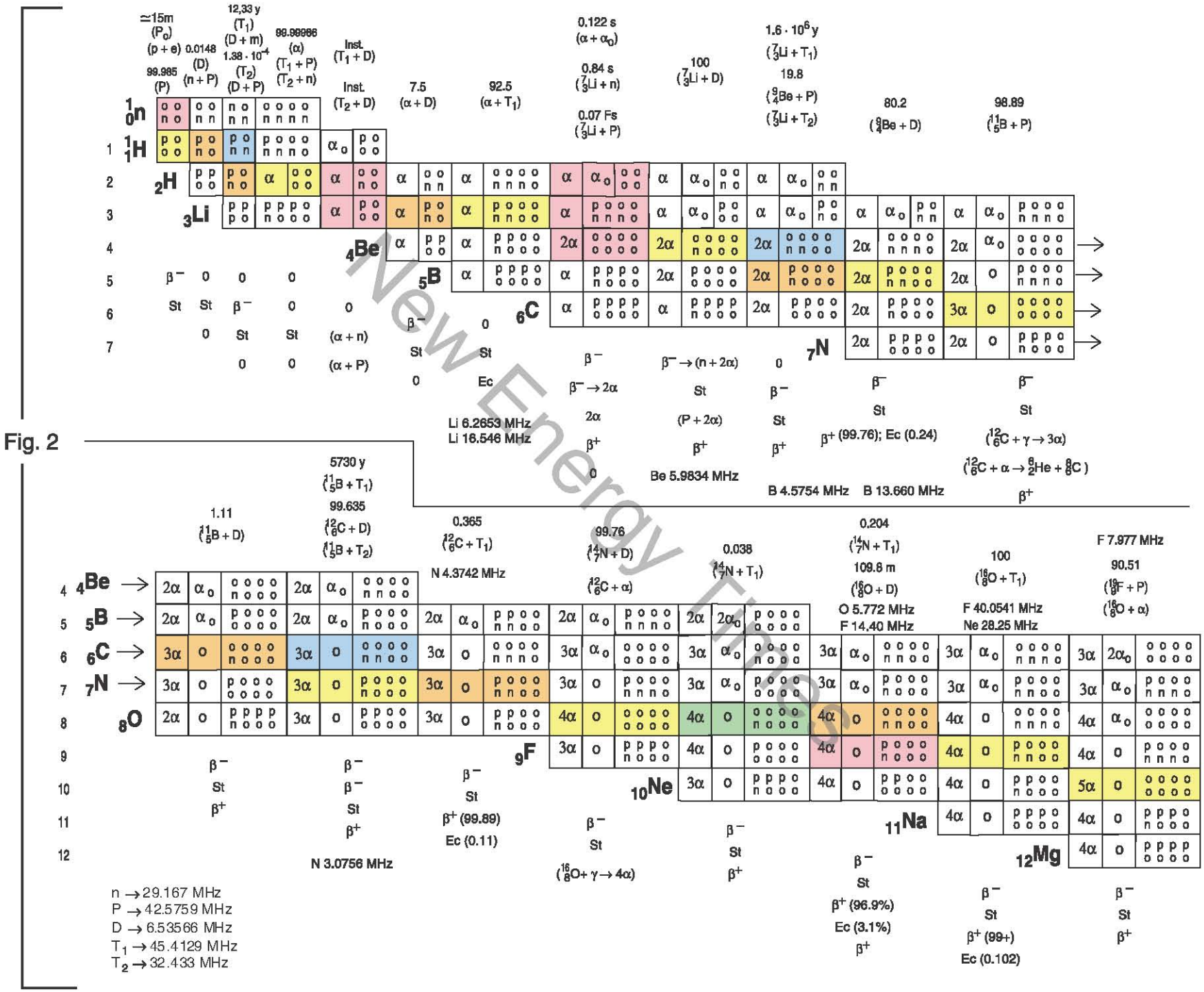

Fig. 2

BLANK - BACK OF FIG. 2

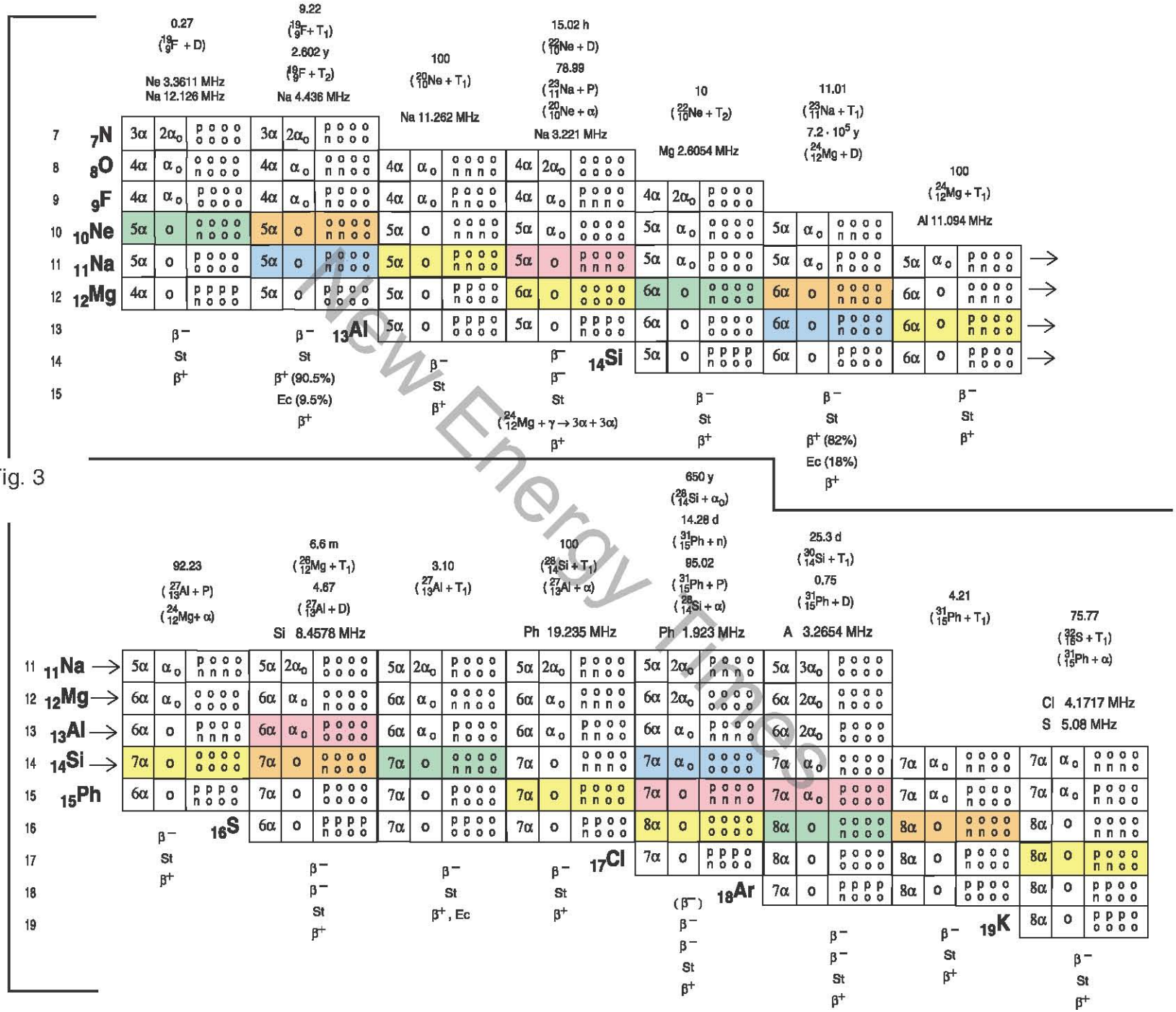

Fig. 3

BLANK - BACK OF FIG. 3

Fig. 4

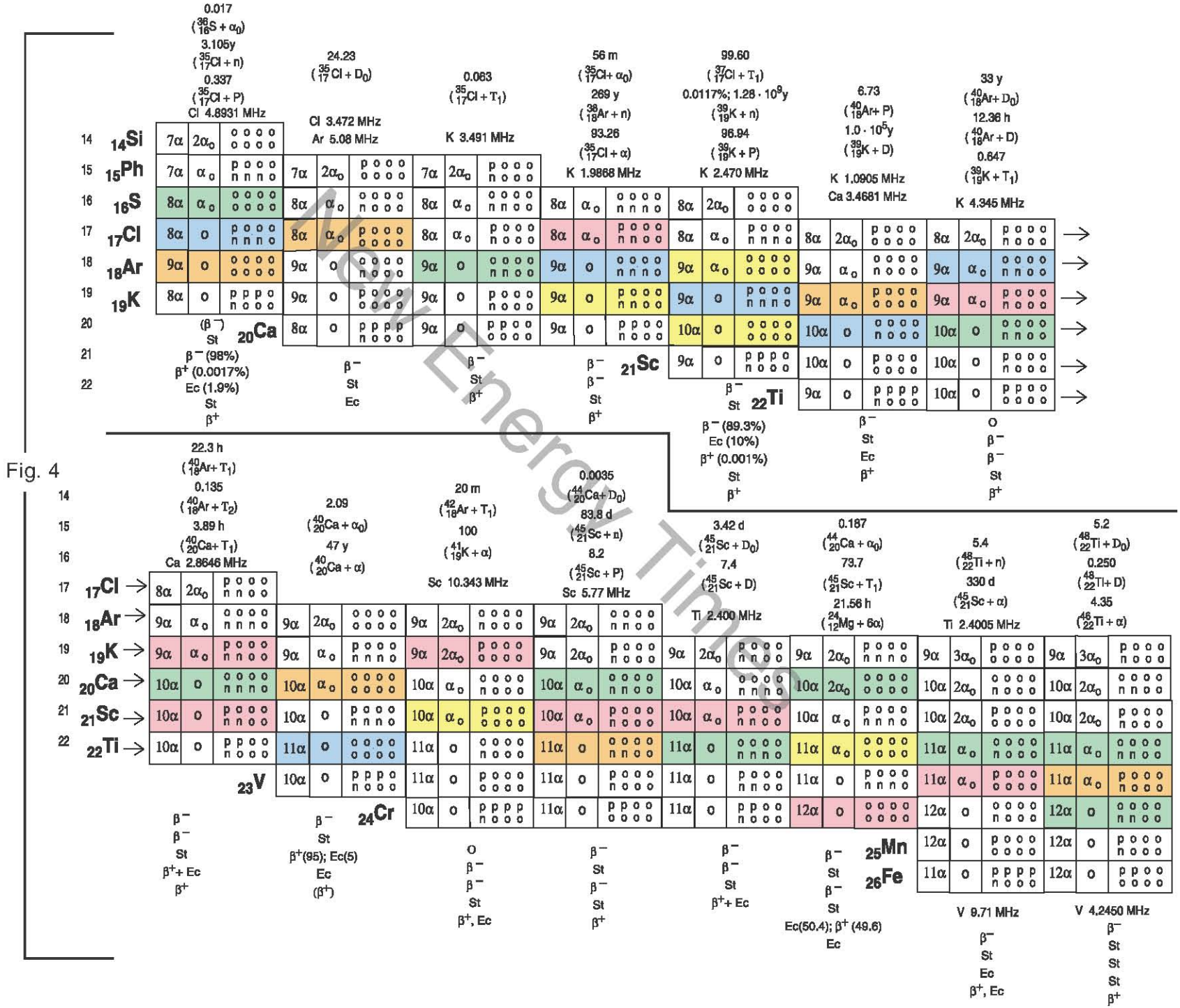

BLANK - BACK OF FIG. 4

GAMOW FACTOR CANCELLATION AND NUCLEAR PHYSICS MECHANISMS FOR ANOMALOUS LOW-ENERGY NUCLEAR REACTIONS

Yeong E. Kim and Alexander L. Zubarev [2]

ABSTRACT

Possible nuclear physics mechanisms are proposed for explaining anomalous effects recently observed in low-energy nuclear reactions. It is recently shown that a near cancellation of the Gamow factor at low energies can occur if one of the final-state nuclei has a weakly bound ("halo") excited state. Another mechanism for the Gamow factor cancellation is a continuum-electron shielding of nuclear charge by a dense electron plasma. If the Gamow factor cancellation occurs, it can lead to a large enhancement of reaction rates and probabilities for anomalous nuclear fusion reaction and nuclear fission, and may provide nuclear physics mechanisms for explaining the anomalous effects observed in low-energy nuclear reactions. Several specific cases of the anomalous effects are discussed in terms of nuclear physics mechanisms, and cluster-impact nuclear reactions.

INTRODUCTION

Since the 1989 announcements of "cold fusion" phenomena [1,2], there have been persistent claims of observing the cold fusion phenomena, and hundreds of experimental papers have been published [3-5]. Most of the reported experimental results are not reproducible at a desirable level of 100%. However, there are a few experimental results which appear to be 100% reproducible [5]. Most recently, observations of low-energy nuclear transmutation have been reported from electrolysis experiments using heavy water and also using water [6-13].

There have been many theoretical models proposed to explain the cold fusion phenomena. Most of those theoretical models claiming to have explained the phenomena appear far from having accomplished their claims [14,15]. Recently, we developed a new alternative theoretical formulation of low-energy nuclear fusion reactions based on the optical theorem [16-18], which is much less model-dependent than previous theoretical approaches, and showed that some of the cold fusion phenomena may be justified theoretically, since a Gamow factor cancellation (GFC) can occur if the imaginary part of the effective nuclear interaction in the elastic channel (ENIEC) has a very weak component with a finite long range (FLR). However, we could not prove nor rule out theoretically the existence of such a FLR component in the imaginary part of ENIEC. In another recent paper [19], we demonstrated (without a rigorous derivation) a possibility of the existence of FLR components if the target nucleus has a weakly bound excited state ("halo" nuclear state). In the most recent paper, we have obtained a rigorous derivation [20] of a new type of FLR interaction in the imaginary party of ENIEC for the case in which one of the final-state nuclei has an excited halo nuclear state.

Another mechanism for GFC is a continuum-electron shielding (CES) of nuclear charge by a dense electron plasma such as one observed in ultra-short-time discharge plasma experiments by Shoulders et al. [21,22].

If GFC occurs, theoretical opposition based on the Gamow factor to the cold fusion [3-5] and low-energy nuclear transmutation [6-13] phenomena may be premature, since it can enhance reaction rates and probabilities for nuclear fusion reaction and nuclear fission, which may provide theoretical explanations of the observed

[2] Department of Physics, Purdue University, West Lafayette, IN 47906.

anomalous effects based on nuclear physics mechanisms. Several specific cases of the observed anomalous effects including recent observations of nuclear transmutation [6-13] are discussed in terms of nuclear physics mechanisms.

2. UNCERTAINTIES OF LOW-ENERGY NUCLEAR REACTION RATES

Nuclear reaction rates and cross-section $\sigma(E)$ at low energies ($\lesssim$ a few keV) are not well determined, since $\sigma(E)$ at low energies, relevant to the cold fusion phenomena and also relevant to the primordial and stellar nucleosynthesis, cannot be measured in the laboratory. They are extracted from the laboratory measurements of $\sigma(E)$ at higher energies by an extrapolation procedure based on nuclear theory [17,18]. Historically, both experimental and theoretical investigations of low-energy ($\lesssim$ 1 keV) nuclear reactions were by-passed and have been neglected by nuclear physics community in favor of investigating nuclear physics phenomena at much higher energies. Therefore, it is now important to turn our attention and efforts to investigating these neglected and unexplored new nuclear physics frontier.

For non-resonance reactions, it is customary to extract the S-factor, S(E), from the experimentally measured $\sigma(E)$ using the following semi-classical formula,

$$\sigma_G(E) = \frac{S(E)}{E} e^{-2\pi\eta(E)}, \tag{1}$$

where $\eta(E) = Z_i Z_j e^2/\hbar u$, $e^{-2\pi\eta(E)}$ is the Gamow factor representing the probability of bringing two charged nuclei to zero separation distance, and S(E) is expected to be a slowly varying function of E. The energy dependence of the nuclear reaction cross-section $\sigma(E)$ cannot be obtained rigorously from first principles. Therefore, one must rely on physically reasonable nuclear reaction models, such as Eq. (1), or phenomenological microscopic models, which may not be reliable nor accurate at low energies for some cases.

For the ambient temperature of E = kT $\approx$ 1/40 eV, the Gamow factor in Eq. (1) has an astronomically small value of $e^{-2\pi\eta(E)} \approx 10^{-2760}$ for two deuterons. Even with the electron screening energy of E_s = 43.4 eV based on Thomas-Fermi model, the Gamow factor has a very small value of $e^{-2\pi\eta(E)} \approx 10^{-65}$, while the claimed observed fusion rates lead to $\sim 10^{-20}$ [1] and $\sim 10^{-30}$ [2]. This extremely small value of $e^{-2\pi\eta(E)} \approx 10^{-65}$ has been one of the main reasons for theoretical opposition [14] and nuclear physics community's rejection of both the cold fusion [3-5] and low-energy transmutation phenomena [6-13].

3. OPTICAL THEOREM FORMULATION

The conventional optical theorem first introduced by Feenberg [23] is given by

$$\sigma_t = \frac{4\pi}{k} Imf(0) \tag{2}$$

where σ_t is the total cross-section and $f(0)$ is the elastic scattering amplitude in forward direction ($\theta = 0$).

To avoid complications associated with the singularity of the forward Coulomb scattering amplitude when we use the convention optical theorem, given by Eq. (2), for scattering of two charged nuclei, we describe a different formulation based on "partial-wave" optical theorem involving angle-integrated and/or angle-independent quantities in the following [16-19].

For the elastic scattering involving the Coulomb interaction and nuclear potential, the scattering amplitude can be written as a sum of two amplitudes:

$$f(\theta) = f^{c}(\theta) + \tilde{f}(\theta), \tag{3}$$

where $f^{c}(\theta)$ is the Coulomb amplitude and $\tilde{f}(\theta)$ is the remainder. $\tilde{f}(\theta)$ can be expanded in partial waves [18] as

$$\tilde{f}(\theta) = \Sigma_{\ell}(2\ell + 1)\, e^{2i\delta_{\ell}^{c}} f_{\ell}^{N(el)} P_{\ell}(\cos\theta), \tag{4}$$

where δ_{ℓ}^{c} is the Coulomb phase shift, $f_{\ell}^{N(el)} = (S_{\ell}^{N} - 1)/2ik$, and S_{ℓ}^{N} is the ℓ-th partial wave S-matrix for the nuclear part. Using Eq. (3) and Eq. (4), the integrated elastic cross section σ^{el} can be written as

$$\sigma^{el}(E) = \sigma^{c} + \sigma^{int} + \sigma^{N(el)}, \tag{5}$$

where σ^{c} is the pure Coulomb cross section (Rutherford scattering), σ^{int} is the interference term, and $\sigma^{N(el)}$ is the nuclear elastic cross section. The partial wave expansion of $\sigma^{N(el)}$ is given by $\sigma^{N(el)} = \Sigma_{\ell}(2\ell + 1)\,\sigma_{\ell}^{N(el)}$ with $\sigma_{\ell}^{N(el)} = \frac{\pi}{k^2}|S_{\ell}^{N} - 1|^2$.

For the reaction cross section $\sigma^{(r)}$, the partial wave expansion is given by $\sigma^{(r)} = \Sigma_{\ell}(2\ell + 1)\,\sigma_{\ell}^{(r)}$ where $\sigma_{\ell}^{(r)} = \pi(1 - |S_{\ell}^{N}|^2)/k^2$. Using the expressions of $\sigma_{\ell}^{(r)}$ and $\sigma_{\ell}^{N(el)}$ derived above, we can write $\sigma_{\ell}^{(r)} + \sigma_{\ell}^{N(el)} = 2\pi(1 - ReS_{\ell}^{N})/k^2$. Combining this with $Imf_{\ell}^{N(el)} = (1 - ReS_{\ell}^{N})/2k$, we obtain the partial wave optical theorem for two-potential scattering case as

$$Imf_{\ell}^{N(el)} = \frac{k}{4\pi}(\sigma_{\ell}^{(r)} + \sigma_{\ell}^{N(el)}) \tag{6}$$

which is a rigorous result.

For low energies, $F_{\ell}^{N(el)} \propto e^{-2\pi\eta/k}$ and hence $\sigma_{\ell}^{N(el)} = 4\pi|f_{\ell}^{N(el)}|^2 \propto e^{-4\pi\eta/k^2}$. Since $\sigma_{\ell}^{(r)} \propto e^{-2\pi\eta/k^2}$, we have $\sigma_{\ell}^{(r)} > \sigma_{\ell}^{N(el)}$ at low energies and hence we can write Eq. (6) as

$$Imf_{\ell}^{N(el)} \approx \frac{k}{4\pi}\sigma_{\ell}^{(r)} \tag{7}$$

which is still a rigorous result at low-energies. We note that Eqs. (6) and (7) are for non-radiative nuclear reactions and need to be modified for radiative nuclear reactions.

In terms of the partial wave T-matrix, T_{ℓ}, the elastic nuclear scattering amplitude, $f_{\ell}^{N(el)} = (S_{\ell}^{N} - 1)/2ik$, can be written as

$$f_{\ell}^{N(el)}(E) = -\frac{2\mu}{\hbar^2 k^2}\langle\psi_{\ell}^{c}|T|\psi_{\ell}^{c}\rangle \tag{8}$$

where ψ_{ℓ}^{c} is the ℓ-th partial wave regular Coulomb function and μ is the reduced mass. Using the low-energy optical theorem Eq. (7) with Eq. (8), we obtain the ℓ-th partial-wave reaction cross section $\sigma_{\ell}(E)$ $(= \sigma_{\ell}^{(r)}(E))$ as

$$\sigma_{\ell}(E) \approx \frac{4\pi}{kE}\int_{0}^{\infty}\psi_{\ell}^{c}(r)\, U_{\ell}(r, r')\, \psi_{\ell}^{c}(r')\, dr\, dr' \tag{9}$$

where $E = \hbar^2 k^2/2\mu$ and $U_\ell(r, r') = -Im \langle r|T_\ell|r' \rangle$ with T_ℓ representing the ℓ-th partial wave contribution of the T-matrix operator. The total reaction cross-section $\sigma(E)$ is given by $\sigma_\ell(E) = \Sigma_\ell (2_\ell + 1)\, \sigma_\ell(E)$.

4. REACTION CROSS SECTION FORMULA

It is recently shown [16, 18, 19] that $Im \langle r|T_\ell|r' \rangle = (-U_\ell(r, r'))$ is separable for the $\ell = 0$ two-channel case, and hence $U_0(r, r')$ in Eq. (9) is also separable for the case of two-channels (elastic and fusion). Therefore, to estimate the S-wave cross section $\sigma_0(E)$ for the two-channel case, we can parameterize $U_0(r, r')$ in Eq.(9) by two parameters λ (strength/length) and β^{-1} (range) in a separable form as

$$U_0(r, r') = \lambda g(r)\, g(r') \tag{10}$$

where β^{-1} is a potential range parameter for g (r) and $\lambda = V_0 \beta / (V_0 > 0)$. λ is expected to be a slowly varying function of energy for the non-resonance case. (For the case of resonance reactions, the energy dependence of λ can be parameterized by the Breit-Wigner expression).

For $\ell = 0$ case, Coulomb wave function $\psi_0^c(r)$ is given by

$$\psi_0^c(r) = C_0(\eta) M_{i\eta,\frac{1}{2}}(2ikr)/2i \tag{11}$$

where $C_0^2(\eta) = 2\pi\eta / (e^{2\pi\eta} - 1)$ and $M_{i\eta,\frac{1}{2}}(2ikr)$ is the Whittaker function. The reaction cross section given by Eq. (9), in the case of $g(r) = e^{-\beta r}/r$, can be written as

$$\sigma_0(E) = \frac{4\pi\lambda}{kE} \left| \int_0^\infty \psi_0^c(r) \frac{e^{-\beta r}}{r} dr \right|^2 = \frac{\pi\lambda}{kE} C_0^2(\eta) \left| \frac{1}{i} \int_0^\infty M_{i\eta,\frac{1}{2}}(2ikr) \frac{e^{-\beta r}}{r} dr \right|^2 \tag{12}$$

The integral in Eq. (12) can be evaluated exactly

$$\sigma_0(E) = \frac{4\pi\lambda}{kE} \left[\int_0^\infty dr \psi_0^c(r) e^{-\beta r}/r \right]^2 = \frac{4\lambda\pi^2}{E} R_B \frac{(e^{-2\phi\eta} - 1)^2}{(e^{2\pi\eta} - 1)} e^{4\phi\eta} \tag{13}$$

with

$$e^{4\phi\eta} = \exp\left[4\alpha \frac{\mu c^2}{\hbar c} \left(\frac{Z_a Z_b}{k} \right) \tan^{-1}\left(\frac{k}{\beta} \right) \right] \tag{14}$$

where $\phi = \tan^{-1}(k/\beta)$ and $R_B = \hbar^2/(2\mu Z_a Z_b e^2)$. The energy dependence of λ is expected to be weak.

The use of more general form for $g(r) = (e^{-\beta r}/r) \Sigma_{i=0}^n c_i r^i$ instead of $e^{-\beta r}/r$ in Eq. (10) also leads to the same enhancement factor $e^{4\phi\eta}$. Therefore, the enhancement factor $e^{4\phi\eta}$ is independent of shape of the separable function $g(r)$ used in Eq. (10). For $g(r) = (e^{\beta r}/r) \Sigma_{i=0}^N c_i r^i$, we obtain for $\sigma_0(E)$ the following

$$\sigma_0(E) = \frac{\tilde{S}_0(E)}{E} e^{4\phi\eta}\, e^{-2\pi\eta} \tag{15}$$

where

$$\tilde{S}_0(E) = 4\pi^2 \lambda \Sigma_{ij} c_i c_j F_i^\beta(E) F_j^\beta(E) \tag{16}$$

with $F_0^\beta(E) = R_B(e^{-2\phi\eta} - 1)$, $F_1^\beta(E) = R_B^{-1}(\beta^2 + k^2)^{-2}$, $F_2^\beta(E) = R_B^{-3}(2R_B\beta + 1)/(\beta^2 + k^2)^4$, etc.

The enhancement factor $e^{4\phi\eta}$ is $e^{2/(R_B\beta)}$ at zero energy and decreases as E increases to $e^{\pi/kR_B} = 1$ for large E, and thus can account for the increase of experimentally extracted S(E) toward lower energies. The enhancement factor $e^{2\phi\eta}$ can be applied to both light nuclei reactions (small Z_a and Z_b) but also to heavy ion reactions (larger Z_a and Z_b) such as sub-barrier heavy ion fusion where $e^{4\phi\eta}$ can be very large. The enhancement factor $e^{4\phi\eta}$ is obtained together with the Gamow factor from our derivation and can be regarded as a modification of the Gamow factor affecting it only at low energies, or as a part of the S-factor if we still wish to keep the conventional semi-classical formula Eq. (1). The new exponential factor is a quantum effect derived from the quantum scattering theory, and may provide new physical insights for the low-energy behavior of the reaction cross-section.

5. EFFECTIVE LONG-RANGE INTERACTION AND GFC

In the limit of $\beta \to 0$ (a long-range limit), we have $\phi = \tan^{-1}(k/\beta) = \pi/2$, and hence $e^{4\phi\eta}$ given by Eqs. (14) approaches to $e^{2\pi\eta}$ which can cancel the Gamow factor $e^{-2\pi\eta}$ in Eq. (15) for $\sigma_0(E)$. Therefore, a Gamow factor cancellation can occur if the interaction range β^{-1} is large (or β is small). If the imaginary part of the effective potential or $g(r)$ in Eq. (10) has a form

$$g(r) = e^{-\beta_1 r}/r + \Lambda e^{-\beta r}/r \tag{17}$$

with $\beta < \beta_1$, the second term could be dominant over the first term even if $\Lambda >> 1$. In the limit of $\beta \to 0$, $\phi = \tan^{-1}(k/\beta) = \pi/2$ and $e^{4\phi\eta} = e^{2\pi\eta}$ which can cancel the Gamow factor $e^{-2\pi\eta}$ in Eq. (15). This shows that a Gamow factor cancellation (GFC) can occur for nuclear fusion reactions if the imaginary part of the effective nuclear interaction in the elastic channel (ENIEC) has a small component of a finite long-range (FLR) interaction. Recently, we have obtained a rigorous derivation of a new type of FLR interaction in the imaginary part of ENIEC for the case in which one of the final-state nuclei has an excited halo nuclear state [20]. The new FLR interaction behaves as $\cos(k_0 r - \eta \ell n 2k_0 r + \delta)\, \psi_n(r)/r^4$ at large distances, where k_0, η, δ, and $\psi_n(r)$ are the final state wave number, the Sommerfeld parameter, the phase shift, and the wave function for the excited p-wave halo nuclear state, respectively.

This demonstrates that we cannot rule out theoretically the GFC effect, and that theoretical opposition based on Eq. (1) to the cold fusion [3-5] and low-energy nuclear transmutation [6-13] phenomena may be premature. Therefore, it is important to investigate both theoretically and experimentally the possibility of the existence of excited halo nuclear states and the finite long range interaction for the imaginary part of the effective potential.

6. GAMOW FACTOR CANCELLATION WITH CONTINUUM-ELECTRON SHIELDING

Recently , we have suggested a possibility of the GFC due to continuum-electron shielding (CES) [25]. For a three-body system (e + p + p) in continuum in which all three particles are mobile, there is a possibility that a solution of the three-body Schroedinger equation may lead to the GFC if the relative velocity υ_{ep} between e and p is smaller than the relative velocity υ_{pp} between two protons, i.e. $\upsilon_{ep} < \upsilon_{pp}$. Since $\upsilon_{ep} = (2E_{ep}/m_e)^{1/2}$ and $\upsilon_{pp} = [2E_{pp}/(m_p/2)]^{1/2}$, condition $\upsilon_{ep} < \upsilon_{pp}$ (or $(\upsilon_{ep}/\upsilon_{pp}) < 1$), becomes $[m_p E_{ep}/(2m_e E_{pp})]^{1/2} < 1$, or

$$\frac{E_{ep}}{E_{pp}} < \frac{2m_e}{m_p} \sim 10^{-3} \tag{18}$$

for the case of (e + d + d) in continuum, the condition $\upsilon_{ed} < \upsilon_{dd}$ corresponds to

$$\frac{E_{ed}}{E_{dd}} < \frac{2m_e}{m_d} \sim 0.5\times10^3 . \tag{19}$$

Conditions for (e + p + nucleus) and (e + d + nucleus) systems are

$$\frac{E_{ep}}{E_{pA}} < \left(\frac{A+1}{A}\right)\left(\frac{m_e}{m_p}\right) \sim \left(\frac{A+1}{2A}\right) \times 10^{-3} , \tag{20}$$

and

$$\frac{E_{ed}}{E_{dA}} < \left(\frac{A+2}{A}\right)\left(\frac{m_e}{m_d}\right) \sim \left(\frac{A+2}{4A}\right) \times 10^{-3} , \tag{21}$$

respectively. The CES condition may be satisfied in a dense electron cluster such as one observed by K. Shoulders [21,22].

Since 1980, K. Shoulders has been investigating dense highly organized micro-size cluster of electrons produced in ultra-short-time discharge plasma experiments [21,22]. The experimental data indicate the existence of a plasma state representing a freely moving, localized packet of electrons. A short Latin acronym EV (electrum validum or electromagnetic vortex) has been adopted to describe this collective plasma state of tightly bound groups of electrons with extremely high densities. The EV's have been reported to be roughly spherically symmetric with radii on the order of 1.0 μm, to travel at speeds on the order of 0.1c (corresponding to the electron kinetic energy of ~ 2.7 keV), to tend to move for distances of 1.0 to 10.0 mm in straight lines, to deflect and accelerate with electron characteristics in experiments, and to have high electron densities on the order of 10^{22} to 10^{24} cm^{-3} with negligible ion content of ~ one ion per 10^6 electrons.

Shoulders [21] reports the principle requirement for generating these EV structures to be a sudden creation of a very high, uncompensated set of electronic charges in a very small volume of space, i.e., a fast emission process coupled to a fast switching process. He notes the times of creation to be considerably less than 10^{-13} sec. The actual threshold initiation times for the particle packet are believed to be $\tau \sim 10^{-15}$ sec. The packet then travels approximately $10^5\tau$ before it catastrophically decays.

Ziolkowski and Tippett [26] interpret the EV theoretically as a stable packet of electrons moving collectively through space-time catalyzed by a localized electromagnetic wave, which can be attributed to localized wave (LW) solutions obtained from Klein-Gordon form of Maxwell equations for a joint system of plasma-fluid and electromagnetic field. Beckmann [27] offers another theoretical interpretation based on oscillating Faraday field surrounding a moving electron.

It has been determined experimentally [22] that the size of EV structure is a function of the high specific energy delivered to the metal. This fact has been recently explained by G. Mesyats in his theoretical analysis [28]. Mechanical storage of energy is thought to be the source for the small EVs produced.

The total number of electrons in a 1 μm diameter EV is ~ 10^{11}. This allows for inclusion of ~ 10^5 ions (or nuclei) which would not be detected in measurements of the charge-to-mass ratio of EV such as time-of-flight measurement, i.e. electrons and nuclei in the EV (NEV) would be collectively accelerated to the velocity of electrons. This could provide a simple nuclear accelerator for accelerating nuclei. Shoulders et al. [22] have

proposed this nuclear acceleration mechanism (leading to cluster-impact nuclear reactions) as a possible explanation of the anomalous nuclear transmutation effect observed by several groups [10-13]. A similar mechanism of nuclear acceleration has been proposed by Rabinowitz and Worledge [29] who pointed out that if a small number of deuterons (or other nuclei) become entrained with a high current density of electrons, the deuterons would attain the same velocity as the electrons. Cluster-impact fusion has been previously investigated both experimentally and theoretically with $(D_2O)_n$ clusters, which is described in the next section 7. For the velocity of $\upsilon = 0.1c$ for the NEV, deuterons entrained in the EV would attain kinetic energy of $M_d\upsilon^2/2 \approx 9.4$ MeV (or proton kinetic energy of ~ 4.7 MeV or oxygen kinetic energy of ~56.3 MeV). Although these higher energy deuterons (or protons) can have large reaction cross-sections, the total reaction rates with the EV's containing ~ 10^5 nuclei per EV are too small for explaining some of the observed reaction rates, unless a substantially large number of the EV is produced per unit time and additional mechanisms such as shock-wave heating are invoked.

Acceleration process of positive ions at higher energies due to electron plasma was observed in 1960 [30] in experiments involving a rapid expansion of plasma in a vacuum spark discharge [31,32]. Plyutto et al. obtained protons with kinetic energies of 4-5 MeV and carbon ions with kinetic energies of 15-20 MeV, when pulsed voltages of only 200-300 kV were used for spark discharge. The average number of 10^{11}–10^{12} per pulse was achieved for accelerated protons or deuterons [33].

If the number of nuclei (deuterons, protons, oxygen, and other nuclei) imbedded in the EV is of the same order as that of electrons (10^{11} electrons in μm diameter size) in the EV, kinetic energies of electrons and nuclei in the NEV become much smaller. However a Gamow factor cancellation due to the continuum-electron shielding can occur if the relative velocities between electrons and nuclei in the NEV are much smaller than the velocity of the NEV. If such a GFC condition and a high production rate of the NEV are achieved, most of the observed anomalous effects [3-5,6-13] can be explained by nuclear physics mechanisms.

Once the GFC is achieved in the entrance channel, nuclear reactions can proceed either via the direct reaction mechanism (i.e. fusion) or via the compound nucleus mechanism (de-excitation by γ-ray or neutron emission, or by fission). The compound nucleus mechanism leading to fission may be consistent with some observations of the anomalous nuclear transmutation [6-13].

For most of the electrolysis experiments, applied voltages are much smaller (~ 10V) than ~2.7kV Shoulders used to generate the EV from his discharge experiments. However, some mechanisms such as the fracto-emission may generate the EV even though the applied voltage is ~10V. Generation of the EV has been observed with applied voltage as low as 50V [22]. If a sufficiently large number of smaller size (< 1μm) EV with lower velocities corresponding to the electron kinetic energy of $\gtrsim$ 10eV can be produced at the surface of the cathode and/or in microcavities and cracks inside the cathode metal, the GFC due to the continuum-electron shielding may occur and provide a consistent explanation for most of the anomalous effects observed in electrolysis experiments, based on nuclear physics mechanisms (fusion, fission, etc.)

7. CLUSTER-IMPACT NUCLEAR REACTION (CINR)

Previous investigations of the cluster-impact nuclear reaction were carried out with heavy-water molecule-clusters, $(D_2O)_n$. Unlike electrons in the NEV, electrons in $(D_2O)_n$ are bound electrons and not continuum electrons, and hence the GFC due to the continuum electron shielding is not applicable. The original claims [34-37] of the anomalous enhancement of $(D_2O)_n$ cluster-impact fusion cross-section were later found to be incorrect [38]. Nevertheless, most of theoretical formulations and models [39-49] developed to describe the cluster-impact fusion phenomena are still applicable to the cluster-impact nuclear reactions with the NEV (CINR/NEV). CINR/NEV is a way of coupling first the input energy into the electronic system and then into the target nuclei as laser induced fusion does. However, CINR/NEV may turn out to be more efficient than the laser induced fusion.

In recent experiments, Beuhler et al. [34-35] observed unexpectedly high rates of ~ 1 - $10s^{-1}$/D pair for deuterium-deuterium (D- D) fusion when singly charged clusters of D_2O molecules ($(D_2O)^+_n$, n = 25 -1300) accelerated to 150 to 325 keV (with a beam current of ~ 1 nA) and were impacted onto TiD, C_2D_4 and $ZrD_{1.65}$ targets [34,35]. In addition, D - D fusion was observed with $(H_2O)^+_{115}$ cluster impacting upon a C_2D_4 target [35]. The results of Beuhler et al. received confirmation by Bae et al. [36] for $(D_2O)^+_{114}$ and $(H_2O)^+_{115}$ cluster beams impacting on a C_2D_4 target. Beuhler et al. [37] reported from their time-of-flight experiments with pulsed cluster beams that light-fragment contaminants cannot be responsible for observed fusion events. The experimental yields for $(D_2O)^+_{100}$ clusters are ~ 10^{25} times higher than that expected [39, 40] from single D^+ clusters at D - D center of mass (CM) energies of 150 eV/D, and ~ 10^{100} times higher than at 15 ev/D for $(D_2O)^+_{1000}$. A number of theoretical models [40-43,50,51] were proposed but they underestimate the observed fusion yields [34-36] by many orders of magnitude for large clusters with n > 100. It was shown [41-43] that heavy atomic partners (such as the oxygen in D_2O) in the molecule play a vital role in explaining the apparently conflicting negative results for $(D)^+_n$ clusters as reported by Fallavier et al. [38].

We developed a cluster-impact fusion theory [41-43] to explain the observed D - D fusion rates [35] for $(D_2O)^+_n$ clusters striking TiD, C_2D_4, and $ZrD_{1.65}$ targets. The theory is expressed in the form of a universal scaling equation with two physically reasonable parameters. We also carried out a theoretical analysis [48] for extracting the effective temperature T_e from the experimentally measured proton energy spectrum, as in the case of D - D fusion in a hot plasma for which the neutron energy spectrum has been used as a diagnostic for the temperature [52-54]. Shock-wave mechanisms for the cluster-impact fusion are investigated in references [44-49] such as pinch instability heating due to magnetic confinement [46,49,55] and shock-wave heating [44,49]. Although the original claims of the anomalous enhancement of $(D_2O)_n$ cluster-impact fusion rate were found to be incorrect and attributed to the contaminants, most of these theoretical models [34-49] are also applicable to CINR/NEV.

8. CONCLUSIONS

It is shown that a near cancellation of the Gamow factor can occur under certain conditions. If one of the final-state nuclei has an excited halo nuclear state, it can lead to a GFC. Another mechanism for obtaining the GFC is due to the continuum-electron shielding and can be achieved by creating high density cluster of mobile electrons and nuclei such as the NEV in which the relative velocity between electron and nucleus in the NEV is much smaller than the velocity between the incident NEV and the target nucleus.

Once the GFC is achieved in the entrance channel, the exit channel can be fusion reaction (via the direction reaction mechanism), or emission of γ-rays, neutrons, or nuclear spontaneous fission from decay of the compound nucleus (the compound nucleus mechanism). These nuclear physics mechanisms may offer a consistent explanation for many of the anomalous effects including the nuclear transmutation observed in low-energy nuclear reaction experiments.

Both the laser induced fusion and the cluster-impact nuclear reaction with the NEV (CINR/NEV) involve coupling first the input energy into the electronic system and then into the target nuclei. However, CINR/NEV may be more efficient. Furthermore, CINR/NEV may offer other advantages such as possible aneutronic reactions. Therefore, it is important to find out whether CINR/NEV can be made more practical than the laser induced fusion.

ACKNOWLEDGEMENT

One of the authors (Y.E.K.) wishes to thank John Bockris, Hal Fox, George Miley, and Ken Shoulders for their helpful discussions on some of the topics described in this paper.

REFERENCES

1. M. Fleischmann, S. Pons and M. Hawkins, *Electroanal. Chem,* vol 261,pp 301 (1989); for some corrections, see *J. Electroanal. Chem.*, vol 263, pp 187 (1989).
2. S.E. Jones, E.P. Palmer, J.B. Czirr, D.L. Becket, G.L. Jensin, J.M. Thorne, S.F. Taylor and J. Rafelski, *Nature*, vol 338, pp 737, (1989).
3. See references in *Transaction of Fusion Technology*, vol 26, (1994), Proceedings of the 4th Intnatl. Conf. on Cold Fusion (ICCF-4), December 6-9, 1993, Lahaina, Mauii, Hawaii, Proceedings of the 5th Intnatl. Conf. on Cold Fusion (ICCF-5), April 9-13, 1995, Monte Carlo, Monaco.
4. E. Storms, *Fusion Technology*, vol 20, pp 433, (1991); ICCF-5, pp- 1-16.
5. T.N. Claytor, D.D. Jackson, and D.G. Tuggle, *J. New Energy,* vol. 1, no l, (1996).
6. J.O'M. Bockris and Z. Minevski, "Two Zones of Impurities Observed After Prolonged Electrolysis of Deuterium on Palladium," *Infinite Energy,* vol 1, no 5 & 6, pp 67-69 (1996), 2 tables, 3 figs, 8 refs.
7. T. Mizuno, T. Ohmori and M. Enyo, "Anomalous Isotopic Distribution in Palladium Cathode after Electrolysis," *J. New Energy,* Summer (1996), vol 1, no 2, 5 figs, 17 refs.
8. R. Notoya, "Low Temperature Nuclear Change of Alkali Metallic Ions Caused by Electrolysis," *J. New Energy,* vol 1, no 1, pp 39-45 (1996).
9. R. Bush, "Electrolytically Stimulated Cold Nuclear Synthesis of Strontium from Rubidium," *J. New Energy*, vol 1, no 1, pp 28-38 (1996).
10. S. Miguet and J. Dash et al., "Microanalysis of Palladium after Electrolysis in Heavy Water," *J. New Energy,* vol 1, no 1, pp 23-27 (1996).
11. G. Miley et al., "Nuclear Transmutations in Thin-Film Nickel Coatings Undergoing Electrolysis," *J. New Energy,* vol 1, no 3, (1996).
12. R. Bass et al., "Electro-Nuclear Transmutation : Low-Energy Nuclear Reactions in an Electrolytic Cell," *J. New Energy,* vol 1, no 3, (1996).
13. R. George and R. Stringham, EPRI Technical Report (1996).
14. V.A. Chechin, V.A. Tsarev, M. Rabinowitz and Y.E. Kim, *International J. Theor. Phys.* vol 33, pp 627, (1994).
15. M. Fleischmann, S. Pons, and G. Preparata, *Nuovo Cimento* A107, pp 143 (1994).
16. Y.E. Kim and A.L. Zubarev, *Nuovo Cimento*, vol 108A, pp 1009 (1995).
17. Y.E. Kim and A.L. Zubarev, *Few-Body Systems Suppl.* vol 8, pp 332 (1995).
18. Y.E. Kim, Y.J. Kim, A.L. Zubarev, and J.H. Yoon, "Optical Theorem Formulation of Low-Energy Nuclear Reactions," Purdue Nuclear Theory Group (PNTG) report PNTG-96-8 (August 1996).
19. Y.E. Kim and A.L. Zubarev, *Genshikaku*, vol 40, no 5 (1995) pp. 27-36.
20. Y.E. Kim and A.L. Zubarev, "Excited Halo Nuclear State and Long Range Interaction in Nuclear Reactions," to be published in *Physical Review*, vol C53, (1996).
21. K.R. Shoulders, EV-A Tale of Discovery, Austin, TX (1987). A historical sketch of early EV work having 246 pages, 153 photos and drawings, 13 references. Available from the author.
22. K. Shoulders and S. Shoulders, "Observations on the Role of Charge Clusters in Nuclear Cluster Reactions," *J. New Energy,* vol 1, no 3 (1996).
23. E. Feenberg, *Phys. Rev.* vol 40, pp 40 (1932).
24. R. Newton, Scattering Theory of Waves and Particles, McGraw-Hill (New York, 1966).
25. Y.E. Kim and A.L. Zubarev, "Three-Body Effects and Uncertainties for the p(pe$^-$, ν_e)d Reaction in Nuclear Astrophysics," Purdue Nuclear Theory Group (PNTG) Report PNTG-96-5 (May 1996).
26. R. Ziolkowski and M.K. Tippett, *Phys. Rev.* vol A43, pp 3066 (1991).
27. P. Beckmann, *Galilean Electrodynamics*, vol 1, p 55 (1990).
28. G.A. Mesyats, "Ecton Processes at the Cathode in a Vacuum Discharge," Proc. XVII Int. Symp. Discharges & Elect. Insulation in Vacuum, (21-26 July 1996) Berkeley, CA, pp 721-731.
29. M. Rabinowitz and D. Worledge, *Fusion Technology*, vol 17, pp 344 (1990).
30. A.A. Plyutto, Soviet Physics JETP, vol 12, p 1106 (1961).
31. A.A. Plyutto, V.N. Ryzhkkov, and A.T. Kapin, Soviet Physics JETP, vol 20, p 328 (1965).
32. P.E. Belensov, A.T. Kapin, A.A. Plyutto, and V.P. Ryzhkov, Soviet Physics - Technical Physics, vol 9, p 1633 (1965).
33. A.A. Plyutto, P.E. Belensov, E.D. Korop, G.P. Mkheidze, V.N. Ryzhkov, K.V. Suladze, and S.M. Temchin, Soviet Physics JETP Letters, vol 6, p 61 (1967).
34. R.J. Beuhler, G. Friedlander, and L. Friedman, *Phys. Rev. Lett.* vol 63, pp 1292 (1989).

35. R.J. Beuhler, Y.Y. Chu, G. Friedlander, L. Friedman, and W. Kunnmann, *J. Phys. Chem.* vol 94, pp 7665 (1990).
36. Y.K. Bae, D.C. Lorents, and S.E. Young, *Phys. Rev.* vol A44, pp 4091 (1991).
37. R.J. Beuhler, Y.Y. Chu, G. Friedlander, L. Friedman, A.G. Alessi, V. LoDestro, and J.P. Thomas, *Phys. Rev. Lett.* vol 67, pp 473 (1991).
38. J. Fallavier, R. Krisch, J.C. Poizat, J. Remillieux, and J.P. Thomas, *Phys. Rev. Lett.*, vol 65, pp 621 (1990).
39. Y.E. Kim, *Fusion Technology*, vol 17, pp 507 (1990).
40. M. Rabinowitz, *Mod. Phys. Lett.* vol B4, pp 665 (1990).
41. M. Rabinowitz, Y.E. Kim, R. A. Rice, and G.S. Chulick, AIP Conference Proceedings, vol 228, pp 846 (1991).
42. Y.E. Kim, M. Rabinowitz, G.S. Chulick, and R.A. Rice, *Mod. Phys. Lett.*, vol B5, pp 427 (1991).
43. Y.E. Kim, R.A. Rice, G.S. Chulick, and M. Rabinowitz, *Mod. Phys. Lett.*, vol A6, pp 2259 (1991).
44. Y.E. Kim, G.S. Chulick, R.A. Rice, M. Rabinowitz, and Y.K. Bae, *Chem. Phys. Lett.*, vol 184, pp 465 (1991).
45. Y.E. Kim, M. Rabinowitz, Y.K. Bae, G.S. Chulick, and R.A. Rice, *Mod. Phys. Lett.*, vol B5, pp 941 (1991).
46. Y.E. Kim, M. Rabinowitz, Y.K. Bae, G.S. Chulick, and R.A. Rice, "Hot Plasma Shock-Wave Theory of Cluster-Impact Fusion," AIP Conference Proceedings, vol 250, pp 321 (1992).
47. Y.E. Kim, M. Rabinowitz, Y.K. Bae, G.S. Chulick, and R.A. Rice, "Cluster Impact Hot Fusion," in Proc. of ICENNES '91, to be published in *Fusion Technology*.
48. Y.E. Kim, J.-H. Yoon, R.A. Rice, and M. Rabinowitz, *Phys. Rev. Lett.*, vol 68, pp 373 (1992).
49. Y.E. Kim, M. Rabinowitz, J.-H. Yoon, and R.A. Rice, "Hot Plasma Model for Cluster Impact Fusion," Laser Interaction and Related Plasma Phenomena (International Conference Series), vol 10, edited by H. Hora and G.H. Miley, *Plenum*, New York (1993), pp. 649-662.
50. C. Carraro, B.Q. Chen, S. Schramm, and S.E. Koonin, *Phys. Rev. Lett.*, vol A42, pp 1379 (1990).
51. P.M. Echenique, J.R. Manson, and R.H. Ritchie, *Phys. Rev. Lett.*, vol 64, pp 1413 (1990).
52. G. Lehner and F. Poh., *Z. Physik*, vol 207, pp 83 (1967).
53. G. Lehner, *Z. Physik*, vol 232, pp 174 (1970).
54. H. Brysk, *Plasma Phys.*, vol 15, pp 611 (1973).
55. A. Hasegawa et al., *Phys. Rev. Lett.*, vol 56, pp 139 (1986).

NATURAL NUCLEAR SYNTHESIS OF SUPERHEAVY ELEMENTS (SHE)

Albert Cau[1]

ABSTRACT

As soon as nuclear scientists became convinced of the possible existence of superheavy elements (SHE) with atomic numbers around 114 and 126, numerous attempts have been made to detect them in natural samples and to synthesize them in heavy ion accelerators. No positive results have been obtained until now since no element higher than 101 have been isolated for chemical study.

A new direction to the research of SHE has been taken. The source of the present work is old alchemy, as described in old treatises written prior 1850. It appears that the key material used by alchemists was pitchblende. The hypothesis that SHE could be peculiar elements only as stable as fluorides is discussed.

The mechanism conducing to the production of SHE in a chemical medium is studied: the main point is that SHE are necessarily produced via *soft fusion*, a synergism of exoenergetic nuclear reactions (proton absorption) and endoenergetical nuclear reactions (light element fusion): a mechanism that allows the creation of macroscopic amount of SHE fluoride in mild [low energy] conditions.

The nuclear reactivity of natural mixtures containing uranium and light elements is described. A 1986 experiment showed an unexpected nuclear activity characterized by very intense neutron bursts. The 1996 experiment shows increases of gamma activity upon heating and the production of a peak around 50 KeV.

PART I - SOURCE OF THE RESEARCH

INTRODUCTION

The understanding of the properties of atoms has been the major goal of science during the XXth century. The problem to-day is to know what is the limit of the series of chemical elements. Using a different approach based on the properties of atom in nature and historical considerations it may be possible to conceive that superheavy elements should really constitute that upper limit of the series of chemical elements. It is the purpose of this research to show that under precise conditions these SHE are created and observable by their action on the chemical medium.

Considering the failure of attempts to detect SHE in nature and to synthesize them in heavy ion accelerators, it has been thought that SHE, because they should constitute the upper limit of the periodic chart of chemical elements, could be a peculiarity of nature regarding their nuclear and chemical properties. The question about the existence of SHE, curiously has a precise answer if we consider the historical fact of a science named alchemy. Going back a thousand years ago, when radioactivity was not yet discovered by science, we find treatises that describes to us the making of two related compounds : A *White Stone* and a *Red Stone*, both having remarkable properties, among them the quantitative nuclear transmutation of mercury (Z=80) into gold (Z=79) using the *Red*

[1] A.R.T. , 18 Boulevard Arago, 75013, Paris (France)

Stone, and the nuclear transmutation of mercury (Z=80) into platinum (Z=78) using the *White Stone* [1]. Moreover it is said in old treatises that the compounds cannot be analyzed via conventional methods because they disappear [2].

Science tells us that the stability of nucleus depends on the number of protons and neutrons. The magic numbers introduced by nuclear physicists in the model of the shell nucleus theory give us the possibility to have two stable superheavy elements [3], probably: Z = 114, N = 184 and Z = 126, N = 184 .

Assuming true the rationality of the alchemy process as described in old treatises, we deduce, *à priori*, that the White Stone and the Red Stone are necessarily chemical compounds of Z = 114 and Z = 126 having the following properties:
1) both SHE are stable as fluorides, and 2) both SHE are disintegrated into powerful neutron/proton beam when the protective shell of associated fluorides is broken.

Therefore we are conduced to suspect that the upper limit of chemical elements, supposed to be these SHE, should be necessarily characterized by peculiar nuclear and chemical properties. The classical concept of atom coming from Greek philosophers, still recognized to-day, presents a failure for the limits of atom series. We know that hydrogen, the lower limit of the atomic series, is the unique element in nature that may coexist in a chemical medium as free nucleus (dissolved, of course) as a result of this property. So the upper limit should present similar features: SHE nuclei should exist only as fluoride compounds. This approach of SHE existence based on philosophical considerations has the advantage to go farther than any existing theory of nucleus since the problem is not to know how the SHE nucleus is built, but how it could exist on Earth and how to create them.

The identity of materials used by alchemists

It seems that the most difficult problem to resolve is to find the precise identity of materials used by alchemists. If we study recent alchemy treatises, as well as many older works, we note that most of searchers were using any kind of materials with the secret hope they had chosen the right materials. Today, the fashion is to unsuccessfully process stibnite because cinnabar has been declared dangerous for health for its mercury content.

A few quotes taken from old alchemy treatises will show you that pitchblende (UO_2) is the right material used by alchemists. The other material is fluorite from which it is possible to create the stabilizing medium to grow the superheavy element fluorides.

Identity of prime materials from alchemy treatises

Of course I will consider only alchemy treatises written before the discovery of radioactivity by Becquerel (1896). This study will also show that metaphorical descriptions are widely used to describe concrete facts. The purpose of selected quotes is to show you that we may find in alchemy treatises the implicit description of a nuclear process based on uranium mineral treatment.

Now I will speak but a very little of the Living Fire, which is hidden in the Earth or Center of the World and there has taken up its most fixed Habitation; and by many Philosophers is called the Corporal Water; but it may better be called the Fire of Bodies. To know this is the most secret Mystery in all our Philosophy. This fixt Fire has a great sympathy with the volatil Fire; for it wanteeth it as an aliment, and to its Nourishment.... But its Operation is invisible and very secret, and yet very powerful, which also few know; for it operates by its heat in all things which lie in the Earth. - Sanguis Naturæ [4]. p. 12 - 13

It is a very interesting quote because it mentions the special action of a principle included in the prime material and that it is responsible of the feasibility of the alchemy process. Because *its Operation is invisible and very*

secret, and yet very powerful, we may deduce that it is a very strong reference to nuclear properties of the material.

For the Power and Virtue of this living Fire is so great, that if that were absent, the Elements would be dead, especially the Heaven, an Element which most of all stands in need of this Light. - Sanguis Naturæ. p. 10

This quote does not describe the prime material, but insist on the fact that the alchemy process is the conjunction of different things. For example, if you have gas, will not get any energy with gas alone, you must add air that contains oxygen, but that mix of gas still does not react, you have to initiate the reaction with a spark. It is the same for alchemy process, the prime material alone serve for nothing if you have not its companions. For this reason some alchemy treatises say that the Subject is waiting for the wise alchemist who will know how to awake him.

For where there is glittering Brightness, there is light; where is Light, there is Heat; where is Heat there is Life and very powerful action; and which is a great matter, in it reign the Elements animated with a living Fire, which is a Celestial vivifying, fertile and greening Spirit; the Light, Force and life of all things. - Sanguis Naturæ, p 18

Underlined text gives you the key to understand any alchemy treatise. The life of minerals has a strong relation with mineral luminescence. The greening Spirit may be associated with the strong green fluorescence of uranyl salts.

This living Fire, with which the Heavens and all things are filled by the Creator, descends through the Elements into the Subject, which is called the Balsom of Nature, Electrum immaturum, Magnesia, The Green Dragon, Azoth Vitreus, The Fire of Nature. - Sanguis Naturæ. p. 41

The *Subject* is the prime material : it contains a *living Fire* , it is called *The Green Dragon , The Fire of Nature* . Uranium agrees with this description : U(IV) salts are green and most of them are luminescent.

The certainty of this Solar Subject may be evidently known, if out of it three Principles of Nature can be separated. What they are I will explain. Sulphur residing in our Matter, is its fiery, most subtile, and most thin part, partaking of a subtile Earth, which indeed is the perfect and absolute Tincture, having power of rubifying and illuminating every Body. Which Sulphur is called the Philosopher's secret Fire, and the luminous part. - Sanguis Naturæ. p. 22

The reference to a *Solar Subject* is quite interesting. We may establish a relation with gold whose symbol is the Sun, that precises the frequent location of the alchemist *Gold*. From this *Subject* we obtain *Sulphur* which is the *Philosopher 's secret Fire*: the uranyl salts are effectively luminescent and nuclear reactions inside the mixture of alchemist produce transmutation of elements and heat. This action on the identity of associated chemical elements is the true dissolving power of what alchemists name *Mercury*.

And that Sulphur which we call the Green Lyon, is the Fire of Nature, which lieths hid in the Center of our Subject... - Sanguis Naturæ. p. 26

Sulphur of alchemists presents some strong relations with natural sulfur (Z=14). We have a relation of color: both are yellow, and a relation of Light. As a matter of fact, normal sulfur may burn in oxygen with a bluish flame to produce sulfur dioxide. Uranyl salts, especially sulfate and nitrate, present a strong green luminescence when excited by UV light. According to old books of physics, and even alchemy theory (preceding quote) light is equivalent to fire because they depend on the same natural principle. Consequently the *Sulphur* of alchemists extracted from the prime material is an uranyl salt. The term *Green Lyon* also refers to *Sulphur*, not only because

of the green luminescence of uranyl salts, but also because of the green color of U(IV); uranium dioxide heated with ammonium bifluoride produces the green uranium tetrafluoride.

Our Gold is not vulgar Gold, which is sold by Gold-smiths, or any thing like it, but it is a certain other Substance more precious than Gold itself, whose Green and Golden colour does sufficiently demonstrate its Original and Excellence. - Sanguis Naturæ. p. 33

When alchemists speak of *their Gold*, of course they want to indicate us how precious is the prime material found in mines, but they are more precise since they also tell us implicitly that this mineral is associated with gold. A typical alchemy saying is *The seed of gold is in gold* which means that where you have gold metal, you will also, not very far away, get alchemist gold. In South Africa, gold mines are in fact uranium ores (pitchblende) associated with gold included in quartz, it is also surprising to note that this gold contains some traces or mercury. In my concern, in 1978 while working in Mexico, I isolated tiny wires of gold associated with metatorbernite (uranium, copper, phosphate).

The gold of alchemists is a black mineral: pitchblende. The mineral is often associated with secondary minerals of a yellow color: autunite, carnotite..., but also some green products, the most frequent being meta-torbernite: a microscopic mineral found as very nice tablets of an emerald color.

In this vile and abject Minera, lies hidden the celebrated Stone of the Philosopher's, whose Essence also by reason of its obscurity nobody can see, unless it be delivered therefrom, and brought to light... The Essence of this minera, whereof the chief colour is green, as a most certain indication of life. - Sanguis Naturæ, p 44

This is a general description of the prime material: a vile and abject *Minera* because it was discarded by miners. Evidently the *Essence* of this *Minera* is its luminescence that is clearly emphasized by reason of its obscurity and brought to light. An other indication is that the chief colour is green as a reference to the color obtained by attack in non-oxidizing conditions, and by the fact that some oxidation products are green colored.

Years ago Pitchblende (UO_2), was a common mineral in some silver mines of which most famous is the Joachimsthal line in Bohemia (on Czechoslovakia border with Hungary). According to Diderot [2] it was a very unwelcome black mineral because of its high density similar to the density of the black silver sulfide.

Let see now some quotes selected from the Hermetic Museum [5].

For this reason the Sages use none but this natural fire, not because it is made by the Sages, but because it is made by Nature. - The Hermetic Museum, p 145

Again we have the relation of Light, the natural fire is not prepared by the alchemist, that means the inner property of the material is *Fire*. Pitchblende is not luminescent, but its derivatives such as nitrate and sulfate are. So the alchemist liberates *the natural fire*: an idea often used.

The distilled water is the Moon; the Sun, or Fire, is hidden in it, and it is the father of all things. It is also called living water, for the life of the dead body is hidden in the water. - The Hermetic Museum. p. 225

We have a confirmation of what has been said before: the *Moon* by its cold nature has to be related with *Mercury*, but this *Mercury* contains the *Sun,* that is to say *Sulphur*, therefore *the living water* is a solution of uranyl salt in hydrofluoric acid derivatives. To know why the Moon is associated with cold is evident: the moon is the Earth satellite we may observe during the night, and it is clear that during the night weather is colder than during the day.

Our gold is twofold; one kind is mature and fixed, the yellow Latten, and its heart or centre is pure fire, whereby it is kept from destruction, and only purged in the fire. This gold is our male, and it is sexually joined to a more crude white gold, the female seed: the two together being indissolubly united, constitute our fruitful Hermaphrodite. - The Hermetic Museum, p 165

We came to a crucial point in the identification of prime materials. Do we need one, two or more materials? The frequent sexual reference indicates with no ambiguity that two materials are necessary. They are of course of same nature, that is to say they own the relation of Light, but they are complementary. The *Gold* is the prime material: the *Yellow Latten* is the clear reference to processed pitchblende; the *White Gold* is the reference to fluorite derivatives that constitute the matrix of all the process.

Know, ye Scrutators of Nature, that fire is the soul of everything, and that God Himself is fire and soul. And the body cannot live without fire. For without fire, the other elements have no efficacy. - The Hermetic Museum p 213

An other reference to that *Fire*, the Key of all the alchemy process. It is a very high point of Philosophy with evidently a reference to the prime material that is considered as *a gift of God*, and justly the heart of this material contains its soul that is to say the *Fire*. The work of the artist is to deliver the soul and to join it with the other element. In clear, it is required to process pitchblende to get raw uranyl salt (the luminescent salt), it contains life; the union with fluorite derivative really initiates the process, but the exact composition of the complementary part of uranyl salt has never been given, only implicitly.

In Gold and Silver our menstrues are not visible to the eye, and are only perceived by their effect. - The Hermetic Museum, p 39

Gold and *Silver* are equivalent to *Sulphur* and *Mercury* of alchemists. That is to say uranyl salt and fluorite derivatives. A menstrue is an acidic solvent (Diderot [5], see mentrue), it is a question in the quote of a dissolving action that may be observed when running in the process. *Sulphur* has the power to destroy identity of *Mercury*: nuclear reactions occur and produce the slow formation of the germ of the seed. This outstanding dissolving power of *Sulphur* is often described, but it must be noted that when both are joined, they produce *Sulphur* or *Mercury* depending authors [sic].

The inward heat is much more powerful than elementary fire, but it is tempered and cooled by the water which pervades and refresh the pores of the earth, otherwise all things would be consumed by its fierceness. - The Hermetic Museum, p 103

Inward heat has the precise meaning we know, and *elementary fire* has to be related with luminescence. This quote gives the description of a kind of small size "nuclear reactor."

It is in fact talking about the process; after the washing of the prime material, you get a product with a very strong gamma activity. It contains most of all radioactive decay products of uranium. In this new *Mercury*, we begin to have nuclear reactions of formation of the germ of the *Stone* (if all conditions are fulfilled), you will know below why the formation of SHE requires the participation of protons, but you may note here that it is not a solution, but a periodical refreshment of the mixture in order to avoid stopping the course of the process. That means the proportion of elements are a major feature of the alchemy process.

Nature cannot work till it has been supplied with a material, the first matter is furnished by God, the second matter by the Sage. But in the philosophical work Nature must excite the fire which God has enclosed in the centre of each thing. The excitation of this fire is performed by the will of Nature, for fire naturally purifies every species of impurity. - The Hermetic Museum, p 140

We have the exact implicit description of required materials. *The first matter is furnished by God* means various things. First: this matter has a soul, and as explained before it contains inside a powerful fire, therefore the material owns a hidden light. Second: the reference to *God* is not allegoric, it is clear that thousand years ago nobody could know the nuclear properties of matter, especially uranium. Consequently the knowledge of the property of pitchblende could be only possible with the help of a real adept. But the mystery remains regarding who transferred that knowledge to mankind.

The second matter is furnished by the Sage, that is to say it is a common chemical work that a skillful chemist may discover: it is the processing of fluorite to obtain derivatives such as potassium fluoride, ammonium fluoride, ammonium bifluoride, ammonium fluoborate, hydrofluoric acid (contaminated with silicihydrofluoric acid)... The *work of Nature* is a reference to precise conditions required in the alchemy process named as *the will of nature*. For example, it is possible to change the yellow color of uranyl salt to a very nice blue color, like lapis-lazuli.

For if the hidden central fire, which during life was in state of passivity, obtains the mastery, it attracks to itself all the pure elements, which are then separated from the impure and form the nucleus of a far purer form of life. It is thus that our Sages are able to produce immortal things, particularly by decomposition of minerals: and you see that the whole process from beginning to end is the work of fire. - The Hermetic Museum, p 142

We know that the prime material *gift of God* must be put in a state of reactivity. The first operation is the separation of the active part and the reaction with the complementary part to obtain the germ of the Stone.

More interesting is that affirmation about *the work of fire*: the synergism of nuclear reactions involving protons and light elements to produce these SHE. Of course it is question of the inward fire that may be helped in some parts of the process to get more favorable conditions.

The outward fire does not enter into the composition as an essential part of it, but only by the effect which it helps to produce. The inward fire is sufficient, if only it has received nutriment from the outward fire, which feeds it as wood feeds elementary fire: in proportion to the quantity of nutriment the inward fire grows and multiplies. - The Hermetic Museum, p 144

As observed experimentally, the total gamma activity of the mixture increases. The inward fire corresponds to the nuclear property of uranium. But the outward fire is different since it corresponds to normal heating of the mixture, and as observed the nuclear activity of the mixture increases by heating.

Sulphur is by no means the least important of the great principles since it is a part of the metals, and even a principal part of the Philosopher's Stone. It illumines all bodies since it is the light of the light, and their tincture. - The Hermetic Museum, p 130

When alchemists say that their *Stone is pure Fire*, and they name it *our Sulphur* they are giving us to understand that there exists a relation of light. One of the properties of the *Philosopher's Stone* is to be luminescent under a certain grade of purity. The same observation has been made by Marie Curie with pure radium salts.

It should be noted that common gold is useless for this purpose, being unsuitable and dead. You must therefore, seek to obtain gold which is a pure living spirit, and of which the sulphur is not yet weakened and sophisticated, but is pure and clear: otherwise the first substance, being spiritual and ethereal will not combine with it. - The Hermetic Museum, p 81

Many people have processed gold (Z=79) to produce the *Philosopher's Stone*. Here, like in many alchemy treatises, it is said that common gold is unsuitable for the work. The Gold of alchemists, their *Gold*, has an other nature, it permits to prepare the *Stone*, it is pitchblende. In this gold we have a living spirit, the luminescence of prepared salts; moreover, the quality of pitchblende is important: *and of which the sulphur is not yet weakened*, that means purified uranyl salt may not be used.

Alchemist: Yet the Sages says that their substance is found on the dung hill.
Mercury: What they say is true, but you understand only the letter, and not the spirit of their injunctions. - The Hermetic Museum, p 81

We get to important points of the identification of pitchblende. Imagine you are four hundreds years ago, you need pitchblende, so you will have to get it from mines where you could find this mineral. There were not so many mines worked for metals, but the most valuable metals were gold and silver. Being clever, and considering that *the seed of gold is in gold*, you choose to investigate the European gold and silver mines, especially in Hungary and Bohemia. It is on the hill of discarded minerals of Joachimsthal (opened since 1510) that you will find pitchblende.

Man have it before their eyes, handle it with their hands, yet know it not, though they constantly tread it under their feet. - The Hermetic Museum, p 78

The author describes miners who select the mineral extracted from the mine according technics used centuries ago. Effectively they recognize the mineral because of its density, but quickly discard it because they do not know its real value.

Sulphur is by no means the least important of the great principles, since it is a part of the metal, and even a principal part of the Philosopher's Stone... The student who knows nothing about it, is in the dark in regard to this matter, as is a blind man in respect to colour. - The Hermetic Museum, p 130

Pitchblende is a black mineral from which is extracted the *Sulphur* of alchemists. So *is in the dark in regard to this matter* is a direct reference to the color of the mineral, that is also expressed by *as is a blind man in respect to colour*. The sum of both sentences gives us *dark blind* that is equivalent to *dark blend* or **pitchblende**. The important point to know is that German was the usual language of Basile Valentin and others alchemists.

Voice: It is true that Sulphur is the true and chief substance of the Stone. Yet you curse it injustly. For it lies heavily chained in a dark prison and cannot do as it would. - The Hermetic Museum, p 150

This quote confirms the identification of pitchblende. The dark prison is the black mineral, its treatment with nitric or sulfuric acid produces the corresponding uranyl salt; both are luminescent and of a yellow color similar to sulfur (Z=16).

Do not think that Salt is unimportant because it is omitted by the Ancients; they could not do without it, even if they did not name it, seeing that is the Key which opens the infernale prison house, where sulphur lies in bonds. - The Hermetic Museum, p 143

This quote also confirms the identification of pitchblende. The author emphasizes that the treatment of the mineral to extract Sulphur requires a *Salt*. The association *Salt* and *Key* gives *Vitriol* since the old symbol of vitriol was a key.

Sictus dit: Sachez tous investigateurs de l'art, que le fondement de cet art pour lequel tout le monde pense, n'est autre chose, que les sages estiment la plus haute qu'aucune nature qui soit, mais les fols la croyent la plus vile de toutes les choses.

Alchimus dit: Prenez Arzent, ce sont vers noirs & venin de vieilles tuiles rouges marines, & ont horrible regard, & les cuisez à feu ni trop chaud ni trop froid; car s'il est froid ils ne s'altèrent point..... - Turba Philosophorum, p 14 - 33

Le minéral connu sous le nom de Pechblende se présente comme on sait, en masses amorphes, à cassures conchoïdales d'un noir éclatant ... le minéral examiné provenait des mines de Joachimsthal en Bohême; la pechblende s'y trouve au milieu d'un calcaire lamelleux de couleur rougeâtre. - Ebelsem, Annales de Chimie & Physique, no 8, 498, (1843)

Both French quotes, which are separated by 250 years, may be easily correlated. The alchemist tells us that we have to take as prime material *Arzent* (silver): we may deduce by the kind of mine of interest, that is to say Joachimsthal where pitchblende is found with silver. Our mineral will be like *black worms, & venom of old red marine tiles*, that is to say amorphous mass of strong black luster, inside a lamellar reddish calcareous matrix.

This correlation and the above explanations of quotes are sufficient to be sure that the true prime material of alchemists was pitchblende, the uranium oxide. It is quite possible to research more old alchemy treatises to find similar correlations. The important point is that when an alchemist described the mineral, he did not care a lot about what occurred elsewhere; he described the mine and the mineral he got. It is the reason why some descriptions present some contradictions.

Identity of prime material from science

It may be possible to use our knowledge of atom to identify the prime mineral used by alchemists. We suppose mercury (Z=80) has been chosen as prime material. It results that the *alchemy treatment* of this material has to produce a change of the isotopic proportions in order to produce a new mercury enriched with neutrons, for example. But experiments show that when an atom Z gets more neutrons it transmutes itself to the element Z+1 more stable. This fact being established it is clear that a hypothetical very high neutron enrichment will have to produce one-by-one the elements (Z+1), (Z+2), (Z+3),... to finally reach uranium and transuranium elements. But the problem is that there does not exist any natural neutron source that can produce this sequence of nuclear reactions. Since we will reach uranium and transuranium elements, we have to choose uranium as prime material first because the best mineral found in nature is pitchblende, and second because uranium contains the energy source required by the process.

The interest of that hypothetical explanation of the behavior of elements submitted to *alchemy process* is that we may understand why we have to use a uranium compound to do the alchemy work, and why the *Philosopher's Stone* is necessarily a compound of SHE.

The others materials required by the alchemy process

It is not enough to know that pitchblende is the prime material, as a matter of fact it is an evidence, but it was very important to identify this material in alchemy treatises in order to prove that alchemy treatises describes a natural nuclear process conducing to two compounds which are necessarily, because of their properties, chemical compounds of SHE. The difficult problem to resolve is to precisely understand the nature of the associated compound that permits the initiation of this nuclear process. Alchemy treatises do not describe this material clearly, so a first approach to the nature of this compound relies on the properties of the Philosopher's Stone. We have seen that the Stone are disintegrated by chemical reaction into powerful radial neutron beam. We also

deduced there must exist a protective surrounding of the active superheavy elements, and that protective shell must be composed of fluorine ions because these ions have a very high electron affinity, and consequently are able to stabilize SHE nuclei. Scientific data regarding the stabilizing effect of fluorine upon radioactive nuclei have been given by *Neve de Mevergnies* [7].

The second material required for the alchemy process is fluorite (CaF_2), of which we may find in alchemy treatises some relevant indications. Vitriol for example corresponds to *Vitri Ol* (Oil , Oleum), *Oil of glass*, thus hydrofluoric acid. More details are given in reference. A quote from Sanguis Naturæ [4] shows how to extract the second component required by the process:

Among the Secrets of Alchemy, the greatest is to draw Water out of a Rock; verily a hard and very difficult Work, unless Chemistry alone had showed us the possibility of this thing; which the Artist ought to endeavour to do by Fire, which in the beginning must be gentle, in the middle strong, and in the end most vehement; so that all the Aeral and Ethereal Spirits of this Rocky Minera, may issue forth into a fit Philosophical Vessel, and there resolve themselves into Water; which Water with wonderful Sympathy loves the Rock, from whence it issued; which Water is called by various Names, as Rock-Water, Argent Vive, a Fume, the Tinging Cœlestial Spirit, Incombustible Sulphur, Wine Vinegar, Succus Acacia, Spirit of Wine, Temperate Water, the Luciferous Virgin; all which Names signifie this Water; which if it be again conjoyned with it, remains Stone, and often operates resting upon it, it acquires a wonderful active power, as all know who are acquainted with this Water. - Sanguis Naturæ [4], page 42

We easily relate the first part of the quote with the extraction of a volatile acid with concentrated sulfuric acid: hydrochloric acid, nitric acid, as described in old chemistry treatises; the relevant point being the variation of regulation of fire. The other relevant point is the action of hydrofluoric acid upon calcium sulfate.

Physics of the creation of SHE in natural conditions

Since we know that pitchblende is the material required by the alchemy process, it is necessary to find how it is possible to obtain this *Philosopher's Stone* identified as a fluoride of SHE. Our logical way of analyzing the problem of alchemy induced us to suspect that the only rational explanation of alchemy relies on the natural nuclear synthesis of two SHE fluoride (*à priori*, Z = 114 and Z = 126), therefore it is quite necessary to have a more precise idea of the mechanism of formation of these SHE. We also have to note that nuclear physics science failed to propose a rational explanation of alchemy (if they did succeed, it is classified information), that means the process should involve a new aspect of atomic behavior in nature.

The alchemy mixture contains several chemical elements: uranium and fluorine; light elements. Radioactive decay products of uranium are minor elements but they have a very important place in the process, at least at the beginning, because alpha emitters initiate fission reactions of uranium via neutrons produced by (α, n) reactions. So we may consider that the alchemy mixture is characterized by a nuclear reactivity of fission and, *à priori*, a nuclear reactivity of fusion conducing to SHE depending on experimental conditions. So the nuclear synthesis of SHE is necessarily a synergism of several kinds of nuclear reactions.

Another point that should be considered very carefully is the so-called *Multiplication* step described in old alchemy treatises. It is said that with an initial part of the final compound it may be possible to increase its power via a reiteration of all the steps of process. If the first reiteration takes 6 months, the second will take 1 month. This is the characteristic nuclear property of an element which is able to be disintegrated in precise chemical conditions in order to initiate new nuclear reactions able to generate it again giving a higher quantity of compound a lot more purer than initially. It also means that during the first process, the yield of favorable events conducing to SHE will be very low, so as expected quite dependent of physico-chemical parameters and composition of the mixture.

EXPERIMENTS

The model of formation of SHE may be easily verified, indications have been given. An alternative way is to use a neutron generator to initiate nuclear reactions on an appropriate mixture of pure uranyl salt free of radioactive decay products. But it must be remembered that the process works like any common geochemical process.

Few indications about the first step of the process are given in old alchemy treatises. So considering the relation alchemy *Sulphur* - uranyl salt, and alchemy *Mercury* - HF , NH_4F, NH_4BF_4 ..., these base materials have been initially used in order to make precise the chemical conditions of the process and to observe any unexpected nuclear activity. It must be clear that the success of experiments depends on the precise knowledge of what is named *Mercury* because, from a chemical point of view, it permits to observe the different colors during the two year process: black, blue, green, white, yellow..., (all colors have been observed using uranyl salt) and it must agree with physics of nuclear reactions conducing to SHE.

A first experiment [3] started in June 1986 has permitted [us] to observe a continuous increase of the gamma activity (see Fig. 1) and intense gamma and neutron bursts during days. This experiment used pure pitchblende and hydrofluoric acid, it demonstrated that old alchemy treatises could contain the description of a natural nuclear process conducing to new elements, necessarily SHE.

A very intense neutron burst has been detected (Fig. 2) via the Ag (n, γ) nuclear reaction, for a background of 2,500 cps, the burst reached 131,000 cps. Because uranium mineral was involved, such nuclear activity may be explained by the disintegration of SHE created *in situ*.

A second experiment started in June 1991 using commercial uranyl nitrate and tetrafluoboric acid, showed that purified uranyl salt are useless for the process. A 30% increase of gamma activity has been observed for an initial gamma counting of 1,000 cps.

A third experiment, starting in March 1996, has been made with pitchblende, not so pure as in the first experiment, and tetrafluoboric acid has given two main results:

♢ gamma activity increases by heating of the mixture from cold to room temperature or in a microwave oven (Fig. 3). Heating has been followed by a notable increase of a peak around 50 KeV (Fig. 4 , Fig. 5 , Fig. 6). Once an electronics failure had occured during the heating, the microwave oven stopped after two seconds and refused to start again, the mix was boiling. The spectrum showed the increase of the 50 KeV peak, and the microwave oven was working properly.

♢ a peak around 50 KeV has appeared. Separation of excess ammonium tetrafluoborate via sublimation has been followed by sublimation of a black compound still unidentified. The peak around 50 Kev was missing on the gamma spectrum (Fig. 7-a , Fig. 7-b , Fig. 7-c) of the remaining part A.

♢ A treatment of the part A with nitric acid 50% gave an insoluble red part , the 50 KeV peak was present. (Fig. 8)

♢ A chemical treatment of uranyl nitrate at room temperature has permitted to observe a color change from yellow to green and black (solid phase) then blue like lapis-lazuli. Gamma spectrum of the blue solution is given (Fig. 9). Color changes are, in part, the result of the presence of fluoboric acid in the mixture.

♢ Gamma spectrum of pitchblende used for the experiment is given (Fig.10).

CONCLUSION

The main feature of this research is that it involves several parts of science in order to get a precise idea of its goal in respect with the work of nature. The assumption that SHE existence is closely related with the problem of limits of matter in nature seems to have some resonance in the history of science. The possibility to produce macroscopic amount of SHE fluoride appears today very realistic. It is quite probable that these elements which have a transitory existence when produced in chemical conditions that do not permit them to be stabilized by fluoride, have been observed during years in laboratories by unexpected neutron bursts escaping from uranyl solutions. Today, the correlation of unexpected bursts of radiation from a mixture of uranium mineral has been possible because of the understanding of old alchemy treatises which describes precisely how to process uranyl salt and fluorite in order to produce new compounds with outstanding properties. The present experiment which permitted to make precise the chemical composition of the mixture from color changes and the effect of temperature upon the nuclear reactivity of the mixture, let's suppose that soon it will be possible to isolate these new chemical elements and to produce them at the laboratory scale.

Among the parameters that should permit to create SHE in chemical medium via a synergism of nuclear reactions: endoenergetic and exoenergetic, composition of the mixture and temperature appear to be the main factors of the process. It is also possible that a nuclear cristallogenenis could permit to reach faster the goal in the future.

The main point I would like to emphasize is that a precise study of phenomena occuring during the treatment of the mix of uranyl salt and fluorite derivatives requires one to be able to follow permanently the gamma activity of the mix, as well as IR emission and temperature. This has not been possible for the three experiments (in the first experiment, gamma activity has been measured with a scintillometer Geometrix which has been damaged by excess of radiations).

REFERENCES (part I)

1. Albert Cau, The Philosopher's Stone - A rational study of alchemy, (1995), Editions Col du Feu Fillient - 74550 Orcier (France). ISBN 2-9503346-7-9.
2. Cyliani, "Hermès dévoilé," (1832), Editions Traditionnelles (1982), Paris (France).
3. Gleen T. Seaborg, W. Loveland, "Superheavy Elements," Contemporary Physics, vol 82, no 1, 1987.
4. Sanguis Naturæ, (1696) available as microfilm at Univ. of Washington, Seattle, WA, USA.
5. Encyclopedia of Diderot, see: blende. Univ. of Washington, Seattle WA, USA (for example).
6. The Hermetic Museum, published at Frankfort in 1678.
7. Wayne C. Wosley, "Variation of Radioactive Decay Rates," *J. Chemical Education*, vol 55, no 5, May 1978, p 302-303.
8. A. Cau, "Alchemy: A set of nuclear reactions that could conduce to SHE," *ION* 11(1), p 181-195, June 1989, Univ. Ind. of Santander, Bucaramanga, Colombia.

PART II - A MODEL FOR THE NATURAL NUCLEAR SYNTHESIS OF SUPERHEAVY ELEMENTS.

The direct formation of element titanium Z = 114, for example, from uranium, in the ideal case of a hypothetical fusion in one step, requires the use of titanium Z = 22, and an anti-Coulomb energy of 211 MeV, a very high value which means that the uranium nucleus considered as projectile will not be close to the titanium nucleus for a direct fusion conducing to a superheavy element. So if one fusion step does not permit the formation of SHE, therefore we have to assume that the natural nuclear fusion process involves several steps of fusion!

Uranium is a key component of the mixture: It owns an energy source required to eventually produce nuclear fusion reactions. The fission of uranium, spontaneous or induced by fast neutrons created in the medium produces an energy of 167 MeV which is taken by both fragments of fission:

$E_f = E_1 + E_2$ Conservation of the energy

$m_1 \cdot v_1 + m_2 \cdot v_2 = 0$ Conservation of the momentum quantity

Each fragment of fission m_1, m_2, carries the kinetic energy:

We deduce: $E_1 = \frac{1}{2} m_1 v_1^2 \quad E_2 = \frac{1}{2} m_2 v_2^2$

so: $E_1 = \frac{m_2}{m} E_f$ and $E_2 = \frac{m_1}{m} E_f$ with $E_f \simeq 167$ MeV

with: $m = m_1 + m_2$ $m \simeq 235$ Taking into account emitted neutrons.

The mixture contains several chemical elements: uranium, fluorine, boron, nitrogen, oxygen, hydrogen. Radioactive decay products of uranium are minor elements but they have a very important place in the process because alpha emitters initiate fission reactions via neutrons produced by interaction of alpha radiations with light nuclei. We may consider that the **alchemy** mixture is characterized by a nuclear reactivity of fission and, *à priori*, a nuclear reactivity of fusion conducing to superheavy elements.

The nuclear fusion between two nucleus implies first that both nuclei come in contact then the fusion process may occur according an endothermic or exothermic reaction.

Principle of the fusion process

A fragment of fission of uranium collides with a chemical element of the mixture and transmits it a part of its energy. The activated element will be involved in a fusion process with other element of the mixture if all energy conditions are fulfilled. The road conducive to superheavy element nuclei requires that uranium is the projectile. The scheme is the following:

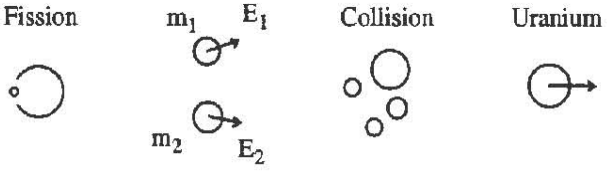

m_1 and m_2 : fragments of fission of uranium, with the energy

$$E_1 = \frac{m_2}{m_1 + m_2} E_{fission} \qquad E_2 = \frac{m_1}{m_1 + m_2} E_{fission}$$

The collision of m_1 or m_2 with an element of the mixture of mass m_o may be represented as follows:

The maximum energy received by the target m_o (case of a frontal collision) is:

$$E_{O_{Max}} = \frac{4 m_1 m_o}{m_1 + m_o} E_1$$

More probable light fragments of uranium fission: $85 \le m_o \le 95$

Energy received by a uranium nucleus: $80.17 \le E_{O_{Max}} \le 81.68$ MeV

Uranium has to receive enough energy to overcome the potential barrier of fusion; this value only depends on the nature of the target nucleus ,that is to say its electric charge Z:

Barrier Energy (MeV) : $V = 1.02857 \frac{Z_U Z_2}{A_U^{1/3} + A_2^{1/3}}$

Fluorine: $^{19}_{9}$F V = 96.06 MeV

Oxygen: $^{16}_{8}$O V = 86.84 MeV

Nitrogen: $^{14}_{7}$N V = 76.95 MeV

Carbon: $^{12}_{6}$C V = 66.90 MeV

Boron: $^{11}_{5}$B V = 56.18 MeV

Hydrogen: $^{1}_{1}$H V = 13.14 MeV

We see that oxygen and fluorine may not participate to a fusion with uranium (some fusion events could be possible). The reason is that uranium projectile has not enough energy to overcome the Coulomb repulsion. For other light elements, carbon, nitrogen, boron and hydrogen the first condition of fusion is fulfilled: the potential barrier between the projectile and the target is overcome.

But it is not so simple, let see the classical case:

$X + x \rightarrow y + Y$ x: target X: projectile

The energy balance is:

$Q = E_y + E_Y - E_X$ or : $Q = (M_X + M_x - M_y - M_Y)\, c^2$

To create a compound nucleus we need a certain amount of energy corresponding to the difference of mass of initial nucleus and final nucleus. It is interesting to note the analogy between chemical energy that involves electrons and nuclear energy that involves nucleons; this fact shows us the similitude of natural laws .

If $Q > 0$,the reaction of formation is endoenergetic that means the reaction will be possible if the projectile overcomes the potential barrier.

If $Q < 0$, the reaction is endoenergetic, that is to say it will occur if the projectile has a minimum energy.

This condition is a consequence of the postulate of positive energy; in the laboratory system, the energy balance is: $Q + E_M$, E_M being the projectile energy in the laboratory system:

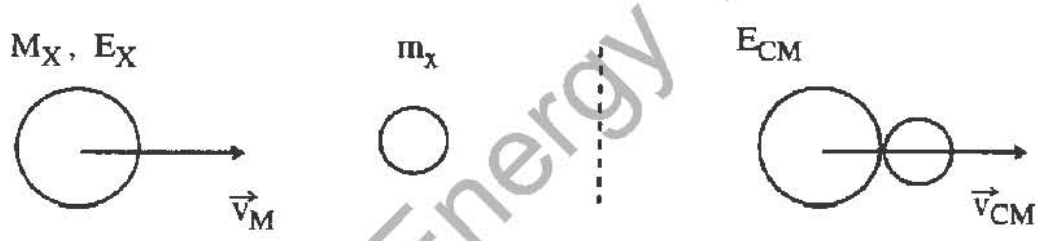

We only consider the formation of the compound nucleus with the step of overcoming of the potential barrier to obtain what I call a **pseudo compound nucleus** $(M_X + m_x)^*$ and after nucleon transfer the compound nucleus $(M_X m_x)^*$ before the step of de-excitation. First we find the relation between energy of projectile nucleus X and energy of the system in the center of mass when nuclei are in close contact .

$\vec{v}_X$ is the velocity of the projectile in the laboratory system, we assume the target x is not moving. At the end of this first step, the velocity of the center of mass is $\vec{v}_{CM}$. The relation deduced from the law of momentum conservation is:

$$M_X \cdot \vec{v}_X = (M_X + m_x) \cdot \vec{v}_{CM} \qquad \text{from which :} \quad \vec{v}_X = \frac{M_X + m_x}{M_X}\, \vec{v}_{CM}$$

Since: $E_x = \frac{1}{2} M_x v^2_X$ and: $E_{CM}\ \frac{1}{2} (M_X + m_x).v^2_{CM}$

we deduce: $$E_{CM} = \frac{M_X}{M_X + m_x}\, E_X$$

The law of energy conservation is: $E_X + M_X.c^2 + m_x.c^2 = E_{CM} + (M_X + m_x)^*.c^2$

By summing this equation with the expression of Q-formation, we get:

$E_X - E_{CM} = -Q$ for example : $E_X = -Q \cdot \frac{M_X + m_x}{m_x}$

This result shows that if Q > 0 the nuclear reaction of fusion will proceed when both nucleus will be in close contact. But if Q< O, the reaction will only occur if the projectile has a minimum energy given by the preceding equation.

Then for the fusion uranium - boron, the condition of fusion is (exact value is given using atomic mass unit):

$E_X > 15. \frac{238 + 11}{11}$ for example : $E_X > 339$ MeV !

Taking into account this result we could think that the natural nuclear fusion is a myth. But our analysis of alchemy treatises show us surprising facts that make it difficult to say that alchemists were using pitchblende and fluorite by a pure coincidence.

In order to solve that obstacle, I considered the present result as an indication of the existence of a new parameter that should be compatible with present knowledge of nuclear physics and should be able to give a realistic approach of the synthesis of superheavy elements.

The solution is obtained from the analysis of the energy balance needed to produce a macroscopic amount of Philosopher's Stone, assumed to be Z = 126 element fluoride. Supposing that one uranium fission is sufficient to produce one SHE nucleus: a maximum probability using the classical concept of nuclear reactivity, it appears that a prodigious amount of energy will be required to produce around 10 grams of SHE: Let 100 MeV the energy useful for fusion of uranium projectile in order to give a SHE nucleus according an unknown process. To produce our 10 grams of SHE, we need:

$100 . 6.02 . 10^{23} . 10/310 = 1.94 . 10^{24}$ MeV this energy corresponds to 74,500 Kg of TNT.

Therefore it seems obvious that a natural nuclear reaction is occurring in order to imitate the consumption of energy from uranium fission: the uranium projectile will have to participate to exoenergetic and endoenergetic nuclear reactions. Since the medium is very rich in hydrogen and that nuclear reaction of fusion with uranium is exoenergetic, it is clear that hydrogen is also the key element of the mixture. Such fact has been explicated by some alchemy authors who recommend to carefully regulate the fire in order to avoid a burning of the initial product.

At that point the understanding of the natural nuclear synthesis of SHE strongly diverges from present methods of searching them using heavy ion accelerators which is characterized by the following parameters:

- Metallic targets are used
- Light projectiles collide the target
- No protons are involved
- No stabilizing agent is present

The main reason is that present methods are still considering the old concept of **atom** (from the Greek word which means **unbreakable**), while in the present study it is supposed that SHE are the limit of the Periodic Table of Elements, and consequently they own a very peculiar characteristic which is their inability to exist as free atoms. Evidently such hypothesis comes from the study of controversial old alchemy treatises, but the fact is that such

hypothesis which perfectly explains these treatises is also easily verified via experiments, since now some cases of unexpected nuclear reactivity may be understood. These experimental facts will be described in the last part.

The goal is to get an idea of the creation path of superheavy nuclei in that chemical medium.

Let see the new changes in our equations, considering the mechanism of fusion has to be related with a **soft fusion process**:

M: Mass of the uranium nucleus

m: Mass of the light nucleus

p: Mass of the proton

E_M: Uranium projectile energy

E_{CMx}, with x = 1,2,3,4: energy in the center of mass

$\vec{v}_{CMx}$, with x = 1,2,3,4: velocity of compound nuclei

Q_x, with x = 1,2,3,4: energy of absorption of nucleons.

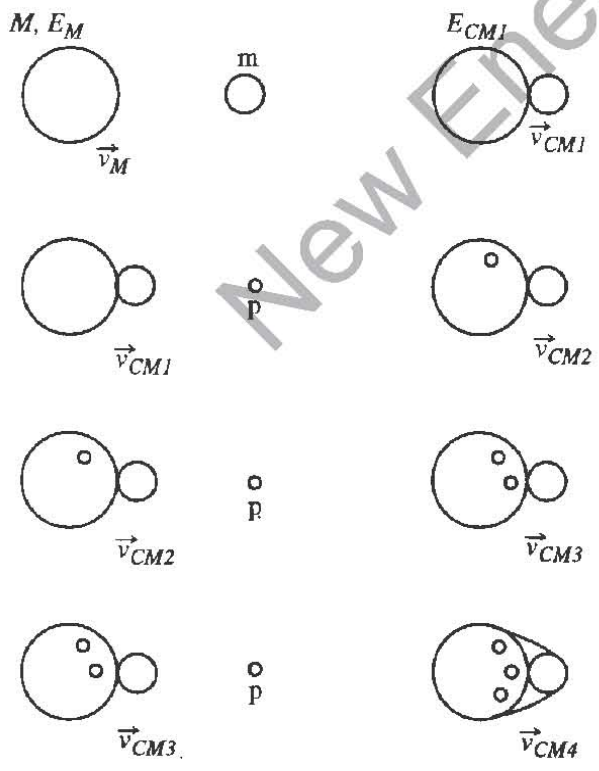

The scheme of this fusion mechanism is a possible approach to reality. The projectile may interact first with proton or a light nuclei. Considering what we know about nuclear reactions: it has been observed that gamma rays of deexcitation of a compound nuclei occur after 10^{-14} second for most nuclear reactions. I think that during

this very short time, the compound nucleus uranium-light element will be able to interact with protons present on its path. It is calculated that it will meet at least 100 protons on a path of about 80 nanometers.

The relations are the following:

$$E_{CM1} = \frac{M}{M + m} E_M \qquad E_{CM2} = \frac{M}{M + mp} E_M$$

$$E_{CM3} = \frac{M}{M + m + 2p} E_M \qquad E_{CM4} = \frac{M}{M + m + 3p} E_M$$

$$E_{CM(n+1)} = \frac{M}{M + m + np} E_M$$

Energy formation relations are:

$Q_1 = M \cdot c^2 + m \cdot c^2 - (M + m) \cdot c^2$

$Q_2 = (M + m) \cdot c^2 + p \cdot c^2 - (M + m + p) \cdot c^2$

$Q_3 = (M + n + p) \cdot c^2 + p \cdot c^2 - (M + m + 2p) \cdot c^2$

$Q_4 = (M + m + 2p) \cdot c^2 + p \cdot c^2 - (M + m + 3p) \cdot c^2$

We assume that $Q_2 = Q_3 = Q_4$ because we have for each case a proton absorption.

Let see now the equations of energy conservation:

$E_M + M.c^2 + m.c^2 = E_{CM1} + (Mm).c^2$

$E_{CM1} + (Mm).c^2 + p.c^2 = E_{CM2} + (Mmp).c^2$

$E_{CM2} + (Mmp).c^2 + p.c^2 = E_{CM3} + (Mm2p).c^2$

$E_{CM3} + (Mm2p).c^2 + p.c^2 = E_{CM4} + (Mm3p).c^2$

The complete fusion may be written:

$(Mm3p) \rightarrow (M + m + 3p)^*$ Excited compound nucleus

The most probable is that each proton absorption will produce a transfer of nucleons of the light element to the uranium projectile, it will result a new interaction between the transuranium nucleus created and the light target.

Summing all the equation we get:

$$E_M - E_{CM4} + Q_1 + Q_2 + Q_3 + Q_4 = (Mm3p).c^2 - (M + m + 3p).c^2$$

The second term of the equation must be zero. The first part of this term corresponds to a union without fusion, while the second part corresponds to the final nucleus before the step of deexcitation. Supposing that protons are not involved, the equation becomes:

$$E_M - E_{CM1} + Q_1 = (Mm).c^2 - (M + m).c^2$$

To get the known result the second term of the equation must necessarily be zero; it results that the equation of interest involving protons will give:

$$E_M - E_{CM4} = - (Q_1 + Q_2 + Q_3 + Q_4)$$

Using the expression of E_{CM4}, we get:

$$E_M \geq - (Q_1 + Q_2 + Q_3 + Q_4) . \frac{M + n + 3p}{M + 3p}$$

This equation gives the minimum energy of uranium projectile to obtain a compound nucleus after three proton absorption.

The important values in the case of the Uranium - Boron fusion are:
Q_1 = 13,80 MeV Energy of formation Uranium - Bore
$Q_2 \simeq$ + 5,5 MeV Energy of one proton absorption

Using numerical values:
Fission energy of uranium: E_f = 167 MeV
Fission fragment: M_o = 94

Energy of fission fragment: E_o = 100.20 MeV
Frontal collision with uranium: so θ = 0
Energy of uranium nucleus: E_U = 81.34 MeV

Target: Bore A = 10, Z = 5
Fusion barrier: $V_{U\text{-}B}$ = 56.59 MeV
Minimum energy required: E_U = 372 MeV

First proton absorption.
Energy required for the complete fusion: $E_{Up} \geq$ 226.36 MeV

Second proton absorption.
Energy required for the complete fusion: $E_{Upp} \geq$ 104.16 MeV

Third proton absorption.
Energy required for the complete fusion: $E_{Uppp} \geq 0$

This explanation of the fusion process Uranium - light element involves the exoenergetic reaction of three proton absorption; it requires that protons present on the path of uranium do react with uranium.

Now we must consider the fusion cross-section when the fusion cross-section is almost equal to the reaction cross-section, that is to say for each interaction between the projectile and the target the fusion will have to occur.

The fusion cross-section involves the energy of the projectile in the system of center of mass. Projectile and target interact as follows:

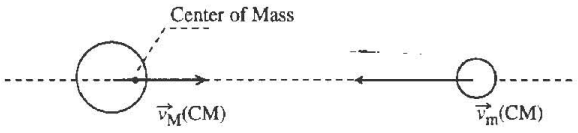

The concept of projectile and target has a precise meaning in the Laboratory system. In the system of Center of Mass equations of the interaction projectile-target are simplest:

$M \cdot \vec{v}_{N(CM)} + m \cdot \vec{v}_{m(CM)} = 0$

We have energy relations:
$M \cdot E_{M(CM)} = m \cdot E_{m(CM)}$

We have also the relations:
$\vec{v}_{M(CM)} = \vec{v} - \vec{v}_{CM}$ and $\vec{v}_{m(CM)} = -\vec{v}_{CM}$

Let compare the following conditions:
- The projectile is the light nucleus, the velocity of the center of mass is:

$$\vec{v}_{CM} = \frac{m}{M+m}\vec{v}_m$$

so : $E_{CM} = \frac{m}{M+m}E_m$ and $E_{m(CM)} = \frac{M^2}{(M+m)^2}E_m$

-The projectile is the heavy nucleus:

$$\vec{v}_{CM} = \frac{M}{M+m}\vec{v}_M$$

so: $E_{CM} = \frac{M}{M+m}E_M$ and $E_{M(CM)} = \frac{m^2}{(M+m)^2}E_M$

When the projectile is the light nucleus we note that $E_{m(CM)}$ is not very different from E_m; the center of gravity of the system is near the heavy nucleus and E_{CM} is small. But when the projectile is the heavy nucleus, $E_{M(CM)}$ is very small, most of all the energy is E_{CM}, and $E_{m(CM)}$ owns the most part of the remaining energy.

We also note that the center of mass is in the uranium nucleus for the distance $R_o < R_U$ while the light nucleus is at a distance 20 times higher.

In the Laboratory system the heavy projectile receives enough energy resulting from the collision the fragment of fission of uranium to overcome the potential barrier of Coulomb. A light projectile for the same value of energy should own a higher velocity to counterbalance its lower mass. **For the heavy projectile a lower action**

velocity is compensated by the inertia effect. The problem of fusion depends on Q, energy of formation of the compound nucleus. As a matter of fact, for $Q > 0$ the reaction is possible if the potential barrier of Coulomb is overcome. But for $Q < 0$ the reaction cannot occur, even if the potential barrier of Coulomb is overcome, because, according the theory, products of the reaction have the energy:

$$E_1 = \frac{m_1}{m_1 + m_2}\left(Q + E_M = \frac{m}{M + m} \right)$$

$$E_2 = \frac{m_2}{m_1 + m_2}\left(Q + E_M = \frac{m}{M + m} \right)$$

It results that the condition of formation of these products of reaction is:

$E_M > -Q\frac{M + m}{m}$ - Minimum energy for the fusion reaction

For the compound nucleus, the sum $E_1 + E_2$ gives:

$$Q + E_M \frac{m}{M + m}$$

This term must be positive; so we obtain the preceding condition of fusion when $Q < 0$. But we also see that the action of protons will make this term positive because for each absorbed proton there will be a gain of $q > 0$, around 5 MeV, and an increase of the ratio:

$$\frac{m}{M + m} \quad \text{to} \quad \frac{m + 1}{M + m + 1}$$

Previous considerations permit to say that in the case of this soft fusion process which is the main feature of the alchemy process:

- The heavy projectile necessarily overcomes the potential barrier if $E_M > V$.
- There is no direct fusion but a very short time of contact between the heavy projectile and the light target. The center of mass of the system carries most of the energy. The subsequent action of protons produces the transfer of nucleons from the light target to the heavy projectile.
- We may suppose that in our case the final fusion cross section depends on the energy of center of mass: E_{CM}, but that fusion cross section is zero until protons initiate the process of nucleon transfer.

The fusion cross section may be given by the formula:

$$\sigma\, fusion = \pi . R_B^2 \left(1 - \frac{V_{R_B}}{E_{CM}} \right) cm^3$$

1 barn = 10^{-24} cm^2

$R_B = 1.4\,(A_1^{1/3} + A_2^{1/3}) \,.\, 10^{-13}$ cm radius of the compound nucleus

$$E_{CM} = \frac{M}{M+m} E_M$$

E_{CM}: Energy of center of mass.
E_M: Energy of projectile in the Laboratory system.
M: Mass of the projectile
m: Mass of the target

During the process of soft fusion the projectile owns a certain amount of internal excitation energy resulting from the collision with the fragment of fission of uranium, that means a lower gain of energy should favor the fusion. If we restrict our thinking to the known theoretical reverse fusion process, it will be necessary to give to uranium an energy of 340 Mev (case Uranium-Boron fusion), the result will be a complete disintegration of the compound nucleus.

We may also note that since the center of mass carries most of the energy this fact is very favorable to the energy transfer process after fusion that allows a new fusion cycle to begin, therefore it becomes possible to produce a macroscopic amount of superheavy nuclei.

	V(MeV)	E_M(MeV)	E_{CM}(MeV)	σ_{fusion} (barn)
Nitrogen	76.95	80.37	75.91	$\simeq 0$
Boron	56.18	80.37	76.82	1.17

It is clear that **Boron** (as well as Beryllium and Carbon) is an interesting element for a complete fusion with uranium:

$^{238}_{94}U + ^{11}_{5}B \rightarrow ^{249}_{97}Bk^*$ Hypothetical compound nucleus

Compound nucleus is in a high excitation state: It is the excess of energy remaining after formation of the compound nucleus. This excitation energy is given by:

$E = E_O + Q$ E_o: energy of projectile
Q: energy of formation of the compound nucleus

Excitation energy depends on the formation energy of the compound nucleus. It means that in the case of an endoenergetic reaction, excitation energy will be lower that in the case of an exothermic reaction of fusion.

Thus the calculus gives:

$E_{CM4} = 92.13$ MeV $V_{RB} = 58.31$ MeV from which : $\sigma_{fusion} = 1.58$ barn

This value makes sense if we compare it with the cross section of fission of uranium by fast neutrons:

$\sigma_{fission} \simeq 0.55$ barn for neutrons with energy: $E_n > 2$ MeV

The mixture does not permit thermal fission because boron is present, therefore fissions of uranium are produced by fast neutrons created in-situ, that means the production of nuclear events of fusion is regulated by the rate of uranium fission.

It must be noted that to obtain a macroscopical amount of superheavy element, we need a very intense nuclear activity of fusion events and that our mixture should behave as a small nuclear reactor. The answer to that question can be obtained from experiments taking in account that our production of Philosophers' Stone implies a minimum of 10 billions favorable events of creation by second.

What could really happen?

This first approach of the mechanism conducing to SHE is necessarily far from reality. It means that as soon as uranium gets kinetic energy, it travels in the medium and may interact with light elements or protons. In the first case, a classical energy transfer to light nucleus should occur. In the second case, proton could effectively react with uranium giving an excited system that is now able to interact efficiently with light nuclei, but it could be a transfer of some nucleons from the light nucleus to uranium; interaction of other proton could produce other nucleon transfer. So the true mechanism could be a continuous interaction projectile - protons - light nuclei until the creation of the first stable superheavy nucleus.

During the first 1986 experiment, as soon the flask was put to rest in a cold place, its nuclear activity starts to increase and continuous burst of radiations have been observed for each measurement of the gamma activity. This fact could be related with the proposed mechanism of formation of SHE, because observed burst of radiations, when working with a uranium mineral, may be only produced and explained by such new kind of nuclear reactions since the medium is not enriched with $^{235}_{92}U$ or $^{239}_{94}Pu$. (A book: Criticality, proceeding of a symposium about this subject of enriched medium has been published around 1975).

The SHE formation

This approach of the first fusion step also indicates how the SHE will be created. It was thought at the beginning of this study that it should exist in the chemical medium some intermediary products, an hypothesis that strongly reduces the possibility of creation of SHE. To pass the instability Z barrier, the excited product of the first fusion owns enough energy to produce new fusion events. On its path in the medium the uranium projectile may interact with protons and light nuclei as long its energy is higher than the potential barrier of fusion. Since the absorption of protons is an exoenergetic nuclear reaction, the compound nucleus will be in an excited state probably favorable to new fusion events with light nuclei until the final compound nucleus get a more stable state and transmits its energy to an uranium nucleus that will start the cycle of fusions. But the final nucleus may also be disintegrated in the medium giving a detectable neutron burst.

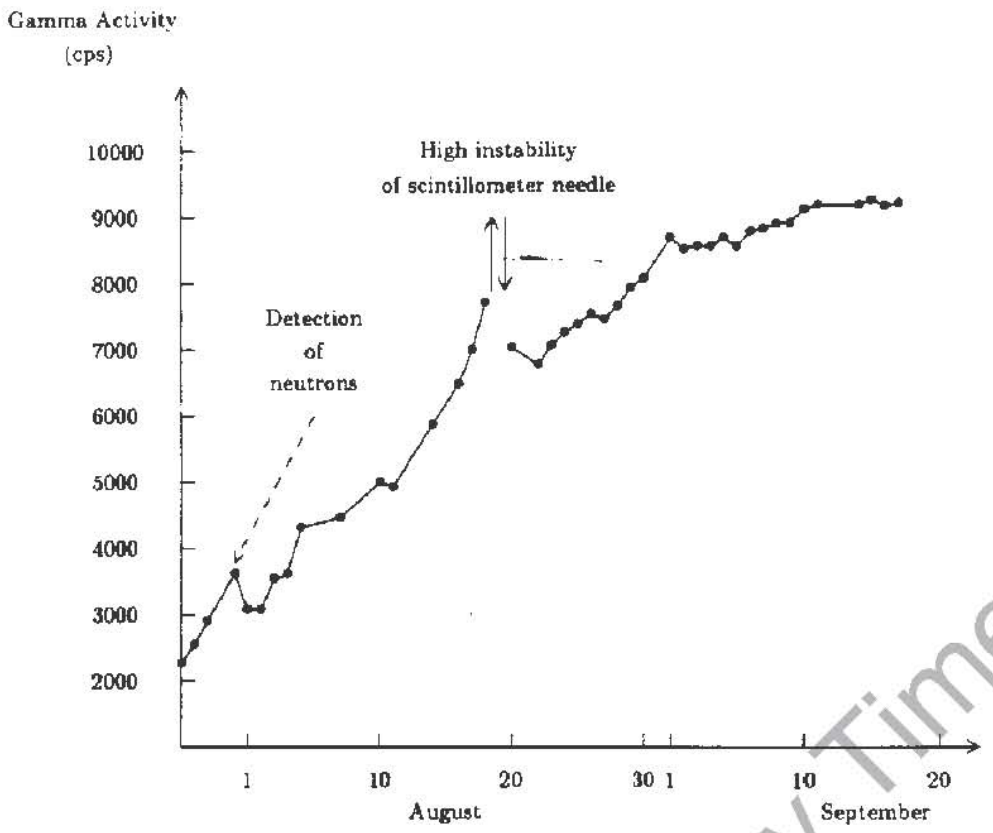

Fig. 1 Flask : Variation of gamma activity

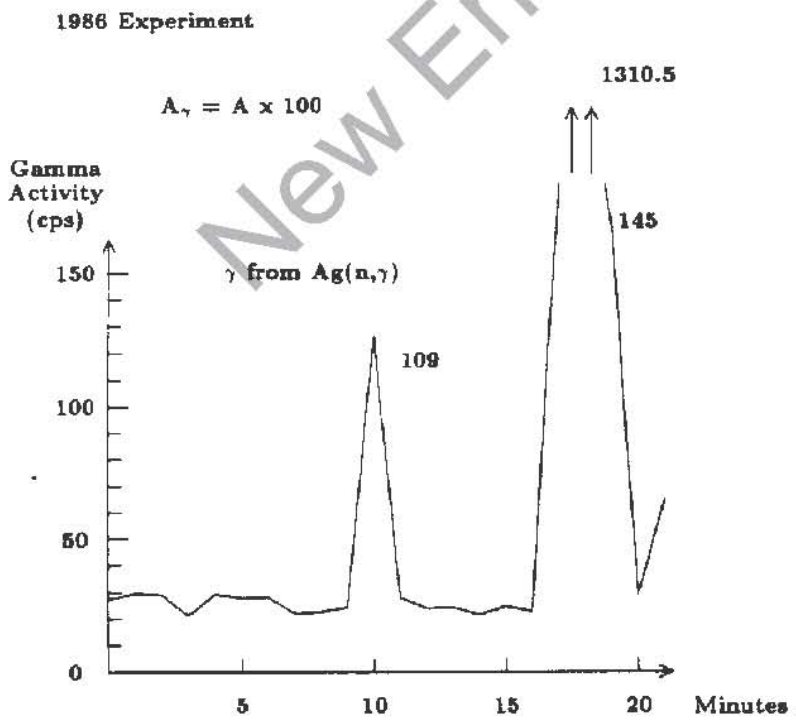

Fig. 2 Detection of neutrons from Ag(n,γ reaction

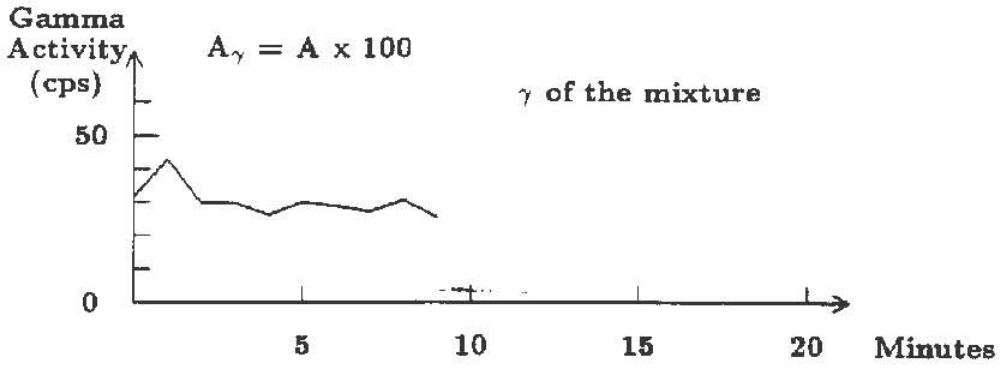

Figure 3

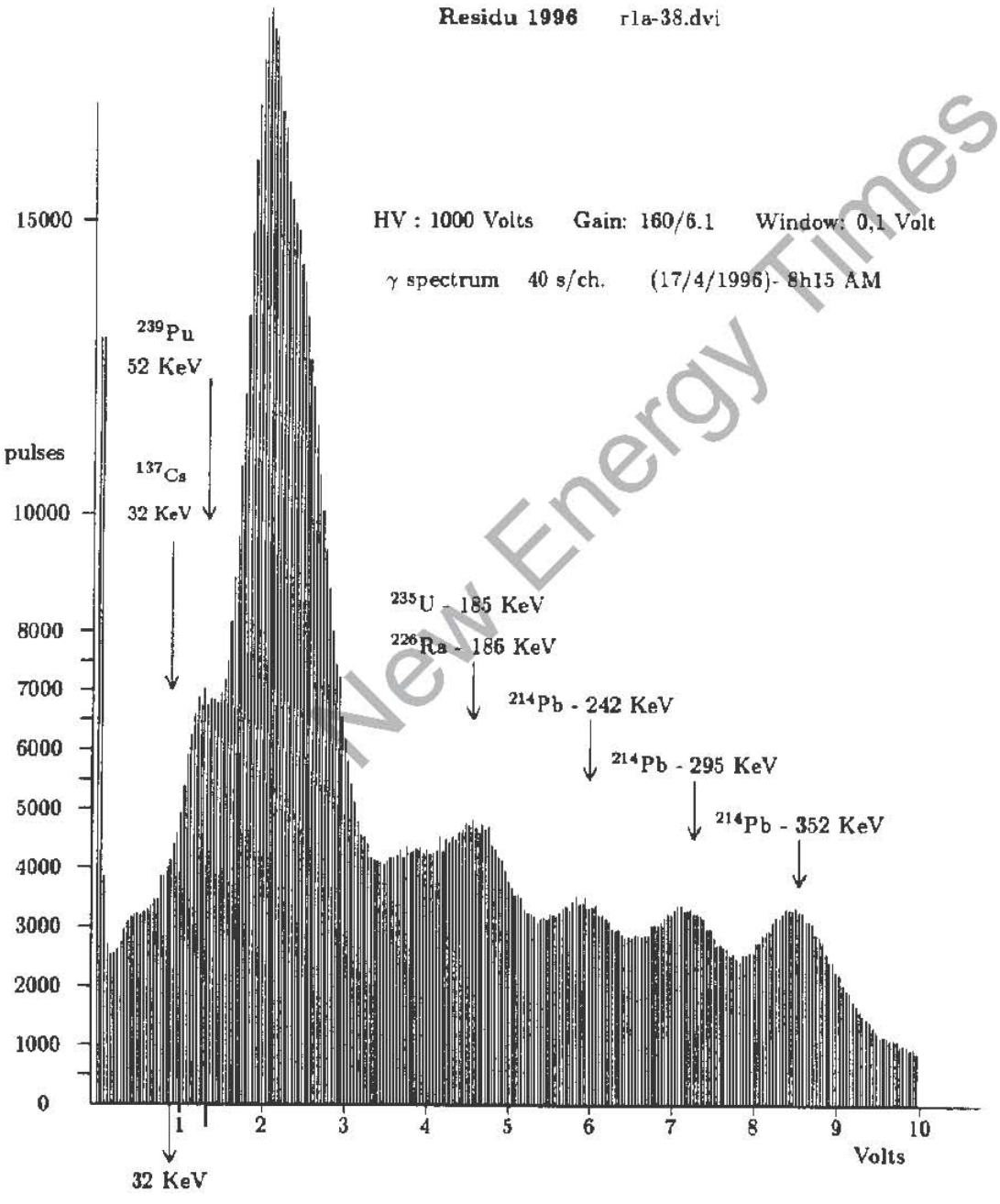

Fig. 4 γ spectrum of the mix before heating

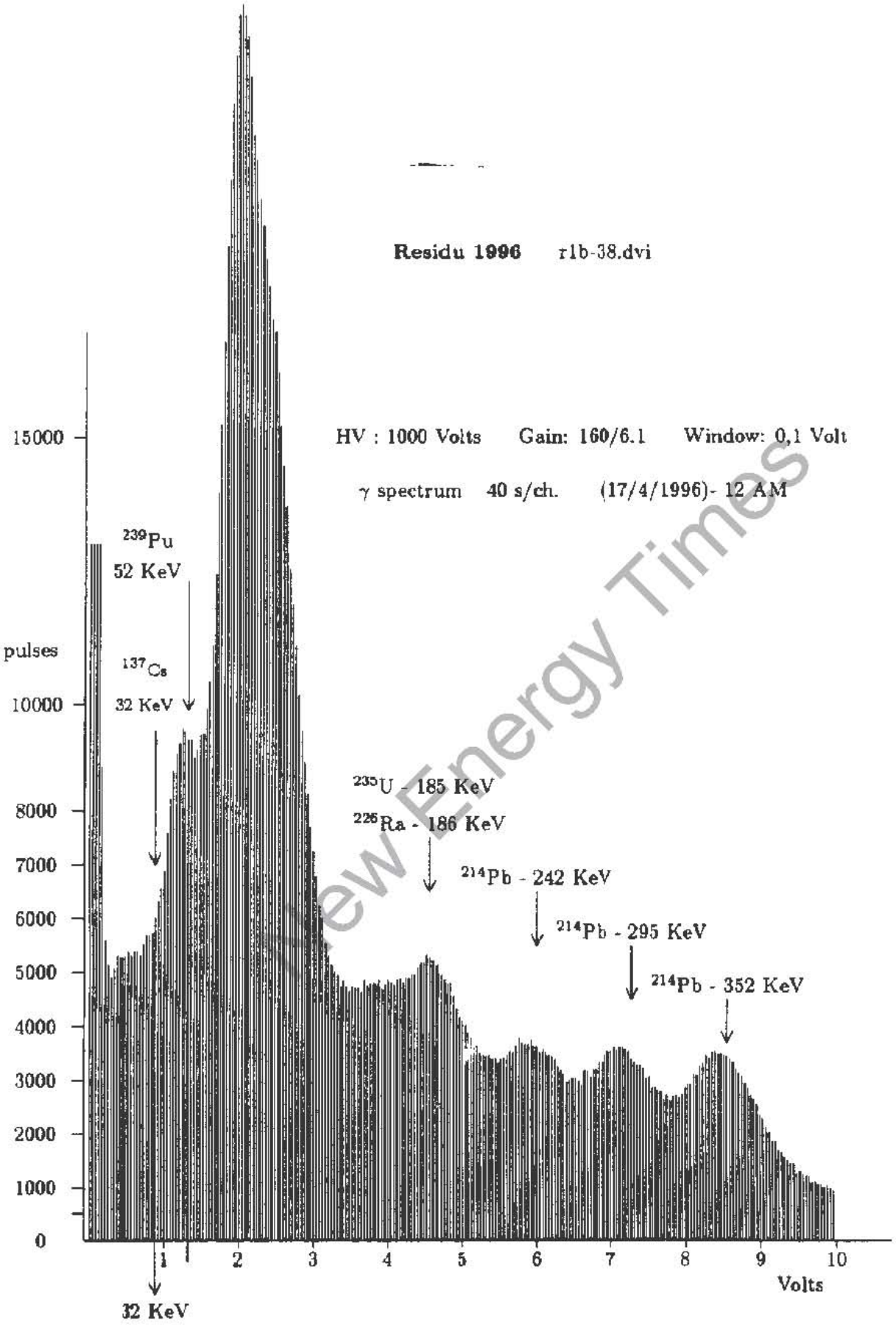

Fig. 5 γ spectrum of the mix after heating

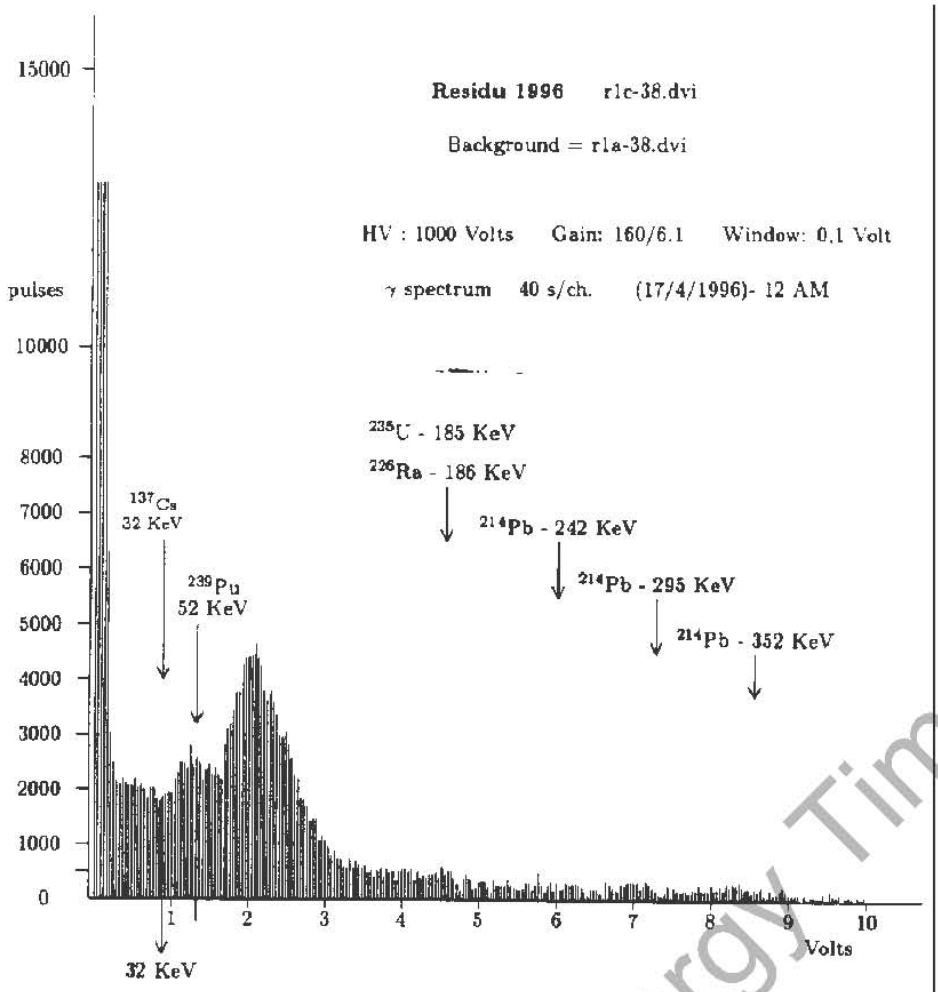

Fig. 6 Increase of γ activity

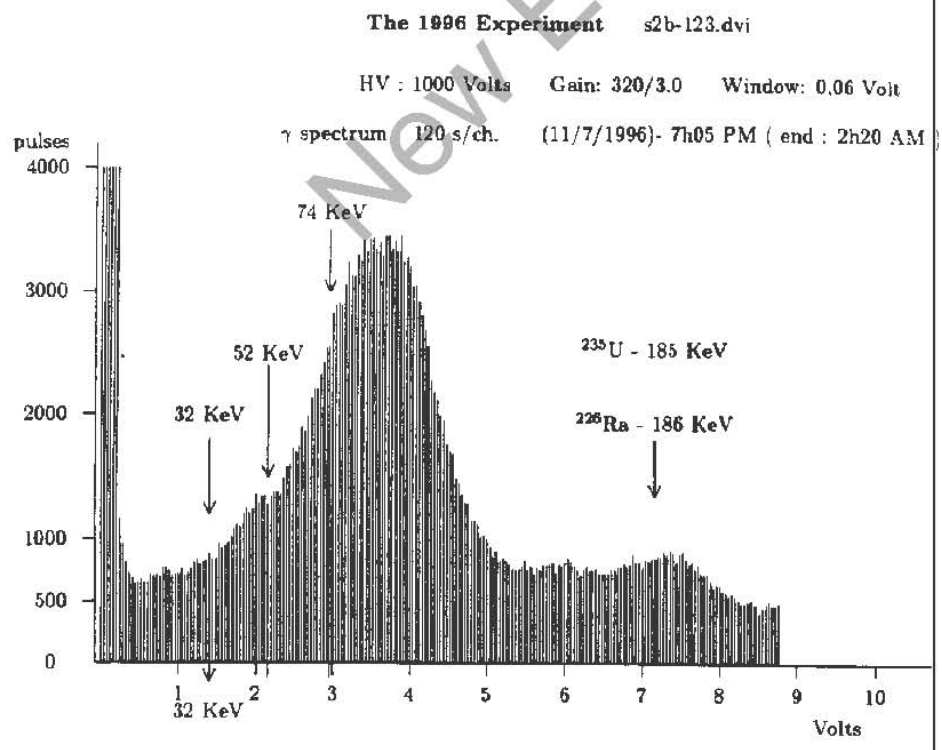

Fig. 7-a Sample to be analyzed

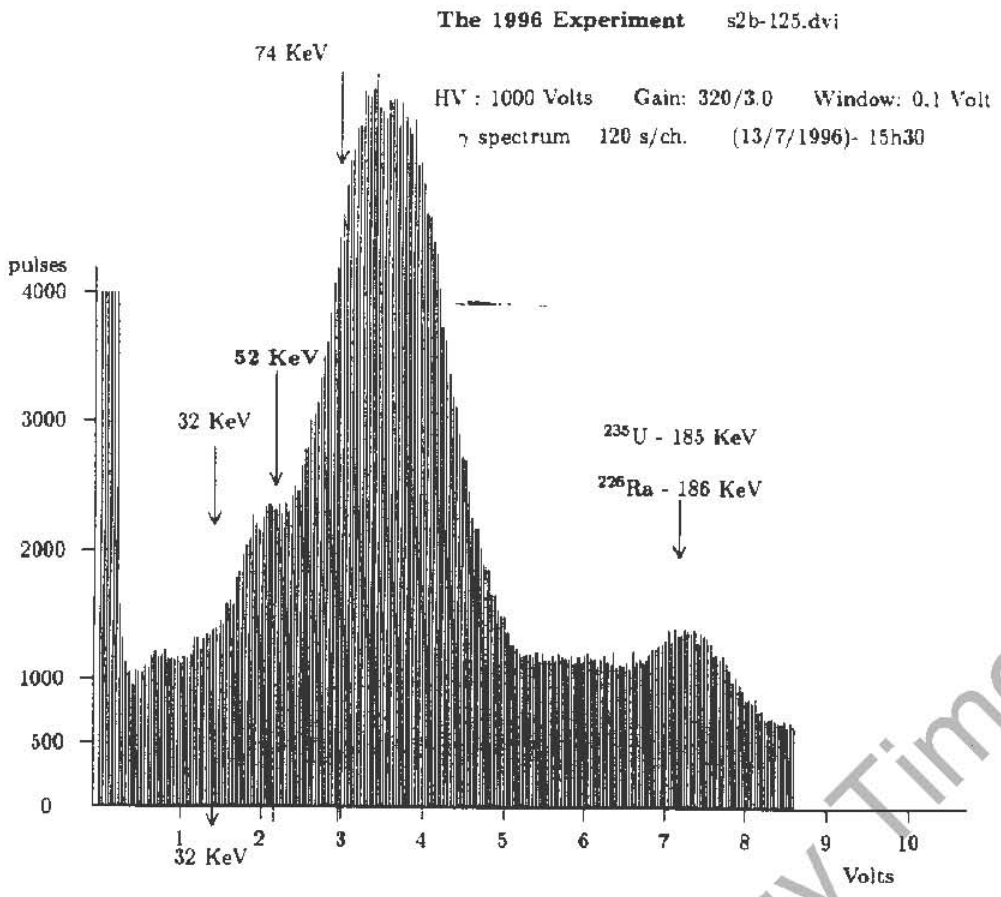

Fig. 7-b Sample after drying to fumes

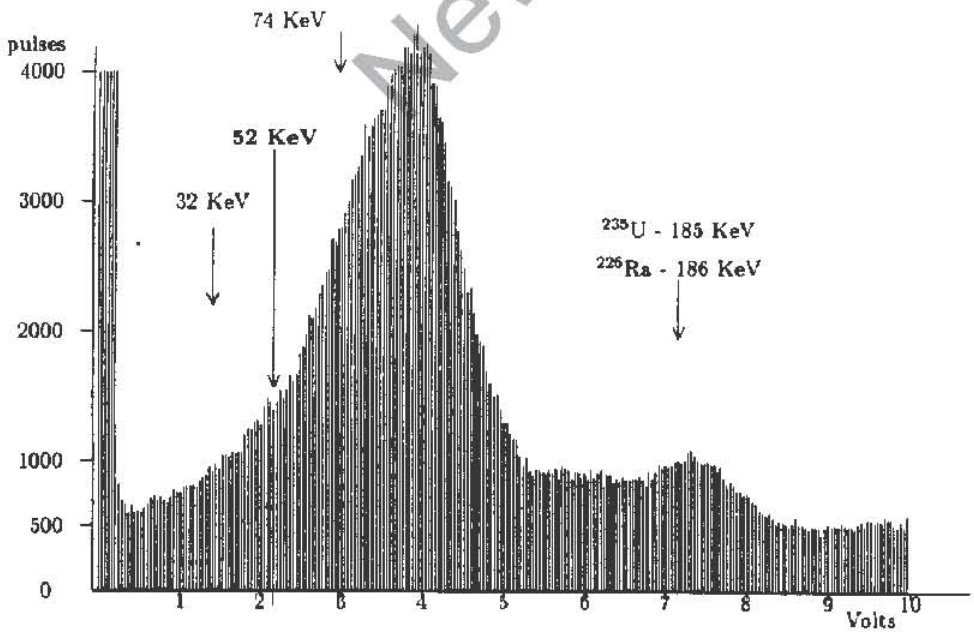

Fig. 7-c Spectrum after sublimation

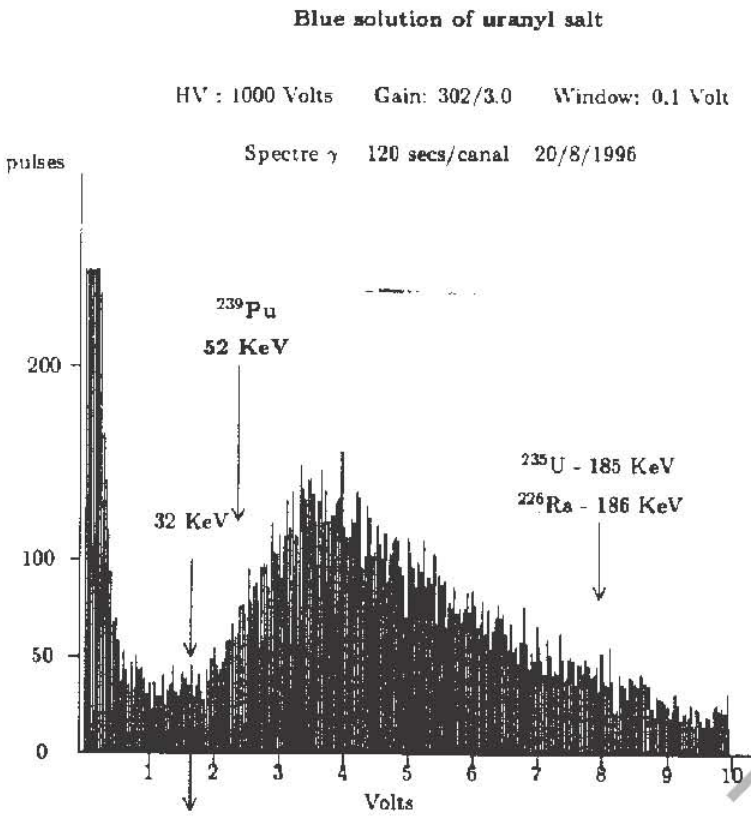

Fig. 8.

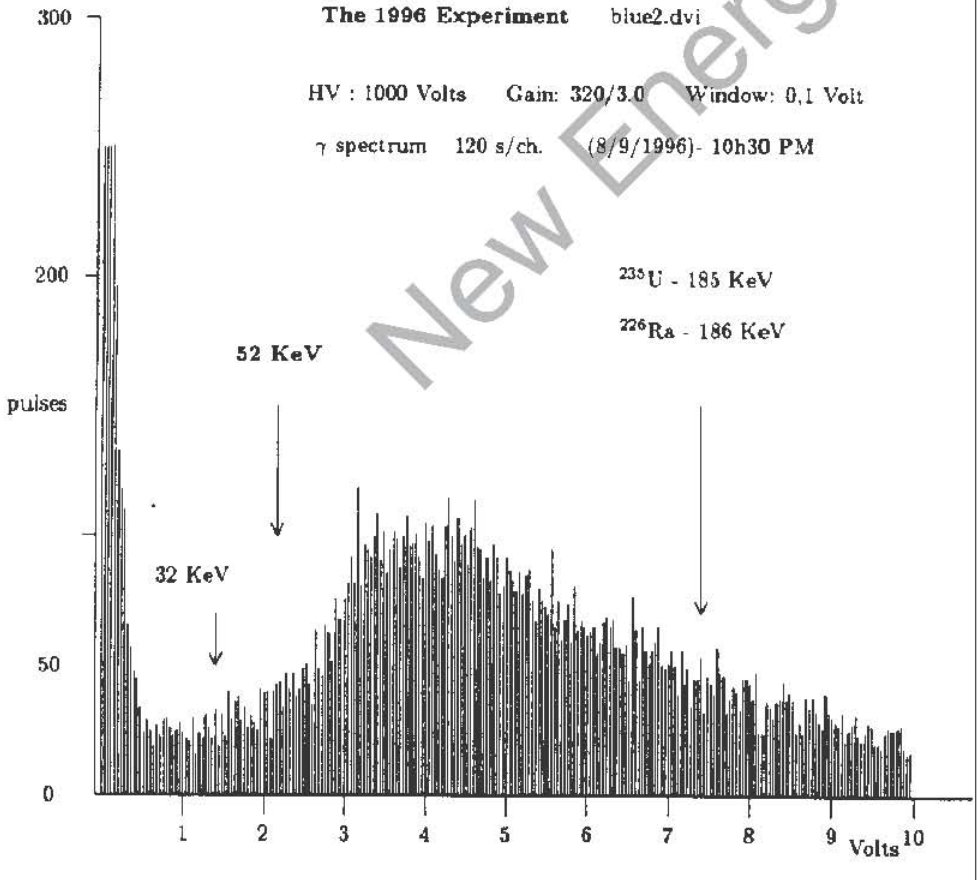

Fig. 9 bis Blue color from uranyl salt

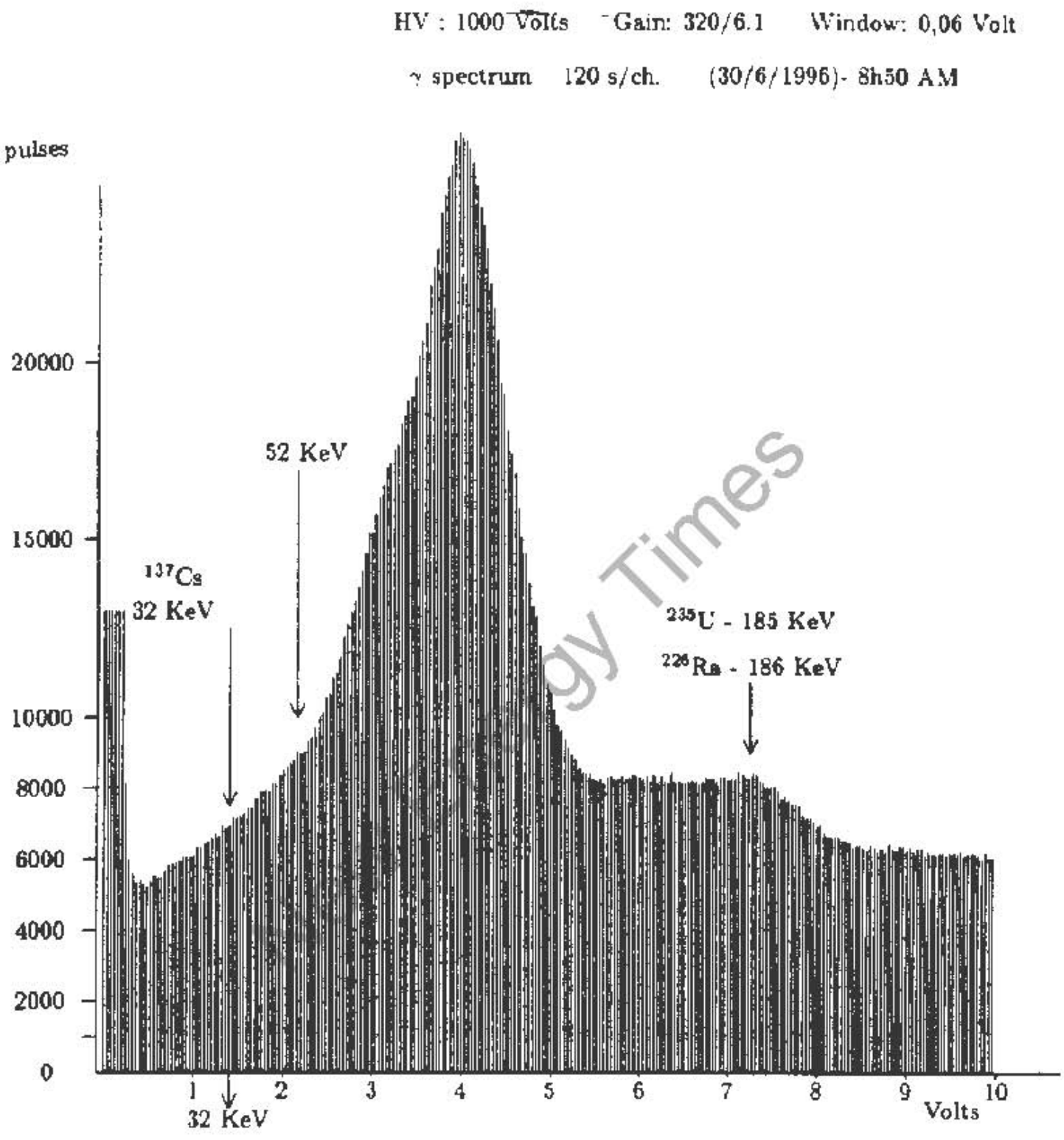

Fig. 10 **Pechblende** (Pech-112.dvi)

NATURAL COLD FISSION – NATURAL NEW ENERGY – NATURAL NEW PHYSICS

Georgiy S. Rabzi [1]

ABSTRACT

"Cold fusion" and "hot fusion" - are two antagonists whose uncompromising struggle will either produce new clean sources of cheap energy and help the world overstep the threshold of the third millennium under the banner of new physics, or prolong investing huge sums in tokamaks. The struggle takes place in your laboratories as well, when in your cold fusion test cells, you observe reaction products, such as elements, particles, and phenomena allegedly inherent solely in high-temperature nuclear reactions. Most often among these are tritium, helium, silver, chlorine, iron, excess energy, as well as protons and neutrons. The variety of cold fusion cells all have a joint in the armor: their structural materials and reacting substances therein are chosen arbitrarily. The attempts to understand the nature of the processes and the phenomena observed stem concomitantly from the results. We have heard about electrolysis, catalysis, chemical affinity, lattice-induced phenomena, and the like.

This author is absolutely positive and has abundant reproducible results to support the conviction that so-called "cold" and "hot" fusion phenomena are the outcome of radioactive-free low-temperature transmutation. In material objects this process is induced by their nature: presence of "-" and "+" electric charge fields which interact continuously with the spatial electric field. It is those interactions that govern all the processes both in the Universe and in our devices. This author's numerous experiments unambiguously suggest that controllable manipulation of the artificially intensified spatial field promotes transmutation.

INTRODUCTION

I invite you to join me in the mental experiment with the ordinary cold fusion test cell (Fig. 1). Let us bring it from its conventional upright position A through 90° into position B. In thus doing, under the same low temperatures you will witness the increased number of the reaction products owing to the summed up fields in the cell with the spatial field.

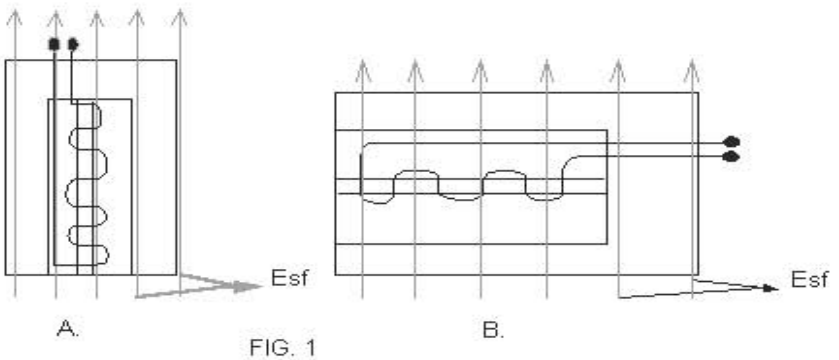

FIG. 1

Fig. 1 Cold Fusion cell with spatial electric field (dotted lines).

[1] Ukrainian International Academy of Original Ideas, Southern Branch, Odessa, Ukraine

Numerous experiments in the likewise-arranged device substantiated an increase in the reaction products to the extent that I name the products as low-temperature transmutation (or fission), but not fusion. The results, along with the samples, were presented at the last-year conference [1].

The spatial field, ignored currently by the experimenters, exerts dramatic impact on every and all material objects. It provokes transmutation which takes place under different but necessarily low temperatures. Thus, at T = 36.6° C the spatial field interaction with carbon C^{13} in our bodies causes its decay into C^{12} signaling the human body's ageing [2].

Such a challenging statement cannot be trusted unless backed up with serious arguments. To these I shall proceed.

THE SPATIAL FIELD

The widely accepted fact that our Universe consists of positive and negative charges lacks one tiny detail: unanimity of opinions as to **what** are these charges. I will show later on that they can be only and exclusively electrons and positrons. So-called "elementary particles" known today - leptons, bosons, hyperons, and the like - are nothing more than the intermediate products of high-temperature bombardment of the nucleus. They have no natural stability, like electron and positron have. Electrons and positrons stand alone among over 300 elementary "ghost"-particles for their highest specific charges $\frac{e^-}{m_{e^+}}$ and $\frac{e^+}{m_{e^+}}$. They are unexterminable and fill the space at random. But their spatial distribution is never changed because an empty space is dielectric [3]. When interacting, electric fields of these charges sum up to form, respectively, spatial charges "+" of positrons and "-" of electrons. The space in between the charges is imbued with electric field lines self-emerged from numerous electron-positron pairs, or neutrinos. Their terminal charges $q_{\nu+} = 0.16 \cdot 10^{-42}$ C and $q_{\nu-} = 0.16 \cdot 10^{-42}$ C connect them, respectively, to the spatial "+" and "-" charges, and **in this manner the spatial material electric field is self-emerged**. It is in this field where all physical events with the objects of the Universe take place [4,5].

The charges of electron and positron are their uncognized essence, something called Logos in the Bible. *"In the beginning was the Word, and the Word was with God, and the Word was God"*. That is, these charges store and under interaction with the field give out all the information about any phenomenon: from gravitation to restructuring in lattices. Their interaction is primary. It is primordial, always the strongest, twin reciprocated. Self-attraction of charges yields self-motion of electron and positron. An oblate electron-positron pair = matter = neutrino is self-emerged [6,7,8]. Great velocity of attraction between those pairs is born, and energy is released when pairs collide (Fig. 2a).

THE NEUTRINO AS A BUILDING BLOCK

Being a particle of matter, a neutrino has both charge $q_{\nu\pm} = 0.16 \cdot 10^{-42}$ C and mass $m_\nu = 0.43 \cdot 10^{-34}$ kg. Since $q_{\nu-}$ and $q_{\nu+}$ charges are unexterminable, hence mass is also unexterminable. Let me please remind you that I determine mass as a measure of the directional interaction between the nonexterminable electric charge and spatial field [1]. Therefore, a neutrino is not a hypothetic particle (as modern physics states) but real non-exterminable matter, the basis of the Universe.

From multiple neutrinos, through self-attraction of their microcharge fields, a neutron (n) is self-generated (Fig. 2b). It is further attracted to positron e^+ producing proton (p) (Fig. 2c). That is why **proton and neutron are essentially one and the same particle with only positron charge differing**.

The above considerations allow for explaining such a phenomenon as self-production of chemical elements in the Universe - from the simplest atom to transuranium ones - solely in terms of electron, positron, and neutrino charges.

ATOMIC FORMATION AND ATOMIC WEIGHTS

The spatial field polarizes the neutron-born proton. Neutrino in thus oriented field acquires spin -1/2 (Fig. 2d). Charge-conjugate interaction of all the neutrinos microcharge fields in neutron with all the anti-neutrinos in proton results in self-generated by mutual attraction a proton-neutron pair. All its charges are compensated, except for the positron charge captured by proton (Fig. 2e). An isolated positron in the atomic nucleus is impossible without simultaneously attracted electron, otherwise the system will not be an isolated one. Hence, according to the full charge conservation law [8] each proton's positron is joined by the attracted from space electron e^- decelerated by the spatial field force $F = e^- E_{sf}$

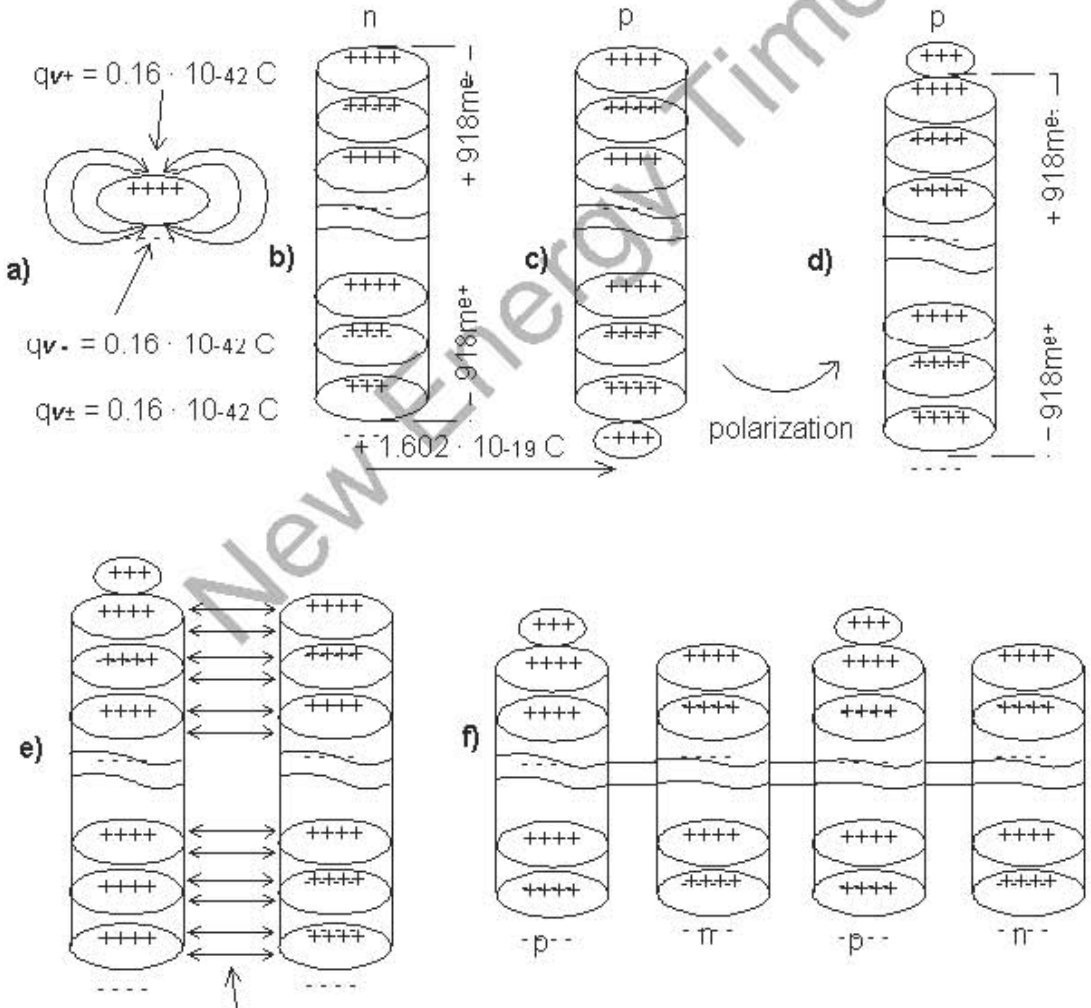

FIG. 2

By analogy with the first p-n pair of an atom, interaction of conjugate charges involves the subsequent pairs whose orbital electrons correspond to the number of the nuclear positrons (Fig. 2f). In this manner self-formation of heavy and super-heavy (transuranium) elements proceeds **only** in those domains of space where low field intensity and about absolute zero temperature are found.

To verify applicability of the discussed theoretical sequence of the chemical atoms self-formation the **absolute atomic weights** of all 104 elements in the Periodic System were calculated using nothing else but electric charges of positron, electron, and neutrino. Absolute atomic weights 100% fitted the relative ones. The adopted model helped place hydrogen, as well as zero group (Table). Note that hydrogen is the first element to be self-generated and the pre-finite one in the complete decay. Calculations and analysis of the atomic masses corroborated the nuclei of all the elements (excluding isotopes) to consist of the differing number of *solely* proton-neutron pairs. Dineutron and diproton cannot inhabit nuclei because they are unstable, decaying in 10^{-21} seconds. [9]

Table I

Initial weight of the sample g	Input voltage (power source) V	Temperature °C	Duration h	Output current intensity obtained from Pb μA	Output voltage obtained from Pb μV	Final weight of the sample g
6.28	2000	780	6	81	139	6.6

My observations show instability to be inherent in all the elements of Periodic System and hence in all objects of the Universe. Instability is directly proportional to the number of the atomic orbital electrons. It is a new undeniable fact whose validity I claim, and insist upon, because nature in the research was identical to the nature of objects under study [13].

Self-generation of elements is accompanied with the release of energy into the space, which elevates its temperature. Energy is accepted also by orbital electrons at the moment of super-heavy elements formation. Weakly bound to the heavy element nucleus, electrons of the desired outer orbit, in their permanent interaction with spatial field, are stripped off the orbit, thus triggering low-temperature transmutation. Without a stripped off electron, its field-bound positron of the proton becomes exposed. According to the law of constant net electric charge of an isolated system (atom), the positron is forced off the proton by the spatial field. Self-emerged is the transmutation of the first proton-neutron pair into neutrino $\nu 1$ and anti-neutrino $\bar{\nu}1$. Fission of the first proton-neutron pair is completed when an isolated system (atom) is created, but of a lighter element.

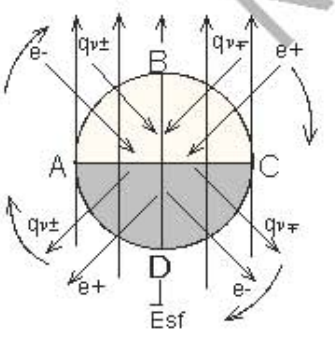

Fig. 3. A - self-emergence starts, decay of heavy elements stops; ABC - self-generation of heavy elements from e^+, e^-, $q_{\nu\pm}$ $q_{\bar{\nu}\mp}$ charges; C - self generation stops, transmutation starts; CDA - transmutation of heavy elements into the final product (e^+, e^-, $q_{\nu\pm}$, $q_{\bar{\nu}\mp}$).

TRANSMUTATION AND ENERGY

Transmutation of an atom involves continuously liberated radiation-free intra-nuclear energy. Released into the surrounding space are also orbital electrons, proton's positrons, certain number of neutrinos and anti-neutrinos as structural material for further self-generation of new elements. The processes of self-generation and transmutation of objects in the Universe are interconnected and proceed under low temperatures. It is by no means intermittent variations in the elements' behavior but a single, circular, continuous, and eternal process of universal transformations. Our Universe is constant in its dynamics, self- emerging and transmuting in a circle (Fig. 3).

Fig. 3 corroborates that both microworld and macroworld – the Universe – are equally based on interactions of charges e^+, e^-, $q_{\nu\pm}$ $q_{\bar{\nu}\mp}$. **The governing motive force that integrates the processes of self-emergence and self-transmutation of heavy elements into a single, strictly sequential, continuous circular process, which is a basis for vital activity of any material object, is the low-temperature spatial field.**

Fission involves liberation of energy which is partly utilized in fission of newly formed lighter elements whose binding energy exceeds that of heavy elements. Therefore, in order that further fission can proceed, elevated temperature is needed, but even in the Earth's core the temperature of fission never exceeds 5000° C. Tremendous temperatures in the central part of the Sun can be related merely to the huge (compared to Earth) mass of the decaying proton-neutron pairs.

Unexplainable bursts of temperatures up to the utter destruction of test cells [10] strongly suggest that, resulting from heating-induced low-temperature transmutation, a new element has self-emerged in the cell accompanied with the excess heat as by-product. Thus I claim that only and exclusively low-temperature transmutation provides a new source of cheap and ecology-friendly energy. And **this** is the basis for physics of the future.

Transmutation of super-heavy elements in their massive aggregations in the Universe **always** involves liberation both of energy and lighter elements, and their gaseous derivatives, like H_2, He, CH_4, NH_3 as the pre-finite stage of their finite transmutation into the charges e^+, e^-, $q_{\nu+}q_{\nu-}$. Electric charges are the products of transmutation, the very "dust" of which the Bible says: *"For dust you are and to dust you will return."* That is why numerous expensive attempts to fuse heavy long-lasting elements at temperatures as high as tens millions of degrees are hopeless. Violated by high temperatures and tremendous energies, Nature will never engender sound offspring, such as cheap abundant energy. New inexhaustible sources of non-polluting energy will be obtained by he who is utilizing the spatial field energy [4,5,11,12] along with the artificial combination of natural low-temperature self-generation of elements and transmutation processes.

During these days we can diversely use energy released during transmutation in bodies and substances. I have conceptual designs of the devices that:

a) help utilize the energy of fission particles to obtain heat energy in the units made of pre-included constituent of heat-generating circuits for heat power plants;
b) enable immediate production of electric energy as by-product of low-temperature transmutation.

To make the above statement valid, the experiments were initiated in February 1995 where Pb underwent transmutation at T = 780° C and standard barometric pressure. Reproducible results showed, besides new elements, microcurrents of electrons from the transmuting Pb.

The paradox of these results cannot but puzzle: transmutation of Pb destined to produce lighter elements induces an increase in the original weight of the sample. Analysis showed that the heaviest element in the Periodic System - osmium - is responsible for eight samples which support the above statement. These samples were handed at the last-year conference to Dr. G.H. Lin to be analyzed.

The discussed theory also gives clues to a number of urgent issues such as controllable enhancement of transmutation to process atomic wastes into commercially feasible non-radioactive products. It enables one to obtain long-lasting super-heavy elements. Following the above considerations, a device was constructed for accelerating and decelerating transmutation processes.

SUMMARY

The listed problems can be easily resolved if approached in terms of concepts introduced by my theory:

1. Nuclei of all elements consist exclusively of proton-neutron pairs.
2. Instability is inherent in all elements.
3. Transmutation proceeds under low temperatures only.
4. Self-generation and transmutation constitute a single continuous circular process of universal changes.

5. Spatial field of the electric charges is the basic factor which governs all the phenomena and transformations of material objects.

My report is supplemented with a tentative list of certain issues that can be understood and effected should the above concepts be accepted by Science. [see Addendum 1]

Let me please conclude with a wish that advent of the new millennium be marked with the advent of new energy and new physics.

REFERENCES

1. G.S. Rabzi, "Mechanism of Low Temperature Transmutation," *The Journal of New Energy*, (1996), vol 1, no 1, pg 46.
2. V.L. Kaznatcheev et al. Proc. Int'l Symp., "Cold Fusion and New Sources of Energy," Minsk, May 24-26, (1994), p. 190 (in Russian).
3. N.M. Mirolyubov et al. Methods of Calculating Electrostatic Fields, Moscow, Vysshaya Shkola Pub. (1963) (in Russian).
4. R.P. Feynman, R.B. Leighton, M. Sands, The Feynman Lectures on Physics, V.5. Electricity and Magnetism, Moscow. Mir Publ. (1966) (in Russian).
5. R.E. Peierls, The Laws of Nature, Moscow. (1959) (in Russian).
6. Fritjof Kapra. Dao of Physics, S.-Petersburg: Otis Publ. (1994) (in Russian).
7. K.N. Mukhin, Introduction to Nuclear Physics, Moscow. Atomizdat. (1968) (in Russian).
8. E.M. Purcell, Berkeley Physics Course, V.2. Electricity and Magnetism, Moscow. Nauka Publ. (1967) (in Russian).
9. Ya. Zeldovich, *Science and Life*, (1976). No. 10, p. 18 (in Russian).
10. E.F. Mallove, "An Italian Cold Fusion Hot Potato," *Cold Fusion*, May 1994, vol 1, no. 1, pp 45.
11. R.V. Pohl, Elektrizitatslehre, vol 2, Moscow, Fizmatgiz Publ., (1962) (in Russian).
12. C.L. Kervran, Transformation l'Energie du Faibles, Paris: Malon, (1975), 210 pp.
13. A.N. Vyalssev, The Lightest Atomic Nuclei, Moscow, (1963), pg 54 (in Russian).

ADDENDUM 1
A List of Challenging Issues Which Are Met Adopting Conceptual Approach of the Works by G.S. Rabzi, "Mechanism of Low-Temperature Transmutation" and "Natural Cold Fission -Natural New Energy - Natural New Physics"

1. Physical essence of gravitation mechanism and zero gravity is disclosed. Twin paradox is explained.
2. Gravity in spacecrafts can be induced.
3. Possibility arises to determine neutron charge which provides for gravitational acceleration and magnetic moment.
4. Explanation is found for the physical essence of the Cavendish experiment on determining the γ constant in the Newton's gravity equation. It is interaction not of ball masses but of their dipoles.
5. Gravitating mass and inertial mass are proved not equal.
6. Four known types of interactions are proved to be the derivatives of the basic and unique interaction provided by Nature - charge, or electric one.
7. All sorts of interactions in the Universe can be described without introduced constants.
8. Elements' atomic size can be calculated without approximations.
9. Disclosed is the origin of $T_{1/2}$ = const half-life stability of elements and $\Delta m \cong 0.001$ mass defect stability.
10. Explanation is found for similar density of the nuclear matter in different atoms not related to the number of nucleons.
11. Understood is the cause of energy-radiating atom stability.
12. Mechanism of true (not averaged) energy quantum emergence is described without approximations.
13. True origin of "+" and "-" charges in the Dirac equation $E = \pm\sqrt{m_e c^{24} + c^2 p^2}$ is shown.
14. Revealed is interference in the Michelson experiment and the resulting inconstancy of absolute velocity C = 300.000 km/sec.
15. Explained is the cause of light beam aberration from a star to the observer on the Earth.
16. Explanation is found for heavy ions to be retained at sufficient height from the Earth surface.
17. Found is the way to generate transuranium long-lasting elements.
18. Atomic nuclei can be constructed from nothing else but proton-neutron pairs; origin of the nucleons motion and their trajectories can be determined.

Mendeleev's Periodic System of Elements with Zero Group (in Grams)

Groups of Elements

Period	Row	0	I	II	III	IV	V	VI	VII	VIII		
1	I	ν 45.696	H 1 14.03						H 2 27.57			
2	II	He 2 32.503	Li 3 39*10	Be 4 43.449	B 5 78.877	C 6 94.584	N 7 113.022	O 8 137.239	F 9 148.966			
3	III	Ne 10 170.136	Na 11 210.487	Mg 12 223.597	Al 13 254.04	Si 14 270.09	P 15 284.277	S 16 306.952	Cl 17 324.751			
4	IV	Ar 18 342.252	K 19 382.488	Ca 20 398.355	Sc 21 418.76	Ti 22 440.339	V 23 463.50	Cr 24 486.705	Mn 25 509.313	Fe 26 523.445	Co 27 546.86	Ni 28 574.16
	V		Cu 29 587.47	Zn 30 613.252	Ga 31 654.78	Ge 32 665.13	As 33 679.95	Se 34 700.045	Br 35 707.017			
5	VI	Kr 36 733.897	Rb 37 839.08	Sr 38 864.45	Y 39 887.35	Zr 40 910.2	Nb 41 934.395	Mo 42 959.6	Tc 43 979.6	Ru 44 1006.5	Rh 45 1028.5	Pd 46 1050
	VII		Ag 47 1074.8	Cd 48 1096	In 49 1113.45	Sn 50 1132.74	Sb 51 1152.2	Te 52 1171.7	I 53 1191.2			
6	VIII	Xe 54 1210.62	Cs 55 1218.7	Ba 56 1226.75	La 57 1246.245	Hf 72 1586.77	Ta 73 1605.1	W 74 1609.68	Re 75 1645.23	Os 76 1664.74	Ir 77 1680.5	Pt 78 1699
	IX		Au 79 1734.65	Hg 80 1742.65	Tl 81 1750.705	Pb 82 1758.74	Bi 83 1760.75	Po 84 1774.78	At 85 1785.1	Rn 86 1793.15		
7	X		Fr 87 1840.21	Ra 88 1848.43	Ac 89 1856.3	Unq 104 2092.308	Unp 105	Unh 106	Uns 107	Une 108		

Lanthanide Series

Ce 58 1274.18	Pr 59 1297.14	Nd 60 1324.64	Pm 61 1343.05	Sm 62 1366.015	Eu 63 1388.97	Gd 64 1408.488	Tb 65 1434.89	Dy 66 1457.89	Ho 67 1480.85	Er 68 1503.76	Tm 69 1533.76	Yb 70 1549.33	Lu 71 1575.04

Actinide Series

Th 90 1864.21	Pa 91 1856.17	U 92 1885.5	Np 93 1906.82	Pu 94 1926.344	Am 95 1945.86	Cm 96 1952.89	Bk 97 1984.89	Cf 98 2004.4	Es 99 2039.99	Fm 100 2043.44	Md 101 2058.36	No 102 2066.24	Lr 103 2074.27

ν - Electron-positron pair - Neutrino, with microcharge e^{4} - $0.16*10^{-44}$ C.
The absolute atomic weights of all the elements are multiplied by 10^{-24} grams

POSSIBLE PALLADIUM-RELATED NUCLEAR REACTIONS

Shang-Xian Jin and Hal Fox [1]

ABSTRACT

The recent discoveries by Bockris and Minevski [1] and by Mizuno et al. [2] of apparent numerous low-temperature nuclear reactions has challenged current atomic models. By making the assumption that standard conservation laws for nuclear reactions would be preserved, a large variety of possible nuclear reactions have been proposed and checked for obeying conservation rules. The purpose of this paper is to present a list of some possible nuclear reactions between palladium isotopes and the following single particles: deuterons, protons, neutrons, and alpha particles.

A. INTRODUCTION

The recent reports of a considerable number of anomalous nuclear reactions reported by Bockris and Minevski [1] plus similar results reported by Mizuno, et al. [2] challenge the current atomic models. In order to get a better understanding of how such nuclear reactions **might possible occur**, the authors have compiled a list of **possible** nuclear reactions. In compiling this list, the authors have used the well-accepted concepts of conservation principles to determine which nuclear reactions involving deuterium (d), protons (p), neutrons (n), and alpha particles (α) could occur. Each resulting nuclear reaction has been checked for obeying the conservation rules of **energy, baryon number, charge, spin, parity, and isospin.** No attempt has been made to explain how the various particles can overcome the Coulomb barrier to cause such nuclear reactions. No attempt has been made to rank the reactions according to probabilities. Also, no attempt has been made to consider all of the possible nuclear reactions between the particles and the secondary nuclides produced. Some of the experimental results given in references [1] and [2] suggest that whatever process is promoting nuclear reactions with the palladium could possibly cause nuclear reactions to occur with isotopes or elements produced by the initial palladium nuclear reactions.

B. LIST OF POSSIBLE NUCLEAR REACTIONS

The following five sections list many (but not all) possible nuclear reactions. Section 1 list the reactions between deuterium and various stable palladium isotopes. Section 2 lists the possible nuclear reactions between protons and various stable palladium isotopes. Section 3 lists possible neutron reactions with stable palladium isotopes. Section 4 lists the possible nuclear reactions with alpha particles and various stable palladium isotopes. In sections 1 through 4, the end products from the nuclear reactions all produce smaller mass elements. In section 5, are listed some of the many nuclear reactions with stable palladium isotopes that can produce higher-mass isotopes and elements.

In all sections, when a radioactive or metastable nuclide results (marked with an *) the natural radioactive decay for that nuclide is shown indented from the left margin. For such nuclides, the half-life is given, and followed

[1] Fusion Information Center, P.O. Box 58639, Salt Lake City, UT 84158

by the chain of radioactive events (with the emission of alpha, beta, or gammas). The energies of the emitted particles are also shown. In all cases, the energy of radiation for alpha and beta particles are shown in Mev and the energy for gamma-ray emissions are shown in Kev.

The following are the list of symbols used:

symbols:		time:	
α	alpha particle	MS	milliseconds
β^-	negative electron	S	seconds
β^+	positron	M	minutes
γ	gamma ray	D	days
p	proton	A	years
d	deuteron		
n	neutron		
t	triton	*	radioactive or metastable nuclide
ε	electron capture	ω	weak
IT	isomeric transition	νω	very weak
e^-	conversion electron		

(energy of radiation in Mev for Alpha and Beta, Kev for gamma)

In section 5 the dotted lines (two places) indicates that there are many other possible nuclear reactions that could occur and obey the various conservation rules. The choices of reactions made by the authors were determined by analyzing data that was provided by Bockris and Minevski [1] and by Mizuno, et al. [2].

1. d + Pd → C + D + ...

$d + {}_{46}Pd^{106} \rightarrow {}_{45}Rh^{104*} + \alpha + 7.75$ Mev
$d + {}_{46}Pd^{108} \rightarrow {}_{45}Rh^{106*} + \alpha + 10.6$
$d + {}_{46}Pd^{110} \rightarrow {}_{45}Rh^{108*} + \alpha + 7.40$
${}_{45}Rh^{104*} \rightarrow$ 42.3 S:β^- 2.44: γ 555.8 $\rightarrow {}_{46}Pd^{104}$
${}_{45}Rh^{106*} \rightarrow$ 29.9S:β^- 3.54: γ 511.9,621.9 $\rightarrow {}_{46}Pd^{106}$
${}_{45}Rh^{108*} \rightarrow$ 17 S:β^- 4.5: γ 433.9, 618.8 $\rightarrow {}_{46}Pd^{108}$

$d + {}_{46}Pd^{102} \rightarrow {}_{3}Li^{6} + {}_{44}Ru^{98} - 0.66$
$d + {}_{46}Pd^{104} \rightarrow {}_{3}Li^{6} + {}_{44}Ru^{100} - 1.14$
$d + {}_{46}Pd^{105} \rightarrow {}_{3}Li^{6} + {}_{44}Ru^{101} - 1.70$
$d + {}_{46}Pd^{106} \rightarrow {}_{3}Li^{6} + {}_{44}Ru^{102} - 1.75$
$d + {}_{46}Pd^{108} \rightarrow {}_{3}Li^{6} + {}_{44}Ru^{104} + 0.619$
$d + {}_{46}Pd^{110} \rightarrow {}_{3}Li^{6} + {}_{44}Ru^{106*} - 2.97$
${}_{44}Ru^{106*} \rightarrow$ 1.02 A:β^- 0.0394 $\rightarrow {}_{45}Ph^{106*} \rightarrow$ 29.9S:β^- 3.54:γ 551.9, 621.9 $\rightarrow {}_{46}Pd^{106}$

$d + {}_{46}Pd^{102} \rightarrow {}_{3}Li^{6} + {}_{42}Mo^{94} + \alpha - 2.89$
$d + {}_{46}Pd^{104} \rightarrow {}_{3}Li^{6} + {}_{42}Mo^{96} + \alpha - 3.99$
$d + {}_{46}Pd^{105} \rightarrow {}_{3}Li^{6} + {}_{42}Mo^{97} + \alpha - 4.24$
$d + {}_{46}Pd^{106} \rightarrow {}_{3}Li^{6} + {}_{42}Mo^{98} + \alpha - 5.17$
$d + {}_{46}Pd^{108} \rightarrow {}_{3}Li^{6} + {}_{42}Mo^{100} + \alpha - 3.72$

$d + {}_{46}Pd^{104} \rightarrow {}_{4}Be^{6*} + {}_{43}Tc^{100*}$ - 8.80
$d + {}_{46}Pd^{106} \rightarrow {}_{4}Be^{8*} + {}_{43}Tc^{100*}$ + 4.14
$\rightarrow {}_{4}Be^{6*} + {}_{43}Tc^{102*}$ - 10.5
$d + {}_{46}Pd^{108} \rightarrow {}_{4}Be^{10*} + {}_{43}Tc^{100*}$ - 0.148
$\rightarrow {}_{4}Be^{8*} + {}_{43}Tc^{102*}$ + 6.27
$d + {}_{46}Pd^{110} \rightarrow {}_{4}Be^{10*} + {}_{43}Tc^{102*}$ - 3.21
$\rightarrow {}_{4}Be^{12*} + {}_{43}Tc^{100*}$ + 4.80
${}_{43}Tc^{100*} \rightarrow$ 15.8 S:β^- 3.4, 2.9; γ 539.5, 590.8 $\rightarrow {}_{44}Ru^{100}$
${}_{43}Tc^{102*} \rightarrow$ 4.4 M:β^- 1.8:γ 475.1, 628.1 $\rightarrow {}_{44}Ru^{102}$
$\rightarrow$ 5.3 S:β^- 4.2, 3.4, 2.2:γ 475.1 $\rightarrow {}_{44}Ru^{102}$

$d + {}_{46}Pd^{104} \rightarrow {}_{4}Be^{6*} + {}_{42}Mo^{99*}$ + p - 18.4
$d + {}_{46}Pd^{105} \rightarrow {}_{4}Be^{11*} + {}_{42}Mo^{95}$ + p - 15.0
$d + {}_{46}Pd^{106} \rightarrow {}_{4}Be^{6*} + {}_{42}Mo^{101*}$ + p - 18.9
$\rightarrow {}_{4}Be^{8*} + {}_{42}Mo^{99*}$ + p - 3.04
$d + {}_{46}Pd^{108} \rightarrow {}_{4}Be^{8*} + {}_{42}Mo^{101*}$ + p - 1.67
$\rightarrow {}_{4}Be^{10*} + {}_{42}Mo^{99*}$ + p - 7.33
$d + {}_{46}Pd^{110} \rightarrow {}_{4}Be^{10*} + {}_{42}Mo^{101*}$ + p - 11.6

$d + {}_{46}Pd^{106} \rightarrow {}_{4}Be^{6*} + {}_{42}Mo^{99*}$ + t - 24.1
$d + {}_{46}Pd^{108} \rightarrow {}_{4}Be^{6*} + {}_{42}Mo^{101*}$ + t - 23.2
$\rightarrow {}_{4}Be^{8*} + {}_{42}Mo^{99*}$ + t - 7.33
$d + {}_{46}Pd^{110} \rightarrow {}_{4}Be^{8*} + {}_{42}Mo^{101*}$ + t - 11.6
$\rightarrow {}_{4}Be^{10*} + {}_{42}Mo^{99*}$ + t - 16.8
${}_{42}Mo^{99*} \rightarrow$ 2.747 D:β^- 1.214:γ 140.5, 739.5 $\rightarrow {}_{43}Tc^{99*} \rightarrow$ 6.01 H; IT 142.7, 2.2(e^-), γ 140.5; β^- 0.435 $\rightarrow {}_{44}Ru^{99}$
${}_{42}Mo^{101*} \rightarrow$ 14.6 M:β^- 0.7, 2.23:γ 191.9, 590.9, 1012.5, 506.0 $\rightarrow {}_{43}Tc^{101*} \rightarrow$ 14.2 M:β^- 1.32:γ 306.8 $\rightarrow {}_{44}Ru^{101}$

$d + {}_{46}Pd^{106} \rightarrow {}_{4}Be^{6*} + {}_{41}Nb^{98*}$ + α - 1.41
$d + {}_{46}Pd^{108} \rightarrow {}_{4}Be^{8*} + {}_{41}Nb^{98*}$ + α + 2.75
$d + {}_{46}Pd^{110} \rightarrow {}_{4}Be^{10*} + {}_{41}Nb^{98*}$ + α - 6.73
${}_{4}Be^{6*} \rightarrow$ 5.0E-21 S: 2p, α
${}_{4}Be^{8*} \rightarrow$ 7E-17 S:2 α 0.0641
${}_{4}Be^{10*} \rightarrow$ 1.6E6 A:β^- 0.556 $\rightarrow {}_{5}B^{10}$
${}_{4}Be^{11*} \rightarrow$ 13.8 S:β^- 11.5, 9.4:γ 2124.5 $\rightarrow {}_{5}B^{11}$
${}_{4}Be^{12*} \rightarrow$ 12, MSβ^- $\rightarrow {}_{5}B^{12*} \rightarrow$ 20.20 MS:β^- 13.37:γ 4439 $\rightarrow {}_{6}C^{12}$
${}_{41}Nb^{98*} \rightarrow$ 51 M:β^- 2.3, 1.9:γ 787.3, 722.7 $\rightarrow {}_{42}Mo^{98}$
$\rightarrow$ 2.9 S:β^- 4.6:γ 787.3, 1024.0 $\rightarrow {}_{42}Mo^{98}$

$d + {}_{46}Pd^{105} \rightarrow {}_{5}B^{10} + {}_{42}Mo^{96}$ + n - 6.60

$d + {}_{46}Pd^{102} \rightarrow {}_{5}B^{12*} + {}_{42}Mo^{92}$ - 1.35
$d + {}_{46}Pd^{104} \rightarrow {}_{5}B^{12*} + {}_{42}Mo^{94}$ - 1.24
$d + {}_{46}Pd^{105} \rightarrow {}_{5}B^{12*} + {}_{42}Mo^{95}$ - 0.93

$d + {}_{46}Pd^{106} \rightarrow {}_{5}B^{12*} + {}_{42}Mo^{96}$ - 1.34
$d + {}_{46}Pd^{108} \rightarrow {}_{5}B^{12*} + {}_{42}Mo^{98}$ + 1.35
$d + {}_{46}Pd^{110} \rightarrow {}_{5}B^{12*} + {}_{42}Mo^{100}$ - 2.39

$d + {}_{46}Pd^{102} \rightarrow {}_{5}B^{10} + {}_{42}Mo^{96}$ + n - 6.60
$d + {}_{46}Pd^{105} \rightarrow {}_{5}B^{8*} + {}_{41}Nb^{98*}$ + p - 22.0
${}_{5}B^{8*} \rightarrow$ 770 MS:β^- 14; (α)8.359, (2α)1.57 $\rightarrow {}_{4}Be^{8}$
${}_{5}B^{12*} \rightarrow$ 20.2 MS:β^- 13.37;γ 4439, (α)0.2 $\rightarrow {}_{6}C^{12}$

$d + {}_{46}Pd^{106} \rightarrow {}_{6}C^{10*} + {}_{41}Nb^{98*}$ - 8.96
$d + {}_{46}Pd^{108} \rightarrow {}_{6}C^{12} + {}_{41}Nb^{98*}$ + 10.1
$d + {}_{46}Pd^{110} \rightarrow {}_{6}C^{14*} + {}_{41}Nb^{98*}$ - 5.29
${}_{41}Nb^{98*} \rightarrow$ 51 M:β^- 2.3, 1.9;γ 787.3, 722.7 $\rightarrow {}_{42}Mo^{98}$
$\rightarrow$ 2.9S:β^- 4.6;γ 787.3, 1024.0 $\rightarrow {}_{42}Mo^{98}$

$d + {}_{46}Pd^{106} \rightarrow {}_{6}C^{10*} + {}_{40}Zr^{97*}$ + p - 15.8
$d + {}_{46}Pd^{108} \rightarrow {}_{6}C^{12} + {}_{40}Zr^{97*}$ + p + 3.25
$d + {}_{46}Pd^{110} \rightarrow {}_{6}C^{14*} + {}_{40}Zr^{97*}$ + p - 15.8
$d + {}_{46}Pd^{112} \rightarrow {}_{6}C^{16*} + {}_{40}Zr^{97*}$ + p - 10.2

$d + {}_{46}Pd^{108} \rightarrow {}_{6}C^{10*} + {}_{40}Zr^{97*}$ + t - 20.1
$d + {}_{46}Pd^{110} \rightarrow {}_{6}C^{12} + {}_{40}Zr^{97*}$ + t - 6.22
$d + {}_{46}Pd^{112} \rightarrow {}_{6}C^{14*} + {}_{40}Zr^{97*}$ + t - 7.18
${}_{6}C^{10*} \rightarrow$ 19.3 S:β^- 1.87;γ 718.3 $\rightarrow {}_{5}B^{10}$
${}_{6}C^{14*} \rightarrow$ 5730 A:β^- 0.157 $\rightarrow {}_{7}N^{14}$
${}_{6}C^{16*} \rightarrow$ 0.75 S:β^- $\rightarrow {}_{7}N^{16*} \rightarrow$ 7.13 S:β^- 4.27, 10.44;γ 6129, 7115 $\rightarrow {}_{8}O^{16}$
${}_{40}Zr^{97*} \rightarrow$ 16.8 H:β^- 1.92;γ 743.3 $\rightarrow {}_{41}Nb^{97*} \rightarrow$ 1.23 H:β^- 1.27; γ 658 $\rightarrow {}_{42}Mo^{97}$

$d + {}_{46}Pd^{102} \rightarrow {}_{7}N^{12*} + {}_{40}Zr^{92}$ - 3.68
$d + {}_{46}Pd^{104} \rightarrow {}_{7}N^{12*} + {}_{40}Zr^{94}$ - 6.36
$\rightarrow {}_{7}N^{14} + {}_{40}Zr^{92}$ + 9.32
$d + {}_{46}Pd^{105} \rightarrow {}_{7}N^{14} + {}_{40}Zr^{93*}$ + 9.0
$\rightarrow {}_{7}N^{12*} + {}_{40}Zr^{95*}$ - 6.96
$d + {}_{46}Pd^{106} \rightarrow {}_{7}N^{14} + {}_{40}Zr^{94}$ + 7.63
$\rightarrow {}_{7}N^{12*} + {}_{40}Zr^{96}$ - 8.68
$d + {}_{46}Pd^{108} \rightarrow {}_{7}N^{12*} + {}_{40}Zr^{98*}$ - 9.46
$\rightarrow {}_{7}N^{14} + {}_{40}Zr^{96}$ + 9.21
$d + {}_{46}Pd^{110} \rightarrow {}_{7}N^{14} + {}_{40}Zr^{98*}$ + 3.21
${}_{40}Zr^{93*} \rightarrow$ 1.5E6 A:β^- 0.060;γ 30.4 $\rightarrow {}_{41}Nb^{93}$
${}_{40}Zr^{95*} \rightarrow$ 64.02 D:β^- 0.366, 0.40;γ 756.7, 724.2 $\rightarrow {}_{41}Nb^{95*} \rightarrow$ 3.61 D:β^- 1.16;γ 204.1 $\rightarrow {}_{42}Mo^{95}$
$\rightarrow$ 34.97 D:β^- 0.160;γ 765.8 $\rightarrow {}_{42}Mo^{95}$
${}_{40}Zr^{98*} \rightarrow$ 30.7 S:β^- 2.2 $\rightarrow {}_{41}Nb^{98*} \rightarrow$ 51 M:β^- 2.3, 1.9;γ 787.3, 722.7 $\rightarrow {}_{42}Mo^{98}$
$\rightarrow$ 2.9 S:β^- 4.6;γ 787.3, 1024.0 $\rightarrow {}_{42}Mo^{98}$

$d + {}_{46}Pd^{105} \rightarrow {}_{7}N^{14} + {}_{38}Sr^{89*} + \alpha + 8.63$
$d + {}_{46}Pd^{106} \rightarrow {}_{7}N^{12*} + {}_{38}Sr^{92*} + \alpha - 13.6$
$\rightarrow {}_{7}N^{14} + {}_{38}Sr^{90*} + \alpha + 0.597$

$d + {}_{46}Pd^{108} \rightarrow {}_{7}N^{12*} + {}_{38}Sr^{94*} + \alpha - 14.4$
$\rightarrow {}_{7}N^{14} + {}_{38}Sr^{92*} + \alpha + 4.25$
$d + {}_{46}Pd^{110} \rightarrow {}_{7}N^{14} + {}_{38}Sr^{94*} + \alpha - 1.75$
${}_{7}N^{12*} \rightarrow \underline{11.0\ M;\beta^-}\ \underline{16.3;\gamma\ 4439;(3\alpha)0.192} \rightarrow {}_{6}C^{12}$

$d + {}_{46}Pd^{102} \rightarrow {}_{9}F^{18*} + {}_{38}Sr^{86} + 8.85$
$d + {}_{46}Pd^{104} \rightarrow {}_{9}F^{18*} + {}_{38}Sr^{88} + 10.6$
$d + {}_{46}Pd^{105} \rightarrow {}_{9}F^{18*} + {}_{38}Sr^{89*} + 10.1$
$d + {}_{46}Pd^{106} \rightarrow {}_{9}F^{18*} + {}_{38}Sr^{90*} + 8.29$
$d + {}_{46}Pd^{108} \rightarrow {}_{9}F^{18*} + {}_{38}Sr^{92*} + 8.66$
$d + {}_{46}Pd^{110} \rightarrow {}_{9}F^{18*} + {}_{38}Sr^{94*} + 2.66$

$d + {}_{46}Pd^{102} \rightarrow {}_{9}F^{19} + {}_{38}Sr^{84} + n - 3.10$
$d + {}_{46}Pd^{104} \rightarrow {}_{9}F^{19} + {}_{38}Sr^{86} + n - 0.71$
$d + {}_{46}Pd^{106} \rightarrow {}_{9}F^{19} + {}_{38}Sr^{88} + n + 2.20$
$d + {}_{46}Pd^{108} \rightarrow {}_{9}F^{19} + {}_{38}Sr^{90*} + n + 3.59$
$d + {}_{46}Pd^{110} \rightarrow {}_{9}F^{19} + {}_{38}Sr^{92*} + n - 1.23$
${}_{38}Sr^{89*} \rightarrow \underline{50.52\ D;\beta^-}\ \underline{1.49;\gamma\ 909.2} \rightarrow {}_{39}Y^{89}$
${}_{38}Sr^{90*} \rightarrow \underline{29.1\ A;\beta^-}\ \underline{0.546} \rightarrow {}_{39}Y^{90*} \rightarrow \underline{2.67\ D;\beta^-\ \nu\omega}\ \underline{2.281;\gamma\ 2186.2} \rightarrow {}_{40}Zr^{90}$
$\rightarrow \underline{3.19\ H;\ IT\ 479.5;\gamma\ 202.5}\beta^-\ \omega;\gamma\ \underline{2318.9} \rightarrow {}_{40}Zr^{90}$
${}_{38}Sr^{92*} \rightarrow \underline{2.71\ H;\beta^-}\ \underline{0.54;\gamma\ 1384.0} \rightarrow {}_{39}Y^{92*} \rightarrow \underline{3.54\ H;\beta^-}\ \underline{3.64;\gamma\ 934.5,\ 1405.4} \rightarrow {}_{40}Zr^{92}$
${}_{38}Sr^{94*} \rightarrow \underline{1.25\ M;\beta^-}\ \underline{2.08;\ \gamma\ 1427.6} \rightarrow {}_{39}Y^{94*} \rightarrow \underline{18.7\ M;\beta^-}\ \underline{4.92;\gamma\ 918.7,\ 1138.9,\ 550.9} \rightarrow {}_{40}Zr^{94}$

$d + {}_{46}Pd^{102} \rightarrow {}_{9}F^{18*} + {}_{36}Kr^{82} + \alpha + 2.50$
$d + {}_{46}Pd^{104} \rightarrow {}_{9}F^{18*} + {}_{36}Kr^{84} + \alpha + 2.86$
$d + {}_{46}Pd^{106} \rightarrow {}_{9}F^{18*} + {}_{36}Kr^{86} + \alpha + 3.20$
${}_{9}F^{18*} \rightarrow \underline{1.830\ H;\beta^-}\ \underline{0.635,\varepsilon} \rightarrow {}_{8}O^{18}$

$d + {}_{46}Pd^{102} \rightarrow {}_{10}Ne^{24*} + {}_{37}Rb^{80*} + 3.29$
$\rightarrow {}_{10}Ne^{22*} + {}_{37}Rb^{82*} + 5.90$
$d + {}_{46}Pd^{104} \rightarrow {}_{10}Ne^{24*} + {}_{37}Rb^{82*} + 7.94$
${}_{37}Rb^{80*} \rightarrow \underline{34\ S;\beta^-}\ \underline{4.1;\ \varepsilon;\gamma\ 616.6} \rightarrow {}_{36}Kr^{80}$
${}_{37}Rb^{82*} \rightarrow \underline{6.47\ H;\ \varepsilon;\beta^-}\ \underline{0.80;\gamma\ 776.5,\ 554.3,\ 619.1} \rightarrow {}_{36}Kr^{82}$
$\rightarrow \underline{1.258\ M;\beta^-}\ \underline{3.4;\ \varepsilon;\gamma\ 776.5} \rightarrow {}_{36}Kr^{82}$

$d + {}_{46}Pd^{102} \rightarrow {}_{10}Ne^{19*} + {}_{36}Kr^{84} + p - 14.0$
$d + {}_{46}Pd^{104} \rightarrow {}_{10}Ne^{19*} + {}_{36}Kr^{86} + p - 2.06$
$d + {}_{46}Pd^{104} \rightarrow {}_{10}Ne^{19*} + {}_{36}Kr^{88*} + p - 6.10$

$d + {}_{46}Pd^{104} \rightarrow {}_{10}Ne^{19*} + {}_{36}Kr^{84} + t - 10.5$

$d + {}_{46}Pd^{106} \rightarrow {}_{10}Ne^{19*} + {}_{36}Kr^{86} + t - 9.85$

$d + {}_{46}Pd^{108} \rightarrow {}_{10}Ne^{19*} + {}_{36}Kr^{88*} + t - 10.4$

${}_{36}Kr^{88*} \rightarrow$ 2.84 H;β^- 0.52, 2.9;γ 2392.1, 196.3 $\rightarrow {}_{37}Rb^{88*} \rightarrow$ 17.1 M;β^- 5.31;γ 1836.1, 898.1 $\rightarrow {}_{38}Sr^{88}$

$d + {}_{46}Pd^{104} \rightarrow {}_{10}Ne^{24*} + {}_{35}Br^{78*} + \alpha + 0.74$

$\rightarrow {}_{10}Ne^{22} + {}_{35}Br^{80*} + \alpha + 5.21$

$d + {}_{46}Pd^{105} \rightarrow {}_{10}Ne^{23} + {}_{35}Br^{80*} + \alpha + 3.33$

$d + {}_{46}Pd^{106} \rightarrow {}_{10}Ne^{24*} + {}_{35}Br^{80*} + \alpha + 2.68$

${}_{10}Ne^{19*} \rightarrow$ 17.22 S;β^- 2.24; $\varepsilon;\gamma$ 109.9, 1356.8 $\rightarrow {}_{9}F^{19}$

${}_{10}Ne^{24*} \rightarrow$ 3.38 M;β^- 1.98;γ 427.3 $\rightarrow {}_{11}Na^{24*}$

${}_{11}Na^{24*} \rightarrow$ 14.96 H;β^- 1.391;γ 1368.6, 2754.0 $\rightarrow {}_{12}Mg^{24}$

$\rightarrow$ 20.2 MS; IT 472.3; β^- ~6 $\rightarrow {}_{12}Mg^{24}$

$d + {}_{46}Pd^{102} \rightarrow {}_{12}Mg^{26} + {}_{35}Br^{78*} + 14.9$

$d + {}_{46}Pd^{104} \rightarrow {}_{12}Mg^{26} + {}_{35}Br^{80*} + 15.8$

$\rightarrow {}_{12}Mg^{28*} + {}_{35}Br^{78*} + 12.2$

$d + {}_{46}Pd^{106} \rightarrow {}_{12}Mg^{28*} + {}_{35}Br^{80*} + 14.1$

${}_{35}Br^{78*} \rightarrow$ 6.45 M;β^- 2.5, $\varepsilon;\gamma$ 613.7 $\rightarrow {}_{34}Se^{78}$

$\rightarrow$ 6.45 M;β^- γ ?ω $\rightarrow {}_{36}Kr^{78}$

${}_{35}Br^{80*} \rightarrow$ 17.66 M;β^- 2.00;γ 616.6 $\rightarrow {}_{36}Kr^{80}$

$\rightarrow$ 17.66 M;ε,β^- 0.85;γ 665.9 $\rightarrow {}_{34}Se^{80}$

$d + {}_{46}Pd^{104} \rightarrow {}_{12}Mg^{27*} + {}_{34}Se^{78} + p + 8.05$

$d + {}_{46}Pd^{106} \rightarrow {}_{12}Mg^{27*} + {}_{34}Se^{80} + p + 8.29$

$d + {}_{46}Pd^{108} \rightarrow {}_{12}Mg^{27*} + {}_{34}Se^{82} + p + 11.5$

$d + {}_{46}Pd^{106} \rightarrow {}_{12}Mg^{27*} + {}_{34}Se^{78} + t - 0.105$

$d + {}_{46}Pd^{108} \rightarrow {}_{12}Mg^{27*} + {}_{34}Se^{80} + t + 4.00$

$d + {}_{46}Pd^{110} \rightarrow {}_{12}Mg^{27*} + {}_{34}Se^{82} + t + 2.02$

$d + {}_{46}Pd^{106} \rightarrow {}_{12}Mg^{24} + {}_{33}As^{80*} + \alpha + 6.50$

$d + {}_{46}Pd^{108} \rightarrow {}_{12}Mg^{26} + {}_{33}As^{80*} + \alpha + 12.2$

$d + {}_{46}Pd^{110} \rightarrow {}_{12}Mg^{28*} + {}_{33}As^{80*} + \alpha + 9.15$

${}_{12}Mg^{22*} \rightarrow$ 3.86 S;β^- 3.1;γ 582, 72.9 $\rightarrow {}_{11}Na^{22*} \rightarrow$ 2.605 A;β^- 0.546, $\varepsilon;\gamma$ 1274.5 $\rightarrow {}_{10}Ne^{22}$

${}_{12}Mg^{27*} \rightarrow$ 9.45 M;β^- 1.75, 1.59; $\varepsilon;\gamma$ 843.8, 1014.4 $\rightarrow {}_{13}Al^{27}$

${}_{12}Mg^{28*} \rightarrow$ 21.0 H;β^- 0.459;γ 30.6, 1342.3 $\rightarrow {}_{13}Al^{28*} \rightarrow$ 2.25 M;β^- 2.86; γ1179.0 $\rightarrow {}_{14}Si^{28}$

$d + {}_{46}Pd^{104} \rightarrow {}_{14}Si^{26*} + {}_{33}As^{80*} + 2.63$

$d + {}_{46}Pd^{105} \rightarrow {}_{14}Si^{27*} + {}_{33}As^{80*} + 8.86$

$d + {}_{46}Pd^{106} \rightarrow {}_{14}Si^{28*} + {}_{33}As^{80*} + 16.5$

$d + {}_{46}Pd^{108} \rightarrow {}_{14}Si^{30} + {}_{33}As^{80*} + 22.8$

$d + {}_{46}Pd^{110} \rightarrow {}_{14}Si^{32*} + {}_{33}As^{80*} + 20.6$

${}_{33}As^{80*} \rightarrow$ 16 S;β^- 5.4, 4.7;γ 665.9 $\rightarrow {}_{34}Se^{80}$

$d + {}_{46}Pd^{104} \rightarrow {}_{14}Si^{29} + {}_{32}Ge^{76} + p + 11.5$
$d + {}_{46}Pd^{106} \rightarrow {}_{14}Si^{29} + {}_{32}Ge^{78*} + p + 9.62$

$d + {}_{46}Pd^{106} \rightarrow {}_{14}Si^{29} + {}_{32}Ge^{76} + t + 3.39$
$d + {}_{46}Pd^{108} \rightarrow {}_{14}Si^{29} + {}_{32}Ge^{78*} + t + 5.33$

$d + {}_{46}Pd^{102} \rightarrow {}_{14}Si^{30} + {}_{31}Ga^{70*} + \alpha + 16.12$
$\rightarrow {}_{14}Si^{32*} + {}_{31}Ga^{68*} + \alpha + 14.0$
$d + {}_{46}Pd^{104} \rightarrow {}_{14}Si^{32*} + {}_{31}Ga^{70*} + \alpha + 14.3$
${}_{14}Si^{26*} \rightarrow \underline{2.23\ S;\beta^-\ 3.83;\gamma\ 829} \rightarrow {}_{13}Al^{26*} \rightarrow \underline{6.345\ S;\beta^-\ 3.21} \rightarrow {}_{12}Mg^{26}$
$\rightarrow \underline{7.3E5\ A;\beta^-\ 1.17;\ \varepsilon;\gamma\ 1808.6} \rightarrow {}_{12}Mg^{26}$
${}_{14}Si^{27*} \rightarrow \underline{4.14\ S;\beta^-\ 3.85;\gamma\ 2210} \rightarrow {}_{13}Al^{27}$
${}_{14}Si^{32*} \rightarrow \underline{1.0E2\ A;\beta^-\ 0.221} \rightarrow {}_{15}P^{32*} \rightarrow \underline{14.28\ D;\beta^-\ 1.709} \rightarrow {}_{16}S^{32}$
${}_{31}Ga^{68*} \rightarrow \underline{1.130\ H;\beta^-\ 1.899,\varepsilon;\gamma\ 1077.3} \rightarrow {}_{30}Zn^{68}$
${}_{31}Ga^{70*} \rightarrow \underline{21.1\ M;\beta^-\ 1.65;\gamma\ 1039,176.2} \rightarrow {}_{32}Ge^{70}$
${}_{33}As^{80*} \rightarrow \underline{16\ S;\beta^-\ 5.4,4.7;\ 665.9} \rightarrow {}_{34}Se^{80}$

$d + {}_{46}Pd^{102} \rightarrow {}_{15}P^{30*} + {}_{32}Ge^{74} + 23.1$
$\rightarrow {}_{15}P^{32*} + {}_{32}Ge^{72} + 22.1$
$\rightarrow {}_{15}P^{34*} + {}_{32}Ge^{70} + 20.6$

$d + {}_{46}Pd^{104} \rightarrow {}_{15}P^{30*} + {}_{32}Ge^{76} + 21.4$
$\rightarrow {}_{15}P^{32*} + {}_{32}Ge^{74} + 21.5$
$\rightarrow {}_{15}P^{34*} + {}_{32}Ge^{72} + 21.1$
$d + {}_{46}Pd^{106} \rightarrow {}_{15}P^{30*} + {}_{32}Ge^{78*} + 19.4$
$\rightarrow {}_{15}P^{32*} + {}_{32}Ge^{76} + 20.8$
$\rightarrow {}_{15}P^{34*} + {}_{32}Ge^{74} + 21.5$
$d + {}_{46}Pd^{108} \rightarrow {}_{15}P^{32*} + {}_{32}Ge^{78*} + 22.7$
$\rightarrow {}_{15}P^{34*} + {}_{32}Ge^{76} + 24.7$
$d + {}_{46}Pd^{110} \rightarrow {}_{15}P^{34*} + {}_{32}Ge^{78*} + 21.4$

$d + {}_{46}Pd^{102} \rightarrow {}_{15}P^{29*} + {}_{32}Ge^{74} + n + 7.51$
$\rightarrow {}_{15}P^{31} + {}_{32}Ge^{72} + n + 14.2$
$\rightarrow {}_{15}P^{33*} + {}_{32}Ge^{70} + n + 14.1$
$d + {}_{46}Pd^{104} \rightarrow {}_{15}P^{29*} + {}_{32}Ge^{76} + n + 5.82$
$\rightarrow {}_{15}P^{31} + {}_{32}Ge^{74} + n + 13.5$
$\rightarrow {}_{15}P^{33*} + {}_{32}Ge^{72} + n + 14.6$
$d + {}_{46}Pd^{105} \rightarrow {}_{15}P^{28*} + {}_{32}Ge^{78*} + n - 4.42$
$d + {}_{46}Pd^{106} \rightarrow {}_{15}P^{29*} + {}_{32}Ge^{78*} + n + 3.89$
$\rightarrow {}_{15}P^{31} + {}_{32}Ge^{76} + n + 12.8$
$\rightarrow {}_{15}P^{33*} + {}_{32}Ge^{74} + n + 15.0$
$d + {}_{46}Pd^{108} \rightarrow {}_{15}P^{31} + {}_{32}Ge^{78*} + n + 14.8$
$\rightarrow {}_{15}P^{33*} + {}_{32}Ge^{76} + n + 18.1$

$d + {}_{46}Pd^{110} \rightarrow {}_{15}P^{33*} + {}_{32}Ge^{78*} + n + 14.9$

${}_{32}Ge^{78*} \rightarrow \underline{1.45\ H;\beta^-}\ \underline{0.70;\gamma\ 277} \rightarrow {}_{33}As^{78*} \rightarrow \underline{1.512\ H;\beta^-}\ \underline{4.3,\ 3.7,\ 3.0,\ 1.7;\gamma\ 613.7,\ 694.9,\ 1308.7} \rightarrow {}_{34}Se^{78}$

$d + {}_{46}Pd^{102} \rightarrow {}_{15}P^{30*} + {}_{30}Zn^{70} + \alpha + 12.5$

$\rightarrow {}_{15}P^{32*} + {}_{30}Zn^{68} + \alpha + 17.1$

$\rightarrow {}_{15}P^{34*} + {}_{30}Zn^{66} + \alpha + 16.5$

$d + {}_{46}Pd^{104} \rightarrow {}_{15}P^{30*} + {}_{30}Zn^{72*} + \alpha + 9.64$

$\rightarrow {}_{15}P^{32*} + {}_{30}Zn^{70} + \alpha + 15.2$

$\rightarrow {}_{15}P^{34*} + {}_{30}Zn^{68} + \alpha + 16.1$

$d + {}_{46}Pd^{106} \rightarrow {}_{15}P^{32*} + {}_{30}Zn^{72*} + \alpha + 13.2$

$\rightarrow {}_{15}P^{34*} + {}_{30}Zn^{70} + \alpha + 15.2$

$d + {}_{46}Pd^{108} \rightarrow {}_{15}P^{34*} + {}_{30}Zn^{72*} + \alpha + 17.2$

${}_{15}P^{28*} \rightarrow \underline{0.270\ S;\beta^-}\ \underline{11.5;\gamma\ 1779.0} \rightarrow {}_{14}Si^{28}$

${}_{15}P^{29*} \rightarrow \underline{4.14\ S;\beta^-}\ \underline{3.94;\gamma\ 1273.4,\ 2425.9} \rightarrow {}_{14}Si^{29}$

${}_{15}P^{30*} \rightarrow \underline{2.50\ M;\beta^-}\ \underline{3.24;\ \varepsilon;\gamma\ 2235.2} \rightarrow {}_{14}Si^{30}$

${}_{15}P_{32*} \rightarrow \underline{14.28\ D;\beta^-}\ \underline{1.709} \rightarrow {}_{16}S^{32}$

${}_{15}P^{33*} \rightarrow \underline{25.3\ D;\beta^-}\ \underline{0.249} \rightarrow {}_{16}S^{33}$

${}_{15}P^{34*} \rightarrow \underline{12.4\ S;\beta^-}\ \underline{5.1,\ 3.2;\gamma\ 2127.7} \rightarrow {}_{16}S^{34}$

$d + {}_{46}Pd^{102} \rightarrow {}_{16}S^{36} + {}_{31}Ga^{68*} + 23.0$

$d + {}_{46}Pd^{104} \rightarrow {}_{16}S^{36} + {}_{31}Ga^{70*} + 23.3$

$\rightarrow {}_{16}S^{38*} + {}_{31}Ga^{68*} + 17.7$

$d + {}_{46}Pd^{106} \rightarrow {}_{16}S^{38*} + {}_{31}Ga^{70*} + 19.0$

${}_{31}Ga^{68*} \rightarrow \underline{1.130\ H;\beta^-}\ \underline{1.899;\gamma\ 1077.3} \rightarrow {}_{30}Zn^{68}$

${}_{31}Ga^{70*} \rightarrow \underline{21.1\ M;\beta^-}\ \underline{1.65;\gamma\ 1039,\ 176.2} \rightarrow {}_{32}Ge^{70}$

$d + {}_{46}Pd^{102} \rightarrow {}_{16}S^{31*} + {}_{30}Zn^{72*} + p + 5.05$

${}_{30}Zn^{72*} \rightarrow \underline{46.5\ H;\beta^-}\ \underline{0.30;\gamma\ 144.7} \rightarrow {}_{31}Ga^{72*} \rightarrow \underline{144.10\ H;\beta^-}\ \underline{0.96,0.64;\gamma\ 834.1,\ 2201.7,\ 630} \rightarrow {}_{32}Ge^{72}$

$d + {}_{46}Pd^{102} \rightarrow {}_{16}S^{38*} + {}_{29}Cu^{62*} + \alpha + 12.5$

$\rightarrow {}_{16}S^{36} + {}_{29}Cu^{64*} + \alpha + 18.9$

$\rightarrow {}_{16}S^{34} + {}_{29}Cu^{66*} + \alpha + 19.0$

$\rightarrow {}_{16}S^{32} + {}_{29}Cu^{68*} + \alpha + 14.9$

$d + {}_{46}Pd^{104} \rightarrow {}_{16}S^{38*} + {}_{29}Cu^{64*} + \alpha + 13.6$

$\rightarrow {}_{16}S^{36} + {}_{29}Cu^{66*} + \alpha + 18.2$

$\rightarrow {}_{16}S^{34} + {}_{29}Cu^{68*} + \alpha + 16.6$

$d + {}_{46}Pd^{106} \rightarrow {}_{16}S^{38*} + {}_{29}Cu^{66*} + \alpha + 13.9$

$\rightarrow {}_{16}S^{38*} + {}_{29}Cu^{68*} + \alpha + 16.9$

$d + {}_{46}Pd^{108} \rightarrow {}_{16}S^{38*} + {}_{29}Cu^{68*} + \alpha + 16.5$

$\rightarrow {}_{16}S^{31*} \rightarrow \underline{2.56\ S;\beta^-}\ \underline{4.39;\gamma\ 1286.2} \rightarrow {}_{15}P^{31}$

$\rightarrow {}_{16}S^{38*} \rightarrow \underline{2.84\ H;\beta^-}\ \underline{0.99;\gamma\ 1941.9} \rightarrow {}_{17}Cl^{38*} \rightarrow \underline{37.2\ M;\beta^-}\ \underline{4.91,\ 1.11;\gamma\ 2167.6,\ 1642.4} \rightarrow {}_{18}Ar^{38}$

$d + {}_{46}Pd^{102} \rightarrow {}_{18}Ar^{40} + {}_{29}Cu^{64*} + 25.7$

$\rightarrow {}_{18}Ar^{42*} + {}_{29}Cu^{62*} + 22.4$

$d + {}_{46}Pd^{104} \rightarrow {}_{18}Ar^{40} + {}_{29}Cu^{66*} + 25.0$

$\rightarrow {}_{18}Ar^{42*} + {}_{29}Cu^{64*} + 23.6$

$d + {}_{46}Pd^{106} \rightarrow {}_{18}Ar^{40} + {}_{29}Cu^{68*} + 23.7$

$\rightarrow {}_{18}Ar^{42*} + {}_{29}Cu^{66*} + 23.9$

$d + {}_{46}Pd^{108} \rightarrow {}_{18}Ar^{42*} + {}_{29}Cu^{68*} + 26.5$

${}_{18}Ar^{42*} \rightarrow \underline{33\ A;\beta^-} \rightarrow {}_{19}K^{42*} \rightarrow \underline{12.36\ H;\beta^-\ 3.52;\gamma\ 1524.6} \rightarrow {}_{20}Ca^{42}$

${}_{29}Cu^{62*} \rightarrow \underline{9.74\ M;\beta^-\ 2.93;\ \varepsilon;\ \gamma\ 1173.0,\ 875.7} \rightarrow {}_{28}Ni^{62}$

${}_{29}Cu^{64*} \rightarrow \underline{12.70\ H;\ \varepsilon;\beta^-\ 0.578;\gamma\ 1345.8} \rightarrow {}_{30}Zn^{64}$

$\rightarrow \underline{12.70\ H;\beta^-\ 0.651} \rightarrow {}_{28}Ni^{64}$

${}_{29}Cu^{66*} \rightarrow \underline{5.10\ M;\beta^-\ 2.63;\gamma\ 1039.3} \rightarrow {}_{30}Zn^{66}$

${}_{29}Cu^{68*} \rightarrow \underline{31\ S;\beta^-\ 3.5,\ 4.6;\gamma\ 1077.3,\ 1261.2} \rightarrow {}_{30}Zn^{68}$

$d + {}_{46}Pd^{104} \rightarrow {}_{19}K^{47*} + {}_{28}Ni^{58} + n + 11.6$

$d + {}_{46}Pd^{106} \rightarrow {}_{19}K^{47*} + {}_{28}Ni^{60} + n + 15.3$

$d + {}_{46}Pd^{108} \rightarrow {}_{19}K^{47*} + {}_{28}Ni^{62} + n + 21.0$

$d + {}_{46}Pd^{110} \rightarrow {}_{19}K^{47*} + {}_{28}Ni^{64} + n + 19.0$

${}_{19}K^{47*} \rightarrow \underline{17.5\ S;\beta^-\ 4.0;\gamma\ 2013.4,\ 586.0} \rightarrow {}_{20}Ca^{47*}$

${}_{20}Ca^{47*} \rightarrow \underline{4.536\ D;\beta^-\ 0.694,\ 1.990;\gamma\ 1297.1} \rightarrow {}_{21}Sc^{47*} \rightarrow \underline{3.349\ D;\beta^-\ 0.439,\ 0.600;\gamma\ 159.4} \rightarrow {}_{22}Ti^{47}$

$d + {}_{46}Pd^{108} \rightarrow {}_{20}Ca^{46} + {}_{27}Co^{64*} + 33.8$

$d + {}_{46}Pd^{110} \rightarrow {}_{20}Ca^{48} + {}_{27}Co^{64*} + 36.1$

${}_{27}Co^{64*} \rightarrow \underline{0.30\ S;\beta^-\ 7.0;\gamma\ 1345.8,\ 931.1} \rightarrow {}_{28}Ni^{64}$

$d + {}_{46}Pd^{105} \rightarrow {}_{22}Ti^{52*} + {}_{25}Mn^{54*} + n + 21.7$

${}_{25}Mn^{54*} \rightarrow \underline{312.2\ D;\ \varepsilon;\gamma\ 834.8} \rightarrow {}_{24}Cr^{54}$

${}_{22}Ti^{52*} \rightarrow \underline{1.7\ M;\beta^-\ 1.8;\gamma\ 124.5,\ 17.0} \rightarrow {}_{23}V^{52*} \rightarrow \underline{3.76\ M;\beta^-\ 2.47;\ \gamma\ 1434.1} \rightarrow {}_{24}Cr^{52}$

2. p + Pd → C + D + . . .

$p + {}_{46}Pd^{105} \rightarrow {}_{5}B^{10} + {}_{42}Mo^{96} - 4.38\ Mev$

$p + {}_{46}Pd^{104} \rightarrow {}_{9}F^{19} + {}_{38}Sr^{86} + 1.51$

$p + {}_{46}Pd^{106} \rightarrow {}_{9}F^{19} + {}_{38}Sr^{88} + 4.42$

$p + {}_{46}Pd^{108} \rightarrow {}_{9}F^{19} + {}_{38}Sr^{90*} + 2.83$

$p + {}_{46}Pd^{110} \rightarrow {}_{9}F^{19} + {}_{38}Sr^{92*} + 0.996$

${}_{38}Sr^{90*} \rightarrow \underline{29.1\ A;\beta^-\ 0.456} \rightarrow {}_{39}Y^{90*} \rightarrow \underline{2.67\ D;\beta^-\ 2.281;\gamma\ 2186.2} \rightarrow {}_{40}Zr^{90}$

$\rightarrow \underline{3.19\ H;\ IT\ 479.5;\gamma\ 202.5;\beta^-\ ;\gamma\ 2318.9} \rightarrow {}_{40}Zr^{90}$

${}_{38}Sr^{92*} \rightarrow \underline{2.71\ H;\beta^-\ 0.54;\gamma\ 1384.0} \rightarrow {}_{39}Y^{92*} \rightarrow \underline{3.54\ H;\beta^-\ 3.64;\gamma\ 934.5,\ 1405.4} \rightarrow {}_{40}Zr^{92}$

$p + {}_{46}Pd^{102} \rightarrow {}_{9}F^{19} + {}_{36}Kr^{80} + \alpha - 6.65$

$p + {}_{46}Pd^{104} \rightarrow {}_{9}F^{19} + {}_{36}Kr^{82} + \alpha - 2.47$

$p + {}_{46}Pd^{106} \rightarrow {}_{9}F^{19} + {}_{36}Kr^{84} + \alpha - 1.12$

$p + {}_{46}Pd^{108} \rightarrow {}_{9}F^{19} + {}_{36}Kr^{86} + \alpha + 0.10$

$p + {}_{46}Pd^{110} \rightarrow {}_{9}F^{19} + {}_{36}Kr^{88*} + \alpha - 2.29$

${}_{36}Kr^{88*} \rightarrow \underline{2.84\ H;\beta^-}\ \underline{0.52, 2.9;\gamma\ 2392.1, 196.3} \rightarrow {}_{37}Rb^{88*} \rightarrow \underline{17.7\ M;\beta^-}\ \underline{5.31;\gamma\ 1836.1, 898.1} \rightarrow {}_{38}Sr^{88}$

$p + {}_{46}Pd^{105} \rightarrow {}_{11}Na^{22*} + {}_{36}Kr^{84} + 6.49$

$p + {}_{46}Pd^{105} \rightarrow {}_{11}Na^{22*} + {}_{34}Se^{80} + \alpha - 0.61$

${}_{11}Na^{22*} \rightarrow \underline{2.605\ A;\beta^-}\ \underline{0.546,\ \varepsilon;\gamma\ 1274.5} \rightarrow {}_{10}Ne^{22}$

$p + {}_{46}Pd^{105} \rightarrow {}_{13}Al^{28*} + {}_{34}Se^{78} + 12.8$

$p + {}_{46}Pd^{105} \rightarrow {}_{13}Al^{28*} + {}_{32}Ge^{74} + \alpha + 6.72$

${}_{13}Al^{28*} \rightarrow \underline{2.25\ M;\beta^-}\ \underline{2.86,\ \varepsilon;\gamma\ 1779.0} \rightarrow {}_{14}Si^{28}$

$p + {}_{46}Pd^{102} \rightarrow {}_{15}P^{29*} + {}_{32}Ge^{74} + 9.73$

$p + {}_{46}Pd^{102} \rightarrow {}_{15}P^{31} + {}_{32}Ge^{72} + 16.4$

$p + {}_{46}Pd^{102} \rightarrow {}_{15}P^{33*} + {}_{32}Ge^{70} + 14.3$

$p + {}_{46}Pd^{104} \rightarrow {}_{15}P^{29*} + {}_{32}Ge^{76} + 8.04$

$p + {}_{46}Pd^{104} \rightarrow {}_{15}P^{31} + {}_{32}Ge^{74} + 15.7$

$p + {}_{46}Pd^{104} \rightarrow {}_{15}P^{33*} + {}_{32}Ge^{72} + 14.8$

$p + {}_{46}Pd^{105} \rightarrow {}_{15}P^{28*} + {}_{32}Ge^{78*} - 2.19$

$p + {}_{46}Pd^{106} \rightarrow {}_{15}P^{29*} + {}_{32}Ge^{78*} + 6.12$

$p + {}_{46}Pd^{106} \rightarrow {}_{15}P^{31} + {}_{32}Ge^{76} + 15.0$

$p + {}_{46}Pd^{106} \rightarrow {}_{15}P^{33*} + {}_{32}Ge^{74} + 15.1$

$p + {}_{46}Pd^{108} \rightarrow {}_{15}P^{31} + {}_{32}Ge^{78*} + 13.9$

$p + {}_{46}Pd^{108} \rightarrow {}_{15}P^{33*} + {}_{32}Ge^{76} + 15.3$

$p + {}_{46}Pd^{110} \rightarrow {}_{15}P^{33*} + {}_{32}Ge^{78*} + 10.2$

${}_{15}P^{28*} \rightarrow \underline{0.270\ S;\beta^-}\ \underline{11.5;\gamma\ 1779.0} \rightarrow {}_{14}Si^{28}$

${}_{15}P^{29*} \rightarrow \underline{4.14\ S;\beta^-}\ \underline{3.94;\gamma\ 1273.4, 2425.9} \rightarrow {}_{14}Si^{29}$

${}_{15}P^{33*} \rightarrow \underline{25.3\ D;\beta^-}\ \underline{0.249} \rightarrow {}_{16}S^{33}$

${}_{32}Ge^{78*} \rightarrow \underline{1.45\ H;\beta^-}\ \underline{0.70;\gamma\ 277} \rightarrow {}_{33}As^{78*} \rightarrow \underline{1.512\ H;\beta^-}\ \underline{4.3, 3.7, 1.7, 3.0;\gamma\ 613.7, 694.9, 1308.7} \rightarrow {}_{34}Se^{78}$

$p + {}_{46}Pd^{105} \rightarrow {}_{21}Sc^{52*} + {}_{26}Fe^{54} + 29.1$

${}_{21}Sc^{52*} \rightarrow \underline{8.2\ S;\beta^-}\ \underline{7.0, 4.6;\gamma\ 1049.7, 1267.9} \rightarrow {}_{22}Ti^{52*} \rightarrow \underline{1.7\ M;\beta^-}\ \underline{1.8;\ \gamma\ 124.5, 17.0} \rightarrow {}_{23}V^{52*} \rightarrow$

$\cdot \rightarrow {}_{23}V^{52*} \rightarrow \underline{3.76\ M;\beta^-}\ \underline{2.47;\gamma\ 1434.1} \rightarrow {}_{24}Cr^{52}$

$p + {}_{46}Pd^{105} \rightarrow {}_{15}P^{34} + {}_{31}Ga^{70} + d + 0.524$

$p + {}_{46}Pd^{105} \rightarrow {}_{23}V^{52*} + {}_{24}Cr^{54} + 27.2$

${}_{23}V^{52*} \rightarrow \underline{3.76\ M;\beta^-}\ \underline{2.47;\gamma\ 1434.1} \rightarrow {}_{24}Cr^{52}$

$p + {}_{46}Pd^{105} \rightarrow {}_{22}Ti^{52*} + {}_{25}Mn^{54*} + 23.9$

${}_{22}Ti^{52*} \rightarrow \underline{1.7\ M;\beta^-}\ \underline{1.8;\gamma\ 124.5} \rightarrow {}_{23}V^{52*} \rightarrow \underline{3.76\ M;\beta^-}\ \underline{2.47;\ \gamma 1434.1} \rightarrow {}_{24}Cr^{52}$

$p + {}_{46}Pd^{105} \rightarrow {}_{20}Ca^{48} + {}_{25}Mn^{54*} + \alpha + 16.2$

${}_{25}Mn^{54*} \rightarrow$ 312.2 D; ε,γ 834.8 $\rightarrow {}_{24}Cr^{54}$

3. n + Pd → C + D + . . .

$n + {}_{46}Pd^{106} \rightarrow {}_{4}Be^{6*} + {}_{42}Mo^{101*}$ - 16.7

$\rightarrow {}_{4}Be^{8*} + {}_{42}Mo^{99*}$ - 0.816

$n + {}_{46}Pd^{108} \rightarrow {}_{4}Be^{8*} + {}_{42}Mo^{101*}$ - 2.89

$\rightarrow {}_{4}Be^{10*} + {}_{42}Mo^{99*}$ - 8.11

$n + {}_{46}Pd^{108} \rightarrow {}_{4}Be^{10*} + {}_{42}Mo^{101*}$ - 9.37

${}_{4}Be^{6*} \rightarrow$ 5.0E-21 S;2p, α

${}_{4}Be^{8*} \rightarrow$ ~7E-17 S;2α .0641

${}_{4}Be^{10*} \rightarrow$ 1.6E6 A; β⁻ 0.556 $\rightarrow {}_{5}B^{10}$

${}_{42}Mo^{99*} \rightarrow$ 2.747 D;β⁻ 1.214;γ 140.5, 739.5 $\rightarrow {}_{43}Tc^{99*} \rightarrow$

${}_{43}Tc^{99*} \rightarrow$ 6.01 H; IT 142.7, 2.2(e⁻); γ140.5; β⁻ .435 $\rightarrow {}_{44}Ru^{99}$

${}_{42}Mo^{101*} \rightarrow$ 14.6 M;β⁻ 7.2, 2.3;γ 191.9, 591, 1013, 5060 $\rightarrow {}_{43}Tc^{101*} \rightarrow$

${}_{43}Tc^{101*} \rightarrow$ 14.2 M;β⁻ 1.32;γ 306.8 $\rightarrow {}_{44}Ru^{101}$

$n + {}_{46}Pd^{105} \rightarrow {}_{5}B^{8} + {}_{41}Nb^{98}$ - 19.75

$n + {}_{46}Pd^{106} \rightarrow {}_{6}C^{10} + {}_{40}Zr^{97}$ - 14.6

$n + {}_{46}Pd^{108} \rightarrow {}_{6}C^{10} + {}_{40}Zr^{99}$ - 18.8

$\rightarrow {}_{6}C^{12} + {}_{40}Zr^{97}$ + 1.48

$n + {}_{46}Pd^{110} \rightarrow {}_{6}C^{12} + {}_{40}Zr^{99}$ - 1.91

$\rightarrow {}_{6}C^{14} + {}_{40}Zr^{97}$ - 0.355

$n + {}_{46}Pd^{102} \rightarrow {}_{10}Ne^{19} + {}_{36}Kr^{84}$ + 0.826

$n + {}_{46}Pd^{104} \rightarrow {}_{10}Ne^{19} + {}_{36}Kr^{86}$ + 0.110

$n + {}_{46}Pd^{106} \rightarrow {}_{10}Ne^{19} + {}_{36}Kr^{88}$ - 3.88

$n + {}_{46}Pd^{108} \rightarrow {}_{10}Ne^{19} + {}_{36}Kr^{90}$ + 7.13

$n + {}_{46}Pd^{102} \rightarrow {}_{14}Si^{29} + {}_{32}Ge^{74}$ + 15.5

$n + {}_{46}Pd^{104} \rightarrow {}_{14}Si^{29} + {}_{32}Ge^{76}$ + 13.8

$n + {}_{46}Pd^{106} \rightarrow {}_{14}Si^{29} + {}_{32}Ge^{78*}$ + 11.0

${}_{32}Ge^{78*} \rightarrow$ 1.45 H;β⁻ 0.70;γ 277 $\rightarrow {}_{33}As^{78*} \rightarrow$ 1.512 H;β⁻ 4.3, 3.7, 3.0;γ 613, 694, 1308 $\rightarrow {}_{34}Se^{78}$

$n + {}_{46}Pd^{102} \rightarrow {}_{14}S^{31} + {}_{30}Zn^{72}$ + 7.27

$n + {}_{46}Pd^{105} \rightarrow {}_{9}F^{17} + {}_{36}Kr^{88}$ + p - 9.40

$\rightarrow {}_{9}F^{19} + {}_{36}Kr^{86}$ + p - 7.70

$n + {}_{46}Pd^{105} \rightarrow {}_{11}Na^{25} + {}_{34}Se^{80} + p - 0.517$

$n + {}_{46}Pd^{105} \rightarrow {}_{13}Al^{29} + {}_{32}Ge^{76} + p + 3.80$

$n + {}_{46}Pd^{104} \rightarrow {}_{4}Be^{11*} + {}_{30}Zr^{90} + \alpha - 15.2$
$n + {}_{46}Pd^{106} \rightarrow {}_{4}Be^{11*} + {}_{30}Zr^{92} + \alpha - 14.5$
$n + {}_{46}Pd^{108} \rightarrow {}_{4}Be^{11*} + {}_{30}Zr^{94} + \alpha - 18.6$
$n + {}_{46}Pd^{110} \rightarrow {}_{4}Be^{11*} + {}_{30}Zr^{96} + \alpha - 15.0$
${}_{4}Be^{11*} \rightarrow \underline{13.8\ S;\beta^-}\ \underline{11.5,\ 9.4;\gamma\ 2124.6} \rightarrow {}_{5}B^{11}$

$n + {}_{46}Pd^{102} \rightarrow {}_{10}Ne^{19} + {}_{34}Se^{80} + \alpha - 6.28$
$n + {}_{46}Pd^{104} \rightarrow {}_{10}Ne^{19} + {}_{34}Se^{82} + \alpha - 7.93$
$n + {}_{46}Pd^{106} \rightarrow {}_{10}Ne^{19} + {}_{34}Se^{84} + \alpha - 10.1$

4. α + Pd → C + D + . . .

$\alpha + {}_{46}Pd^{102} \rightarrow {}_{4}Be^{6*} + {}_{44}Ru^{100} - 14.4$
$\alpha + {}_{46}Pd^{104} \rightarrow {}_{4}Be^{6*} + {}_{44}Ru^{102} - 16.3$
$\alpha + {}^{46}Pd^{105} \rightarrow {}^{4}Be^{6*} + {}_{44}Ru^{103} - 17.1$
$\rightarrow {}_{4}Be^{8*} + {}_{44}Ru^{101} - 3.00$
$\rightarrow {}_{4}Be^{10*} + {}_{44}Ru^{99} - 11.0$
$\alpha + {}_{46}Pd^{106} \rightarrow {}_{4}Be^{6*} + {}_{44}Ru^{104} - 17.8$
${}_{4}Be^{6*} \rightarrow \underline{5.0E\text{-}21\ S;\ 2p,\alpha}$
${}_{4}Be^{8*} \rightarrow \underline{\sim 7E\text{-}17\ S;2\alpha\ ,0641}$
${}_{4}Be^{10*} \rightarrow \underline{1.6E6\ A;\beta^-\ 0.556} \rightarrow {}_{5}B^{10}$

$\alpha + {}_{46}Pd^{102} \rightarrow {}_{6}C^{10*} + {}_{42}Mo^{96} - 12.8$
$\rightarrow {}_{6}C^{12} + {}_{42}Mo^{94} - 2.91$
$\rightarrow {}_{6}C^{14*} + {}_{42}Mo^{92} - 1.72$
$\rightarrow {}_{6}C^{16*} + {}_{42}Mo^{90} - 18.7$
$\alpha + {}_{46}Pd^{106} \rightarrow {}_{6}C^{10*} + {}_{42}Mo^{100} - 17.0$
$\rightarrow {}_{6}C^{12} + {}_{42}Mo^{98} - 0.630$
$\rightarrow {}_{6}C^{14*} + {}_{42}Mo^{96} - 1.70$
$\rightarrow {}_{6}C^{16*} + {}_{42}Mo^{94} - 12.8$
$\alpha + {}_{46}Pd^{110} \rightarrow {}_{6}C^{10*} + {}_{42}Mo^{104} - 21.4$
$\rightarrow {}_{6}C^{12} + {}_{42}Mo^{102} - 2.32$
$\rightarrow {}_{6}C^{14*} + {}_{42}Mo^{100} - 2.75$
$\rightarrow {}_{6}C^{16*} + {}_{42}Mo^{98} - 11.5$
${}_{6}C^{10*} \rightarrow \underline{19.3S;\beta^-\ 1.87;\gamma\ 718.3} \rightarrow {}_{5}B^{10}$
${}_{6}C^{14*} \rightarrow \underline{5730\ A;\beta^-\ 0.157} \rightarrow {}_{7}N^{14}$
${}_{6}C^{16*} \rightarrow \underline{0.75\ S;\beta^-} \rightarrow {}_{7}N^{16*} \rightarrow \underline{7.13\ S;\beta^-\ 4.27,10.44;\gamma\ 6129,7115} \rightarrow {}_{8}O^{16}$

$\alpha + {}_{46}Pd^{104} \rightarrow {}_{6}C^{10*} + {}_{42}Mo^{98} - 17.6$
$\rightarrow {}_{6}C^{12} + {}_{42}Mo^{96} - 1.81$
$\rightarrow {}_{6}C^{14*} + {}_{42}Mo^{94} - 1.60$
$\rightarrow {}_{6}C^{16*} + {}_{42}Mo^{92} - 13.9$
$\alpha + {}_{46}Pd^{108} \rightarrow {}_{6}C^{10*} + {}_{42}Mo^{102} - 19.2$
$\rightarrow {}_{6}C^{12} + {}_{42}Mo^{100} - 0.916$
$\rightarrow {}_{6}C^{14*} + {}_{42}Mo^{98} - 2.01$
$\rightarrow {}_{6}C^{16*} + {}_{42}Mo^{96} - 12.0$

$\alpha + {}_{46}Pd^{102} \rightarrow {}_{8}O^{14*} + {}_{40}Zr^{92} - 5.06$

$\alpha + {}_{46}Pd^{104} \rightarrow {}_{8}O^{14*} + {}_{40}Zr^{94} - 7.73$

	→	${}_{8}O^{16} + {}_{40}Zr^{90}$	- 10.4		→	${}_{8}O^{16} + {}_{40}Zr^{92}$	- 12.2
	→	${}_{8}O^{18} + {}_{40}Zr^{88*}$	- 1.11		→	${}_{8}O^{18} + {}_{40}Zr^{90}$	+ 2.56
	→	${}_{8}O^{20*} + {}_{40}Zr^{86*}$	- 11.37		→	${}_{8}O^{20*} + {}_{40}Zr^{88}$	- 7.18
$\alpha + {}_{46}Pd^{105}$	→	${}_{8}O^{14} + {}_{40}Zr^{95*}$	- 8.33	$\alpha + {}_{46}Pd^{106}$	→	${}_{8}O^{14*} + {}_{40}Zr^{96}$	- 10.1
	→	${}_{8}O^{16} + {}_{40}Zr^{93*}$	- 12.5		→	${}_{8}O^{16} + {}_{40}Zr^{94}$	- 13.9
	→	${}_{8}O^{18} + {}_{40}Zr^{91}$	- 2.69		→	${}_{8}O^{18} + {}_{40}Zr^{92}$	+ 1.75
	→	${}_{8}O^{19} + {}_{40}Zr^{90}$	- 0.557		→	${}_{8}O^{20*} + {}_{40}Zr^{90}$	- 2.51
$\alpha + {}_{46}Pd^{108}$	→	${}_{8}O^{14} + {}_{40}Zr^{98}$	- 13.8	$\alpha + {}_{46}Pd^{110}$	→	${}_{8}O^{16} + {}_{40}Zr^{98}$	- 18.3
	→	${}_{8}O^{16} + {}_{40}Zr^{96}$	- 15.4		→	${}_{8}O^{18*} + {}_{40}Zr^{96}$	+ 0.290
	→	${}_{8}O^{18} + {}_{40}Zr^{94}$	+ 0.945		→	${}_{8}O^{2} + {}_{40}Zr^{94}$	- 2.45
	→	${}_{8}O^{20*} + {}_{40}Zr^{92}$	- 2.40				

${}_{8}O^{14*} \rightarrow$ 70.60 S:β^- 1.81; γ 2312.7 $\rightarrow {}_{7}N^{14}$

${}_{8}O^{20*} \rightarrow$ 13.5 S:β^- 2.75;γ 1056.8 $\rightarrow {}_{9}F^{20*} \rightarrow$ 11.0 S:β^- 5.40;γ 1633.6 $\rightarrow {}_{10}Ne^{20}$

$\alpha + {}_{46}Pd^{102}$	→	${}_{10}Ne^{24*} + {}_{38}Sr^{82}$	- 3.97	$\alpha + {}_{46}Pd^{104}$	→	${}_{10}Ne^{24*} + {}_{38}Sr^{84}$	- 0.398
	→	${}_{10}Ne^{22} + {}_{38}Sr^{84}$	+ 3.16		→	${}_{10}Ne^{22} + {}_{38}Sr^{86}$	+ 5.55
	→	${}_{10}Ne^{20} + {}_{38}Sr^{86}$	+ 6.05		→	${}_{10}Ne^{20} + {}_{38}Sr^{88}$	- 7.96
	→	${}_{10}Ne^{18*} + {}_{38}Sr^{88}$	- 2.92		→	${}_{10}Ne^{18*} + {}_{38}Sr^{90*}$	- 6.38
$\alpha + {}_{46}Pd^{105}$	→	${}_{10}Ne^{23} + {}_{38}Sr^{86}$	+ 3.67	$\alpha + {}_{46}Pd^{106}$	→	${}_{10}Ne^{24*} + {}_{38}Sr^{86}$	+ 2.98
	→	${}_{10}Ne^{20} + {}_{38}Sr^{89*}$	+ 7.25		→	${}_{10}Ne^{22} + {}_{38}Sr^{88}$	+ 8.46
	→	${}_{10}Ne^{18} + {}_{38}Sr^{91}$	- 7.62		→	${}_{10}Ne^{20} + {}_{38}Sr^{90*}$	- 5.49
					→	${}_{10}Ne^{18} + {}_{38}Sr^{92*}$	- 9.08
$\alpha + {}_{46}Pd^{108}$	→	${}_{10}Ne^{24*} + {}_{38}Sr^{88}$	+ 6.76	$\alpha + {}_{46}Pd^{110}$	→	${}_{10}Ne^{24*} + {}_{38}Sr^{90*}$	+ 5.96
	→	${}_{10}Ne^{22} + {}_{38}Sr^{90*}$	+ 6.85		→	${}_{10}Ne^{22} + {}_{38}Sr^{92*}$	+ 5.03
	→	${}_{10}Ne^{20} + {}_{38}Sr^{92*}$	+ 2.06		→	${}_{10}Ne^{20} + {}_{38}Sr^{94*}$	- 0.133
	→	${}_{10}Ne^{18*} + {}_{38}Sr^{94*}$	- 13.7				

${}_{38}Sr^{89*} \rightarrow$ 50.52 D:β^- 1.49; γ 909.2 $\rightarrow {}_{39}Y^{89}$

${}_{38}Sr^{90*} \rightarrow$ 29.1 A:β^- 0.546 $\rightarrow {}_{39}Y^{90*}$

${}_{39}Y^{90*} \rightarrow$ 2.67 D:β^- 2.281;γ 2186.2 $\rightarrow {}_{40}Zr^{90}$

$\rightarrow$ 3.19 H; IT 479.5;γ 202.5;β^- ;γ 2318.9 $\rightarrow {}_{40}Zr^{90}$

${}_{38}Sr^{91*} \rightarrow$ 9.5 H;β^- 1.09, 2.70, 1.36;γ 555.6, 1024.3, 749.7 $\rightarrow {}_{39}Y^{91*} \rightarrow$ 49.7 M; IT 555.6 $\rightarrow {}_{40}Zr^{91}$

$\rightarrow$ 58.5 D;β^- 1.545;γ 1205 $\rightarrow {}_{40}Zr^{91}$

${}_{38}Sr^{92*} \rightarrow$ 2.71 H;β^- 0.54γ 1384.0 $\rightarrow {}_{39}Y^{92*} \rightarrow$ 3.54 Hβ^- 3.64;γ 934.5, 1405.4 $\rightarrow {}_{40}Zr^{92}$

${}_{38}Sr^{94*} \rightarrow$ 1.25 M;β^- 2.08;γ 1427.6 $\rightarrow {}_{39}Y^{94*} \rightarrow$ 18.7 M;β^- 4.92; 918.7, 1138.9, 550.9 $\rightarrow {}_{40}Zr^{94}$

$\alpha + {}_{46}Pd^{102}$	→	${}_{12}Mg^{22*} + {}_{36}Kr^{84}$	- 2.69	$\alpha + {}_{46}Pd^{104}$	→	${}_{12}Mg^{22*} + {}_{36}Kr^{86}$	- 3.34
	→	${}_{12}Mg^{24} + {}_{36}Kr^{82}$	+ 9.02		→	${}_{12}Mg^{24} + {}_{36}Kr^{84}$	+ 9.38
	→	${}_{12}Mg^{26} + {}_{36}Kr^{80}$	+ 8.60		→	${}_{12}Mg^{26} + {}_{36}Kr^{82}$	+ 9.82
	→	${}_{12}Mg^{28*} + {}_{36}Kr^{78}$	+ 3.66		→	${}_{12}Mg^{28*} + {}_{36}Kr^{80}$	+ 5.93
$\alpha + {}_{46}Pd^{105}$	→	${}_{12}Mg^{25} + {}_{36}Kr^{84}$	+ 9.64	$\alpha + {}_{46}Pd^{106}$	→	${}_{12}Mg^{22*} + {}_{36}Kr^{88*}$	- 7.39
	→	${}_{12}Mg^{22} + {}_{36}Kr^{87*}$	- 4.90		→	${}_{12}Mg^{24} + {}_{36}Kr^{86}$	+ 9.72
					→	${}_{12}Mg^{26} + {}_{36}Kr^{84}$	+ 11.2
					→	${}_{12}Mg^{28*} + {}_{36}Kr^{82}$	+ 8.13

$\alpha + {}_{46}Pd^{108} \rightarrow {}_{12}Mg^{24} + {}_{36}Kr^{88*} + 6.53$
$\rightarrow {}_{12}Mg^{26} + {}_{36}Kr^{86} + 12.4$
$\rightarrow {}_{12}Mg^{28} + {}_{36}Kr^{84} - 10.3$
$\alpha + {}_{46}Pd^{110} \rightarrow {}_{12}Mg^{26} + {}_{36}Kr^{88*} + 6.00$
$\rightarrow {}_{12}Mg^{28} + {}_{36}Kr^{86*} + 12.4$

${}_{36}Kr^{87*} \rightarrow$ 1.27;β⁻ 3.5, 3.9;γ 402.6 $\rightarrow {}_{37}Rb^{87}$
${}_{36}Kr^{88*} \rightarrow$ 2.84 H;β⁻ 0.52, 2.9;γ 2392.1, 196.3 $\rightarrow {}_{37}Rb^{88*} \rightarrow$ 17.7 M;β⁻ 5.31;γ 1836.1, 898.1 $\rightarrow {}_{38}Sr^{88}$
${}_{12}Mg^{22*} \rightarrow$ 3.86 S;β⁻ 3.1;γ 582, 72.9 $\rightarrow {}_{11}Na^{22}* \rightarrow$ 2.605 A;β⁻ 0.546, ε;γ 1274.5 $\rightarrow {}_{10}Ne^{22}$
${}_{12}Mg^{28*} \rightarrow$ 21.0 H;β⁻ 0.459;γ 30.6, 1342.3 $\rightarrow {}_{13}Al^{28}* \rightarrow$ 2.25 M;β⁻ 2.86; γ1179.0 $\rightarrow {}_{14}Si^{28}$

$\alpha + {}_{46}Pd^{102} \rightarrow {}_{14}Si^{26*} + {}_{34}Se^{80} - 0.60$
$\rightarrow {}_{14}Si^{28} + {}_{34}Se^{78} + 13.0$
$\rightarrow {}_{14}Si^{30} + {}_{34}Se^{76} + 14.2$
$\rightarrow {}_{14}Si^{32*} + {}_{34}Se^{74} + 10.8$
$\alpha + {}_{46}Pd^{105} \rightarrow {}_{14}Si^{25} + {}_{34}Se^{84*} - 13.9$
$\rightarrow {}_{14}Si^{27} + {}_{34}Se^{82} + 3.98$
$\alpha + {}_{46}Pd^{104} \rightarrow {}_{14}Si^{26*} + {}_{34}Se^{82} - 2.25$
$\rightarrow {}_{14}Si^{28} + {}_{34}Se^{80} + 12.2$
$\rightarrow {}_{14}Si^{30} + {}_{34}Se^{78} + 15.5$
$\rightarrow {}_{14}Si^{32*} + {}_{34}Se^{76} + 9.32$
$\alpha + {}_{46}Pd^{106} \rightarrow {}_{14}Si^{26*} + {}_{34}Se^{84*} - 4.41$
$\rightarrow {}_{14}Si^{28} + {}_{34}Se^{82} + 11.6$
$\rightarrow {}_{1}4Si^{30} + {}_{34}Se^{80} + 14.7$
$\rightarrow {}_{14}Si^{32*} + {}_{34}Se^{78} + 13.6$

$\alpha + {}_{46}Pd^{108} \rightarrow {}_{14}Si^{28} + {}_{34}Se^{84*} + 10.3$
$\rightarrow {}_{14}Si^{30} + {}_{34}Se^{82} + 14.9$
$\rightarrow {}_{14}Si^{32*} + {}_{34}Se^{80} + 14.7$
$\alpha + {}_{46}Pd^{110} \rightarrow {}_{14}Si^{30} + {}_{34}Se^{84*} + 14.3$
$\rightarrow {}_{14}Si^{32} + {}_{34}Se^{82} + 15.8$

${}_{14}Si^{26*} \rightarrow$ 2.23 S;β⁻ 3.83;γ 829 $\rightarrow {}_{13}Al^{26*} \rightarrow$ 6.345 S;β⁻ 3.21 $\rightarrow {}_{12}Mg^{26}$
${}_{14}Si^{32*} \rightarrow$ 1.0E2 A;β⁻ 0.221; $\rightarrow {}_{15}P^{32*} \rightarrow$ 14.28 D;β⁻ 1.709 $\rightarrow {}_{16}S^{32}$
${}_{34}Se^{84*} \rightarrow$ 3.3 M H;β⁻ 1.41;γ 408.2 $\rightarrow {}_{35}Br^{84*} \rightarrow$ 6.0M;β⁻ 2.2;γ 1463, 424, 881.7 $\rightarrow {}_{36}Kr^{84}$
$\rightarrow$ 31.8M;β⁻ 4.65, 3.8, 2.7;γ 881.7, 1897.7 $\rightarrow {}_{36}Kr^{84}$

$\alpha + {}_{46}Pd^{102} \rightarrow {}_{16}S^{30*} + {}_{32}Ge^{76} + 1.77$
$\rightarrow {}_{16}S^{32} + {}_{32}Ge^{74} + 13.9$
$\rightarrow {}_{16}S^{34} + {}_{32}Ge^{72} + 17.0$
$\rightarrow {}_{16}S^{36} + {}_{32}Ge^{70} + 15.7$
$\alpha + {}_{46}Pd^{104} \rightarrow {}_{16}S^{30*} + {}_{32}Ge^{78} - 1.14$
$\rightarrow {}_{16}S^{32} + {}_{32}Ge^{76} + 12.2$
$\rightarrow {}_{16}S^{34} + {}_{32}Ge^{74} + 16.4$
$\rightarrow {}_{16}S^{36} + {}_{32}Ge^{72} + 16.3$

$\alpha + {}_{46}Pd^{106} \rightarrow {}_{16}S^{32} + {}_{32}Ge^{78*} + 10.3$
$\rightarrow {}_{16}S^{34} + {}_{32}Ge^{76} + 15.7$
$\rightarrow {}_{16}S^{36} + {}_{32}Ge^{74} + 16.6$
$\alpha + {}_{46}Pd^{110} \rightarrow {}_{16}S^{36} + {}_{32}Ge^{78*} + 16.5$
$\alpha + {}_{46}Pd^{108} \rightarrow {}_{16}S^{34} + {}_{32}Ge^{78*} + 14.6$
$\rightarrow {}_{16}S^{36} + {}_{32}Ge^{76} + 16.8$
$\rightarrow {}_{16}S^{38} + {}_{32}Ge^{74} + 13.2$

${}_{16}S^{30*} \rightarrow$ 1.18 S;β⁻ 4.42, 5.09;γ 667.2 $\rightarrow {}_{15}P^{30*} \rightarrow$ 2.50M;β⁻ 3.24; ε;γ 2235.2 $\rightarrow {}_{14}Si^{30}$
${}_{32}Ge^{78*} \rightarrow$ 1.45 H;β⁻ 0.70;γ 277 $\rightarrow {}_{33}As^{78*} \rightarrow$ 1.512 H;β⁻ 4.3, 3.7, 1.7, 3.0;γ 613.7, 694.9, 1308.7 $\rightarrow {}_{34}Se^{78}$

$\alpha + {}_{46}Pd^{102} \rightarrow {}_{18}Ar^{34*} + {}_{30}Zn^{72*} + 1.02$
$\rightarrow {}_{18}Ar^{36} + {}_{30}Zn^{70} + 14.3$
$\rightarrow {}_{18}Ar^{38} + {}_{30}Zn^{68} + 19.2$
$\rightarrow {}_{18}Ar^{40} + {}_{30}Zn^{66} + 18.4$
$\rightarrow {}_{18}Ar^{42*} + {}_{30}Zn^{64} + 14.9$
$\alpha + {}_{46}Pd^{104} \rightarrow {}_{18}Ar^{36} + {}_{30}Zn^{72*} + 11.4$
$\rightarrow {}_{18}Ar^{38} + {}_{30}Zn^{70} + 17.3$
$\rightarrow {}_{18}Ar^{40} + {}_{30}Zn^{68} + 18.1$
$\rightarrow {}_{18}Ar^{42} + {}_{30}Zn^{66} + 16.3$
$\alpha + {}_{46}Pd^{106} \rightarrow {}_{18}Ar^{38} + {}_{30}Zn^{72*} + 15.4$
$\rightarrow {}_{18}Ar^{40} + {}_{30}Zn^{70} + 17.1$
$\alpha + {}_{46}Pd^{108} \rightarrow {}_{18}Ar^{40} + {}_{30}Zn^{72*} + 16.1$
$\rightarrow {}_{18}Ar^{42*} + {}_{30}Zn^{70} + 16.9$

$\rightarrow \quad {}_{18}Ar^{42*} + {}_{30}Zn^{68} \quad + 16.9$

$\alpha + {}_{46}Pd^{110} \rightarrow \quad {}_{18}Ar^{42*} + {}_{30}Zn^{72*} \quad + 16.6$

${}_{18}Ar^{34*} \rightarrow \underline{844\ MS;\beta^-\ 5.037,\ 666.5,\ 461,\ 2580} \rightarrow {}_{17}Cl^{34*} \rightarrow$

${}_{17}Cl^{34*} \rightarrow \underline{32.2\ M;\beta^-\ 2.5,\ 1.3;\gamma\ 2127.7,\ 1176,\ 3303.6} \rightarrow {}_{16}S^{34}$

$\rightarrow \underline{1.528\ S;\beta^-\ 4.47} \rightarrow {}_{16}S^{34}$

${}_{18}Ar^{42*} \rightarrow \underline{33\ A;\beta^-} \rightarrow {}_{19}K^{42*} \rightarrow \underline{12.36\ H;\beta^-\ 3.52;\gamma\ 1524.6} \rightarrow {}_{20}Ca^{42}$

${}_{30}Zn^{72*} \rightarrow \underline{46.5\ H;\beta^-\ 0.30;\gamma\ 144.7} \rightarrow {}_{31}Ga^{72*} \rightarrow \underline{14.10\ H;\beta^-\ 0.96,\ 0.64;\gamma\ 834.1,\ 2201.7,\ 630} \rightarrow {}_{32}Ge^{72}$

$\alpha + {}_{46}Pd^{105} \rightarrow \quad {}_{19}K^{41} + {}_{29}Cu^{68*} \quad + 15.0$

$\rightarrow \quad {}_{19}K^{43*} + {}_{29}Cu^{66*} \quad + 16.9$

$\rightarrow \quad {}_{19}K^{45*} + {}_{29}Cu^{64*} \quad + 16.1$

${}_{29}Cu^{64*} \rightarrow \underline{12.70\ H;\varepsilon;\beta^-\ 0.578;\gamma\ 1345.8} \rightarrow {}_{30}Zn^{64}$

$\rightarrow \underline{12.70\ H;\beta^-\ 0.651} \rightarrow {}_{28}Ni^{64}$

${}_{29}Cu^{66*} \rightarrow \underline{5.10\ M;\beta^-\ 2.63;\gamma\ 1039.3} \rightarrow {}_{30}Zn^{66}$

${}_{29}Cu^{68*} \rightarrow \underline{31\ S;\beta^-\ 3.5,\ 4.6;\gamma\ 1077.3,\ 1261.2} \rightarrow {}_{30}Zn^{68}$

${}_{19}K^{45*} \rightarrow \underline{22.3\ H;\beta^-\ 0.83;\gamma\ 372.8,\ 617.5} \rightarrow {}_{20}Ca^{43}$

${}_{19}K^{45*} \rightarrow \underline{17.8\ M;\beta^-\ 2.1;\gamma\ 174.2,\ 1705.6} \rightarrow {}_{20}Ca^{45} \rightarrow \underline{162.7\ D;\beta^-\ 0.258;\gamma\ 12.4} \rightarrow {}_{21}Sc^{45}$

$\alpha + {}_{46}Pd^{102} \rightarrow \quad {}_{20}Ca^{48} + {}_{28}Ni^{58} \quad + 7.97$

$\rightarrow \quad {}_{20}Ca^{46} + {}_{28}Ni^{60} \quad + 19.0$

$\rightarrow \quad {}_{20}Ca^{44} + {}_{28}Ni^{62} \quad + 22.1$

$\rightarrow \quad {}_{20}Ca^{42} + {}_{28}Ni^{64} \quad + 22.7$

$\rightarrow \quad {}_{20}Ca^{40} + {}_{28}Ni^{66*} \quad + 20.1$

$\alpha + {}_{46}Pd^{106} \rightarrow \quad {}_{20}Ca^{50*} + {}_{28}Ni^{60} \quad + 16.6$

$\rightarrow \quad {}_{20}Ca^{48} + {}_{28}Ni^{62} \quad + 23.5$

$\rightarrow \quad {}_{20}Ca^{46} + {}_{28}Ni^{64} \quad + 22.8$

$\rightarrow \quad {}_{20}Ca^{44} + {}_{28}Ni^{66*} \quad + 20.0$

$\alpha + {}_{46}Pd^{104} \rightarrow \quad {}_{20}Ca^{50*} + {}_{28}Ni^{58} \quad + 12.8$

$\rightarrow \quad {}_{20}Ca^{48} + {}_{28}Ni^{60} \quad + 21.0$

$\rightarrow \quad {}_{20}Ca^{46} + {}_{28}Ni^{62} \quad + 22.9$

$\rightarrow \quad {}_{20}Ca^{44} + {}_{28}Ni^{64*} \quad + 21.6$

$\rightarrow \quad {}_{20}Ca^{42} + {}_{28}Ni^{66} \quad + 17.6$

$\alpha + {}_{46}Pd^{108} \rightarrow \quad {}_{20}Ca^{50*} + {}_{28}Ni^{62} \quad + 19.2$

$\rightarrow \quad {}_{20}Ca^{48} + {}_{28}Ni^{64} \quad + 24.2$

$\rightarrow \quad {}_{20}Ca^{46} + {}_{28}Ni^{66*} \quad + 22.1$

${}_{28}Ni^{66*} \rightarrow \underline{54.6\ H;\beta^-\ 0.20} \rightarrow {}_{29}Cu^{66*} \rightarrow \underline{5.10\ M;\beta^-\ 2.63;\gamma\ 1039.3} \rightarrow {}_{30}Zn^{66}$

${}_{20}Ca^{50*} \rightarrow \underline{14\ S;\beta^-\ 3.12;\gamma\ 256.9,\ 1519.3,\ 71.6,\ 1590.8} \rightarrow {}_{21}Sc^{50*}$

${}_{21}Sc^{50*} \rightarrow \underline{1.71\ M;\beta^-\ 3.69;\gamma\ 1553.8,\ 1121,\ 523.8} \rightarrow {}_{22}Ti^{50}$

$\alpha + {}_{46}Pd^{102} \rightarrow \quad {}_{22}Ti^{46} + {}_{26}Fe^{60*} \quad + 20.1$

$\rightarrow \quad {}_{22}Ti^{48} + {}_{26}Fe^{58} \quad + 25.1$

$\rightarrow \quad {}_{22}Ti^{50} + {}_{26}Fe^{56} \quad + 26.5$

$\rightarrow \quad {}_{22}Ti^{52*} + {}_{26}Fe^{54} \quad + 20.2$

$\alpha + {}_{46}Pd^{106} \rightarrow \quad {}_{22}Ti^{50} + {}_{26}Fe^{60*} \quad + 25.4$

$\rightarrow \quad {}_{22}Ti^{52*} + {}_{26}Fe^{58} \quad + 24.1$

$\alpha + {}_{46}Pd^{104} \rightarrow \quad {}_{22}Ti^{48} + {}_{26}Fe^{60*} \quad + 22.9$

$\rightarrow \quad {}_{22}Ti^{50} + {}_{26}Fe^{58} \quad + 26.6$

$\rightarrow \quad {}_{22}Ti^{52*} + {}_{26}Fe^{56} \quad + 23.1$

$\alpha + {}_{46}Pd^{108} \rightarrow \quad {}_{22}Ti^{52*} + {}_{26}Fe^{60*} \quad + 23.8$

${}_{22}Ti^{52*} \rightarrow \underline{1.7\ M;\beta^-\ 1.8;\gamma\ 124.5,\ 17.0} \rightarrow {}_{23}V^{52*} \rightarrow \underline{3.76M;\beta^-\ 2.47;\gamma\ 1434.1} \rightarrow {}_{24}Cr^{52}$

${}_{26}Fe^{60*} \rightarrow \underline{1.5E6\ A;\beta^-\ 0.147;\gamma\ 58.6} \rightarrow {}_{27}Co^{60*} \rightarrow \underline{10.47\ M;\ IT\ 58.69\ e^-;\beta^-\ 1.6;\gamma\ 1322.5} \rightarrow {}_{28}Ni^{60}$

$\rightarrow \underline{5.271\ A;\beta^-\ 0.318;\gamma\ 1322.5,\ 1173.2} \rightarrow {}_{28}Ni^{60}$

$\alpha + {}_{46}Pd^{105} \rightarrow \quad {}_{11}Na^{23} + {}_{36}Kr^{84} \quad + d - 7.16$

$\rightarrow \quad {}_{11}Na^{21*} + {}_{36}Kr^{86} \quad + d - 13.7$

${}_{11}Na^{21*} \rightarrow \underline{22.48\ S;\beta^-\ 2.51;\gamma\ 350.7} \rightarrow {}_{10}Ne^{21}$

$\alpha + {}_{46}Pd^{105} \rightarrow {}_{12}Mg^{27*} + {}_{35}Br^{80*} + d - 8.65$

${}_{12}Mg^{27*} \rightarrow \underline{9.45\ M;\beta^-}\ \underline{1.75, 1.59;\ \varepsilon;\gamma\ 843.8, 1014.4} \rightarrow {}_{13}Al^{27}$

${}_{35}Br^{80*} \rightarrow \underline{17.66\ M;\beta^-}\ \underline{2.00;\gamma\ 616.6} \rightarrow {}_{36}Kr^{80}$

$\rightarrow \underline{17.66\ M;\varepsilon\ \beta^-}\ \underline{0.85;\gamma\ 665.9} \rightarrow {}_{36}Kr^{80}$

$\alpha + {}_{46}Pd^{105} \rightarrow {}_{17}Cl^{37} + {}_{30}Zn^{70} + d + 2.20$

$\alpha + {}_{46}Pd^{105} \rightarrow {}_{19}K^{43*} + {}_{28}Ni^{64} + d + 4.57$

$\rightarrow {}_{19}K^{45*} + {}_{28}Ni^{62} + d + 4.24$

$\rightarrow {}_{19}K^{41} + {}_{28}Ni^{66*} + d + 2.49$

${}_{19}K^{43*} \rightarrow \underline{22.3\ H;\beta^-}\ \underline{0.83;\gamma\ 372.8, 617.5} \rightarrow {}_{20}Ca^{43}$

${}_{19}K^{45*} \rightarrow \underline{17.8\ M;\beta^-}\ \underline{2.1;\gamma\ 174.2, 1705.6} \rightarrow {}_{20}Ca^{45*} \rightarrow \underline{162.7\ D;\beta^-}\ \underline{0.258} \rightarrow {}_{21}Sc^{45}$

$\alpha + {}_{46}Pd^{105} \rightarrow {}_{11}Na^{20*} + {}_{36}Kr^{88*} + p - 20.4$

$\rightarrow {}_{11}Na^{20*} + {}_{36}Kr^{86} + t - 24.5$

${}_{11}Na^{20*} \rightarrow \underline{447\ MS;\beta^-}\ \underline{11.25;\gamma\ 1633.6} \rightarrow {}_{10}Ne^{20}$

${}_{36}Kr^{88*} \rightarrow \underline{2.84\ H;\beta^-}\ \underline{0.52, 2.9;\gamma\ 2392.1, 196.3} \rightarrow {}_{37}Rb^{88*} \rightarrow \underline{17.7\ M;\beta^-}\ \underline{5.31;\gamma\ 1836.1, 898.1} \rightarrow {}_{38}Sr^{88}$

$\alpha + {}_{46}Pd^{105} \rightarrow {}_{17}Cl^{36*} + {}_{30}Zn^{72*} + p + 4.38$

$\rightarrow {}_{17}Cl^{36*} + {}_{30}Zn^{70} + t - 1.86$

${}_{17}Cl^{36*} \rightarrow \underline{3.01\ E5\ A;\beta^-}\ \underline{0.709} \rightarrow {}_{18}Ar^{36}$

$\underline{3.01\ E5\ A;\varepsilon,\beta^-}\ \underline{0.12} \rightarrow {}_{16}S^{36}$

${}_{30}Zn^{72*} \rightarrow \underline{46.5\ H;\beta^-}\ \underline{0.30;\gamma\ 144.7} \rightarrow {}_{31}Ga^{72*} \rightarrow \underline{144.10\ H;\beta^-}\ \underline{0.96, 0.64;\gamma\ 834.1, 2201.7, 630} \rightarrow {}_{32}Ge^{72}$

5. a + Pd → C (a = d or α)

$d + {}_{46}Pd^{104} \rightarrow {}_{47}Ag^{106*} + 10.7$

${}_{47}Ag^{106*} \rightarrow \underline{24.0\ M;\beta^-}\ \underline{1.96;\gamma\ 511.9} \rightarrow {}_{46}Pd^{106}$

$d + {}_{46}Pd^{106} \rightarrow {}_{47}Ag^{108*} + 10.8$

${}_{47}Ag^{108*} \rightarrow \underline{2.39\ M;\varepsilon,\beta^-}\ \underline{1.65;\gamma\ 633.0} \rightarrow {}_{48}Cd^{108}$

$\rightarrow \underline{2.39\ M;\varepsilon;\beta^-}\ \underline{0.88;\gamma\ 433.9, 618.8} \rightarrow {}_{46}Pd^{108}$

$d + {}_{46}Pd^{108} \rightarrow {}_{47}Ag^{110*} + 11.1$

${}_{47}Ag^{110*} \rightarrow \underline{24.6\ S;\beta^-}\ \underline{2.981;\gamma\ 657.8} \rightarrow {}_{48}Cd^{110}$

$d + {}_{48}Cd^{110} \rightarrow {}_{49}In^{112*} + 10.8$

${}_{49}In^{112*} \rightarrow \underline{14.4\ M;\beta^-}\ \underline{0.86} \rightarrow {}_{50}Sn^{112}$

$\rightarrow \underline{14.4\ M;\varepsilon,\beta^-}\ \underline{1.56;\gamma\ 617.4, 606.7} \rightarrow {}_{48}Cd^{112}$

$d + {}_{48}Cd^{112} \rightarrow {}_{49}In^{114*} + 11.1$

${}_{49}In^{114*} \rightarrow \underline{1.198\ M;\beta^-}\ \underline{1.984;\gamma\ 1299.9} \rightarrow {}_{50}Sn^{114}$

$\rightarrow \underline{1.198\ M;\varepsilon,\beta^-}\ \underline{0.40;\gamma\ 558.4, 576} \rightarrow {}_{48}Cd^{114}$

$d + {}_{48}Cd^{114} \rightarrow {}_{49}In^{116*} + 11.4$

${}_{49}In^{116*} \rightarrow \underline{14.1\ s;\beta^-}\ \underline{3.3;\gamma}\ \underline{1293.6} \rightarrow {}_{50}Sn_{116}$

$d + {}_{50}Sn^{116} \rightarrow {}_{51}Sb^{118*} + 9.57$

${}_{51}Sb^{118*} \rightarrow \underline{3.6\ M;\beta^-}\ \underline{2.65;\gamma}\ \underline{1229.7} \rightarrow {}_{50}Sn^{118}$

$d + {}_{50}Sn^{118} \rightarrow {}_{51}Sb^{120*} + 9.57$

${}_{51}Sb^{120*} \rightarrow \underline{15.89\ M;\varepsilon,\beta^-}\ \underline{1.72;\gamma}\ \underline{1171.4} \rightarrow {}_{50}Sn^{120}$

$\alpha + {}_{46}Pd^{102} \rightarrow {}_{48}Cd^{106} + 1.63$

$\alpha + {}_{46}Pd^{104} \rightarrow {}_{48}Cd^{108} + 2.26$

$\alpha + {}_{46}Pd^{105} \rightarrow {}_{48}Cd^{109*} + 2.55$

${}_{48}Cd^{109*} \rightarrow \underline{462.0\ D;\varepsilon;\gamma}\ \underline{88.0} \rightarrow {}_{47}Ag^{109}$

$\alpha + {}_{46}Pd^{106} \rightarrow {}_{48}Cd^{110} + 2.87$

$\alpha + {}_{46}Pd^{108} \rightarrow {}_{48}Cd^{112} + 3.47$

$\alpha + {}_{46}Pd^{110} \rightarrow {}_{48}Cd^{114} + 4.10$

$\alpha + {}_{48}Cd^{108} \rightarrow {}_{50}Sn^{112} + 1.82$

$\alpha + {}_{48}Cd^{110} \rightarrow {}_{50}Sn^{114} + 2.58$

$\alpha + {}_{48}Cd^{112} \rightarrow {}_{50}Sn^{116} + 3.37$

$\alpha + {}_{48}Cd^{114} \rightarrow {}_{50}Sn^{118} + 4.06$

$\alpha + {}_{50}Sn^{116} \rightarrow {}_{52}Te^{120} + 0.305$

$\alpha + {}_{50}Sn^{118} \rightarrow {}_{52}Te^{122} + 1.08$

$\alpha + {}_{54}Te^{120} \rightarrow {}_{54}Xe^{124} + 2.47$

$\alpha + {}_{54}Te^{122} \rightarrow {}_{54}Xe^{126} + 1.29$

$d + {}_{54}Te^{120} \rightarrow {}_{53}I^{122} - 0.817$

.....

.....

$\alpha + {}_{70}Yb^{170} \rightarrow {}_{72}Hf^{174} - 2.56$

$\alpha + {}_{70}Yb^{172} \rightarrow {}_{72}Hf^{176} - 2.26$

$\alpha + {}_{70}Yb^{174} \rightarrow {}_{72}W^{178*} - 2.92$

${}_{74}W^{178*} \rightarrow \underline{21.6\ D;\varepsilon} \rightarrow {}_{73}Ta^{178*} \rightarrow \underline{2.4\ H;\varepsilon;\gamma}\ \underline{426.4,\ 235.5,\ 178,\ 213.4,\ 88.9} \rightarrow {}_{72}Hf^{178}$

$\rightarrow \underline{2.29\ M;\varepsilon,\beta^-}\ \underline{0.89,\ 0.80;\gamma}\ \underline{93.2,\ 1350.6,\ 1340.9} \rightarrow {}_{72}Hf^{178}$

$\alpha + {}_{72}Hf^{176} \rightarrow {}_{74}W^{180} - 2.48$

$\alpha + {}_{72}Hf^{178} \rightarrow {}_{74}W^{182} - 1.79$

$\alpha + {}_{72}Hf^{180} \rightarrow {}_{74}W^{184} - 1.67$

$d + {}_{72}Hf^{178} \rightarrow {}_{73}Ta^{180*} - 9.55$

${}_{73}Ta^{180*} \rightarrow \underline{8.15\ H;\varepsilon;\gamma}\ \underline{93.3;\beta^-}\ \underline{0.71,\ 0.61,\ \gamma}\ \underline{103.4} \rightarrow {}_{74}W^{180}$

$\alpha + {}_{74}W^{180} \rightarrow {}_{76}Os^{184} - 3.07$

$\alpha + {}_{74}W^{182} \rightarrow {}_{76}Os^{186}$ - 2.83

$\alpha + {}_{76}Os^{184} \rightarrow {}_{78}Pt^{188*}$ - 3.07

${}_{78}Pt^{188*} \rightarrow$ 10.2 D; ε; γ 187.5, 195.0 $\rightarrow {}_{77}Ir^{188*}$

${}_{77}Ir^{188*} \rightarrow$ 1.72 D; εβ⁻ 1.65, 1.13; γ 155.1, 2214.7, 663.1, 478.0 $\rightarrow {}_{76}Os^{188}$

$\alpha + {}_{76}Os^{186} \rightarrow {}_{78}Pt^{190}$ - 3.24

$\alpha + {}_{76}Os^{188} \rightarrow {}_{78}Pt^{192}$ - 2.42

$\alpha + {}_{78}Pt^{190} \rightarrow {}_{80}Hg^{194*}$ - 2.69

${}_{80}Hg^{194*} \rightarrow$ 520 A; ε $\rightarrow {}_{79}Au^{194*} \rightarrow$ 1.64 D; ε, β⁻ 1.49; γ 328.5, 293.6 $\rightarrow {}_{78}Pt^{194}$

$\alpha + {}_{78}Pt^{192} \rightarrow {}_{80}Hg^{196}$ - 1.99

$\alpha + {}_{78}Pt^{194} \rightarrow {}_{80}Hg^{198}$ - 1.33

$\alpha + {}_{80}Hg^{196} \rightarrow {}_{82}Pb^{200*}$ - 3.06

${}_{82}Pb^{200*} \rightarrow$ 21.5 H; ε; γ 147.6 $\rightarrow {}_{81}Ti^{200*} \rightarrow$ 1.087 D; ε, β⁻ 1.07; 1.44; γ 368.0, 1205.7 $\rightarrow {}_{80}Hg^{200}$

$\alpha + {}_{80}Hg^{198} \rightarrow {}_{82}Pb^{202*}$ - 2.49

${}_{82}Pb^{202*} \rightarrow$ 5.3 E4 A; ε $\rightarrow {}_{81}Ti^{202*} \rightarrow$ 12.23 D; ε, β⁻ γ 439.6 $\rightarrow {}_{80}Hg^{202}$

.....

.....

C. SUMMARY

Without addressing the issues of how deuterons, protons, neutrons, or alpha particles can overcome the Coulomb barrier [3], a list of some of the **nuclear reactions permitted by energy, baryon number, charge, spin, parity, and isospin conservation rules has been presented.** This list should help the experimenter examine some of the possible nuclear reactions that could explain the results observed in recent experiments [1,2]. This work has been accomplished assuming that the conservation rules **will be observed in all low-energy nuclear reactions.** Any replicated experimental evidence to the contrary will assure that the current atomic model should be revised.

The authors would appreciate any corrections and/or additions to the above list.

REFERENCES

1. J. O'M. Bockris & Z. Minevski, "Two Zones of 'Impurities' Observed After Prolonged Electrolysis of Deuterium on Palladium," *Infinite Energy*, vol 1, no 5&6, 1996, pp 67-69, 8 refs, 3 figs, 2 tables.
2. T. Mizuno, T. Ohmori & M. Enyo, "Anomalous Isotopic Distribution in Palladium Cathode after Electrolysis", *J. New Energy,* vol 1, no 2, Summer 1996, 5 figs, 17 refs.
3. Hal Fox, "Cold Fusion and the Coulomb Barrier," *J. New Energy*, vol 1, no 2, pp 23-26, 2 figs, 10 refs.

THE COMPLEX CONDITIONS NEEDED TO OBTAIN NUCLEAR HEAT FROM D-Pd SYSTEMS

J. O'M. Bockris [1]

ABSTRACT

The D/Pd system does not show nuclear effects until after several hundred hours of electrolysis although cathodes become saturated with D in 1% of this time. Even then, only a small fraction (10-20%) of electrodes manifest nuclear reactions. More than one-half of the anomalous heat arises from nuclear reactions involving the metal atoms, with gain or loss of protons. The gap in time between the saturation of the substrate and the **switch on** of anomalous heat is taken up by the gradual spread throughout the electrode material of a state of damage. The damage gives rise to an increase in an internal dislocation concentration. On the dislocated areas, adsorbed protons lose their charge and are susceptible to incorporation into the substrate nuclei.

The irreproducibility arises from the effect of adsorbed impurities from the solution. These influence the desorption mechanism for H or D evolution which in turn cause changes in the internal fugacity of H_2 or D_2 and thus affects the spreading of internal damage, and cracking. Traditional concepts of cracking refer to extreme cracking when a massive number of connected cracks reach the surface and decrease the internal fugacity of deuterium. Internal factors affecting reproducibility arise because the technique making the Pd (or etc.) varies the grain size and this affects the spread of the dislocation-loaded areas.

Anodes of Pt dissolve and the Pt contaminates the surface of the electrode. Doped TiO_2, NiO_2 and $LaNiO_3$ are good anodes. D_2 and H_2 anodes eliminate anode dissolution. Insufficiently investigated are alloying and its effects on mechanical properties and the spread of damage.

INTRODUCTION

When Fleischmann and Pons [5] reported their discovery of anomalous heat production in D-Pd cathodes, they did not mention two characteristics of such systems.

(1) Using small cylindrical electrodes, it is necessary (usually) to electrolyze for more than 300 hours before anomalous effects are seen.

(2) Even then, only about 1/5 of the electrodes show the anomalous behavior within 600 hours.

This (rather than prejudice) is the heart of the difficulty in acceptance of the phenomenon. It is so difficult to find the conditions which give anomalous results.[2] Nevertheless, some of the experiments will repay the patient experimenter with a display of astounding and entirely anomalous nuclear phenomena (X rays, heat, tritium,

[1] Department of Chemistry, Texas A&M University, College Station, TX 77843-3255

[2] In the original announcement on TV, it was stated by Fleischmann that – contrary to appearances – it was a difficult experiment. In retrospect, this seems to have been understood in British idiom. Translated into American it reads: "Terribly difficult, needing enormous patience, time, and much skill."

helium, other new nuclei) as has been shown by several hundred scientists in dozens of countries (in more than 1000 publications) over the last seven years.

This paper provides some insight into ways in which this frustrating situation may be interpreted, - and perhaps improved.

THE FACTS OF THE IRREPRODUCIBILITY

The gross facts have already been stated above. The likelihood of success depends little on the pretreatment of the electrode (cold working, polished surface, Pd black, etc.) [1] Three pieces of Pd from the same rod may be "dead" (i.e., behave classically) while the fourth produces tritium [1], or helium [2] and heat, etc. The purity of the solution has a counter-intuitive effect, i.e., solutions specially purified are less likely to be the source of "on" displays than solutions made from ordinary distilled water. Some additives (e.g., thiourea) increase the likelihood of observing anomalous heat. [25]

There are several ways of increasing the likelihood of producing heat, and two of them are related.

1. **Saw-toothed cycling**. One cathodically polarizes, gradually making the potential more negative over (e.g.) one hour and then reducing the overpotential to zero and beginning to rise towards the negative again. Repeating the saw tooth for several days tends to produce anomalous heat more quickly than does steady state polarization. [3]

2. **Cathodic-anodic pulsing**. There is evidence [4] that pulsing the electrode from the potential for hydrogen evolution to that of oxygen many times is effective in stimulating nuclear activity. However, the period in timing and potential amplitude have not been studied.[3]

Is a Post-Saturation Effect a Vital in Obtaining Significant Heat?

1. **The switch-on time.**

Since 1989, it has been assumed that a D + D reaction is the origin of the nuclear phenomena which are alleged to give heat.[4]

Thus, the reaction

$$D + D \rightarrow He^4 + \gamma$$

[3] Apart from the basic difficulty that the US government funds cold fusion work only in its own laboratories (no external funding), another matter is that few of the researchers engaged are physical electrochemists. One finds, e.g., that an experienced researcher with several publications reporting low temperature nuclear phenomena, will ask: "What is overpotential?" However, the log-rate of tritium production has been found to be linear with the overpotential [2]. Lack of observation of the individual electrode potential controlling the rate of the tritium production exponentially is one cause of the large variation in rate reported.

Unfortunately, this absence of researchers who understand potential measurement and control of individual electrodes, who know Luggin capillaries and reference electrodes, - applies particularly to the well-funded Japanese group in the Institute devoted to low temperature nuclear reactions in Sapporo.

[4] Most persons aware of what is misleadingly called "Cold Fusion" believe that the studies were begun by Fleischmann and Pons. It seems likely, that this was the honest opinion of these workers. However, low temperature nuclear phenomena were reported in modern times by Borghi. [6] French work was led by Kervran [7] and Japanese work by Kushi. [8] Most remarkable is that an intense study of the production of neutrons by passing a strong current through wires was carried out is US Government labs in the 1970's/ [9] It seems strange that his was not brought out in the violent rejection of Fleischmann et al's early work.

has been cited as a **possible** mechanism. [10] However, measurements of He^4 from electrodes under high overpotential [10] gave only about 1/3 - 1/2 the He^4 in the gas phase necessary to serve as basis for the observed heat in the Pd-D system, i.e., somewhat more than one-half the heat arises in some other way.

There have been a number of reports in the last few years which describe proton capture reactions, i.e., nuclear reactions **in solids** containing dissolved Hisotopes in which not only isotopes of Pd but also new nuclear species are detected from reactions in the cold. There is evidence for fission and fusion. The reaction rate is small but unmistakable, in some cases being measurable by γ-ray spectroscopy. In experiments other than those in the original D-Pd system as much as 56% of stable (non-radioactive) new nuclei have been found present.

According to Kucherov et al. [11], new nuclei (other than H^3 and He^4) found as a result of plasma formation between Pd electrodes in a D_2 atmosphere may contribute significantly to the anomalous heat arising in such systems. The formation of many new nuclei in solid systems, some containing H or D, was reported by Karabut et al. [11]. Similar findings have been reported more recently by Bush [12], Mizuno [13], Ohmori and Enyo [14], Dash [15] and others.

On this basis, it seems reasonable to hypothesize that in D-Pd cells, in general, reactions of the kind:

$$Pd \pm H \text{ or } D \rightarrow \text{New Nuclei}$$

can occur and that the formation of such nuclei forms a component of the heat observed in the Fleischmann-Pons phenomena. Circumstances necessary for the function of these reactions must be taken into account in any consideration of the several hundred hours of electrolysis which may be necessary to bring about a **switch on** of nuclear activity in D-Pd cells.

Thus, the time to reach saturation with D after the **switch on** of electrolysis will be dependent on the electrode's shape. Detailed solutions to Fick's Second Law for objects of varying shapes are given in Moelwyn-Hughes [16]. However, the time it takes for a diffusion front to reach a distance R (the radius of cylindrical electrode) can be roughly computed from von Schmolokowski's simple equation.

$R^2 = 2D\tau$ where D is the diffusion rate and τ is elapsed time.

Then, with $D = 10^{-6}$ cm^2 sec^{-1} and $\Delta = 1.5$ mm, $\tau = 5.10^4$ sec $\simeq$ 3 hours. But this is much less than the many **hundreds** of hours reported as the **switch on** time for the commencement of nuclear activity. The value of D used above is for the initial diffusion into the metal. As the D/Pd ratio increases, D falls [17]. However, it would have to fall to less than 10^{-8} cm^2 sec^{-1} with increasing D concentration to give the correct order of magnitude for the **switch on** time and this decrease seems unlikely. Indeed, there is evidence that the heat producing activity occurs in the surface layer, e.g., 1μ deep, and the H diffusion front would reach such distances in around a millisecond after switch on. The **switch on** of nuclear activity needs hundreds of hours and hence some additional factor apart from D/Pd $\simeq$ 1. We know that this factor depends intimately on the crystal structure of the Pd; and on the surface concentration of impurities, for this factor affects the surface activity of the adsorbed D intermediate in D_2 evolution which in turn (together with the overpotential) controls the fugacity, [18] of the dissolved D, and that of D_2 in internal voids (in which pressures > 10^4 atmospheres can be reached).

Is the factor, to start proton capture reactions of the type described above, the attainment of highly concentrated dislocation areas **within** the Pd? Is the formation of such areas rate-determined by the gradual spread of damage. (See Fig. 1)

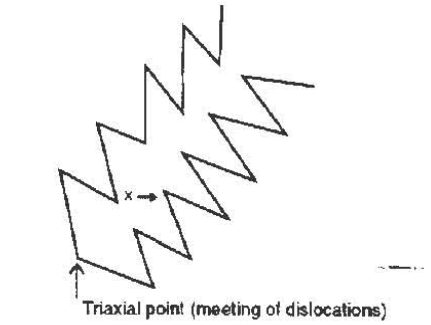

a) Internal crack, serrated surface. Void contains D2 at high fugacity, which helps spread of cracking

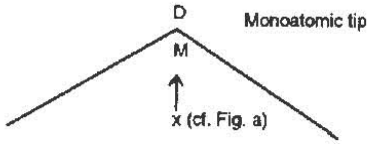

b) Speculative promontory as site of nuclear activity.

FIG. 1. Possible sites of internal damage at which nuclear activity may be initiated.

It may be that the need for impurities in the solution (adsorbed, therefore, on the electrode), is to affect the mechanism of the hydrogen evolution reaction so as to give high internal D_2 fugacity in voids in the metal. Thus, it seems reasonable to suppose that the **right degree** of internal cracking is the prerequisite for nuclear activity. **The need for this to occur to a sufficient extent may be the factor which delays for so long the onset of nuclear activity.** Cracking is usually regarded by workers in this field as a factor inimical to the **switch on** of nuclear phenomena. Indeed, cracks which reach the surface leak D_2 out of the system and reduce the fugacity of D in the metal.

Before the work of Minevski [39], it was not realized that internal damage begins inside Pd electrodes at quite low overpotentials ($\eta \sim 0.2$ v) and hence is always present within a few hours after initiating an experiment. Workers who talk about "cracking" mean **sufficient cracking** to give channels to the interface (i.e., D_2 escape).

Bockris and Flitt [20] published photographs of the **sporadic** movement of cracks under mechanical stress in Fe saturated with H. Such cracks develop large numbers of dislocations. Bockris and Subramaniam [21] calculated an increase of H activity at dislocations (as a function of overpotential) and found that it reached several orders of magnitude over the D_{Ad} activity on planar surfaces [22]. Do the dislocations arising from the spreading of cracks (Fig. 1), which cause super high surface activity of adsorbed deuterons which is the factor leading to proton capture (D^+ with Pd)? Is the key to the observation of anomalous heat and new nuclei the spread of D (or H) damage up to but **not** including the condition for escape from the surface?

Such a hypothesis would lead to some interpretation of the irregular and unpredictable functioning of the phenomena would come within the horizon of explanation. Uncontrolled surface impurities from the solution would determine, adventitiously, the mechanisms of D_2 evolution, **hence the magnitude of the internal** D_2 **fugacity**, and in turn, the degree type of cracking. High overpotential would increase the internal D fugacity though the extent of this factor would depend on the mechanism of hydrogen evolution) but the extent of adsorbed H atoms likely to undergo proton capture is schematically displayed in Fig. 1, would depend on the degree of internal **broken areas** and **voids**. The spread of internal damage with time would lead to **switch on** and the bursts of activity characteristic of the phenomena (including the sporadic spreading of cracks: then stopping, then moving on, etc., observed by Flitt, Revie and Bockris [20]. Each new burst in the crack spreading would give greater heat than the last as more internal surfaces were created, a phenomenon clearly observed by Hodko and Bockris [22].

Thus, to obtain nuclear phenomena would need several conjoint happenings: one of these is the right degree and type of impurities in solution to give adsorbed surface material which in turn influences the mechanism of

hydrogen or deuterium desorption and thus, the internal fugacity and tendency to crack.[5] Another is sufficiently high overpotential to create a sufficiently high internal fugacity for the deuterium evolution mechanism to be operative.

But why do some pieces of Pd work, others not, - from the same rod? Is it possible that relatively small changes in grain size can affect the internal spread of cracks? Could such local changes in internal structure arise from thermal irregularities in solidification or cold working in rod manufacture? Or is the function of certain Pd specimens always due to the surface impurity content which could vary with each solution?

K. Shoulders [40] has recently suggested a model for the occurrence of nuclear reactions within solids in the cold and his model also depends, as the present one, on damage. It would thus also be consistent with the several hundred hours delay before **switch on**. The rest of Shoulders model involves a concept of "clusters" of electrons which would undergo acceleration under local electric fields. The energy of these accelerated electrons, would be the origin of the nuclear reaction.

Importance of the Substrate Thickness and Mechanical Properties

Although one critical factor for the attainment of nuclear activity has been put forward as intermediate degree of internal damage, other factors are important.

Thus, the thickness of the electrode (controlling the time to saturation) is important. It might be thought that the thinnest continuous surface film of Pd on some non-interactive substrate (e.g., Ni) might be optimal. However, according to the experiments performed by Minevski [19], the formation of new nuclei does not begin in Pd until a depth of ~ 1μ [23]. Hence, a thickness **greater than 1μ** but as thin as is practical with this condition (say, 10μ) may be the most appropriate thickness.

The ductility of the electrodeposits is easily controlled by means of a variation of the overpotential and by the nature of concentration of additives [24]. Because of the importance of the right degree of cracking, the ductility of Pd becomes of importance and this may also be varied by means of electrochemical techniques [24] (control of overpotential, pulsing regimes, superimposed a.c., etc.).

Codeposition of D_2 with Pd.

The reversible deposition potential for

$$Pd^{2+} + 2e \rightarrow Pd$$

is +0.951 on the normal H scale; and that of H_2 at pH 14, 1^s -0.812. Hence, at any overpotential (and also with acid solution) Pd will be co-deposited with D_2 evolution.

This co-deposition increases the advantage of the electrochemical method for the formation of a successful system. This effect was first evidenced by Szpak and Boss [25] (cf. also Hodko and Bockris [26]), who codeposited Pd and D_2 onto Au substrates and found that it greatly reduced **switch on** time (~ 50 hrs) for the production of nuclear residues compared with those for a solid cylindrical electrode (~ 500 hrs).

[5] In an erudite and detailed discussion of the factors which have to be conjointly present if one is to obtain a **switch on** of nuclear activity, Storms [38] dismisses cracking as wholly negative. But he means "cracks which reach the surface and release D_2 into the ambience." Storms concentrates on D + D reactions and neglects the Pd + D → new nuclei aspects.

Importance of a Non-dissolving Anode

The adsorption of impurities on the cathode is helpful if the impurity (as tends to be the case) increases the deuterium overpotential for a given cathodic reaction rate [27]. The walls of the cell and the dissolution of the anode are important sources of impurities (SiO_2, Pt). A platinum anode (frequently used by many workers in this field) has a reversible potential for

$$Pt^{2+} + 2e \rightarrow Pt \text{ of } 1.118v \text{ (Normal H Scale).}$$

At pH = 14 the reversible potential for O_2 evolution is + 0.42 (Normal H Scale). At a current density of 1 amp cm^{-2}, the oxygen over potential on Pt at 25°C can be roughly estimated by the approximate equation [28]:

$$\eta = 2RT/F \ln i/i_o$$

where R is the molar gas constant in J per mol per °K, T is temperature in °K, F is the Faraday, or charge on 1 mol of ions in Coulombs.

If i_o is taken at 10^{-10} amps cm^{-2} and η = 1 atmosphere cm^{-2}; $\eta \simeq$ = 1.12. Hence, the Pt dissolution would occur under an overpotential of (1.52 - 1.12) = + 0.40 v. Were there to be no other reaction occurring on the Pt surface, the dissolution rate would be (with $i_o = 10^{-6}$ amp cm^{-2}).

$$i = 10^{-6} \times 10^{4} = 10^{-2} \text{ amps cm}^2$$

However, the **partial** rate will be much less than this because of the competing O_2 evolution. If this reduction is given by the ratio of the calculated Pt dissolution to that of O_2 evolution at 1 amp cm^{-2} (both for 1 sq cm of occupancy), the effective rate is $\sim 10^{-4}/10^{2} = 10^{-2}$. A rate of 10^{-2} amps cm^{-2} on a bare surface without competition would become an effective rate per sq cm of $10^{-2}/10^{2} = 10^{-4}$ amps cm^{-2}.

These very rough estimates[6] suggest that Pt could have a concentration in a 100 cc cell after 100 hrs as high as $3\ 10^{-3}$ moles per liter and a limiting current for the deposition of Pt of around ($i_L \simeq 0.025$ nc) 100μ amp cm^{-2}. Because of the codeposition of D_2 the effective current density will be less than this perhaps) $1/10^{-4} \sim 10^{4}$ less, i.e., about 10^{-2} amps Cm^{-2}. After 100 hrs, up to 100 monolayers of Pt could be on the Pd cathode. Such predictions have been confirmed by the direct measurements of Minevski [29].

Such deposition acts to **catalyze** D_2 evolution and **decrease** the internal fugacity of D_2, and hence diminish the probability of a nuclear switch on. Thus, **Pt anodes should not be used in cells in which it is hoped to manifest nuclear activity**.

Among possibilities [30] for non dissolving anodes would be Pd itself, but also, (doped) TiO_2, NiO_2, CoO_2, La_xNiO_3 [31]. Valuable work in this direction has been done by Tseung and by Conway and Liu. [32] It is of value to have large ("black") deposits on the anode to decrease the current density and hence the anode potential. Various geometric arrangement of cells to increase the area are possible [33].

[6] There will be further cause for reduction of the current density below that calculated because of the formation of thin oxide films likely to impede Pt dissolution by ~ 10^{2} times.

Importance of Alloying; Other Cathode Materials

Pd easily forms alloys with other metals, e.g., Pd-Ni alloys (particularly with 25-85% by weight Pd). There are two purposes in alloying. One is to influence and control the surface reaction. But the most important, – in view of the central position given in this paper to internal cracking, – is to control the ductility of the alloy compared with Pd.

It has been suggested that the ability of a structure to set off nuclear effects is related somewhat parabolically to the degree of cracking and time of electrolysis (Fig. 1). Although this **right degree of internal damage** is a prime key to the interpretation of irreproducibility, long time delays in starting, and bursts in heat output (Fig. 1 and Fig. 2), it is accepted that **too much cracking** is harmful.[7]

Alloying of Pd with Ni [34] may be a way to control this. Pd-Ni alloys are less sensitive to H-induced cracking than Pd. Conversely, they are more susceptible than is Pd to stress cracking. These properties are perhaps the reason for the success of the (Clean Energy Technology, Inc.) cells, which used Pd alloys. The mechanical properties of the electrode, how it depends on the concentration of D, and the switch on of heat evolution, demand research.

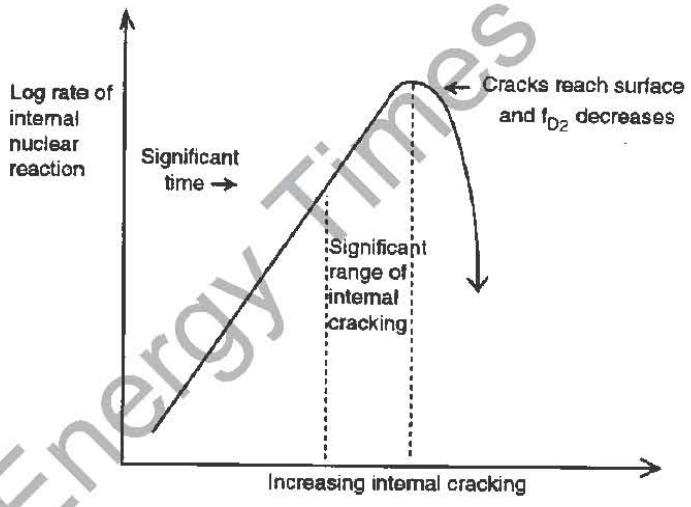

FIG. 2. Schematic of the nuclear reaction rate assumed to depend on the degree of internal cracking. What is often referred to perjoratively as "cracking" is the condition whereby the cracks reach the surface and D_2 escapes from the system, reducing D and, hence, the likelihood of nuclear reaction velocity.

Investigation of other metals and their ability to promote nuclear burning of H and D will be important. According to Kim [35] proton capture by heavy metals may be more likely than with light ones. Other H absorbers such as Ti, Ta, Nb, V provide attractive possibilities. The relation of the nuclear side to structure needs study. What of Th, U, Np as cathodes?

SUMMARY

The hypothesis suggested here is that the right degree of internal cracking and structural damage inside Pd is a necessary prerequisite to the manifestation of nuclear effects. If cracking is too much, the cracks reach the surface and D_2 escapes. Internal cracks increase the internal dislocation concentration per cc. At dislocations, adsorbed D activity is known to be greatly increased [37]. Proton capture (metal + H or D → new nuclei) is postulated to be a maximum at pointed and serrated edge sites within the damaged surfaces. The quirkiness of the phenomena is due to the fact that the following have to occur together: a sufficiently high internal D_2 fugacity and an optimal degree of internal damage (Fig. 1). Cracks develop and spread in bursts [20], which correspond to those of the

[7] Most workers in this field do not understand that internal damage and cracking in Pd begins at overpotentials of -0.3v. When they refer to "cracking," they mean "cracking which reaches the surface and reduces f_{D2}."

heat evolution. The long wait in the experiments is for sufficient cracks to form. The touchy dependence on grain size built in during manufacture of the samples serves to interpret "**live**" and "**dead**" pieces of Pd.

Impurities in solutions may increase D surface coverage and hence internal D_2 fugacity (hence cracks). Overpotential must be high, though if too high, cracks will reach the surface and decrease of internal fugacity.

The optimal electrode thickness is around 10 microns. Cylinders and thicker plates will be poor performers. Electrodeposition, under a superimposed ac regime, and codeposition of Pd and D_2 will reduce $\tau_{switch\ on}$.

Pt as an anode will reduce the probability of observing phenomena because it converts the Pd surface [29] to a Pt one and catalyzes D_2 **evolution**, reducing internal fugacity and hence the presence of adsorbed D at internal dislocations where its surface activity is maximal. Pd itself, or oxide anodes, e.g., doped TiO_2. $La_x\ NiO_3$ or anodic D_2 dissolution from Pd may be optimal [37] for the anodic O_2 evolution.

Alloy electrodes provide a means of controlling the optimal amount of internal cracking. Pd-Ni is a favored system.

REFERENCES

1. R.C. Kainthla, O. Velev, G.H. Lin, N.J.C. Packham, M. Szklarczyk, J. Wass and J.O'M. Bockris, "Sporadic Observation of the Fleischmann-Pons Heat Effect," *Electrochim. Acta*, vol 34, (1989), pg 1315.
2. C.C. Chien, D. Hodko, Z. Minevski and J.O'M. Bockris, "On an Electrode Producing Massive Quantities of Tritium and Helium," *J. Electroanalyt. Chem.*, vol 33, no 8, (1992), pg 189.
3. J.O'M. Bockris, R. Sundaresan, Z. Minevski and D. Letts, "Triggering of Heat and Sub-Surface Changes in Pd-D Systems," *J. Fusion Technology*, vol 26, (1994), pg 267.
4. J.O'M. Bockris, D. Hodko and Z. Minevski, "The Mechanism of Deuterium Evolution on Palladium: Relation to Heat Bursts Provoked by Fluxing Deuterium Across the Interface," The Science of Cold Fusion: Proceedings of ICCF-2, Como, (1991).
5. S. Pons, M. Fleischmann, and M. Hawkins, "Electrochemically Induced Nuclear Fusion of Deuterium," *J. Electroanalyt. Chem.* vol 261, (1989), pg 301.
6. D.C. Borghi, *Nuovo Cimento, Savie Nova*, vol 1, (1943), pg 1.
7. C.L. Kervran, Proofs in Geology and Physics of Low Energy Transmutation, Malvine (Personal communication) 1973.
8. Kushi, Private communication to R.A. Monti, 1991.
9. P. Graneau, "Capillary Fusion," *J. Sci. Exploration*, vol 8, (1944), pg 428.
10. Milburn Miles, B.F. Bush, G.S. Ostrom and J.J. Lagowski, "Heat and Helium Production id Cold Fusion Experiments," The Science of Cold Fusion: Proceedings of ICCF2, Como, Italy, 1991, pg 363.
11. A.B. Karabut, Y.R. Kucherov, I.B. Savatimova, "Gamma-Spectrometry at Glow Discharge in Deuterim," Frontiers of Cold Fusion: Proceedings of ICCF3, Nagoya, Japan, 1992, pg 165.
12. R.T. Bush and R.D. Eagleton, "Calorimetric Studies of an Electrolytic Excess Heat Effect Employing Light-Water-Based Electrolytes of Some Alkali Salts," Frontiers of Cold Fusion: Proceedings of ICCF3, Nagoya, Japan, (1993), pg 405.
13. T. Mizuno and M. Enyo, " Formation of ^{197}Pt Radioissotopes in Solid State Electrolyte Threated by High Temperature Electrolysis in D_2 Gas," *Infinite Energy*, Sept-Oct 1995, pg 9.
14. J. Ohmori, et al., "Isotopic Distrubutions of Heavy Metal Elements Produced During the Light Water Electrolysis on Au Electrode," *New Energy News*, vol 3, no 2 (1995); *The Journal New Energy*, vol 1, no 2 (1996).
15. J. Dash, "Excess Heat and Unexpected Elements from Electrolysis of Acidified Heavy Water with Titanium Cathodes," *The Journal of New Energy*, vol 1, no 3, (1996).
16. E.A. Moelwyn-Hughes, *Physical Chemistry, Pergamon*, (1968).
17. M. Kubalka and B. Baranowski, "Diffusion Coefficients of Hydrogen and Deuterium in Highly Concentrated Palladium Hydride and Deuteride Phases," *Bet. Dun.- esell*, vol 78, (1974), pg 335. See also: S. Majorowski and B. Baranowski, *J. Phys. Chem. Solids*, vol 4, no 3, (1982), pg 1119.
18. P.K. Subramaniam, "Electrochemical Aspects of Hydrogen in Metals," in *Comprehensive Treatise of Electrochemistry*, vol 4, *Plenum*, (1981).

19. J.O'M. Bockris and Z. Minevski, "Two Zones of 'Impurities' Observed after Prolonged Electrolysis of Deuterium on Palladium," *Infinite Energy*, vol 5-6, (1996), pg 67.
20. H.J. Flitt, R.W. Revie and J.O'M. Bockris, "Hydrogen Evolution in Stress Corrosion Cracking," *Australian J. Corrosion*, vol 1, (1976), pg 4.
21. J.O'M. Bockris, W. Beck, M.A. Genshaw, P.K. Subramaniam, and F.S. Williams, "The Effect of Stress on the Chemical Potenital of Hydrogen in Iron and Steel," *Acta Metallurgica*, vol 19, (1971), pg 1205.
22. J. Gittus and J.O'M. Bockris, "Explorations of Cold Fusion," *Nature*, vol 105, (1989), pg 339; see also, D. Hodko and J.O'M. Bockris, Frontiers of Cold Fusion; Proceedings of ICCF3, Nagoya, Japan, (1992), pg 342.
23. J.O'M. Bockris and Z. Minevski, *Infinite Energy*. See [19]
24. J.O'M. Bockris and A.K. Reddy, "Electrodes: More Fundamentals," *Modern Electrochemistry*, vol. 2, chapter 9, *Plenum*, (1970).
25. J. Szpak and P. Boss, "On the Behavior of Pd Deposited in the Process of Evolving Deuterium," *J. Analytical Chem.*, vol 302, pg 244, (1991)
26. D. Hodko and J.O'M. Bockris, "Possible Excess Tritium Production on Pd Codeposited with Deuterium," *J. Electroanalyt. Chem.*, vol 353, (1992), pg 33.
27. H.J. Flirt and J.O'M. Bockris, "Concerning Absorbed and Adsorbed Hydrogen On and In Ferrous Metals," *Int. J.H. Energy*, vol 7, (1982), pg 41.
28. J.O'M. Bockris and A.K. Reddy, Electrodics," *Modern Electrochemistry*, vol. 2, chapter 8, (1976). See also [29].
29. J.O'M. Bockris and Z. Minevski, The Science of Cold Fusion; Proceedings of ICCF2, Como, Italy, (1991)
30. J.O'M. Bockris and S.U.M. Khan, *Surface Electrochemistry*, pg 345, *Plenum*, New York, (1992).
31. J.O'M. Bockris and T. Ottagawa, "Mechanism of Oxygen Evolution on Perovskites," *J. Phys. Chem.*, vol 87, (1983), pg 2960.
32. B.E. Conway and T.C. Liu, Discussion Meeting, Bunsen Society, Sept. 2, 1986.
33. J.O'M. Bockris and S.U.M. Khan, *Surface Electrochemistry*, pg 651, *Plenum*, NY, (1993).
34. R.J. Morrisey, *Metal Finishing*, vol 92, (1994), pg 258.
35. Y.E. Kim and A.L. Zubarev, "Optical Theorum and Effective Finite-Range Nuclear Interactions for Low-Energy Nuclear-Fusion Reactions," *Nuovo Cimento*, vol 1084, (1995), pg 1009.
36. J.O'M. Bockris and T. Ottagawa, *J. Electrochem. Soc.*, vol 131, (1986), pg 1984.
37. F.G. Will, K. Cedynska and D.L. Linton, "Possible Tritium Generation in Elcetrochemical Cells Exploying Palladium Cathodes with High Deuterium Loading," *J. Electroanalyt. Chem.*, vol 360, (1993), pg 161.
38. E. Storms, "How to Produce the Posn-Fleischmann Effect," *Fusion Technology*, vol 29, (1996), pg 261; See also, *Infinite Energy*, vol 5,6, (1996), pg 77.
39. Z. Minevski, Thesis, "Studies of Protective Layers on Aluminum and Aluminum-Tantalum Alloy," Texas A&M University, (1995).
40. K. Shoulders, "Observations on the Role of Charge Clusters in Nuclear Cluster Reactions," *The Journal of New Energy*, vol 1, no 3, September, 1996.

IMPROVED CALCULATIONS INVOLVING ENERGY RELEASE USING A BUOYANCY TRANSPORT CORRECTION

Mitchell Swartz
JET Energy Technology, Inc. [1]

ABSTRACT

Measurement of energy release in the evaluation of fusion systems may rely upon flow calorimetric systems susceptible to Bernard instability which may have inadvertently impacted the calorimetry. Such thermal-driven convection can produce the appearance of "excess heat", or a magnified excess heat, because of unanticipated thermal-driven mass transfer. A semiquantitative correction to enthalpic calculations is suggested after separation of the observed Power output ($P_{derived}$) into two terms, the actual power out (P_{out}) and a second bouyancy-flow-related error term (P_{error}).

DISCUSSION

Measurement and documentation of energy release are critical in the evaluation of fusion, or other putative over-unity systems. Reliance upon flow calorimetric systems are being increasingly used by some to detect enthalpic changes secondary to putative nuclear reactions in condensed phases [1,2,3,4,5]. The equation used to derive the estimated power output, and therefore the presence of any excess heat involves the applied fluid flow, the specific heat of the water, and the temperature differential. Although this equation may be dimensionally correct, it does not appear to be always valid for low flow rates [6], such as in certain cases where Bernard instability [7,8] may inadvertently have an impact upon the calorimetry. Previously qualitatively examined has been the time-varying distribution of temperature in a quasi-one-dimensional model, for both horizontal and vertical flow calorimetry, both with and without convection [6]. There can be thermal redistribution in a vertical system with the addition of upward thermal-driven convection, driven by thermal-induced buoyancy instability. As a result, there can be shift of the isothermal lines away from the intrinsic symmetry exhibited by horizontal flow calorimetric systems with zero applied convective flow, producing the appearance of "excess heat", or a magnified excess heat, even in the absence of applied convection. Thus, the quoted efficiencies of energy generated by classical calculation may not be correct. There may be an apparent error "signal" for zero flow because of the thermal instability which can create mass transfer. This brief note suggests a semiquantitative correction for the enthalpic calculations using a first order term for heat transport secondary to buoyant forces generated by unstable thermal inhomogeneities.

If η_B is the ratio of heat transported by the buoyant forces to all of the heat transported including that by the applied solution convection, then the Q1D model of heat and mass transfer [6] indicates that what is generally correct for horizontal calorimetric systems may not be correct for vertical systems, when the non-dimensional number ($= \eta_B$) is significantly greater than zero.

The buoyant heat flow ratio, η_B, in real systems may also depend upon other non-dimensional factors including the Archimides non-dimensional number, which is the ratio of the buoyant force to the viscous force, and possibly the Rayleigh non-dimensional number, which is the ratio of gravity to thermal conductivity.

For this simplification, we suggest the separation of the observed Power output ($P_{derived}$) into two terms, the actual power out (P_{out}) and a second buoyancy-flow-related error term (P_{error}). Because the total observed signal -- the delta-T in the face of the applied convention ($v_{convection}$) and incidental thermal buoyant convection ($v_{buoyancy}$) -- results from their combined velocity, then to zeroth order one can write

$$P_{observed} = P_{out} + P_{error} = C_p * \Delta T * V_{total} \cong C_p * \Delta T * (V_{convection} + V_{buoyancy}) \quad \text{(eq. 1)}$$

The error term is thus first order on the non-dimensional ratio η_B .

$$P_{error} \approx C_p * \Delta T * V_{total} * \eta_B \quad \text{(eq. 2)}$$

We assume that η_b is small and therefore $V_{total} \approx V_{convection}$. This is also an approximation because the chain rule from calculus, and consideration of possible coolant redistribution, suggest that there are other higher order terms also potentially arising from the impact of the buoyant flow.

$$\frac{\delta P_{error}}{\delta_{\eta_B}} \approx (C_p * \Delta T * V_{total}) + [C_p * V_{total} * \eta_B * \frac{\delta \Delta T}{\delta \eta_B}] \quad \text{(eq. 3)}$$

Thus, the second term in the equation, involving $\frac{\delta \Delta T}{\delta \eta_B}$, may depend upon several additional factors involving at least the total tank volume just outside the reactor (or capacity of the thermal control) and the actual input temperature boundary condition.

Ignoring in this approximation the terms of higher order, and using the approximations above, the linear correction to the observed power becomes corrected as

$$P_{corrected} \approx P_{observed} - (C_p * \Delta T * V_{convection} * \eta_B) \quad \text{(eq. 4)}$$

Thus, a more accurate estimate of purported over-unity power gain (π) could be directly derivable, from the correction to first order, as

$$\pi_{corrected} = \pi_{observed} * (1 - \eta_B) \quad \text{eq. 5)}$$

Since the submission of this manuscript, the correction technique of subtracting for the buoyant uplift in flow calorimetric systems has been experimentally applied independently by Dr. Barry Merriman and P. Burchard [9]. In that system, the correction is taken as a direct calibration to set the null signal. Based on this paper, it may also be possible to semiquantitatively derive both terms in some systems.

In summary, the extent of any such reported 'excess heat' may be inflated, if the information was collected with a vertical flow calorimetric system, without confirmatory calibrations under low to moderate flow conditions where the non-dimensional number (η_B) is not trivial. Equations 4 and 5 offer semiquantitative corrections to the observed calculations of present verticle flow calorimetric systems used to investigate heat producing reactions in the condensed phase. These can be used even in the presence of buoyant flow in vertical flow calorimetric systems, using a linear correction based upon the measured, or estimated, values of η_B.

REFERENCES

1. R.D. Armstrong, E.A. Charles, I. Fells, L. Molyneux, M. Todd, "Some Aspects of Thermal Energy Generation During the Electrolysis of D_2O using a Palladium Cathode," *Electrochim. Acta*, vol 34 (1989), p 1319.
2. L. Bertalot, F. De Marco, A. De Ninno, A. La Barbera, F. Scaramuzzi, V. Violante, P. Zeppa, "Study of Deuterium Charging in Palladium by the Electrolysis of Heavy Water Heat Excess Production," *Nuovo Cimento*, vol 15 D (1993), p 1435.
3. D. Cravens, "Flowing Electrolyte Calorimetry," Proceedings of 5th International Conference on Cold Fusion, pp 79-86 (1995).
4. M.C.H. McKubre, S. Crouch-Baker, R.C. Rocha-Filho, S.I. Smedley, F.L. Tanzella, T.O. Passell, J. Santucci, "Isothermal Flow Calorimetric Investigations of the D/Pd and H/Pd Systems," *J. Electroanal. Chem.*, vol 368 (1994), p 55.
5. O.A. Velev, R.C. Kainthla; "Heat Flow Calorimeter with a Personal-Computer-Based Data Acquisition System," *Fusion Technol.*, vol 18 (1990), p 351.
6. M. Swartz, " Potential for Positional Variation in Flow Calorimetric Systems," *Journal of New Energy*, vol 1, pp126-130 (1996)
7. J. Melcher, Continuum Electromechanics, MIT Press, Cambridge, pp 10.13-10.18 (1981).
8. S. Chandrasekhar, Hydrodynamic and Hydromagnetic Stability, Clarendon Press, Oxford, 9-75 (1961).
9. B. Merriman, P. Burchard, "An Attempted Replication of the CETI Cold Fusion Experiment," http://www.math.ucla.edu/~barry/CF/reportcover.html (1996)

JET Energy Technology, Inc.
P.O.Box 81135
Wellesley Hills, MA 02181

PLASMA-INJECTED TRANSMUTATION

By Hal Fox [1], Robert W. Bass, Shang-Xian Jin

ABSTRACT

Several recent developments of devices that produce low-energy nuclear reactions are explained by the deliberate or fortuitous production of Shoulders' high-density charge clusters, also called EVs (for Electrum Validum). Some and perhaps most of the nuclear reactions in a variety of fluids and devices including the Pons-Fleischmann discovery (palladium/heavy water systems), in nickel/light water systems, in Patterson Power Cells™, in low-pressure deuterium gas devices, in sparking-in-hydrogen devices, in exploding resistors, in plasma-focus devices, in the abundance of elements in the earth's surface, and in the Neal-Gleeson Process are explained by the creation, launching, and impingement of high-density charge clusters on a target element or elements. This paper presents a hypothesis and computations that explains these various discoveries and experimental results that have resulted in the filing of a broad patent application. Excess heat from various so-called **cold fusion** discoveries are substantiated.

A. INTRODUCTION

High-density charge clusters, as taught by Kenneth Shoulders [1], can be formed in a near vacuum by a short pulse of negative potential applied to a specially-designed cathode (such as using a conical point). The charge cluster was designated by Shoulders as an EV or **electrum validum** (Latin and Greek for strong electron). A typical EV will impact a witness plate (a thin metal foil placed near the anode) and leave various-sized holes or blisters in the metal foil. Single EVs and EV clusters may vary in size from less than a micron to 50 microns as produced in the laboratory. It is believed that with appropriate input energy levels larger EVs may be produced.

EVs are formed by many types of electrical discharges. Nearly all electrical sparks, filaments, streamers, or lightning bolts will produce EVs. These EVs are evident when a spark impacts a metal surface. Spark erosion may be primarily the effect of EV action. For one skilled in the art, the strike pattern of a EV is often readily identified [2]. Because the EV consists of 10^8 to 10^{13} electrons and are relatively small, the energy density is large. Provided that the energy of the EV exceeds a certain energy level, the EV can cause nuclear reactions to occur as reported by Shoulders [2].

As taught in Shoulders' patents [1] EVs can be stripped of most positive ions. In other embodiments, the EV can be produced so that it carries or transports a small percent of positive ions [2]. Such EVs, especially when more energetic than a threshold energy value, can produce nuclear reactions [2].

When an EV, of sufficient energy level, and carrying positive ions, impacts some types of target materials a nuclear reaction is produced. The difference between the strike of a typical EV and an EV that causes nuclear reactions, can be easily be seen on microphotographs. Shoulders has shown several typical pictures in his paper [2] where the difference between such an EV strikes are readily apparent. The following Fig. 1a (from Shoulders) is the electron microscope micrograph of an impact of an EV. Fig. 2a (from Shoulders) is a similar micrograph of the result of the impact of a stronger EV. In Fig. 1a the metal has been melted by the released energy of the

[1] President, Fusion Information Center, Inc., P.O. Box 58639, Salt Lake City, UT 84158.
Phone 801-583-6232. Fax 801-583-2963.

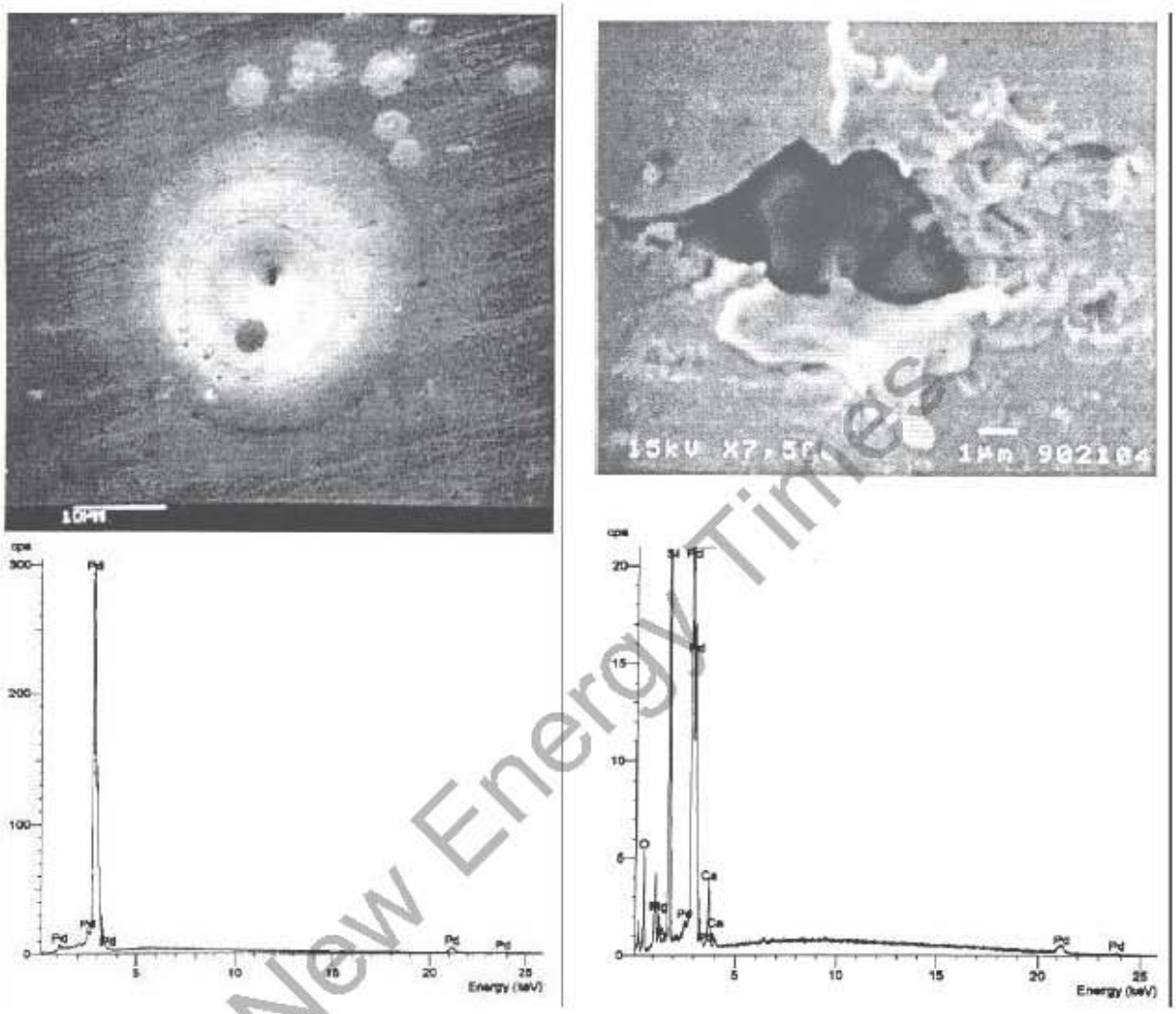

Fig. 1b

EV impact but there is no evidence of nuclear reactions, as shown by the X-ray micro analysis in Fig. 1b. In Fig. 2a the EV has caused a vigorous explosion with measurable nuclear changes as shown by the X-Ray microanalysis in Fig. 2b. The figures are reproduced from Shoulders [2].

The EV is observed to maintain a stable cluster configuration even though consisting primarily of electrons. Therefore, there must be a highly dynamic nature to the EV so that electrodynamic forces are stronger than the repulsive forces of the electron charges. The possibility of the existance of an essentially single-specie plasma state represented by a stable packet of charged particles moving collectively through space-time was examined by Ziolkowski [22]. Robert Bass [3] has shown that a solution of Maxwell's equations is valid for a toroid or a infinitely-long cylinder. From Bass's mathematical description, one of us (Fox) has proposed that the form of the EV is probably a toroid. That assumption has not been firmly established. The size and number of EV clusters is determined by formation parameters, especially by the magnitude and shape of the electrical pulse used to create the EV. Typically, single EVs can vary from one-half to three microns. Higher formation energies produce clusters of EVs which then tend to form a necklace of smaller EVs. The EV necklace is typically about

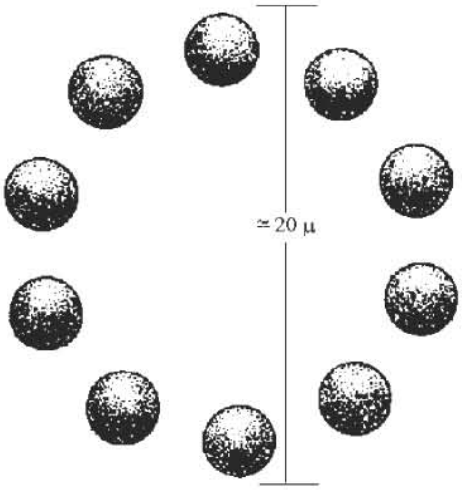

Fig. 3. EV Necklace

20 microns in diameter and appears to travel in a direction perpendicular to the plane of the necklace, much like a smoke ring travels. Fig. 3, after Shoulders [1], illustrates a 20-micron cluster of smaller EVs.

B. THE KINETIC ENERGY CAPABILITY OF AN EV

The energy density of an EV can be shown to be large. The numerical density of electrons in an EV is about equal to Avogadro's Number (about 6 x 10^{23} per cubic cm.). The total number of electrons in a typical EV, one micron in diameter, is about 10^{11} according to Shoulders [2]. Assume that the size of the EV is a sphere one micron in diameter and that the number of electrons in the EV is 10^{11} electrons. The mass of an electron is 9.1095 x 10^{-28} grams. The mass-to-charge ratio of the EV is about the same as the mass-to-charge ratio of an electron [15]. According to Shoulders [1,2] an EV can carry or be embedded with about 1 to 10 positive ions for every million electrons. In other words, if the EV has 10^{11} electrons there may be an attached plasma of 10^5 to 10^6 positive ions. The source of these ions can come from a low-pressure hydrogen atmosphere or from low-pressure water vapor in the near-vacuum environment in which the EVs are produced [1].

An EV, if created and launched in the presence of a strong electric field, is subject to the same accelerating potential as an electron placed in the same electric field. The velocity achieved by an EV in such an electric field is about the same as the velocity achieved by a single electron. Although the EV may be carrying a large number of positive ions, the ratio of electrons to positive ions is so large (10^5 to 10^6) that the positive ions embedded in or attached to the EV have very little effect on the velocity imparted to the EV by the electric field.

The velocity gained by the EV provides a large kinetic energy to the charge cluster. In classical electrodynamics, the kinetic energy of a charge cluster is determined by the potential difference (or electric field strength) between the emitter (cathode) and target (anode). The kinetic energy of the charge cluster at the point or surface of the emitter is considered to be zero and to increase as the charge cluster approaches the target or anode.

When an ion, with mass M_i and charge Z e, is accelerated by a electric field potential difference V, the ion will attain an energy W increase of $\Delta W = Z\ e\ V$, where Z is the charge number of the ion and e is the unit electron charge. The velocity increase v_i in the non-relativistic case is

$$v_i = (2\ Z\ e\ V / M_i)^{1/2}, \quad (1)$$

where we assume that the initial velocity of the ion is zero.

Now consider a high-density charge cluster (an EV) with N_e electrons and N_i positive ions with mass M_i and charge Z e. When this charge cluster accelerates through the same potential difference V as given above, the cluster will gain energy equal to $(-N_e\ e + N_i\ Z\ e)V$ and the velocity increase in the non-relativistic case is

$$v = [2\ (-N_e\ e + N_i\ Z\ e)V / (N_e\ m_e + N_i\ M_i)]^{1/2}, \quad (2)$$

where M_e is the electron mass and M_i is the positive ion mass and zero initial velocity of the cluster is assumed.

In the EV with positive ions case, the ratio of the number of positive ions to the number of negative electrons N_i / N_e is about 10^{-6}. Then equation (2) can be approximated by

$$|v_{EV}| = (2\ e\ V / m_e)^{1/2}, \quad (3)$$

The ratio of v_{EV} to v_i for the same potential difference V is given by

$$|v_{EV}| / v_i = (M_i / Z\ m_e)^{1/2}. \quad (4)$$

and the ratio of the kinetic energy, $K_{i,EV}$, attained by a positive ion embedded in the EV and the kinetic energy, K_i, gained by a positive ion in a cluster of only positive ions is then

$$K_{i,EV} / K_i = 1/2\ M_i\ v^2_{EV} / 1/2\ M_i\ v_i^2 = M_i / Z\ m_e \text{ approx} = 1836\ A/Z, \quad (5)$$

where A is the mass number and Z is the charge number of the positive ion, respectively.

This concept that high kinetic energy can be imparted to positive ions by an EV which has been formed with relatively low-energy means is important! As an example of the extent of the kinetic energy developed in a positive ion, when 5 kilovolts potential difference is applied, a proton (deuteron) in the case of a pure proton (deuteron) cluster will attain 5 KeV energy. However, a proton (deuteron) embedded in an EV, using the same accelerating potential of 5 kilovolts could attain a kinetic energy of 9.18 (18.36) mega-electron volts! This additional kinetic energy is now sufficient to overcome the Coulomb barrier of a typical target nucleus and produce nuclear reactions. When a large number of such EVs, **with accompanying positive ions**, are produced and accelerated to a target anode, the nuclear reaction rate can be quite high.

As the EV research and development matures, it is likely that this technique of promoting high kinetic-energy positive ions will become one of the least expensive and easiest methods to study nuclear reactions. A table-top, compact, charged-particle accelerator may no longer be a dream but become a reality. Such a device is proposed to replace large, expensive, particle accelerators. In the near future, small colleges and even secondary schools could afford to have a laboratory particle accelerator.

C. THE EV AND COLD FUSION DEVICES

As detailed above, when an EV is accelerated in an electric field (and is carrying perhaps 10^6 positive ions), there is sufficient energy to create nuclear reactions by transporting the positive ions into the nuclei of the target material. This statement can be clearly demonstrated by replicating the experiments of Shoulders [2]; George [4]; Dash [5]; Matsumoto [6]; Dufour [7]; Samgin, et al.,[8]; Savvatimova, et al; [9] Miley and Patterson [10]; Reiter and Faile [11]; Rout, Srinivasan, et al. [12]; and many others. The parameters of the experiment must be selected so that EVs are produced and carry positive ions. Conceptually, the difference between an EV and an EV with positive ions can be determined by the difference between the charge-to-mass ratio. Alternatively, to determine if EVs are carrying positive ions, it is better if the experiment is run for only a short time and the metal target is viewed before the target electrode looks like the moon's surface with too many strike patterns obstructing the view. Scanning electron microscopy can be used to determine if there are nuclear changes in the vicinity of the EV strike. If not, then the strike was likely an EV with insufficient energy to promote nuclear reactions.

If we examine other types of experiments such as Bockris [13] where pure carbon electrodes were caused to arc under pure water and iron was produced, we would suggest that EVs were produced. On the other hand, in a replication of the Bockris experiment, Grotz found no significant results [14]. According to the **hypothesis** presented in this paper, Bockris has nuclear reactions because his experiment produced EVs. Grotz has negative results because his experimental procedure was not sufficiently energetic and no ion-bearing EVs were produced.

A dramatic evidence for the power of an EV is pictured in Ken Shoulders' book [15] where he shows the trail left by an EV necklace (a number of EVs can form into a type of a smoke-ring pattern having a dimension of about 20 microns in diameter, this combination is named an EV necklace). One picture shows the hole drilled by an EV through several times it own diameter of aluminum oxide. The EV apparently vaporized the aluminum oxide and the vapor was then deposited on the inner surface of the "EV-drilled" cylindrical hole. See Fig. 4 from Shoulders [15].

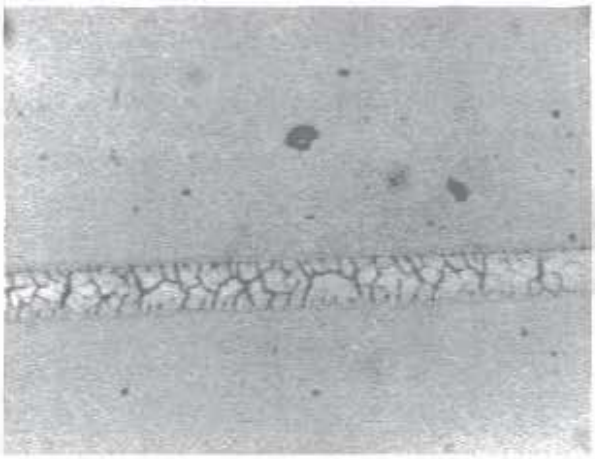

Fig. 4

It is interesting to note that Shoulders' experimental work on high-density charge clusters, covering more than a decade has been rediscovered in Russia by G.A. Mesyats [23]. Mesyats states, "A commonly used way to initiate an **ecton** is to induce a vacuum discharge over a dielectric being in contact with a metal." [23, pg 725]. (Mesyats' **ecton** is Shoulders' **EV**. Compare with Shoulders' patents [1,2]).

D. SIMPLE TEST FOR EV PRODUCTION

If you are working with devices in which EVs are expected to be produced, the following procedure is suggested. Place a small transistor radio near the suspected EV source. Tune to an AM (amplitude modulated) part of the radio band where there are no AM stations on the air. Turn up the volume and listen for "cracks" of static. When an EV strikes it will emits sufficient electromagnetic energy to hear on such a radio. Remember that FM (frequency modulation) clips these bursts of EM radiation and that static discharges will not be heard on FM stations. (Note: Travelers in country where flash floods can be caused by thunderstorms use this technique with their auto radios to listen for any lightning flashes. If lightning cracks are prevalent, wary travelers do not camp in stream beds.)

If you question whether EVs can do damage to metal surfaces, just disconnect the capacitor that is wired across the breaker points of a distributor in a gasoline-fueled internal combustion engine. You will soon find that you will need to replace the distributor breaker points. The capacitor is sufficient to prevent the formation of EVs.

E. GEOLOGIC IMPLICATIONS OF NEVs

Every lightning strike will produce an abundance of strong EVs. If one desires to check that statement, place a polished metal sheet at a place frequented by lightning strikes. After a lightning bolt has hit near the metal sheet, examine it for EV patterns. To consider the long-term effect of lightning-produced EVs, assume that lightning is a source of many strong EVs. The end result would be a flurry of nuclear reactions with every lightning strike. Over the millions of years that the earth's atmosphere has been characterized by frequent or occasional thunder storms, it would be expected that the geological surface of the earth would be enriched by elements characteristic of EV-caused nuclear reactions.

In his verbal presentation of his paper Shoulders [2] used the term "dirt" to describe the conglomeration of new elements produced by an EV strike onto a palladium target. The term "dirt" was chosen to describe the combination of calcium, potassium, carbon, aluminum, iron, etc. of the elements that appear to be abundantly produced by an EV strike on a metal target and the resulting nuclear reactions.

Therefore, it is suggested that the elements found in the earth's crust have been produced, in part, by the action of lightning during the earth's many years of atmospheric thunderstorms. Here is a list of the twenty most abundant elements found in the earth's crust with their atomic numbers [16]: Oxygen 8; Silicon 14; Aluminum 13; Iron 26; Calcium 48; Sodium 11; Potassium 19; Magnesium 12; Titanium 22; Hydrogen 1; Phosphorus 15; Manganese 25; Sulfur 16; Carbon 12; Chlorine 17; Rubidium 37; Fluorine 9; Strontium 38; Barium 56; and Zirconium 40. The reader will find it interesting to compare the elements produced by EV strikes on metal targets with this list. Shoulders' verbal designation of "dirt" for the elements found at an EV strike appears most appropriate. See Appendix A for a list of possible nuclear reactions with a palladium target from a paper by Jin & Fox [18].

F. IMPROVING THE NEAL-GLEESON PROCESS FOR TRANSMUTATION

In a paper presented by one of us (Fox) [17] the Neal-Gleeson Process for low-energy nuclear reactions was partially described. In the Neal-Gleeson Process, a relatively simple configuration of an electro-nuclear cell is connected to a suitable medium-voltage source (several hundred volts). With the proper cell, electrode, and electrolyte configuration, heavy elements in the electrolyte can be transmuted to lower mass elements. This process has been developed over the past two years in a series of over one hundred experiments with gradually-improving results. Naturally-radioactive thorium and naturally-radioactive uranium have been processed with the result that the radioactivity has been dramatically reduced (up to 77 percent reduction in radioactivity). This is a clear indication that the radioactive elements have been transmuted. Mass spectroscopy analysis of before and after samples show that elements not present in the **before samples** are present in the **after samples.**

It is the basis of the hypothesis presented in this paper that the mechanism for the reduction of radioactivity, using the Neal-Gleeson Process (patent pending), is that many EVs are produced at the electrodes and injected into the heavy elements dissolved in the electrolyte. Therefore, if one desires to improve on the Neal-Gleeson Process it will be by improving the manner in which EVs are produced and injected into the nuclei of selected target elements.

G. THE PENETRATION OF A NUCLEI BY AN EV

It remains to be determined as to what extent an energetic EV can carry positive ions, such as hydrogen, deuterium, or lithium ions and cause such ions to penetrate the Coulomb barrier of the nuclei. We know that EVs travel at velocities up to a reasonable fraction of the speed of light [1, 2, 15]. The velocity of an EV is strongly dependent on the accelerating voltage supplied. As detailed above, the kinetic energy imparted to an EV can be sufficient to carry the positive ions into the nucleus of nearby elements (in the vicinity of an EV strike), overcome the Coulomb barrier, causing such ions to become a part of the nuclei of some fraction of such target nuclei (by EV-ion collisions), and promoting a nuclear reaction (such as the spontaneous fissioning of heavy elements).

While this type of nuclear reaction could be considered to be a high-energy plasma physics reaction, the initiating process is low-energy (often less than 1,000 volts). The process of the nuclear reaction begins with the creation of a high-density charge cluster by low-energy means. However, the charge cluster has a high energy potential. The impact of the EV, with at least some types of matter, then produces nuclear reactions. The question that should be addressed is: "Is it expected that the nuclear reactions caused by EVs will have the same branching ratios as nuclear reactions observed in high-energy plasma physics?" It is suggested that the over 600 papers reporting on **cold fusion** successes is replete with evidence that the branching ratios, for at least some low-energy-generated nuclear reactions, are different from the branching ratios found in high-energy gas-plasma physics nuclear reactions. The fact that the reactions occur in or near the surface of a metal lattice is asufficiently different from the environment that occurs in high-energy gas-plasma physics to produce different results.

However, it is believed that the nuclear reactions produced by EVs in a low-pressure gas environment will be similar to the experimental results from a similar bombardment of a target material with high-energy positive ions.

H. SUMMARY

This paper presents a hypothesis which is intended to guide further experiments to determine to what extent the EVs are responsible for nuclear reactions in various types of cold fusion devices and also in the Neal-Gleeson Process. This hypothesis explains many of the anomalies observed in a variety of cited experiments. The hypothesis has the advantage of not requiring any unusual new physics principles to be invoked. The acceptance of the formation of and the development of high kinetic-energy potential of the EVs has sufficient merit to critically investigate this hypothesis with both experiments and for further mathematical analysis to determine the range of possible application of this hypothesis in explaining previous experiments (beginning with Pons and Fleischmann [21]) and extending the important discoveries of Shoulders' work and of the Neal-Gleeson Process into new realms of experimental investigation. If this hypothesis is correct, then a new world of nuclear physics is opened to further development, complete with transmutation, power generation, and thousands of new inventions for the benefit of man and beast.

ACKNOWLEDGEMENTS: As seen by the references, the authors have had the privilege of communicating with some of today's geniuses through personal contact with many scientists, engineers, and inventors. The authors' contributions are one of gathering and rearranging scraps from the intellectual feasts of the scientific elite. The financial support of the Fusion Information Center, Inc. is acknowledged.

REFERENCES

1. Kenneth R. Shoulders, "Energy Conversion Using High Charge Density", U.S. Patent 5,018,180, issued May 21, 1991, see also "Circuits Responsible to and Controlling Charged Particles", U.S. Patent 5,054,047, issued Oct. 1, 1991.
2. Kenneth and Steven Shoulders, "Observations on the Role of Charge Clusters in Nuclear Cluster Reactions", *Journal of New Energy*, vol 1, no 3, Fall 1996.
3. Robert W. Bass, "New Solutions of Maxwell's Equations", *Fusion Facts*, August 1992, pp 20-21.
4. Russ George, Paper presented at second Low-Energy Nuclear Reactions conference, College Station, Texas, September 13-14, 1996.
5. S. Miguet, John Dash (Portland State University), "Microanalysis of Palladium after Electrolysis in Heavy Water", *Journal of New Energy*, vol 1, no 1, January 1996, pp 23, 5 figs, 3 refs.
6. Takaaski Matsumoto (Hokkaido Univ), "Cold Fusion Experiments by Using Electrical Discharge in Water", in Proceedings: ICCF4, Volume 3: Nuclear Measurements Papers, December 6-9, 1993, Maui, Hawaii, pp10-1 to 10-6, 4 refs, 2 figs.
7. J. Dufour, "Cold Fusion by Sparking in Hydrogen Isotopes," *Fusion Technology*, **1993,** vol 24, p 205ff.
8. A.L. Samgin, A.N. Baraboshkin, I.V. Murigin, S.A. Tsvetkov, V.S. Andreev, G. Vakarin (Inst. High-Temp. Electrochem., Rus. Acad. Sci., Ekaterinburg), "The Influence of Conductivity on the Neutron Generation Process in Proton Conducting Solid Electrolytes," Proceedings of ICCF4, Volume 3: Nuclear Measurements Papers, December 6-9, 1993, Maui, Hawaii, pp 5-1 to 5-7, 9 refs, 3 figs.
9. Irina Savvatimova, Yan Kucherov, & Alexander Karabut, "Impurities in Cathode Material Before and after Deuterium Glow Discharge Experiments", *Fusion Technology*, vol 26, no 4T, Dec 1994, pp 389-394. ICCF-4, Maui, Hawaii, Dec 6-9, 1993.

10. George H. Miley and James A. Patterson, "Nuclear Transmutations in Thin-Film Nickel Coatings Undergoing Electrolysis", *Journal of New Energy*, vol 1, no 3, Proceedings of the Second Low-Energy Nuclear Reactions Conference, Sept 13-14, 1996, College Station, Texas.
11. Reiter and Faile, "Spark Gap Experiments", *New Energy News*, Sept 1996, p 11ff.
12. R.K. Rout, M. Srinivasan, A. Shyam and V. Chitra (BARC, India), "Detection of High Tritium Activity on the Central Titanium Electrode of a Plasma Focus Device," *Fusion Technology*, vol. 19, March 1991, pp 391-394.
13. R. Sundaresan & J.O'M. Bockris, "Anomalous Reactions During Arcing between Carbon Rods in Water", *Fusion Technology*, vol 26, Nov. 1994.
14. Toby Grotz, "Investigations of Reports of the Synthesis of Iron via Arc Discharge through Carbon Compounds", *Journal of New Energy*, vol 1, no 3, Fall 1996, 3 figs, 10 refs.
15. Kenneth R. Shoulders, EV - A Tale of Discovery, 265 pages, illus., c1987, privately published and available from the author.
16. Robert C. Weast, Editor, CRC Handbook of Chemistry and Physics, 59th Edition, CRC Press, Inc. ©1978, p F-199.
17. Robert Bass, Rod Neal, Stan Gleeson, & Hal Fox, "Electro-Nuclear Transmutations: Low-Energy Nuclear Reactions in an Electrolytic Cell", *Journal of New Energy*, vol 1, no 3, Fall 1996.
18. Shang-Xian Jin & Hal Fox, "Possible Palladium-Related Nuclear Reactions", *Journal of New Energy*, vol 1, no 3, Fall 1996.
19. Ron Brightson, "Application of the Neutron Cluster Model to Experimental Results", *Journal of New Energy*, vol 1, no 1, pp 68-74.
20. Roberto Monti, "Low-Energy Nuclear Reactions: Experimental Evidence for the Alpha Extended Model of the Atom", *Journal of New Energy*, vol 1, no 3, Fall 1996, Proceedings of the Second Low-Energy Nuclear Reactions Conference.
21. M. Fleischmann, S. Pons, and M. Hawkins, "Electrochemically Induced Nuclear Fusion of Deuterium." *J. Electroanalytical Chem.*, vol. 261, pp 301-308, and erratum, vol. 263, p 187, 1989.
22. Richard W. Ziolkowski & Michael K. Tippett, "Collective effect in an electron plasma system catalyzed by a localized electromagnetic wave", *Physical Review A*, vol 43, no 6, 15 Mar 1991, pp 3066-3072, 1 fig, 7 refs.
23. G.A. Mesyats (Inst. of Electrophysics, Ekaterinburg, Russia), "ECTON Processes at the Cathode in a Vacuum Discharge", Proceedings ISDEIV, XVIIth International Symposium on Discharges and Electrical Insulation in Vacuum, Berkeley, Calif., July 21-26, 1996, Volume II, pp 720-731, 10 figs, 5 tables, 38 refs.

APPENDIX A

Elements that potentially could be produced by non-neutral plasma injection into a palladium target.

The following data is taken from the Jin & Fox paper, "Possible Palladium-related Nuclear Reactions", *Journal of New Energy*, vol 1, no. 3 [18].

In this case only palladium is considered as a target material. Only the reactions with deuterium, protons, and alpha particles as payload elements are listed below. Only those nuclear reactions that are consistent with conservation rules are included. It is obvious that as other target elements are considered and as other payload elements may be considered, the entire spectrum of the periodic table may be amenable to formation by the EV-payload-accelerator-target process. In fact, if the new elements produced do not leave the target material, many additional elements could be created by the plasma-injection process with secondary target elements. It is stated in the patent application that it is obvious that one skilled in the art can produce just about any element desired.

Payload Element: deuteron. Possible Pairs of Elements Produced:

Rhodium & helium; lithium & ruthenium; lithium & molybdenum; beryllium and tellurium; beryllium & molybdenum; beryllium & niobium; boron & molybdenum; carbon & niobium; carbon & zirconium; nitrogen & zirconium; nitrogen & strontium & helium; fluorine & strontium; fluorine & krypton; neon & rubidium; neon & krypton; neon & bromine; magnesium & bromine; magnesium & selenium; magnesium & arsenic & helium; silicon & arsenic; silicon & germanium; silicon & gallium; phosphorus & germanium; phosphorus & zinc; sulfur & gallium; sulfur & copper; argon & copper; potassium & nickel; calcium & cobalt; titanium & manganese.

Payload Element: proton. Possible Pairs of Elements Produced:

Boron & molybdenum; fluorine & krypton; sodium & krypton; sodium & selenium; aluminum & germanium; phosphorus & germanium; scandium & iron; phosphorus & gallium; vanadium & chromium; titanium & manganese; calcium & manganese; manganese & chromium.

Payload Element: helium-4. Possible Pairs of Elements Produced:

Beryllium & ruthenium; carbon & molybdenum; oxygen & zirconium; neon & strontium; magnesium & krypton; silicon & selenium; sulfur & germanium; argon & zinc; krypton & copper; potassium & copper; calcium & nickel; titanium & iron; sodium & krypton; magnesium & bromine; chlorine & zinc.

A cautionary note: The above list of possible elements makes no assumptions about the inner construction of the nucleus. If Ron Brightson [19] is correct in his nuclear cluster model, many of these possible reactions are favored and others are not. If Roberto Monti [20] is correct in his alpha-cluster model, then the same statement is true. **It is expected that a series of experiments will be required to produce the type of data that will provide the basis for improved understanding of the inner structure of the nucleus.**

NOTE: Those who may be interested in commercial rights to this technology should contact Hal Fox, 801-583-6232, Fax 801-583-2963.

LETTER TO THE EDITOR

A Comment to the paper of E.E. Antonov et al.
[*JNE* vol 1, no 2]

The authors proposed a plasma-chemical discharge method of water conversion in gaseous phase for hydrogen production and a theoretical model and provided some experimental results. The method is interesting and the results of research are worth referring to.

The method may be quite effective for hydrogen production from water vapor, however the installation cost on the combustion engine is more expensive than the electrolysis methods in future use.

The proposed theoretical model has contributed to comparison and analysis of the experimental data. A more accurate model, however, is needed for deeper understanding of the processes. A non-equilibrium kinetic model which could determine the distribution function of each component in the system under given boundary conditions is recommended.

Dr. S.X. Jin

[Dr. Jin is a *JNE* peer-reviewer. --Ed.]

JOURNAL OF NEW ENERGY

An International Journal of New Energy Systems Vol. 1, No. 3, 1996

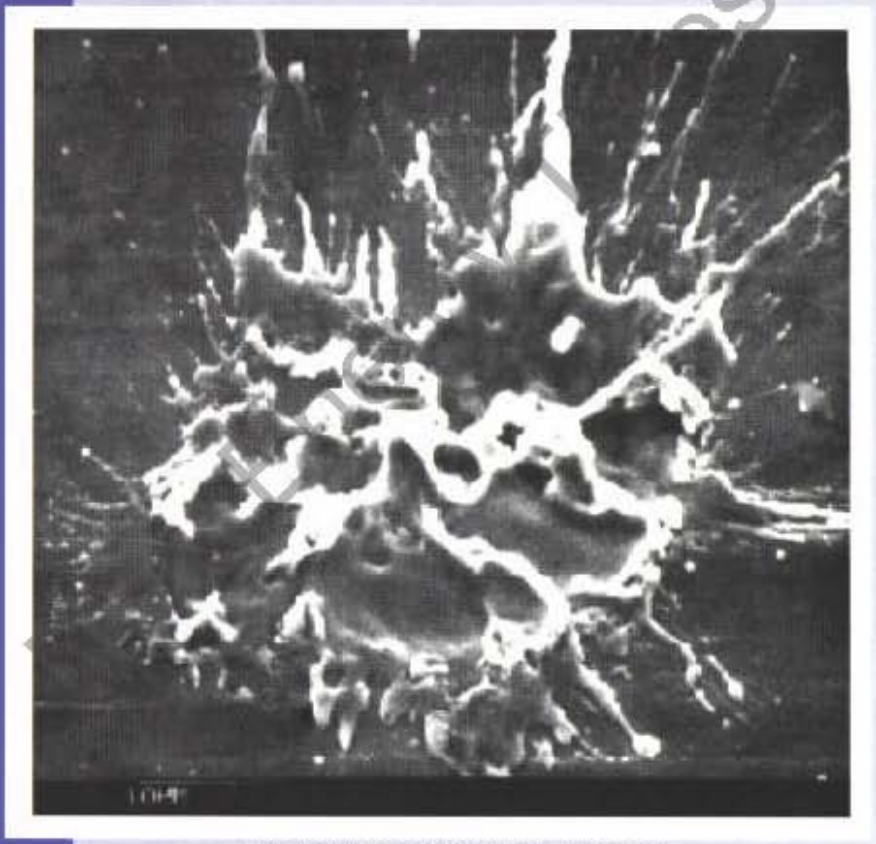

Micro-photograph of a K. Shoulders experiment.

Journal of JNE

Proceedings of the Second Conference on Low-Energy Nuclear Reactions held September 13-14, 1996.

Fall 1996
ISSN 1086-8259

Fall 1996 **Vol. 1, No. 3**

JOURNAL OF NEW ENERGY

An International Journal of New Energy Systems

The Journal of New Energy is published quarterly by Fusion Information Center, Inc., with offices at the University of Utah Research Park, Salt Lake City, Utah.

ISSN: 1086-8259

Mailing address:
Journal of New Energy
P.O. Box 58639
Salt Lake City, Utah 84158-0639
(801) 583-6232 FAX: (801) 583-2963

JNE Staff:
Hal Fox, Editor
Dineh Torres, Publications Dir., Graphics
Robyn Harris, Circulation Mgr.

Printed in the U.S.A

Instructions to Authors:

Professional papers on cold fusion and other enhanced energy systems are solicited from scientists, engineers, inventors, and students. Papers from recognized professionals may be published immediately with an accompanying invitation for peer-review comments. Other papers will be submitted for peer review. Names and addresses of any reviewers will be sent to authors with reviewers' comments.

The Journal of New Energy (JNE) is devoted to publishing professional papers with experimental results that may not conform to the currently-accepted scientific models. The topics to be covered in this journal include cold nuclear fusion, low-energy nuclear reactions, high-density charge cluster technology (including some plasma circuits where enhanced energy is produced), high-efficiency motors or generators, solid-state circuits that appear to provide anomalous amounts of output energy, and other new energy devices. Papers with experimental data are preferred over theoretical papers. Standard alternative energy topics such as hydrogen fuel, wind power, solar power, tidal power, and geothermal power are not solicited.

Authors should submit abstracts. If the abstracts are favorably considered for publication, the author will be sent an author's kit of instructions for the preparation of the paper. The editor and the editorial advisory board are responsible for making publication decisions.

Authors or their employers will be invoiced for production costs sufficient to cover the cost of publication in excess of subscription funds received. The JNE will try to match donors with authors from developing countries so that all acceptable manuscripts can be published. **Donors are requested to contact the JNE and they will be specially honored in the Journal.**

Editor Hal Fox is the leading founder of the Fusion Information Center which publishes both *Fusion Facts*, a monthly technical newsletter designed to keep subscribers informed of the latest developments in cold fusion and energy research, and *New Energy News*, a monthly newsletter covering all areas of new energy research for members of the Institute for New Energy and other worldwide subscribers.

JOURNAL OF NEW ENERGY

An International Journal of New Energy Systems Vol. 1, No. 3, 1996

Published by the
Fusion Information Center
P.O. Box 58639
Salt Lake City, Utah 84158-0639

A Quarterly Journal
Subscription: $150 for 4 issues
Single issues: $45

Fall 1996

ISSN 1086-8259

FUSION INFORMATION CENTER

FIC OFFERS LICENSE RIGHTS TO NEW TECHNOLOGY

FIC has acquired rights to a new invention which provides for the creation and control of a variety of nuclear reactions. One of the embodiments of this invention is the methodology for constructing a table-top particle accelerator that can accelerate positive ions to achieve impact energy previously achieved only by accelerators using millions of volts. Other embodiments of the invention aid in reducing radioactivity and providing thermal energy from aneutronic nuclear reactions. See the paper, "Plasma-Injected Transmutation" in this issue. For further information call Hal Fox.

Fusion Information Center, Inc.
P.O. Box 58639, Salt Lake City, UT 84158-0639
(801) 583-6232 FAX: (801) 583-2963

INSTITUTE FOR NEW ENERGY

The Institute for New Energy is an international organization to promote new and renewable energy sources. Its monthly newsletter is **New Energy News,** reporting worldwide on all facets of new and enhanced energy.

The Institute for New Energy
P.O. Box 58639
Salt Lake City, UT 84158-0639
Phone: 801-583-6232
FAX: 801-583-2963
E-mail: inc@padrak.com
Web Site: www.padrak.com/inc/

New Energy News

New Energy News (NEN) is the monthly newsletter for the Institute for New Energy,. containing 20 to 30 pages per issue.
It is *FREE* with your membership.

Membership

- Membership to the INE is $35.00 per year for individuals in the U.S.A.
- $40.00 for Canada, and Mexico
- $50.00 for all other countries, *and*
- $60.00 per year for Corporations and Institutions

Call the INE for additional information at the above address, *or*
Contact the INE President: Dr. Patrick G. Bailey — inc@padrak.com